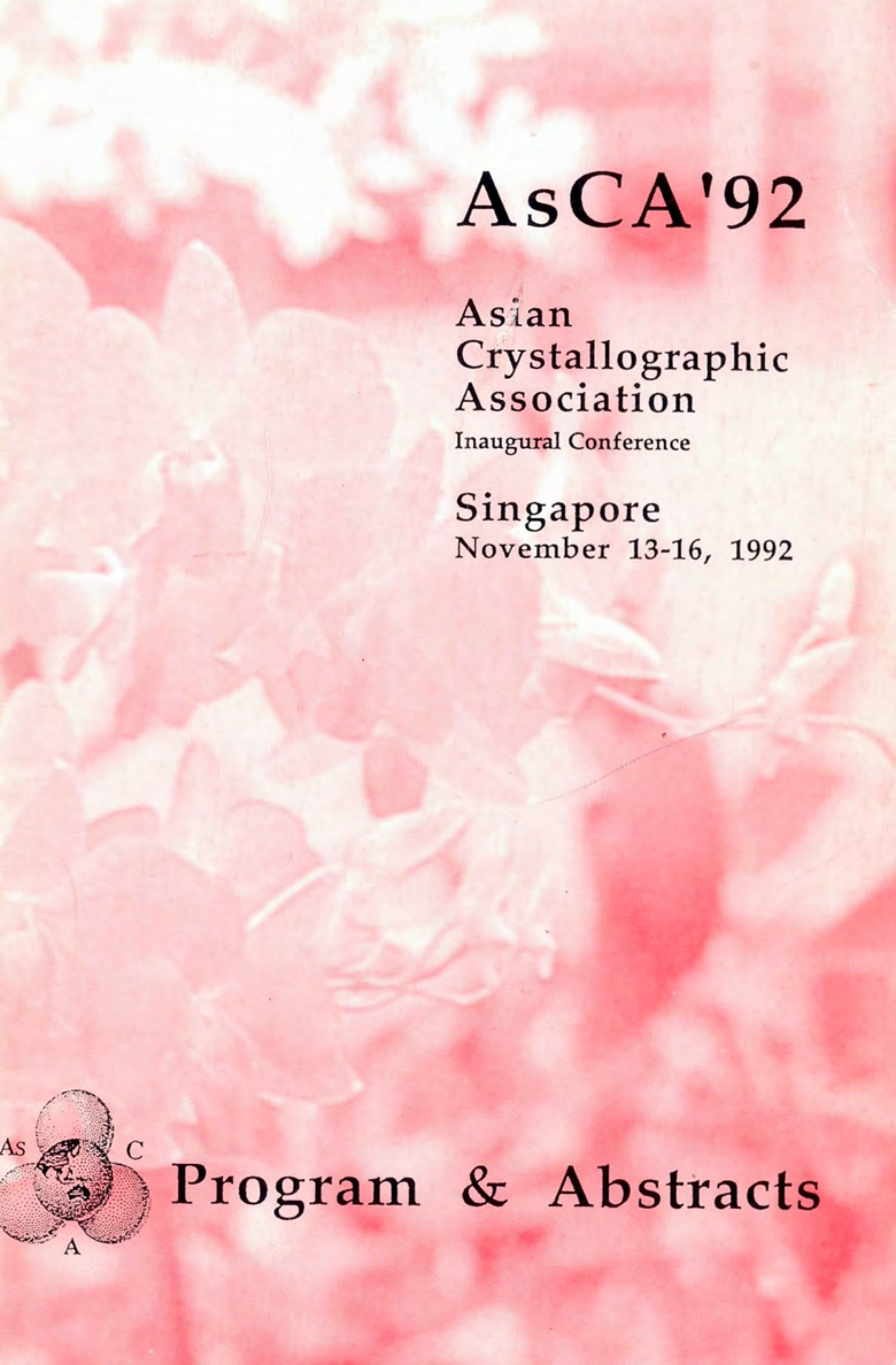

AsCA'92

Asian Crystallographic Association

Inaugural Conference

Singapore
November 13-16, 1992

Program & Abstracts

AsCA'92

Asian Crystallographic Association

Inaugural Conference

Singapore

November 13-16, 1992

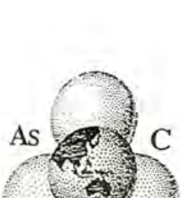

Program & Abstracts

AsCA'92 is the inaugural conference of the **Asian Crystallographic Association.**

Its organisation has been supported financially and administratively by the
Crystallographic Association of Japan and
Society of Crystallographers in Australia.

Grants for young scientists attending this conference have been possible because of contributions from the
International Union of Crystallography,
Crystallographic Society of Japan and
Society of Crystallographers in Australia.

AsCA is also grateful for assistance from the **National University of Singapore.**

Table of Contents

International Organising Committee

Nobutami Kasai (Ch.)	*Japan*
Hans C Freeman	*Australia*
Sydney R Hall	*Australia*
Hiroo Hashizume	*Japan*
Jimpei Harada	*Japan*
Hiroshi Iwasaki	*Japan*
Lip Lin Koh	*Singapore*
Fumiyuki Marumo	*Japan*
Fang-ming Miao	*China*
Yu Wang	*Taiwan*
John W White	*Australia*

International Program Committee

Edward N Maslen (Ch.)	*Australia*
Bryan F Anderson	*New Zealand*
Tamaichi Ashida	*Japan*
Hans C Freeman	*Australia*
Siba P Sen Gupta	*India*
Jimpei Harada	*Japan*
Kum-fun Mok	*Singapore*
Mei-cheng Shao	*China*
Michiyoshi Tanaka	*Japan*
Allan H White	*Australia*

Coordinating Committees

Cr S J

Hiroo Hashizume (Ch.)
Jimpei Harada
Hiroyuki Horiuchi
Hiroshi Iwasaki
Nobutami Kasai
Fumiyuki Marumo
Yuji Ohashi
Kazumasa Ohsumi
Satoshi Sasaki
Michiyoshi Tanaka
Takuyuki Uragami

S C A

Sydney R Hall (Ch.)
Hans C Freeman
Edward N Maslen
Max R Taylor
John W White
Geoff A Williams

Singapore

Lip Lin Koh (Ch.)
Lawrence Chia
John O Hill
Kum-fun Mok

General Information

Registration Desk

The AsCA'92 conference registration desk will be open from 15:00 to 21:00 on Friday November 13 and from 8:00 to 18:00 on Saturday November 14 to Monday November 16. The registration deck is located on the ground floor of the Regional Language Centre, 30 Orange Grove Road (see map on inside front cover). The local phone numbers for the conference organisers are 737 9044 and 733 6108.

The registration desk is responsible for all participant registration and the issuing of conference satchels and badges. It will post notices and relay messages to participants. All bookings of *ad hoc* sessions should be arranged through the registration desk.

Notices

All notices will be placed on the conference Notice Board which is located on the ground floor of the RELC outside the auditorium. General messages and mail for conference participants will be available from the registration desk. Notice of any changes in the scientific program will be posted on the Notice Board.

Conference Badges

The conference name badge must be worn at the Opening Ceremony, all scientific sessions, exhibitions, lunches and social events. Badges are colour-coded as follows:

White	Full and student participants
Yellow	Accompanying persons
Pink	Members of the Organising and Program Committees

Travel Arrangements

International flights must be reconfirmed with your airline at least 24 hours prior to departure. The local Singapore Airlines number is 223 8888.

Meals and Refreshments

Morning and afternoon coffee

Morning and afternoon coffee for all full and student participants will be served from 10:30 to 11:00 and from 15:15 to 15:45 in the ground floor lobby and the restaurant foyer of the RELC on the Saturday, Sunday and Monday, November 14-16.

Lunch

Lunch will be served free of charge to all full and student participants in the RELC restaurant from 12:30 to 13:30 on the Saturday, Sunday and Monday, November 14-16. Conference badges must be worn.

NUS Campus Bus

A minibus will depart from Sheares Hall for the RELC at 8:15 on the mornings of Saturday, Sunday and Monday, November 14-16. This will be free of charge for AsCA'92 registrants. There will be no return bus to the NUS campus but taxis in Singapore are inexpensive, especially when shared by several participants.

Social Events

Welcoming Reception

A welcoming reception and get-together will be held in the RELC lobby from 19:00 to 22:00 on Friday November 13 for all registrants (full, student and accompanying persons). Refreshments and snacks will be served. The reception is sponsored by *Siemens.*

Evening Refreshments

Soft drinks and beer will be served from 17:00 to 19:00 on the Saturday and Sunday evenings in the restaurant foyer, courtesy of *MAC Science* and *Enraf Nonius*.

Farewell Banquet

A farewell banquet for all registrants (full, student and accompanying persons) will be held in the RELC restaurant from 19:00 to 22:30 on Monday November 16. Dress is casual. The banquet is sponsored by *Rigaku*.

Opening Ceremony

The opening ceremony for AsCA'92 will be held in the RELC auditorium from 8:30 to 9:00 on Saturday November 14. The welcoming speakers will be

Professor Nobutami Kasai, President, Asian Crystallographic Association
Professor Andre Authier, President, International Union of Crystallography
Professor Hsing Hua Huang, Deputy Vice Chancellor, National University of Singapore

This ceremony will be followed by the opening plenary lecture from N Sakabe entitled "Biological Application of Synchrotron Radiation".

Society Meetings

The following meetings of crystallographic societies have been scheduled.

Asian Crystallographic Association		
Saturday November 14	19:00	Council meeting, Casuarina theatre
Crystallographic Society of Japan		
Friday November 13	17:00	Council meeting, Casuarina theatre
Monday November 16	18:00	Annual meeting, auditorium
Society of Crystallographers in Australia		
Monday November 16	18:00	General meeting, Casuarina theatre

Commercial Sponsors

The organisers wish to thank the following companies for sponsoring various aspects of this conference. Their assistance has kept the registration fee for this meeting to a minimum.

Enraf Nonius
Rigaku Corporation
MAC Science
Philips
Siemens
Singapore Airlines

Scientific Program Summary

The scientific program schedule for each of the three days of the conference will be:

9:00-10:30	Main Lectures **A** in the auditorium, ground floor.
11:00-12:30	Microsymposia **B** in the auditorium, ground floor.
13:45-15:15	Microsymposia **C** in the auditorium, ground floor.
9:00-10:30	Microsymposium **X** in the Casuarina theatre, second floor on Monday
11:00-12:30	Microsymposia **Y** in the Casuarina theatre, second floor.
13:45-15:15	Microsymposia **Z** in the Casuarina theatre, second floor.
11:00-17:45	Poster sessions **P**, **Q** and **R** in restaurant foyer, second floor.
11:00-17:45	Poster sessions **S**, **T**, **U**, **V** and **W** in main poster hall, second floor.

The left-hand column on each page of the Program Schedule indicates the times of the oral contributions.

The right-hand column on each page of the Program Schedule comprises the abstract numbers in the style of the Abstracts list at the rear of the Program book.

Exhibitors

A commercial exhibition will be held on ground floor lobby, and the second floor main poster hall, from 9:00 to 17:30 each day of scientific sessions.

The exhibitors are:

Enraf Nonius BV, X-ray Diffraction, Roentgenweg 1, 2624BD Delft, The Netherlands.
Fax 31 15 698500

MAC Science, 2-25-16 Nakano Ue Machi, Hachioji, Tokyo 192, Japan. Fax: 81 426 24 2723

Rigaku International Corporation, Sanseido Shinjuku Blding. 7F, 4-15-3 Nishi-Shinjuku, Shinjuku-ku, Tokyo 160, Japan. Fax: 81 3 3299 6364

Siemens AG, X-ray Analytical Systems, Oestliche Rheinbruckenstr. 50, D-7500 Karlesruhe 21, Germany. Fax: 49 45 2845733

Xray Research, Grosse Theatrestr. 42, D-2000 Hamburg 26, Germany. Fax: 49 40 8315916.

Microsymposia Topics

Saturday November 14

Orals

9:00-10:30	**A** Synchrotron Radiation	
11:00-12:30	**B** Organic & Organometallic Structures	**Y** Powder Diffraction
13:45-15:15	**C** Maximum Entropy Methods	**Z** Films & Surfaces

Posters

- **P** Macromolecular Structures I
- **R** Interactions in Biological Molecules
- **T** Minerals, Inorganics & Alloys I
- **V** Phase Transitions & Solid State
- **Q** Macromolecular Structures II
- **S** Electron Scattering & Microscope Imaging
- **U** Minerals, Inorganics & Alloys II
- **W** Crystal Growth & Preparation

Sunday November 15

Orals

9:00-10:30	**A** Electron Scattering	
11:00-12:30	**B** Biological Structures	**Y** Theory
13:45-15:15	**C** Minerals & Inorganic Materials	**Z** Crystal Growth

Posters

- **P** Synchrotron Radiation
- **R** Techniques Other than Diffraction
- **T** Carbon & Organic Structures I
- **V** Electron Distributions
- **Q** Diffractometry & Data Analysis
- **S** Neutron Diffraction
- **U** Organometallic Structures I

Monday November 16

Orals

9:00-10:30	**A** Neutron Diffraction	**X** Phase Transitions
11:00-12:30	**B** Interactions in Biological Structures	**Y** Extinction
13:45-15:15	**C** Diffraction Physics	**Z** Crystallographic Information

Posters

- **P** Interfaces, Films & Surfaces I
- **R** Organic Structures II
- **T** Enzyme Structures
- **V** Phase Transitions & Solid State
- **Q** Interfaces, Films & Surfaces II
- **S** Organometallic Structures II
- **U** Small Biological Structures

Program Schedule

Saturday November 14

Session **14A** SYNCHROTRON RADIATION *(Auditorium)*

9:00 **Biological Application of Synchrotron Radiation** 14A-1
by *N Sakabe*, K Sakabe, T Higashi, A Nakagawa and N Watanabe

9:30 **A Multi-purpose Beam-line Facility** by R F Garrett 14A-2

9:50 **Design Concept of the Spring-8 Undulator Beamline for Macromolecular Crystallography** 14A-3
by *N Kamiya*, H Iwasaki, T Ueki, M Yamamoto, T Uruga and H Yamaoka

10:10 **The Scope for Improved Insertion Devices** by S Yamamoto 14A-4

10:30 *Coffee*

Session **14B** CARBON AND ORGANIC STRUCTURES and ORGANOMETALLIC STRUCTURES *(Auditorium)*

11:00 **Crystal Structures of Some Substituted Ethanes** 14B-1
by *L L Koh* and H H Huang

11:25 **Preparation of Carbon Nanotubes by DC ARC-Discharge Evaporation** 14B-2
by *Y Ando* and S Iijima

11:45 **Crystal Structure and Nonlinear Optical Properties of m-Nitrobenzoic Acid Diethanol Amine Adduct** 14B-3
by *X K Yao*, H G Wang, R J Wang and J M Zheng

12:00 **Structural Aspects of the Trivalent Group 15 Metal(II) (As,Sb,Bi) Complexes with α-hydroxy Acids** by *G Smith*, D S Sagatys and R C Bott 14B-4

12:15 **Studies on Organometallic Compounds: Structure and Activity of Organostannyl Carboxylates** 14B-5
by B B Maji, S Biswas, K L Ghatak, S N Ganguly and *Asok Banerjee*

12:30 *Lunch*

Session **14Y** POWDER DIFFRACTION *(Casuarina Theatre)*

11:00 **Powder Diffraction** by S P Sen Gupta 14Y-1

11:20 **α$TiOSO_4$: Structure Determination from Powder XRD Data and Relationships to other $MoXO_4$ Structures** by *I E Grey* and R Stranger 14Y-2

11:40 **Crystallography of $REAlO_3$ (RE=La, Ce, Pr and Nd)** 14Y-3
by *M Tanaka*, H Horiuchi, T Shishido and T Fukuda

Saturday November 14

12:00 **Crystal Structure Analysis with High-resolution Powder Diffractometer Data** by *T O Ochiai* and H Toraya 14Y-4

12:15 **Structures of the Two Polymorphs of Magnesium Boron Nitride Determined from X-ray Powder Diffraction Data** by H Hashizume, *N Sudo*, H Hiraguchi, O Fukunaga, C Gilmore and G Bricogne 14Y-5

12:30 *Lunch*

Session **14C** MAXIMUM ENTROPY METHODS *(Auditorium)*

13:45 **Electron Density Distributions of Crystalline Materials Obtained by the Maximum Entropy Method** by M Sakata 14C-1

14:15 **Maximum Entropy Method Analysis of Neutron Powder Diffraction Data** by M Sakata, T Uno, M Takata and *C J Howard* 14C-2

14:35 **Analysis of an Approximation in the Maximum Entropy Method** by *S Kumazawa* and M Sakata 14C-3

14:55 **Direct Investigation of Thermal Vibrations of Be Metal by the Maximum Entropy Method Applied to Single Crystal Neutron Diffraction Data** by *M Takata*, M Sakata, F K Larsen, Y Kubota and B B Iversen 14C-4

15:15 *Coffee*

Session **14Z** INTERFACES, FILMS AND SURFACES *(Casuarina Theatre*

13:45 **Accurate Determination of the Unit Cell for an Epitaxial Layer of $Hg_{1-x}Cd_xTe$ Deposited by MOCVD on GaAs** by Zhu Nanchang, *A W Stevenson* and Li Runshen 14Z-1

14:05 **Evaluation of the Roughness of Crystal Surface by X-ray Scattering – Theoretical Consideration** by J Harada 14Z-2

14:25 **Grazing Angle X-ray Standing Wave Study of As-adsorbed Si Surface** by *H Kurashina*, O Sakata and H Hashizume 14Z-3

14:40 **Axial Symmetry Quasicrystal Structure in Some Thin Films, Coatings and Vegetable Fibres — An ESR Study** by *Nguyen Van Tri*, Pham The Vung and Le Hai Hung 14Z-4

14:55 **Double Crystal X-ray Characterization of II-V Multilayered Specimens by Selective Etching** by S Swaminathan 14Z-5

15:15 *Coffee*

Saturday November 14

Section 14P MACROMOLECULAR STRUCTURES I *(Foyer)*

Crystallization and Preliminary X-ray Crystallographic Study of Lysozyme Produced by *Streptomyces globisporus* by *C Uematsu*, H Naitoh, S Harada, Y Kai and N Kasai 14P-1

Preliminary Crystallographic Study of Cytochrome *c'* from *Achromobacter xylosoxidans* NCIB 11015 by *N Shibata*, T Inoue, Y Kai, S Harada, N Kasai, T Kohzuma, S Suzuki, H Iwasaki, and S Shidara 14P-2

Crystal Structure of *Streptomyces erythraeus* Trypsin at 2.7Å Resolution by *T Yamane*, A Suzuki, T Ashida, Y Kawata and F Sakiyama 14P-3

Crystal structure of [2Fe-2S] Ferredoxin I from the *Equisetum arvense* at 1.8Å Resolution by *M Bando*, Y Morimoto, T Tsukihara, S Ikemizu and K Fukuyama 14P-4

Crystal Structure of the TFIID TATA-box Binding Protein: A Novel DVA binding Motif that Recognizes the Minor Groove by D B Nikolov, A -H Hu, J P Lin, A Gasch, A Hoffmann, M Horikoshi, N -H Chua, R G Roeduer and *S K Burley* 14P-5

Section 14Q MACROMOLECULAR STRUCTURES II *(Foyer)*

Crystallographic Refinement of Trichosanthin at 1.9Å Resolution by *Lin YuJuan*, Pan KeZhen, Fu ZhuJi and Zhou KangJing 14Q-6

Crystal Structures of Two Blue Copper Proteins by *T Inoue*, Y Kai, S Harada, N Kasai, S Suzuki, T Kohzuma, J Tobari, S Shidara, and H Iwasaki 14Q-7

High Resolution Electron Crystallography of an α-Helical Coiled Coil Protein by P A Tulloch, Y Fujiyoshi and Y Kimura, *A W S Johnson*, P W Dyson and A E C Spargo 14Q-8

Crystallographic Studies on Double Shelled Spherical Virus, Rice Dwarf Virus (RDV) II by *Y Morimoto*, T Tomizaki, T Sato, T Tsukihara, M Koizumi, T Omura, H Kano and H Mizuno 14Q-9

Crystal Structural Analyses of Spherical Viruses, Tobacco Necrosis Virus (TNV) and Rice Dwarf Virus (RDV) by *T Tsukihara*, Y Morimoto, K Fukuyama, M Koizumi, T Omura, K Kano and H Mizuno 14Q-10

The Structure and Function of Mos Kinase by *B K Sathyanarayana*, W Matten, R Zhou, N Kew, I Daar, T Copeland, G F Van de Woude, J Erickson and R Rubin 14Q-11

Saturday November 14

Section 14R INTERACTIONS IN BIOLOGICAL STRUCTURES *(Foyer)*

Drug-Protein Interaction: Refinement and Modelling of Sulfonamide Drugs Bound to Human Carbonic Anhydrase I Enzyme 14R-12
by *S Chakravarty* and K K Kannan

Crystal Structure of Glutathione Synthetase with Adenosine(5')tetraphospho-(5')pyridoxal by *T Hibi*, H Kato, T Nishioka, J Oda, K Yamaguchi and Y Katsube 14R-13

Active Site Conformation of Cytoplasmic Cyclophilin of *Eschrichia coli.* Steric Hindrance and Attachment of Cyclospolin A 14R-14
by *M Ito*, M Konno, T Hayano, M Suzuki, S Sato and N Takahashi

Alkaline Metal Ion Bound in Human Lysozyme 14R-15
by *M Matsushima*, A Pähler, K Morikami and K Inaka

Structure of *P. stutzeri* G4-amylase and its Complex with Maltotetraose 14R-16
by *Y Matsuura*, Y Morishita, Y Yoshioka, M Sato, Y Katsube and M Kubota

Study of Conformational Difference Between a Dihydropyridine Calcium Channel Antagonist and a Non Antagonist 14R-17
by *S Mehdi* and K Ravi Kumar

Crystal Structure of the Complex between Porcine Pancreatic Elastase and Macrocyclic Inhibitor by *T Tada*, T Yasuda, S Harada, Y Kai and N Kasai 14R-18

Variations on the Same Theme — Crystal Structure of L-Asparaginase and the Uniqueness of its Structural Fold 14R-19
by *J K Mohana Rao*, M Gribskov, D Housset, M Jaskolski, J Lubkowski, M Miller, B K Sathyanarayana, A Swain and A Wlodawer

Binding and Catalytic Roles of the Active Site Metal in Zinc Proteinases 14R-20
by *G Shoham*, H M Greenblatt and H Feinberg

Section 14S ELECTRON SCATTERING, AND MICROSCOPE IMAGING OF STRUCTURE *(Main Hall)*

Use of Atomic Force Microscope in Determination of Space Groups by X-ray Diffraction Analysis of Crystals by *N Masaki*, K Machida, H Kado, K Yokoyama, T Tohda, Y Yoshimura and M Kitamura 14S-31

Electron Microscopy and Diffraction Study of the Direct Reaction of Iron and Carbon and the Formation of a New Iron Carbide 14S-32
by *S Nagakura*, T Komekyu, M Ando and S Odawara

Modulation Modes of $Bi_2Sr_2(Ca_{1-x}Ln_x)Cu_2O_{8+\delta}$ Crystals Studied by High-Resolution Reverse Imaging by T Onozuka 14S-33

Saturday November 14

EELS Study of the Temperature Dependence of the Volume-Plasmon Energy in Aluminium by *M Terauchi,* H Abe, R Kuzuo and M Tanaka	14S-34
Modulated Structures in Fe-Doped Bi-Sr-Cu-O Superconductors Studied by High-Resolution TEM by *K Yanagisawa,* Y Matsui, T Koizumi and T Hasegawa	14S-35
Search for Crystal Structure of Long-period Bi-Mn Alloy Phase — an Example of Structure Analysis by High Resolution Electron Microscopy by *K Yoshida,* T Kawai and K Shimonishi	14S-36

*Section **14T*** MINERALS, INORGANICS & ALLOYS I *(Main Hall)*

Crystal Structure of a New Ternary Chalcogenide $Ta_2Ni_2(\mu_3\text{-}Se)_2(\mu_4\text{-}Se)_2(\mu_5\text{-}Se)_2$ by *S-X Liu,* B Zhang, Z-M Wang and J-L Huang	14T-38
Crystal Structures of Iron-Containing Ternary Layered Tellurides by *Huang Jin-Ling,* S-X Liu and G-L Cal	14T-39
Structure of $Na_4SrSi_3O_9$ and its Relationship to Other $M'_4M''(TO_3)_3$ Compounds by R P Gunawardane	14T-40
Plurality of Si and Co Sites in Co-Akermanite by *K Hagiya,* M Ohmasa and K Iishi	14T-41
Crystal Structure of Duftite Polymorphs by *Kharisun,* M R Taylor and A Pring	14T-42
Polarization Study of Magnetic X-ray Scattering of $(Ba,Sr)_2Zn_2Fe_{12}O_{22}$ by E Tsuji, S Kumazawa, H Katoh, N Momozawa, *K Ishida,* K Ohshima, J Harada and S Kishimoto	14T-43
Single Crystal X-ray Diffraction and EXAFS Studies on R_3TaO_7 (R=Ho,Y,Yb) by *T Tanaka,* N Ishizawa, M Yoshimura, K Tanaka, H Oyanagi, and F Marumo	14T-44
Structure Analysis of Lead Orthovanadate $Pb_3(VO_4)_2$ in the Ferroelastic and Ferroelectric Phases by *T Umeki,* H Kasatani and H Terauchi	14T-45
Structural Variability in γ-Alumina by *B K Gan,* B H O'Connor and C J Howard	14T-46
A New FCC Phase of Y_2O_3 by *S K Katagiri,* N Ishizawa and F Marumo	14T-47

*Section **14U*** MINERALS, INORGANICS & ALLOYS II *(Main Hall)*

Crystal Structure and Lattice Parameters of $Zn_{1-x}Co_xS$, $Zn_{1-x}V_xS$ Diluted Magnetic Semiconductors by *D Gómez de Andérez,* S A López-Rivera and W Giriat	14U-48

Saturday November 14

Structure and Symmetry of PTCR Perovskites 14U-49
by *N J Calos*, J S Forrester, T J White and S Myhra

Structure of $Ba_{6-3x}Sm_{8+2x}Ti_{16}O_{54}$ by *H Ohsato*, T Ohhashi and T Okuda 14U-50

Microcrystalline Keatite — A Fibrous SiO_2-Phase by B Martin 14U-51

The Intersite Distribution of a Small Amount of Mn Ion in Olivine 14U-52
by *Y Ono*, M Tokonami, H Horiuchi, N Aikawa and S Sasaki

Local Crystal Structures of an Ilvaite Single Crystal 14U-53
by *Y Takeuchi*, Y Matsushita, H Sawada and H Taniguchi

Local Structure of Intercalants in Layered Compound Cu_xTiS_2 14U-54
by *K Ohshima*, R Maruta and A Makita

The Zr-N-F and Y-O-F Composite Modulated Structures 14U-55
by *S Schmid*, R L Withers and J G Thompson

X-ray Anomalous Dispersion Determination of $PbZrO_3$ Superstructure 14U-56
by K Nagino, M Iida, Y Itoh, *Y Soejima* and K F Fischer

Changes in Morphology of Periodic Antiphase Boundaries in One-Dimensional Long Period Superstructures 14U-57
by *M Itakura* N Kuwano, S Iwasaki, K Kajiwara, A Matsumoto and K Oki

Diffuse Scattering in an Yttria-Stabilised Cubic Zirconia, $(Zr_{0.61}Y_{0.39}O_{1.805})$ 14U-58
by *T R Welberry*, R L Withers, J G Thompson and B D Butler

Section **14V** PHASE TRANSITIONS and SOLID STATE REACTIONS *(Main Hall)*

X-ray Study of Phase Transition in a C_{60} Single Crystal 14V-59
by *H Kasatani*, H Terauchi, Y Hamanaka and S Nakashima

Crystalline State Racemization of a Bulky Chiral Group 14V-60
by *Y Sakai*, Y Ohashi, Y Arai, Y Ohgo, N Kamiya and H Iwasaki

X-ray Diffraction Study on the Phase Relation of $BaZnGeO_4$ 14V-61
by *S Takai*, T Atake, N Ishizawa, F Marumo and A Hamano

Domain Distributions Around Cubic-Tetragonal Phase Transitions 14V-62
by *T Koga*, N Aomine, Z Lu, Y Soejima and A Okazaki

Chiral-to-racemic Transformation in a Cobaloxime Crystal on Exposure to Visible Light by *T Nemoto* and Y Ohashi 14V-63

Photoisomerization Rates Before and After a Reversible Thermal Phase Transition by *H Tatsuki*, A Sekine and Y Ohashi 14V-64

Section **14W** CRYSTAL GROWTH AND PREPARATION *(Main Hall)*

Structural Features in Some Rapidly Solidified Aluminium Alloys by *Lecong Dzuong*, Ha Thanh Binh, Le Duc Lap and Nguyen Thanh Do 14W-66

Growth of Pure Cadmium Iodide Crystals and Study of Laser Induced Cracks in Them by S K Chaudhary 14W-67

Vapour Growth and Characterization of Cadmium Chloride Doped Crystals of Cadmium Iodide by *Ritu Dhingra* and G C Trigunayat 14W-68

Growth and Characterization of $CdBr_2$ Doped Dendritic Single Crystals of CdI_2 by *Binay Kumar*, G L Bhalla and G C Trigunayat 14W-69

Epitaxial $BaTiO_3$ Crystals (I) on $SrTiO_3$ Substrates by *H Terauchi*, Y Yoneda, Y Watanabe, H Kasatani, K Kamigaki, Y Yano, T Terashima and Y Bando 14W-70

Epitaxial $BaTiO_3$ Crystals (II) on [Pt/MgO] Substrate by *Y Yoneda*, H Yabuno, H Kasatani, H Terauchi, Y Yano,T Terashima and Y Bando 14W-71

Characterization of Barium Titanate Powder Prepared by Chemical Precipitation by T Tunkasiri and *G Rujijanagul* 14W-72

Hydrothermal Synthesis and Structural Characterization of $A_{0.5}VOPO_4.yH_2O$ (A=Alkali, Alkaline Earth and Transition Metals) by *K H Lii*, H Y Kang and S L Wang 14W-73

Defect Substructures and Mechanical Properties of Mullite Prepared by Coprecipitation by *Shu-Cheng Yu* and Jiann-Shing Lee 14W-74

Method to Control Microstructure by Electron Channeling Pattern (ECP) in Presence of Suppressing Contrast Forming Mechanisms by A N Efimov 14W-75

Lattice Metric Match at Heteroepitaxy: Non-cubic Crystals by A N Efimov and *A O Lebedev* 14W-76

Sunday November 15

Session 15A ELECTRON SCATTERING, AND MICROSCOPE IMAGING OF STRUCTURE *(Auditorium)*

9:00 **High Resolution Electron Microscopy** by K Hiraga 15A-1

9:30 **X-ray and Electron Diffraction from Twisted Quartz Crystals** by *M Fehlmann* and A F Moodie 15A-2

9:50 **Electron Microscope Study of Incommensurate Lattice Modulation in Layered Composite Crystal PbS–VS_2** by *N Yamamoto*, K Akiyama, K Yagi, Y Gotoh and Y Oosawa 15A-3

10:10 **High-Resolution EELS Study of the Electronic Structures of Semiconductors Containing Lattice Defects** by *M Terauchi* and M Tanaka 15A-4

10:30 *Coffee*

Session 15B BIOLOGICAL STRUCTURES *(Auditorium)*

11:00 **Crystal Structural Analyses of Spherical Viruses, Tobacco Necrosis Virus (TNV) and Rice Dwarf Virus (RDV)** by *T Tsukihara*, Y Morimoto, K Fukuyama, M Koizumi, T Omura, K Kano and H Mizuno 15B-1

11:30 **Crystal Structure of Uncomplexed NC41 Anti-neuraminidase Fab in its Uncomplexed Form** by *M C Lawrence*, R Malby, A Kortt, V Staton, P M Colman, and R G Webster 15B-2

11:50 **Studies on the Structures of Insulin Analogues and the Binding of Insulin Interaction with its Receptor** by *W R Chang* and D C Liang 15B-3

12:10 **Enzyme Substrate Interactions: Refined Structure of Human Carbonic Anhydrase I (HCAI)-HCO_3^- Complex** by *Vinay Kumar* and K K Kannan 15B-4

12:30 *Lunch*

Session 15Y THEORY *(Casuarina Theatre)*

11:00 **Enhanced Phase Effect in Four-beam X-ray Diffraction — Triplet Phases from Four-beam Diffraction** by Y S Tsai, M T Huang and *Shih-Lin Chang* 15Y-1

11:20 **Phase Determination and Refinement by Density Modification; Low Density Elimination** by M Shiono 15Y-2

11:35 **Restoring the Original Electron Distribution of Lipid Bilayers – A Simulation Study** by *S Yamamura*, M Takata, M Sakata, H Takahashi and I Hatta 15Y-3

11:55 **The Role of Anomalous Dispersion in the Comparative Refinement of Modulated Crystal Structures** by A D Rae 15Y-4

12:10 **Optical Transforms** by T R Welberry 15Y-5

12:30 *Lunch*

Session 15C MINERALS, INORGANICS & ALLOY STRUCTURES *(Auditorium)*

13:45 **Computer Simulation of the Structural and Physical Properties of the $MgSiO_3$ Polymorphs** by M Matsui 15C-1

14:20 **Photorefractive KNSBN Crystals with A-sites Unfulfilled Tungsten Bronze Structure** by *H C Chen*, D L Sun and Q Z Jiang 15C-2

14:40 **Modulation Wave Approach to Structural Parameterization and Rietveld Refinement of the C9-cristobalite Related, Low Carnegieite Structure** by *R L Withers* and J G Thompson 15C-3

15:00 **Low-Carnegieite — Why Previous Attempts to Study its Structure Were Unsuccessful** by *J G Thompson*, R L Withers, A K Whitaker and R M Traill 15C-4

15:15 *Coffee*

Session 15Z CRYSTAL GROWTH AND PREPARATION *(Casuarina Theatre)*

13:45 **Holographic Studies of the Solid-Liquid Interface Boundary Layer in Flux Crystal Growth** by *Xiling Yu*, Youchen Liu and Xuefeng Yue 15Z-1

14:05 **Growth and Characterization of Bi-Sr-Ca-Cu-O Single Crystals** by *Alka Jain* and G C Trigunayat 15Z-2

14:25 **Pressure Dependence of Cell Dimensions in NiS_2 Crystals Grown under Different Sulfur Vapour Pressures** by T Komori, N Ishizawa, *F Marumo* and Y Noda 15Z-3

14:45 **The Synthesis and Structure of $Cu_3Bi_4V_2O_{14}$** by G B Deacon, B M Gatehouse and *G N Ward* 15Z-4

15:00 **Synthesis and Characterization of Ni_3S_2 (Heazlewoodite) Crystals** by S M Dharmaprakash 15Z-5

15:15 *Coffee*

Sunday November 15

Section 15P SYNCHROTRON RADIATION *(Foyer)*

The Australian National Beamline Facility by *R F Garrett*, J W Boldeman, D J Cookson, G Foran, D C Creagh, F Johnson, S Janky and S W Wilkins P-00

Proposed Synchrotron X-ray Study of Monolayers at the Photon Factory by G T Barnes and *C H L Kennard* 15P-2

An Instrument for X-ray Surface Studies by G Barnes, C Kennard, D C Creagh, *I Jamie* and J W White 15P-3

X-ray Evaluation of a Lapped Si Single Crystal by *H Shiwaku*, M Ando, K Hyodo, Xiao-Jing Wu and S Horiuchi 15P-4

Intensity Enhancement in Asymmetric Diffraction with Parallel-Beam Synchrotron Radiation by *H Toraya*, T C Huang and Y Wu 15P-5

Structure Refinement of Submicrometer-Sized Twinned Domains by Laue Method using Synchrotron Radiation by *K Ohsumi*, K Hagiya, T Takase, Y Shimizugawa, M Ohmasa and M Miyamoto 15P-6

Ultramicro-single-crystal Diffraction Study on Barium Titanate using SR by *M Kataoka*, K Suda, N Ishizawa, F Marumo, Y Shimizugawa and K Ohsumi 15P-7

Diffraction from Composite $Nd_{13}Fe_{46}B_{41}$ Crystal by Synchrotron Radiation by *T Ohba*, S Sasaki, M Takata and Y Komura 15P-8

Section 15Q DIFFRACTOMETRY and DATA ANALYSIS *(Foyer)*

Micro-area X-ray Diffraction in Crystallographic Analyses of Mineral Textures and Tiny Single Crystals by *H Horiuchi*, M Tanaka, S Nojima, T Mitsuki, and I Minato 15Q-9

Microstructure and Crystallinity of Luminescent Porous Silicon by Diffraction Techniques by *K Takemoto*, Y Nakamura and O Nittono 15Q-10

Design of New Type Four Circle Diffractometer with Movable Rotating Anode X-ray Source by *J Harada*, I Takahashi, T Shimura, T Miyazaki, K Yamada and K Masuda 15Q-11

Fundamental Study of a Time-resolved Laue Method for Protein Crystallography by *N Watanabe*, N Sakabe, and K Sakabe 15Q-12

High Resolution Data Collection from Protein Crystals on R-axis IIC Diffractometer by *T Sato*, T Higashi and T Tada 15Q-13

Structure Determination of Organic Compounds by a Rapid X-ray Measurement System by *F Iwasaki*, M Sakuratani, M Yasui, N Kamiya and H Iwasaki 15Q-14

Fully Automatic Structure Elucidation
by *K Yamaguchi*, E Yasudome and G Matsumara 15Q-15

***XTAL* 3.2: A New System Release** by E Blanc, D Schwarzenbach, D M Collins, D D Dexter, D A Grossie, H D Flack, *S R Hall*, G S D King, B G Kruger, R Olthof-Hazekamp, J M Stewart and K D Watenpaugh 15Q-16

Section 15R TECHNIQUES OTHER THAN DIFFRACTION *(Foyer)*

Electron Irradiation Defect Studies on Quartz Crystals at Constant Electron Energy (200 kV) by B Martin 15R-17

The Polarity of Thermal Conductivity in $LiNbO_3$ and $LiTaO_3$ by *M Tokonami*, O Tachikawa, Y Ono, T Suetsugu, S Kan, K Yamamoto and J Hikita 15R-18

Smectic Layer Structure of Ferrocene Containing Liquid Crystals
by *N Nakamura*, T Hanasaki and K Onoi 15R-19

Cumulative Distribution Functions of Normalized Intensity, Allowing for Atoms at Special Positions in the Unit Cell by B Pal and *G D Nigam* 15R-20

Section 15S NEUTRON DIFFRACTION *(Main Hall)*

Refinement of the Crystal Structures of Cu_6O_8InCl and $Cu_6O_8Cu_2Cl$ by Neutron and X-ray Powder Diffraction
by *H Hayakawa*, E Akiba, S Ono, H Ihara, F Izumi and H Asano 15S-32

Neutron Powder Diffraction Study of Deuterated Benzene from 4K to the Melting Point by C J Craven, P D Hatton, G S Pawley and *C J Howard* 15S-33

A Neutron/X-ray Diffraction Study of Simulated Radiation-Waste Element Substitution in Synroc by *W Kalceff*, E A Xuereb and D N Argyriou 15S-34

Section 15T CARBON AND ORGANIC STRUCTURES I *(Main Hall)*

Influence of ^{13}C Isotope Concentration on the Structure of Diamond
by *T Yamanaka*, S Morimoto, H Kansaki and S Sasaki 15T-36

Single-Crystal X-ray study on *fcc* and *hcp* C_{60}
by *T Kitamoto*, S Sasaki, H Hashizume, T Atake, T Tanaka, H Kawaji, K Kikuchi, K Saito, S Suzuki, Y Achiba and I Ikemoto 15T-37

Sunday November 15

An X-ray Study of a Twinned n-Tetracosane Crystal 15T-38
by S C Nyburg and *A R Gerson*

Molecular Aggregation of Cationic Surfactants and Aromatic Compounds 15T-39
by *T Kitamura*, H Uekusa, Y Ohashi and H Hirata

Lattice Instability Coupled with Molecular Internal Degrees of Freedom in Biphenyl and bis(4-chlorophenyl)sulfone 15T-40
by *T Atake*, T Tanaka, H Kawaji, K Saito, K Kikuchi and I Ikemoto

Directed Heteromolecular Hydrogen Bond Interactions in Carboxylic Acid Cocrystals by *D E Lynch*, G Smith and C H L Kennard 15T-41

Crystal and Molecular Structures and Thermal Properties of Mesogenic 2,5-bis-(4-ethylbenzoyl)oxystyrene and 2,5-bis(4-methoxybenzoyl)oxybenzaldehyde 15T-42
by *Yang Qingchuan*, Dai Sheng, Zhou Hongbing, Zhou Qifeng and Tang Youchi

Unusually Short Ethylene Bond Length and Large Amplitude Torsional Motion of (*E*)-stilbenes in Crystals 15T-43
by *K Ogawa*, S Yoshimura, Y Takéuchi, T Sano and K Toriumi

Unusual Structure of Pentafluoronitrosobenzene 15T-44
by H G Ang, W L Kwik, K K Ong and *W Y Leong*

Section 15U ORGANOMETALLIC STRUCTURES I *(Main Hall)*

Crystal Structure of [Isothiocyanato(1,4,8,12-tetra–azacyclopentadecane) copper(II)] Thiocyanate 15U-46
by *Tsong-Jen Lee* , C –T Tsai, Wei-Jen Lan and Chung-Sun Chung

Structure of a Hexanuclear Bimetallic Cluster (μ–H)$Os_5Cu(CO)_{18}PPh_3$ 15U-47
by H G Ang, W L Kwik and *K H Ng*

Structural Studies of Complexes of Copper(I) Halides with Ethylene Thiourea and *sym*-diphenylthiourea by P Thavornyutikarn, Y Wattanakanjana, *C Pakawatchai*, B W Skelton and A H White 15U-48

The Role of NCS^- Ion in Structures of Cu(II) Complexes with Deformed Diazadioximes and Tetraamines 15U-49
by *T H Tahirov*, Tian-Huey-Lu, Yun-Long Hseih and Chung-Sun Chung

Magneto-Structural Correlations of Dimeric Copper(II) Trichloroacetates 15U-50
by *H Uekusa* and S Ohba

The Structural Characterization of [$(cy)_3PIAgpyAgIP(cy)_3$] 15U-51
by *Effendy* and A H White

Novel Interpenetrating Molecular Frameworks Derived from AgTCM 15U-52
by *S R Batten*, B F Hoskins and R Robson

Ag(I) As(III) Complexes with α-hydroxy acids: Structures of the Isomorphous Complexes {$Ag_5As_4(C_4H_2O_6)_4(H_2O)_5(X)\}_n$,{$C_4H_2O_6$ = (+)tartrate(4-) and X=NO_3^-, ClO_4^-}, with Ag-As Bonds by *G Smith*, R C Bott and D S Sagatys 15U-53

The Crystal Structure of $Au(PPh_3)_2(PhCS_2)$ by Ju-Chun Wang 15U-54

Crystal Structure of a Platinum(II) Complex of L-methionyl-glycine 15U-55
by *D Shi*, T W Hambley and H C Freeman

Structure of Potassium Theobrominium Tetrakis(thiocyanato) Palladate(II) 15U-56
by T Giraldi, *M R Taylor*, M I Moreno-Vida, J Ruis-Sanchez,
J M Salas-Peregrín and E Colacio

Pt, Pd and Rh Complexes with Metalapentalene Framework 15U-57
by *M Yasui*, S Yoshida and F Iwasaki

Thallium-containing Platinum Sulphur Complexes: Crystal Structure of $TlS_2Pt_2(PPh_3)_4PF_6$ by M S Zhou, L L Koh, *Y Xu*, T S A Hor, P H Leung and K F Mok 15U-58

Symmetry Axis of the Vanadyl Complex in VO^{2+} Doped $Cd(C_4H_2O_4).2H_2O$ Single Crystals by *R S Bansal* and V P Seth 15U-59

Unprecedented Framework Structures: New Derivatives of $Cd(CN)_2$ 15U-60
by B F Abrahams, *M J Hardie*, B F Hoskins, R Robson and G A Williams

Section 15V ELECTRON DISTRIBUTIONS *(Main Hall)*

Bonding Deformation and Superposition Effects in the Electron Density 15V-62
by *I Olovsson*, G J McIntyre and H Ptasiewicz-Bak

Extinction Corrections from Equivalent Reflection Intensities 15V-63
by *E N Maslen* and N Spadaccini

Electron Density Distribution for the High Melting Substance TiN 15V-64
by *M J Kisono*, Y Kubota, M Takata and M Sakata

Electron Distribution in a Crystal of $NiS_{2-x}Se_x$ 15V-65
by *U Tanaka*, N Ishizawa, F Marumo and T Miyadai

The Electron Distribution in Dipotassium Tetrafluoronickelate, K_2NiF_4 15V-66
by S K Yeh, S Y Wu and *Yu Wang*

Synchrotron Radiation Vibration Amplitudes and $\Delta\rho$ Maps for K_2SiF_6 and K_2PdCl_4 by *J R Hester*, E N Maslen, N Spadaccini, N Ishizawa and Y Satow 15V-67

Sunday November 15

Synchrotron X-ray Study of the Electron Density in Corundum Al_2O_3 15V-68
by E N Maslen, *V A Streltsov*, N Ishizawa and Y Satow

Synchrotron X-ray Study of $\Delta\rho$ in Y_2BaCuO_5 by *R M Hsu* and E N Maslen 15V-69

Structure and Electron-density Studies of a $Tl_2CaBa_2Cu_2O_8$ Superconductor Synchrotron X-rays by *S Sasaki*, T Mori, K Kawaguchi and M Nakao 15V-70

A Hydrogen Bonding Study with Charge Density Distribution and Interaction Energy by *Kuan-Jiuh Lin* and Yu Wang 15V-71

Spin and Charge Transfer through Hydrogen Bonding in $[Co(NH_3)_5(OH_2)][Cr(CN)_6]$ by B N Figgis and *E S Kucharski* 15V-72

The Electron Distribution in $Nd_2Fe_{14}B$ by *D du Boulay* and E N Maslen 15V-73

Electron Density in AlN from X-ray Powder Data by the Maximum Entropy Method by N Nakahigashi, *H Ishibashi*, S Minamigawa and M Kogachi 15V-74

Electron Density in Pure Metals by the Maximum Entropy Method 15V-75
by *Y Kubota*, M Takata and M Sakata

On the Reproducibility of Electron Density Maps for Ideal Perovskites 15V-76
by E N Maslen and *N R Streltsova*

Monday November 16

Session **16A** NEUTRON DIFFRACTION *(Auditorium)*

9:00 **Neutron Sources and their Crystallographic Applications** 16A-1
by R Chidambaram

9:30 **Scattering Length Variations in Neutron Diffraction** by J W White 16A-2

10:00 **Structure of Orthorhombic HfO_2 by Neutron Powder Diffraction** 16A-3
by *O Ohtaka*, T Yamanaka, N Hara, H Asano and F Izumi

10:15 **Bragg and Diffuse Neutron Scattering Studies of Cubic Zirconia** 16A-4
by *D N Argyriou* and M M Elcombe

10:30 *Coffee*

Session **16X** SOLID STATE REACTIONS and PHASE TRANSITIONS *(Casuarina Theatre)*

9:00 **Nitro-nitrito Linkage Photoisomerization in Crystals of Nitropenta-amminecobalt(III) Dichloride** by S Ohba 16X-1

9:20 **Crystalline-state Photoisomerization of Cobaloxime Complexes** 16X-2
by *A Sekine* and Y Ohashi

9:40 **Phase Transition and Crystal Structures of 1-Br-Adamantane** 16X-3
by *H Takakura*, N Ichiwa and M Shiono

10:00 **X-ray Study of Ferridistortive Phase Transition in $\{N(CH_3)_4\}_2CoBr_4$** 16X-4
by *Y Nishihata*, A Sawada, H Kasatani and H Terauchi

10:15 **Phase Transitions of the Halogen-Bridged M(II)-X-M(IV) Mixed-Valence Complexes. Structural Studies of High- and Low-Temperature Phase of $[Pt(en)_2][PtBr_2(en)_2](ClO_4)_4$** 16X-5
by *K Toriumi*, M Yamashita, S Kurita, I Murase and T Ito

10:30 *Coffee*

Session **16B** INTERACTIONS IN BIOLOGICAL STRUCTURES *(Auditorium)*

11:00 **DNA Conformation in Crystals** by M Sundaralingam 16B-1

11:30 **Probing the Interaction Between Platinum Anti-Cancer Drugs and DNA** 16B-2
by *T W Hambley*, G W Allen, F R Fenton, E C H Ling and K Patser

11:50 **Electrostatic Potential in $tRNA^{Asp}$ Recognition by Aspartyl-tRNA Synthetase** by *A Takenaka*, J Cavarelli, J C Thierry and D Moras 16B-3

Monday November 16

12:10 **Biophysical and Crystallographic Study of DNA Recognition by a Basic-Helix-Loop-Helix-Zipper Protein** 16B-4
by *A R Ferré-D'Amaré*, P Pognonec, R G Roeder and S K Burley

12:30 *Lunch*

Session 16Y **EXTINCTION** and **ELECTRON DISTRIBUTIONS** *(Casuarina Theatre)*

11:00 **The Exact Solution of Dynamical Diffraction in a Distorted Crystal and its Applications** by N Kato 16Y-1

11:15 **Experimental Test of the Statistical Dynamical Theory of Extinction** 16Y-2
by *T Takama* and T Kihara

11:35 **A General Theory of Extinction in Crystals** by T M Sabine 16Y-3

11:50 **Neutron Diffraction Study of KCl: Test of the Sabine Extinction Formalism** by *S Maheswaran* and T M Sabine 16Y-4

12:10 **X-ray 5d-Orbital Analysis of PtP_2 and Multiple Diffraction Free Intensity Measurement** by *K Tanaka*, S Kumazawa, S Maruno and I Shirotani 16Y-5

12:30 *Lunch*

Session 16C **DIFFRACTOMETRY AND DIFFRACTION PHYSICS** *(Auditorium)*

13:45 **Direct Observation of Anomalous Transmission of X-rays through Thin Natural Diamond Crystals with Varying Degrees of Crystal Perfection** 16C-1
by *Krishnan Lal*, S Niranjana, N Goswami and Ajit Ram Verma

14:05 **Single Crystal Diffractometer on an Open Tube X-ray Generator with Maximum Tube Voltage 200KV** 16C-2
by *F P Okamura*, K Yukino, K Yamamoto, T Hori, S Yoshimachi, R Yokoyama, H Kawasaki, K Tsukamoto and H Izawa

14:25 **Texture Analysis by Four Circle Goniometer in Polycrystalline Materials** 16C-3
by *A ul Haq* and A Q Khan

14:45 **A System for Analysing Thin Film Structure by Grazing Incidence diffraction: I. Grazing Incidence Diffractometer** 16C-4
by *H Toraya* and T Ochiai

15:00 **Measurement of Radii of Curvature of Slightly Bent Crystals Using a Reticon Detector** by *D Gao*, S W Wilkins and A W Stevenson 16C-5

15:15 *Coffee*

Session 16Z CRYSTALLOGRAPHIC INFORMATION *(Casuarina Theatre)*

13:45 **The World Directory of Crystallographers, Electronic Mail, and Communication with Crystallographers in the Asian Region** by *H Hashizume* and Y Epelboin 16Z-1

14:05 ***CIFtbx*: Fortran Routines for Manipulating CIF's** by S R Hall 16Z-2

14:25 **XAFS: Can This Important Technique Achieve Respectability?** by D C Creagh 16Z-3

14:45 ***SHELXL-92* A New Least-Squares Refinement Program for Use With Single Crystal Diffraction Data** by G M Sheldrick and *W T Robinson* 16Z-4

15:00 **Integrated X-ray Measurement and Computation System for Protein Crystallography** by *N Yasuoka*, Y Higuchi, S Misaki, Y Morimoto and I Fujii 16Z-5

15:15 *Coffee*

Section 16P INTERFACES, FILMS & SURFACES I *(Foyer)*

Morphological Investigation of the (0001) Surface of Ice I_h Crystal by X-ray Crystal Truncation Rod Scattering by *A Goto*, K Akiya, T Shimura, I Takahashi, J Harada, Y Furukawa and T Hondoh 16P-1

$CaSrF_2$/GaAs and CaF_2/S/GaAs Interface Structures Revealed by X-ray Standing Waves and Crystal Truncation Rods by *H Hashizume*, T Niwa, M Sugiyama, O Sakata and S Maeyama 16P-2

X-ray Diffraction Study of the Air Cleaved NaCl(100) Surface by *I Takahashi*, T Kakiuchi, T Shimura and J Harada 16P-3

Structures of Multilayered Ag/Cu and Ag/Pb Films by X-ray Diffraction by K Hazama, J Kozaki, S Ando and *O Nittono* 16P-4

Epitaxial Growth of (110) Ag Thin Film on NaCl in a Knudsen Gas of Ar by I Ogura 16P-5

Section 16Q INTERFACES, FILMS & SURFACES II *(Foyer)*

Crystal Structure Changes in Oxygen-Deficient $YBa_2Cu_3O_{7-\delta}$ Superconducting Thin Films by *J Ye*, A Ishii and K Nakamura 16Q-6

Structural Characterization of Fe/X (X:Ag,Cu,Ta) Multilayer Films Prepared by DC Sputtering by *Y Haga*, T Sugiyama, Y Nakamura and O Nittono 16Q-7

Monday November 16

X-ray Standing Waves in 100Å–Thick Epilayers Under Grazing-incidence Diffraction Conditions by *O Sakata*, I Kawamoto and H Hashizume 16Q-8

Observation of the CTR Scattering from AlAs Molecular Layers in GaAs using Imaging Plate Detector by *T Shimura* and J Harada 16Q-9

Misfit Accommodation of Pt/Au/buffer Ag Trilayers Grown onto Si, MgO and NaCl Substrates by *A Sugawara* and O Nittono 16Q-10

X-ray Diffraction Analysis of RTP Processed Cu/In/Se Stacked Thin Layers by *F Camillo*, M Donat, H Galindo, A B Vincent, J M Martin and D Gómez de Andérez 16Q-11

Section 16R ORGANIC STRUCTURES II *(Foyer)*

Crystal Structures of Adenylyl2'-5'-adenosine Trihydrate and Tetrahydrate: Molecular Conformation Under Different Hydrations by *R Krishnan* and T P Seshadri 16R-12

Crystal Structures of 2,6-di(2-furyl)-3,5-dimethyl Piperidin-4-one by *N Sukumar*, M N Ponnuswamy, J C Thenmozhiyal and R Jeyaraman 16R-13

Structural Study of 1-octadecanol by the PSPC System by *H Kobayashi* and N Nakamura 16R-14

Crystal Structures of Meso-1,1'-dicyano-1,1'-diphenylethane (1) and Meso-1,1'-dinitro-1,1'-diphenylethane (2) by *L L Koh*, H H Huang, K Y Sim, Y L Lam and Y Xu 16R-15

Effect of Trimethylsilyl Substituent on C-O Bond Lengths at the Beta Position: Some Structural Studies by *J M White* and G B Robertson 16R-16

Sequential Base-promoted Cleavage of C-S Bonds in a Coordinated Crown Thioether by M A Bennett, L Y Goh and *A C Willis* 16R-17

Structure and Properties of Bilayer-forming Amphiphiles, $C_nAzoC_mN^+Br^-$ by *Guiqing Xu*, K Okuyama and M Masatsugu 16R-18

Crystal Structure of 1,18-Dibromooctadecane by *T Yamamoto*, N Nakamura and Y Yoshimura 16R-19

2D-NMR Study on the Conformation of a Dodecacyclopeptide by *L H Lai*, L B Ma, Z W Miao and X J Xu 16R-20

Section 16S ORGANOMETALLIC STRUCTURES II *(Main Hall)*

Metal Complexes of Benzoquinonediimine and Related Diimines 16S-31
by Shie-Ming Peng

Crystal Structures of Four Transition Metal Complexes 16S-32
by *Tian-Huey Lu*, Tahir Tahirov, Bor-Hann Chen and Chung-Sun Chung

Complexes of Some First Transition Series Elements with 16S-33
4,4'-dipyrazolylmethane by J A Broomhead, G Camm and *M Sterns*

Polymorphic Structures of $M(HCOO)_2.2(NH_2)_2CO$: M=Mn,Cd,Co,Mg,Zn 16S-34
by *N Achiwa* , M Fujino, H Takakura, M Shiono, N Koyano, Ridwan,
I Shibuya and K Yamagata

Crystal and Molecular Structure of Zinc(II) and Cobalt(II) Complexes with 16S-35
4,5–Diazafluoren-9-one
by *N Venkata Lakshmi,* K Ravikumar, G Prasuna and M V Rajasekharan

Study of Bis{*trans*-[bis(diphenylphosphino)ethylene]}-tricarbonyliron(0) 16S-36
and *cis*-[bis(diphenylphosphino)-ethylene]tricarbonyliron(0)
by Lung-Shiang Luh and *Ling-Kang Liu*

Structure of Iodine{[3,3'-(1,3-propanediyldinitrilo)bis(2-butanoneoximato)]- 16S-37
N,N'N",N'"}(2,2,2-trifluoroethyl)cobalt(III)
by S Geremia, *Asadur Rahman*, E Zangrando and L Randaccio

EXAFS Studies of Monomeric/Dimeric Equilibria of Nitridotechnetium(VI) 16S-38
Complexes in Solution
by *G A Williams,* L J Martin, D M Samuels and M Nomura

X-ray Structural Studies of a Novel Delocalised Triphosphazene 16S-39
$(CF_3)_2P{=}N{=}P(CF_3)_2{=}N{=}PPh_3$ and the Triosmium Cluster Complexes
$Os_3(CO)_{11}[(CF_3)_2P{=}N{=}P(CF_3)_2{=}N{=}PPh_3]$ by H G Ang, W L Kwik and *Y M Cai*

Structures of $(CF_3)_2As{=}N{=}PPh_3$,$[Os_3(CO)_{11}((CF_3)_2As{=}N{=}PPh_3)]$ and 16S-40
$[Os_3(CO)_9(\mu{-}H)_2((CF_3)_2As{=}N{=}PPh_3)]$ – Novel Neutral Molecules
Containing As=N=P Moiety by H G Ang, W L Kwik, *Y W Lee* and A L Rheingold

X-ray Crystal Structure of $[\{WCl_3(PMe_2Ph)_2\}_2\{(\mu{-}NC_6H_4N{-}1,4)\}]$– 16S-41
The First Structural Characterisation of a Binuclear Complex Containing
a 1,4-phenylene Diimido Bridge
by W Clegg, R J Errington, *D C R Hockless,* J M Kirk and C Redshaw

Molecular Structure of Tungsten Phenoxide 16S-42
by *N Kanehisa,* Y Kai, N Kasai H Yasuda, Y Nakayama and A Nakamura

Stereochemistry and Crystal Structure of Diphenyltin Dichloride Complexes with meso- or rac-Bis-(phenylsulfinyl)ethane 16S-43
by *H-G Wang*, X K Yao, R J Wang, J X Bao and P X Shao

Coordination of Tetramethylethylenediamine with Halogen Bridged Lead(II) 16S-44
by *H Miyamae*, Y Hatanaka, Y Iijima, G Hihara and M Nagata

Section 16T ENZYME STRUCTURES *(Main Hall)*

Crystallisation and Preliminary X-ray Studies of Calotropin DII, a Cystein Protease from *Calotropis gigantea* by B Das, S Ghosh, S Pain, I Dey, G Biswas , B P Mukhopadhyay, N K Sinha and *Asok Banerjee* 16T-45

Crystallization of Protein Disulfide Isomerase from Bovine Liver 16T-46
by *G Kurisu*, C Uematsu, T Shiba, S Harada, Y Kai and N Kasai

Crystallization and X-ray Diffraction Study of Phospholipase A2 from the Venom of *Agkistrodon halys* Pallas by *Gui Lulu*, Niu Xiutian, Yang Jian, Bi Ruchhang, Liu Zhengjiong, Zhou Yuanchong and Lin Nianqin 16T-47

Two Crystal Forms of Bovine Heart Cytochrome c Oxidase by *E Yamashita*, Y Morimoto, T Tsukihara, Y Fukumoto, K Shinzawa-Ito and S Yoshikawa 16T-48

Structure Analysis of *Serratia* Protease from *Serratia* sp. E-15 16T-49
by *K Hamada*, H Hiramatsu, T Fujiwara, Y Katsuya, Y Hata, M Sato and Y Katsube

Structure Analysis of Neutral Protease from *Streptomyces caespitosus* 16T-50
by *A Nagara*, T Kinoshita, S Harada, Y Kai, N Kasai , S Tunazawa and F Sakiyama

Three-dimensional Structure of Oligo-1,6-glucosidase at 3Å Resolution 16T-51
by *Y Hata*, H Kizakai, K Watanabe, Y Suzuki and Y Katsube

Three-Dimensional Structures of Aspartate Aminotransferase from *Escherichia coli* at 1.8 Å Resolution by A Okamoto, *K Hirotsu* and T Higuchi 16T-52

Structure of the Active-site Mutants of *Escherichia coli* Aspartate Aminotransferase by *I Miyahara*, K Hirotsu, T Higuchi and O Okamoto 16T-53

X-ray Structural Analysis of Aspartic Proteinase from *Irpex lacteus* 16T-54
by *H Mizuno*, N Oogami, H Kobayashi, K Kasamo, I Kasukabe and K Murakami

Structure of Chimeric 3-isopropylmalate Dehydrogenase and its Thermostable Mutants by M Sakurai, K Onodera, *H Moriyama*, N Tanaka, K Numata, H Kirino, T Oshima, Y Katsube and M Sato 16T-55

Crystal Structure of Ribonuclease U2 at 1.8Å Resolution 16T-56
by *S Noguchi*, Y Satow, C Sasaki, T Matsuzaki and T Uchida

Structure Analysis of Phospholipase A2 from the Venom of *Trimeresurus flavoviridis* by E Matsueda, *A Suzuki*, T Yamane and T Ashida 16T-57

Crystal Structure of Chicken Gizzard G Actin•DNase I Complex at 2Å Resolution by *K.Sasaki*, K.Sakabe, N. Sakabe, H. Kondo and M.Shimonura 16T-58

Structure of Buffalo Carbonic Anhydrase II: Comparison with Other Known Carbonic Anyhdrase (CA) Structures by *V Kumar* and K K Kannan 16T-59

Metal-Protein Interaction: Binding of Mercury to Human Carbonic Anhydrase I Enzyme by *S Chakravarty*, V S Yadava and K K Kannan 16T-60

Section **16U** SMALL BIOLOGICAL MOLECULES AND FRAGMENTS *(Main Hall)*

Structure and Molecular Motion in the Alkali Metal Salts of Penicillin V by *A J Edwards*, C K Prout, M Dobson, J Fattah, S J Heyes, J E Taguchi, J M Twyman, D J Watkin and M Wendeler 16U-61

Crystal Structure of the DNA Fragment d(CCGGGCCCGG) by M A Viswamitra, *D Champion C S Kumar* and N Gautham 16U-62

Molecule Structure of an RNA Duplex with Four Successive non-Watson-Crick Base Pairs by S *Fujii*, Y Tanaka, T Sakata, H Hiroaki, S Uesigi, and T Tanaka, 16U-63

Crystal Structure of Boc-d-Val-Ala-Leu-Ala-OMe by *V Pattabhi*, C Sadasivan, S Durani and V Bohde 16U-64

Unusual Conformational Flexibility in n^1-Substituted Uncommon Purine Nucleotides: Structures of 1-allyl-isoguanosine and 1-allyl-xanthosine by *Yen-Chywan Liaw*, Ji-Wang Chern and Andrew H -J Wang 16U-65

Conformational Analyses of AC-ring Bicyclic Colchicine Analogues by R J Greenwood and *M F Mackay* 16U-66

Absolute Configuration and Conformation of a Novel Antiallergic Agent KW4099 by *N Hirayama*, T Sugaya, S Tomioka, E Ohshima and N Obase 16U-67

Structure Determination of the Blue Flower Pigment, Commelinin, from *Commelinia communis* by *A Nakagawa*, K Yoshida, T Kondo, T Kawai and the late T Goto 16U-68

Structural Studies on β(1→3) Linked Oligosaccharides by *K Noguchi*, K Okuyama, S Kitamura and K Takeo 16U-69

Crystal Structures of Modified Nucleosides 5'-o-Tosyl Adenosine and 2'–o-Tosyl Adenosine by *D Prahadeeswaran* and T P Seshadri 16U-70

Monday November 16

Metal Ion-purine Base Interactions, Zn(II) and Cd(II) Complexes of 8-methylthiotheophylline. X-ray Crystal Structure and Solution Structure of Bis(8-methylthiotheophyllinato)diaquazinc(II) by *M H Skipworth*, M R Taylor, J C Avila-Roson, M A Hidalgo, J Suarez-Varela and E Colacio 16U-71

Section **16V** PHASE TRANSITIONS and SOLID STATE REACTIONS *(Main Hall)*

Molecular Libration and a Possible Structural Phase Transition in Crystalline 4,4''-Difluoro-*p*-Terphenyl by *H Saitoh*, K Saito, Y Yamamura, H Matsuyama, K Kikuchi, M Iyoda and I Ikemoto 16V-72

X-ray Diffraction Study of Phase Transitions and Structures of $(KBr)_{1-x}(KCN)_x$ Mixed Crystals by *Y Yoshimura*, T Okazaki and K Shimaoka 16V-73

Packing Effect in Solid-State Polymerization of Diethynylbenzene Derivatives by γ-irradiation 16V-74
by *R Kitagawa*, N Kanehisa, Y Kai, N Kasai, Y Yamamoto and S Takahashi

Asymmetric Photosynthesis in Chiral Crystal Environment 16V-75
by *H Kogo*, A Sekine, Y Ohashi, R Matsukawa, K Miyamoto and F Toda

Scientific Abstracts

14A–1

BIOLOGICAL APPLICATION OF SYNCHROTRON RADIATION

N. Sakabe, K. Sakabe*, T. Higashi+, A. Nakagawa & N. Watanabe,
Photon Factory, KEK, Tsukuba 305, Japan.
* Department of Chemistry, Faculty of Science, Nagoya University, Chikusa, Nagoya 464, Japan.
+ Rigaku Corporation, Matsubara, Akighima Tokyo 1966, Japan.

The advantages of synchrotron radiation (SR) are high brilliance, highly parallel nature and tunability. An X-ray diffraction data collection system for macromolecular crystallography, with a Weissenberg camera, imaging plate and image reader BA100, was constructed using SR at the Photon Factory. The basic ideas in using a Weissenberg camera for macromolecular crystallography are: 1) A cylindrical film cassette provides high resolution easily 2) Background noise decreases approximately as $1/r^2$ (r is the film cassette radius), whereas Bragg reflections vary less strongly with r. 3) More data will be recorded on a film, when Weissenberg geometry is applied. 4) Bijvoet pairs are recorded with high accuracy on the same film, as simultaneous reflections. 5) Almost all X-ray paths should be evacuated or filled with helium gas to reduce scattering and absorption by air.

The fundamental requirements when detecting X-ray diffraction from protein crystals are: 1) high detection quantum efficiency, 2) wide dynamic range, 3) linearity of response, 4) high spatial resolution, 5) large detector area 6) uniformity of response, 7) high counting rate capability and 8)low background noise. An imaging plate(IP), a new type of X-ray integrated-type area detector, is most suitable for collecting X-ray diffraction data from protein crystals. The combination of camera, IP and SR X-ray is very powerful (N. Sakabe, *Nucl. Instr. and Meth.*, 1991, A**303**, 448). The type 3 camera using IP was designed for station BL6A2 at the Photon Factory. Normally, one data set around an axis is recorded on 10-30 IP sheets, while consuming only one or two crystals. In 24 hours 6-10 data sets can be collected. As 43 groups from overseas and 45 domestic groups have requested use of this data collection system, there is a long queue to secure just two days beam time per year. To alleviate this situation, another station is under construction at L18B, which will also be used for time resolved LAÜE experiments. Applications of this system will be presented and future data collection systems will be discussed.

It is contrary to common sense that X-ray crystallography should elucidate only the static aspects of structure, whereas synchrotron radiation should enable us to elucidate time dependent structures of proteins. For this purpose we have made a time-resolved Laüe camera with data processing software. Evaluation of the Laüe data and applications of this method at the Photon Factory will be presented.

14A-2

A MULTI-PURPOSE BEAM LINE FACILITY

R F Garrett, ANSTO, Applications of Nuclear Physics, Private Mail Bag 1, Menai NSW 2234, Australia

A multi-purpose beam-line is being constructed at the Photon Factory, Tsukuba, Japan to provide users with routine access to synchrotron radiation in the hard X-ray region. The beam-line will deliver either monochromatic light, in the 5-20keV range, or white light to the experimental hutch. The main experimental instrument will be a multi-configuration vacuum diffractometer which combines a two-circle diffractometer with a large Weissenberg mode Imaging Plate camera. The diffractometer is optimised for protein crystallography, high resolution powder diffraction, small angle scattering and single crystal diffraction. Details of the beamline, monochromator and diffractometer design will be presented.

In addition the white or monochromatic beam can pass through the diffractometer to a secondary table-top station, allowing other white beam techniques to be performed. This secondary station will be available in late 1992 for white beam experiments.

14A–3

DESIGN CONCEPT OF SPRING-8 UNDULATOR BEAMLINE FOR MACROMOLECULAR CRYSTALLOGRAPHY

N. Kamiya, H. Iwasaki, T. Ueki, M. Yamamoto, T. Uruga and H. Yamaoka, The Institute of Physical and Chemical Research (RIKEN), Hirosawa 2-1, Wako, Saitama, 351-01, Japan.

SPring-8 (Super Photon, ring-8GeV), a new synchrotron radiation source for basic science and advanced technology, is now being constructed by the JAERI-RIKEN SPring-8 Project Team at Harima Science Garden City in Hyogo Prefecture. (Commissioning of the storage ring will start in 1997-98.) SPring-8 is characterized by low emittance and the thirty-eight straight sections for insertion devices such as undulators and wigglers. The storage ring energy, 8GeV, provides the undulator fundamental X-ray energy of 10-20 keV, which is very useful for macromolecular crystallography.

X-ray crystallography is a most powerful technique to determine three-dimensional structures of biological macromolecules, which have contributed so much to recent progress in molecular biology. However, the technique is limited now by the MIR and MAD phasing (MIR with the heavy atom derivatives of low occupancy, and MAD for the macromolecules with relatively large molecular weight such as 50,000 daltons) and by the data collection for small crystals less than 100μm or for very large macromolecules such as ribosomal proteins. All these limitations are imposed by the accuracy of the reflection data available. Since diffraction intensities from macromolecular crystals are intrinsically weak, data accuracy is determined mainly by the background level of X-ray measurement, which depends on X-ray optics and on the detector utilized in data collection.

From the undulator of SPring-8, very intense X-rays with energy resolution of 10^{-4} could easily be obtained in a small size (<100μm) and with small divergence (~30μrad), although the high heat load problem must be resolved for the optical elements. High quality incident X-rays may decrease the background scattering from the sample crystal itself, from air, etc.. For macromolecular crystallography, the Imaging Plate is one of the most suitable X-ray detectors available, with a very low noise level, but the spatial resolution now achieved (~150μm) should be improved to ~50μm for recording diffraction spots less than 100μm. The design concept of the SPring-8 undulator beamline for macromolecular crystallography will be discussed in terms of these considerations.

14A-4

THE SCOPE FOR IMPROVED INSERTION DEVICES

Shigeru Yamamoto, Photon Factory, National Laboratory for High Energy Physics (KEK), 1-1 Oho, Tsukuba, Ibaraki 305, Japan.

Insertion devices have been recognized as important sources of synchrotron radiation for physical and chemical sciences including crystallography, due to their very high brilliance, quasi-monochromaticity, tunability of wave length and polarization characteristics. Further recent progress in accelerator science is opening the way towards producing coherent synchrotron radiation at very short wavelength region using insertion devices.

In the Photon Factory, we have developed various undulators and wigglers with special features, and installed them in the 2.5-GeV Photon Factory (PF) storage ring and the 6.5-GeV TRISTAN Accumulation Ring (AR). As a whole these insertion devices provide users with synchrotron radiation that covers the wide spectral range from 10eV to 100keV, and the degree of circular polarization from 0 to 1 for both left- and right-handed circular polarization. The brilliance of the radiation from these insertion devices ranges from 10^{15} to 10^{16} photons/s/mm^2/mrad^2/0.1% bandwidth, which corresponds to a region of brilliance 10^2-10^3 times that of the bending radiation both from the PF 2.5-GeV ring and the AR. Spectral features of each insertion device will be described in detail in the presentation.

The above activities at the PF and AR can be regarded as "Research and Development" studies towards a future project in which very long (70m) undulators are to be constructed in the TRISTAN Main Ring (MR), which is to be renewed to very low emittance (about 1 nm rad) after high energy experiments using the MR are terminated in a few years. The brilliance of the radiation will exceed that of the so-called third generation synchrotron light source by three orders of magnitude. A brief description will also be given of the possibility of producing coherent radiation in a 4-nm region by driving a free electron laser installed in the MR.

14B-1

CRYSTAL STRUCTURES OF SOME SUBSTITUTED ETHANES

L. L. Koh and H. H. Huang
Chemistry Department, National University of Singapore
Singapore 0511

Crystal structures of a number of substituted ethanes have been determined by X-ray diffraction. The substituent groups included nitro, cyano, phenyl, alkyl and cyclic alkyl groups The following observations have been made.

1. The main factors that determine the conformation of the molecules appear to be the steric and polar interactions between the substituent groups. Bulky groups at 1 and 1' positions tend to be *trans* to each other whereas nitro groups tend to be *gauche*.

2. The central C-C bond length is very much affected by steric effects. The observed length ranges from 1.488(3)Åin 1,2-dinitroethane to 1.630(3) Å in 1,1' -diphenyl-bicycloheptyl.

3. For diastereoisomeric meso and (±) pairs, the meso isomer tends to have higher density than the (±) isomer. The ratio of the densities ranges from 1.024 to 1.054.

4. Most of the crystals have monoclinic cells. The internal symmetry of the compound is usually not fully utilized in the solid state packing.

14B–2

PREPARATION OF CARBON NANOTUBES BY DC ARC-DISCHARGE EVAPORATION

Y.Ando, Department of Physics, Meijo University, Tenpaku-ku, Nagoya 468, Japan, and S. Iijima, Fundamental Research Laboratories, NEC Corporation, 34 Miyukigaoka, Tsukuba, Ibaraki 305, Japan.

Carbon fullerenes such as C_{60} (Kroto et al. (1985)) can be prepared by dc arc-discharge evaporation between two graphite electrodes in rarefied inert gas. Part of the positive electrode is evaporated and deposited on the negative electrode. Carbon nanotubes with helical structure (Iijima (1991), Iijima et al.(1992)) were found in the deposit by high resolution TEM.

In this experiment, carbon evaporation was carried out in three different kinds of atmospheric gas, He, Ar and CH_4. The deposit on the negative electrode in each gas, with different gas pressures, was sectioned by a diamond cutter. By measuring the thickness of the deposit, its growth rate was obtained as shown in Fig. 1. There exist optimum conditions on the growth rate of the deposit for each gas. The existence of carbon nanotubes in the deposit section was confirmed by SEM and TEM for every gas within the pressure range 20-200 Torr. Coexistence of whisker-like nanotubes and small graphitic particles was observed by SEM. In addition to the two typical morphologies, graphitic sheets were observed by TEM. It is also concluded that the production of carbon nanotubes has been completed in a very short time by arc-discharge.

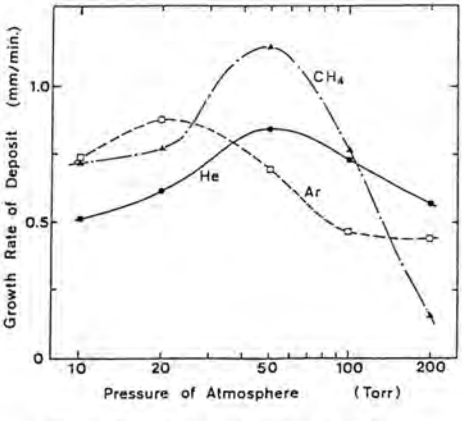

Fig.l. Growth rate of carbon deposit

Iijima,S. (1991). Nature **354**, 56-58.
Iijima,S., Ichihashi,T. and Ando,Y. (1992). Nature **356**, 776-778.
Kroto,H.W., Heath,J.R., O'Brien,S.C., Curl,R.F. and Smalley,R.E. (1985) . Nature **318**. 162-163.

14B–3

CRYSTAL STRUCTURE AND NONLINEAR OPTICAL PROPERTIES OF *m*-NITROBENZOIC ACID DIETHANOL AMINE ADDUCT

X.K.Yao, H.G.Wang, R.J.Wang and J.M. Zheng, Central Laboratory and Department of Chemistry, Nankai University, Tianjin, 300071, China.

Various molecular organic compound with one or more aromatic systems in conjugated positions have been studied actively for the last twenty years (Bailey *et al* ., 1991; Qin *et al* ., 1990) . Some criteria for a molecular crystal engineering approach have been formulated (Zyss *et* al., 1990). The 1:1 adduct of *m*-nitrobenzoic acid and diethanol amine (*m*-NBA-DEA) was obtained and a bulk single crystal with dimension 15 x 45 x 20 mm was grown by slow-cooling. This crystal, when irradiated by laser light at 1064 nm (Nd^{3+}:YAG) generates a second-harmonic wave at 532 nm. The structure of *m*-NBA-DEA has been determined by X-ray diffraction, monoclinic, *Cc*, a = 22.892(8), b = 4.612(2), c = 14.809(5)Å, β = 124.77 (2)°, Z = 4. T = 110K. R = 0.025. The *m*-NBA carboxyl group's hydrogen atom has been transferred to the amino group of DEA. Six hydrogen bonds make the title compound a two-dimensional network structure stretching on the (010) plane and the benzene ring planes are perpendicular to the (010) plane. Thus the dipole moment of the molecules enhance each other and macroscopic non-linearities may, therefore, be manifested. From molecular mechanics calculations it is shown that the molecular dipole moment of the ground state reduced the original 6.25D to the current 5.80D owing to the shift of the H atom and the resulting hydrogen bond generation. The head-to-end arrangement of molecules is favourable to enhancing the value of second order nonlinear optical coefficient β (Ye & Fang, 1990). It is also known that there is no obvious difference between the conformation of the title compound in the crystal and its ideal conformation predicted by molecular mechanics. This helps to explain why *m*-NBA and DEA are good partners for a nonlinear optical material.

Bailey, R.T., Cruickshank, F.R., Pugh, D. & Sherwood, J.N. (1991) *Acta Cryst.* **A47**, 145-155.
Qin, J.G. & Liu, D.Y. (1990) *Huaxue Tongbao*, No.10, 23-30.
Zyss, J. & Tsoucaris, G. (1990) *Structure and Properties of Molecular Crystals,* edited by M. Pierrot, pp. 97-350, Netherlands: Elsevier Science Publishers B.V.
Ye, Cheng & Fang, Shibi (1990) *Huaxue Tongbao,* No.6, 5-12.

14B–4

STRUCTURAL ASPECTS OF THE TRIVALENT GROUP 15 METAL (As, Sb, Bi) COMPLEXES WITH α–HYDROXY ACIDS

Graham Smith, Dalius S. Sagatys and Raymond C. Bott, Centre for Instrumental and Developmental Chemistry, Queensland University of Technology, Brisbane, 4000, Australia.

The Group 15 metals constitute a pharmacologically important series of elements used primarily for the treatment of a number of exotic diseases, eg Schistosomiasis and Leishmaneisis (tartar emetic). However, because of the acute toxicity of these elements, current usage is mainly limited to the less toxic bismuth compounds which are cheap and efficacious in the treatment of amoebic stomach infections and peptic ulcer disease (Gilman et al., 1991). The most common means of producing suitable water soluble compounds for pharmaceutical use is with α-hydroxy acids and despite their historical significance, little is known about their mode of action or about their structural chemistry [except for the antimony tartrates of the tartar emetic type (Mu, 1966)]. A project aimed at the systematization of the structural aspects of antimony(III) and other Group 15 metals with α-hydroxy acids has provided a number of examples of complex species involving these metals and both citric acid and (+)-tartaric acid, stabilized by various counter cations. Structural types include monomers such as $[\mathrm{LiSb(citrate^{2-})_2(H_2O)}]\cdot 2\mathrm{H_2O}$, $[\mathrm{NaSb(citrate^{2-})_2(H_2O)_2}]\cdot \mathrm{H_2O}$ (Hartley et al., 1991): dimers, eg $[\mathrm{AgSb(citrate^{2-})_2}]_2$ (Hartley et al., 1991) and polymers $[\mathrm{Ag_4Sb_4(tartrate^{4-})_4(H_2O)_4}]_n$ (Sagatys et al., 1991). Examples also include those with metal-metal bonds $\{[\mathrm{Ag_5As_4(tartrate^{4-})_4(H_2O)_5X}]_n\}$ ($X = \mathrm{NO_3^-}, \mathrm{ClO_4^-}$) and mixed-valence citrate species $\{[\mathrm{CuSb(citrate^{2-})(citrate^{3-})(H_2O)}]\cdot 2.5\mathrm{H_2O}$ (Smith et al., 1992); $[\mathrm{K_2Sb_4(citrate^{n-})_8\,(H_2O)_8}$ ($n = +1$ to $+3$)]. Only one bismuth example is described, a polymeric species, $(\mathrm{NH_4})_n\ [\mathrm{Bi(tartrate^{4-})_2(H_2O)}]_n$ (Sagatys et al., 1992).

Gilman, A.G., Rall, T.W., Nies, A.S. & Taylor, P., in '*Pharmacological Basis of Therapeutics*', 8th Edn. (Pergamon; New York, 1991).

Hartley, D.W., Smith, G., Sagatys, D.S. & Kennard, C.H.L. (1991). *J. Chem. Soc. Dalton Trans.*, 2735-2739.

Mu, H.-C. (1966). *K'o Hseuh T'ung Pao* **17**, 502.

Sagatys, D.S., Smith, G., Lynch, D.E. & Kennard, C.H.L. (1991). *J. Chem. Soc. Dalton Trans.*, 361-264.

Sagatys, D.S. O'Reilly, E.J., Patel, S., Bott, R.C., Lynch, D.E., Smith, G. & Kennard, C.H.L. (1992). *Polyhedron* **11**, 631-634.

Smith, G., Sagatys, D.S., Bott, R.C., Lynch, D.E. & Kennard, C.H.L. (1992). *Polyhedron* **11**, 631-634.

14B–5

STUDIES ON ORGANOMETALLIC COMPOUNDS: STRUCTURE AND ACTIVITY OF ORGANOSTANNYL CARBOXYLATES

B.B.Maji*, S.Biswas, K.L.Ghatak†, S.N.Ganguly#, A.Banerjee,
Bose Institute, Biophysics Department, Calcutta 700054.
* Presidency College, Calcutta 700073, India.
† Durgapur Govt. College, West Bengal, India.
\# Bose Institute, Calcutta 700009,India.

The synthesis, structure determination [B.C. Das et al., (1992)] and biological activity of organo-stannyl carboxylates [Maji, Ghatak, Ganguly, Ray (1989)] are described. Orange red crystals were obtained by interaction of O-arylaminoazobenzene-2'-carboxylate at 298K. A single-crystal X-ray diffraction analysis revealed a strictly planar $COOSnBu^n_3$ moiety. This unique structural feature could be correlated with the compound's biological property, which was due to the presence of both the metal and the β-azoic nitrogen in the reactive site of the molecule. The biological potency of these organostannyl carboxylates is associated with the nucleophilic character of the β-azoic nitrogen. The more the nucleophilicity, the greater will be the activity.

This was explained on the basis of intercalation of the (gly-gly) dipeptide, into two specific and properly oriented binding sites of the organotin compound, resulting in the formation of a stable complex. Such an intercalation mechanistic approach for arresting bacterial growth was supported by chemical as well as by spectral studies. A computer simulated intercalated model (Silicon Graphics) nicely corroborates the experimental results.

Das B.C., Biswas G., Ghosh S., Maji B.B., Ghatak K.L., Ganguly S.N., & Banerjee A. (1992) *Acta Cryst. C* (in press).

Maji B.B., Ghatak K.L., Ganguly S.N., & Ray P.G.(1989). *Trans Bose Res. Inst.* **52** (4), 97-100.

14Y-1

POWDER DIFFRACTION

S P Sen Gupta, Department of Materials Science, Indian Association for the Cultivation of Science, Calcutta 700032, India.

[Abstract will be supplied at conference]

14Y–2

αTiOSO$_4$: STRUCTURE DETERMINATION FROM POWDER XRD DATA AND RELATIONSHIPS TO OTHER MOXO$_4$ STRUCTURES.

I.E. Grey, CSIRO Division of Mineral Products, Port Melbourne, Vic. 3207, Australia, and R. Stranger, Department of Chemistry, University of Queensland, Q. 4072, Australia.

αTiOSO$_4$ forms as a leach-resistant phase during the digestion of altered ilmenite concentrates in concentrated sulphuric acid. It contains about 7 wt% Fe$_2$O$_3$ and its composition can be expressed as $Ti_{.85}Fe_{.15}O_{.85}(OH)_{.15}SO_4$. It has monoclinic symmetry, space group C2/c, with unit cell parameters a = 5.1175(2), b = 13.7675(6), c = 9.5035(4) Å, β = 91.097(3)°. Its structure was determined using powder X-ray diffraction data and refined using the Rietveld method to R_{wp} = 0.059, R_B = 0.022, G of Fit = 1.56 for 706 reflections to 2θ = 140°, CuKα radiation. The structure comprises a 3-D framework of corner-linked Ti1O$_6$ and Ti2O$_6$ octahedra and SO$_4$ tetrahedra, with 6-sided channels running parallel to both [100] and [001]. Alternating corner-shared octahedra and tetrahedra form 4-member rings which link together into ribbons via the constituent octahedra. Ribbons containing Ti1O$_6$ and Ti2O$_6$ octahedra lie along [001] and [100] respectively, and differ in the relative positions of the pairs of octahedral vertices that are utilised in the formation of the 4-member rings.

Variation of the acid leaching conditions in the digestion experiments led to the formation of two other (Ti,Fe)(O,OH)SO$_4$ polymorphs, structurally related to Ge(OH)PO$_4$ and βNbOPO$_4$ respectively, as well as various double sulphates. Structural relationships between αTiOSO$_4$ and these other phases will be described.

14Y-3

CRYSTALLOGRAPHY OF REAlO$_3$ (RE = La, Ce, Pr and Nd)

M. Tanaka, Photon Factory, National Laboratory for High Energy,
Physics, 1-1 Oho, Tsukuba, Ibaraki 305, Japan,
H. Horiuchi, Mineralogical Institute, Faculty of Science,
University of Tokyo, Hongo 7-3-1, Tokyo 113, Japan,
T. Shishido and T. Fukuda, Institute for Material Research,
Tohoku University, Katahira, Sendai 980, Japan.

The crystal lattices of the title compounds were carefully investigated by X-ray powder diffraction profile analysis. All lattices are very slightly distorted from the so called 'ideal' cubic perovskite structure. The LaAlO$_3$ and NdAlO$_3$ structures are rhombohedral, but two different crystal systems, rhombohedral and tetragonal have been suggested for CeAlO$_3$ and PrAlO$_3$ [1-4]. Powder samples of these four compounds were carefully prepared, in a graphite crucible under He gas atmosphere to prevent oxidation[5], particularly as Ce and Pr prefer valency 4+ to 3+ in air. X-ray powder diffraction data were collected in the 2θ range 10 to 135 degrees, by 0.02 degree step scanning, counting for 10 seconds at each step with multiple measurements. Cu $K\alpha$ radiation (35kV and 22.5mA) monochromatized by pyrolytic graphite, with Si as external standard, on a JEOL/DX-GO-S2 diffractometer. The 2θ angles determined precisely for each peak by profile fitting program PROFIT [6] were used to evaluate lattice constants by least squares methods. The results indicate that REAlO$_3$ with La, Pr and Nd crystallize in the rhombohedral system, but CeAlO$_3$ has a tetragonal structure. According to a single crystal structure analysis of CeAlO$_3$ [7], some O atom shapes deviate markedly from spherical. This might be due to averaging over statistical arrangements of very fine scale domains with symmetry structure lower than tetragonal. The lattice distortion from an ideal cubic perovskite type structure is smaller in LaAlO$_3$ and greater in NdAlO$_3$.

[l] Geller S. & Bala V.B. (1956). *Acta. Cryst.* **9**, 1019.

[2] Margolis N.V., Toropov N.A. & Udalov Yu P (1964). *Soviet Physics Crystallography*, **9**, 328.

[3] Kim,Y.S. (1968). *Acta Cryst.,* B**24**, 295.

[4] Zachariasen, W.H. (1949). *Acta Cryst.* **2**, 388.

[5] Shishido T., Tanaka M., Horiuchi, H. & Fukuda T. (1992). *Bull. Chem. Soc. Japan,* **6**,47.

[6] Toraya, S.(1986). *J. Appl. Cryst.* **19**, 440.

[7] Tanaka M., Shishido T., Horiuchi H., Toyota N., Shindo D. & Fukuda,T. (1992). *Proceedings in 'Rare Earth 92'*, in print.

CRYSTAL STRUCTURE ANALYSIS WITH HIGH-RESOLUTION POWDER DIFFRACTOMETER DATA

T. Ochiai and H. Toraya, Ceramics Research Laboratory, Nagoya
Institute of Technology, Asahigaoka, Tajimi 507, Japan

There has been growing interest in the use of high-resolution powder diffractometer data for crystal structure analysis (Louer and Langford, 1988, Kurahashi, Honda, Goto, Inari & Katayama, 1991). In the present paper, the quality of the data measured on a commercial-type high-resolution powder diffractometer was assessed. The advantages and disadvantages of its use in structure analysis have been studied.

The diffractometer used was a Rigaku RINT system, equipped with a Johanson-type Ge(lll) crystal monochromator on the incident-beam side to remove the Kα2 component. In order to compensate for loss of intensity due to monochromatization, it was installed on a rotating anode generator (Cu target), which at maximum load could be operated at 18 kW. Powder samples of α-SiO_2 ($\mu = 96.4$ cm^{-1}) and CeO_2 ($\mu = 2240$ cm^{-1}) were used as reference standards for investigating the variation of profile shape with 2θ. Their powder patterns were analyzed by profile fitting. The pseudo-Voigt function gave a better fit than the Pearson VII function in the full-2θ range. The minimum full-width at half maximum (FWHM) for a receiving slit (RS) width of 0.l5mm of 0.068° at $2\theta = 33°$ decreased to 0.057° with loss of intensity for an RS width of 0.05mm. The profile shape varied almost linearly from Gaussian to Lorentzian with increasing 2θ as observed by Louer and Langford (1988). The shapes for the Kαl singlet were almost symmetric for CeO_2 sample with a narrow Soller slit (aperture = 2°). However, the profile slightly broadened and became asymmetric for α-SiO_2, possibly because of displacement-type aberration due to specimen transparency.

In order to study the dependence of pattern decomposition on the resolution of the data, powder patterns for monoclinic-ZrO_2 observed by using diffractometers of the present high-resolution type, of normal type, and with parallel-beam synchrotron radiation were analyzed by whole-powder-pattern fitting techniques. Two overlapping reflections at a distance of a quarter of FWHM from each other could be decomposed when the high-resolution type diffractometer data were used, giving much better resolution than that by a normal-type diffractometer. The effect of data resolution on the refined positional and occupancy parameters of several inorganic materials is also under investigation.

Louer D. and Langford, J. I. (1988). *J. Appl. Cryst.* **21**, 430-437.
Kurahashi M., Honda K., Goto M., Inari Y., and Katayama C. (1990)
J. Appl. Cryst. **24**, 61-63

14Y–5

STRUCTURES OF THE TWO POLYMORPHS OF MAGNESIUM BORON NITRIDE DETERMINED FROM X-RAY POWDER DIFFRACTION DATA

H. Hashizume, N. Sudo, H. Hiraguchi, O. Fukunaga (*), C. Gilmore (+)
and G. Bricogne ($), Research Laboratory of Engineering Materials,
Tokyo Institute of Technology, Yokohama 227, Japan.
(*) Dept. of Inorganic Materials, Tokyo Institute of Technology.
(+) Dept. of Chemistry, University of Glasgow, Scotland.
($) LURE, Orsay, France and MRC, Cambridge, England.

The crystal structures of magnesium boron nitride Mg_3BN_3 in the low- and high-pressure forms have been determined *ab initio* from X-ray powder data. The steps used are to decompose the powder pattern to extract integrated intensity data, calculate Patterson functions and build try-and-error structure models, followed by test powder pattern calculations and Rietveld refinements. 54 and 21 reflections observed on a laboratory $\theta-\theta$ diffractometer were used to solve the structures of $Mg_3BN_3(L)$ and $Mg_3BN_3(H)$ respectively. The effective data resolution is 0.9Å for $Mg_3BN_3(L)$ and 1.25Å for $Mg_3BN_3(H)$. Low-pressure $Mg_3BN_3(L)$ has a hexagonal cell (space group $P6_3/mmc$, $Z = 2$) with $a = 3.54453(4)$ and $c = 16.0353(3)$Å while the high-pressure $Mg_3BN_3(H)$ cell is orthorhombic ($Pmmm$, $Z = 1$) with $a = 3.0933(2)$, $b = 3.1336(2)$ and $c = 7.7005(5)$Å. The two structures commonly include linear N=B=N molecular anions, which are thought to play a role in catalyzing the reaction BN(hexagonal) → BN(cubic) at high pressure-temperatures.

A very similar structure has been obtained by applying standard direct methods to the same $Mg_3BN_3(L)$ intensity data. Refinements revealed unimportant anisotropic thermal vibrations for each of the Mg, B and N atoms, which are supported by quasispherical distributions of the atomic electrons in the density maps calculated from the phased structure factors by entropy maximization. The maximum-entropy maps also show significant electron densities between the N and B atoms, supporting the double-bond N=B=N molecules. An attempt to solve the $Mg_3BN_3(L)$ structure from the unphased structure factors using the procedure devised by Gull, Livesey and Sivia [*Acta Cryst.* A43, 112 (1987)] did not work. A separate application of a multisolution method of phase determination by combined maximization of entropy and likelihood [C. Gilmore *et al.*, *Acta Cryst.* A47, 830 (1991)] yielded a clean map which revealed the positions of all the Mg, B and N atoms for $Mg_3BN_3(L)$. Inclusion of overlapped reflections was essential. The same $Mg_3BN_3(L)$ structure was thus obtained by the three independent structure determinations.

14C–1

ELECTRON DENSITY DISTRIBUTIONS OF CRYSTALLINE MATERIALS OBTAINED BY THE MAXIMUM ENTROPY METHOD

M. Sakata, Department of Applied Physics, Nagoya University, Chikusa-ku, Nagoya, 464-01, Japan.

This is a review of recent studies on electron density distributions of crystalline materials obtained by the Maximum Entropy Method (MEM) done by our group. The studies to be reviewed are limited to ones which deal with the Fourier transformation of crystal structure data in order to estimate the electron-density distribution of a crystal. The MEM provides us with the least-biased deduction which is compatible with certain given information. In the present case, the given and missing information corresponds to the observed and unmeasured structure factors, respectively. Since the materials for which the electron density distributions have been obtained by MEM analysis so far have very simple structures, it is assumed that the phase could be determined without any significant ambiguities.

The first work to restore the precise electron density distribution by the MEM analysis was performed for Si by Sakata & Sato [M. Sakata & M. Sato (1990) Acta Cryst. **A46**, 263]. The data used in the analysis were collected by Saka & Kato [T. Saka & N. Kato (1986) Acta Cryst. **A42**, 469]. They measured the structure factors for 30 net planes by the *Pendellösung* method on an absolute scale. In their data set, however, so-called forbidden reflections were not included because of experimental difficulties. In the conventional Fourier method, the core electrons could be easily seen in the electron density distribution but it was not possible to restore the covalent bond electrons due to probably lack of forbidden reflections, which arise from purely the contribution of bonding electrons at room temperature. On the other hand, the electron density distribution of Si obtained by the MEM analysis by using the same data set clearly showed the covalent bond electrons between Si atoms as well as core electrons. It was also shown that the MEM density map had much higher peak height at atomic position than that of conventional Fourier map; roughly speaking twice. In other word, it could be said that the resolution of MEM density distribution is very high. Furthermore it was revealed that unmeasured forbidden reflections could be well predicted from the MEM map of Si.

The method was extended so as to treat X-ray powder data. Modern powder diffraction has been greatly improved in various ways, particularly, profile refinement and decomposition. It is possible to evaluate integrated intensities for each Bragg reflection unless the peak overlap is very severe. At this point, high resolution diffractometer utilizing synchrotron radiation has a great advantage. The extension was made to handle the severely overlapped peaks as a combined structure factor. By this extension, the method is now having a versatility. So far about 10 compounds have been already analyzed by the present method, such as CeO_2, CaF_2, TiO_2, Be, Mg, Al, Cu, ice Ih, LiF, LiH, etc and the number is increasing quite rapidly. It is notable from the results that the structure of hcp and fcc metals in electron level are characteristically different; hcp metals forms electronic layer by three center bond but fcc metals. It is also notable that the electron density distribution of hydrogen is strongly influenced by the existence of hydrogen bond.

Methodologically further extension is going on, such as trying to solve the negative scattering problem in neutron diffraction case or trying to find out small structure change with either temperature, pressure or composition by simply subtracting MEM density map of two states.

14C–2

MAXIMUM ENTROPY METHOD ANALYSIS OF NEUTRON POWDER DIFFRACTION DATA

M. Sakata, T. Uno, M. Takata, Department of Applied Physics, Nagoya University, Nagoya, Japan ; and C. J. Howard, Australian Nuclear Science & Technology Organization, Lucas Heights, NSW 2234, Australia.

It is often said that X-ray and neutron diffraction is complementary. In X-ray powder diffraction, X-ray photons are scattered by electrons in materials, while neutron beams are diffracted by nuclei in neutron powder diffraction case assuming that there is no magnetic interactions. What could be observed from X-ray and neutron powder diffraction data is, therefore, the electron and nuclear density distribution of the crystalline materials, respectively. There have been, however, not known how to restore such electron and/or nuclear density distribution directly from the observed structure factors by powder diffraction without using any structural model.

Recently Sakata & Sato [M. Sakata & M. Sato (1990) Acta Cryst.A**46**, 263] has successfully applied the Maximum Entropy Method (MEM) to restore the precise electron density distribution from the accurately determined structure factors by the *Pendellösung* method. It is possible to measure the accurate Bragg intensities free from extinction effects by a powder diffraction experiment. The success of the method depends on the fact that the electron density is always positive. In order to analyze neutron diffraction data by the MEM, it is necessary to overcome the difficulty of negative scattering length for some atoms, such as H, Ti and Mn. Though a method to tackle this negative scattering problem was presented in the XVIIth Meeting of the Society of Crystallographers in Australia, it was not fully satisfactory. The reason is that it had to use the calculated structure factors in order to reverse the contribution of negative scatterers. The results of this method necessarily depend on the structural model used.

In this work, the new method has developed. The new approach is based, not on scattering length densities, but on nuclear densities which are always positive. Two equations are obtained, one for atoms with nuclei of positive scattering length and the other for atoms with negative scattering length. Using these two equations, nuclear densities of Ti and O atoms can be calculated separately. This procedure, like its X-ray counterpart, requires no structural model. MEM analysis of the rutile data by this approach has been successfully completed. As expected, and in contrast to the electron density distribution obtained by the MEM [Sakata, Uno, Takata, Mori. (1992) Acta Cryst. **B48**, in press], the map shows both Ti and O nuclear densities localized within very small regions around the atomic centres. It is concluded that the MEM applied to a neutron powder diffraction data is much superior to conventional Fourier transformation and, in spite of the longer computation time, is well worthwhile.

14C–3

AN ANALYSIS OF APPROXIMATION OF THE MAXIMUM ENTROPY METHOD

Shintaro Kumazawa, Department of Physics, Science University of Tokyo, Noda, Japan, and
Makoto Sakata, Department of Applied Physics, Nagoya University, Nagoya, Japan.

A new method has recently been developed for accurate structure analysis, that is, the Maximum Entropy Method(MEM) [1]. The MEM is a very powerful method for visualizing detail in electron and nuclear densities without using any structural model. In an increasing number of examples, such as Si[1], CeO_2 [2], TiO_2 [3], etc the MEM was successfully applied. In this work, the MEM fundamental equation was solved under the conditions; 1) to satisfy symmetry requirements, 2) to conserve the number of electrons, 3) to adopt 0-th order single pixel approximation [4]. The MEM solution is thus obtained iteratively, starting from the maximum entropy state of uniform density. Among the conditions, 1) and 2) are consequences of our knowledge of crystallography. However condition 3) is needed to solve the equations numerically at each iteration. It is therefore desirable to examine the validity of this approximation. The purpose of the work is to examine the validity of the 0-th order single pixel approximation and to analyse the MEM by simulation.

First we consider a very simple case of a 1-dimensional electron density with a center of symmetry where only two pixels exists. In this case it is possible to solve the MEM equation analytically at each iteration. There is virtually no difference between the exact and approximated solutions as long as the value of Lagrange multiplier, λ, is sufficiently small. As λ increases, the discrepancy between the two solutions becomes larger.

Secondly, the MEM was examined by 1 and 2 dimensional simulation and compared with the conventional Fourier synthesis. When all non-zero structure factors are used, the MEM and the Fourier synthesis give the same density distribution which is, of course, identical to the original density. For a limited number of structure factors, the MEM solution reaches the original density much faster than the Fourier synthesis as the number of structure factors increases. It is concluded from these simulations that the MEM is greatly superior to the conventional Fourier synthesis for restoring the original electron density when the available structure factors are limited, which is likely in practical cases.

[1] Sakata M & Sato M. (1990) *Acta Cryst.* A**46**, 263.
[2] Sakata, M. et al. (1990) *J.Appl.Cryst.* **23**, 526.
[3] Sakata, M. et al. (1992) *Acta Cryst.* B**48**, in press.
[4] Wilkins, S.W. et al.(1983) *Acta Cryst.* A**39**, 892.

14C-4

A DIRECT INVESTIGATION OF THERMAL VIBRATIONS OF Be METAL BY THE MAXIMUM ENTROPY METHOD APPLIED TO SINGLE CRYSTAL NEUTRON DIFFRACTION DATA

M.Takata, M.Sakata, F.K.Larsen*, Y.Kubota & B.B.Iversen*
Dept. of Applied Physics, Nagoya Univ., Nagoya, 464-01, JAPAN
*Dept. of Chemistry, Aarhus Univ., DK-8000 Aarhus C, DENMARK

A conventional approach for describing the atomic thermal vibrations is to assume that the vibrations are determined by an effective one-particle potential which is expanded according to the atomic site symmetry. The corresponding atomic thermal smearing function is thus temperature dependent. The Maximum Entropy Method (MEM) directly yields the nuclear density distribution, which is equivalent to the thermal smearing function, from even a limited number of accurate neutron diffraction data[1]. Therefore, the MEM enables us to investigate thermal vibrational features directly without using a model. The purpose of this study is to examine the capability of the MEM for the direct investigation of thermal vibrations and Be was chosen as a test case.

Mean-square atomic displacement and antisymmetric atomic vibrations in Be at room temperature have been determined from short-wave length neutron data by conventional analysis. The same data have been treated by the MEM. In one analysis, the 48 reflections up to the $\sin\theta/\lambda = 1.41\text{Å}^{-1}$ are used and the unit cell is divided into 120X120X120 pixels in order to get good spatial resolution. The density distribution at the presumed nuclear site in the basal and in the (100) plane which is perpendicular to the basal plane of the hcp structure are shown in Fig.1 (a) and (b), respectively.

In Fig.1(a), a characteristic triangular feature is clearly visible. We interpret this as being caused by 3rd order anharmonic vibrations in the basal plane. In Fig.1(b), the nuclear density shows significant difference from the expected oblate shape for harmonic vibrations. We interpret this feature as being due to a significant quartic term of the one-particle potential function. In the conventional approach, it is very difficult to prove the existence of a quartic anharmonic term since there is a very high correlation between second and fourth order parameters. So far, only inconclusive results have been provided for the quartic anharmonicity in Be. However, in this study it seems that the MEM density maps have revealed the existence of 3rd order as well as 4th order anharmonic vibration. Curve fits to the MEM density profiles along different directions are being calculated in order to derive the quantitative values for the anharmonic terms directly from the MEM map. Results will be presented at the meeting.

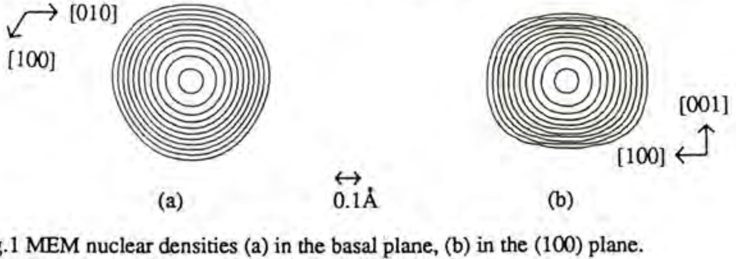

(a) (b)

Fig.1 MEM nuclear densities (a) in the basal plane, (b) in the (100) plane. The contour lines are drawn in logarithmic scale.

1) Sakata,M., Takata,M., Kubota,Y., Uno,T., Kumazawa,S., & Howard,C.J., (1992) to be published in Advances in X-ray Analysis
2) Larsen,F.K., Lehmann,M.S., & Merisalo,M.(1980) Acta Cryst.,**A36**,159

14Z–1

ACCURATE DETERMINATION OF THE UNIT CELL FOR AN EPITAXIAL LAYER OF $Hg_{1-x}Cd_xTe$ DEPOSITED BY MOCVD ON GaAs

Zhu Nanchang[*], Andrew W. Stevenson[#] and Li Runshen[*]
[*]Shanghai Institute of Metallurgy, Academia Sinica, 865 Chang Ning Rd., Shanghai 200050, China
[#]CSIRO Division of Materials Science and Technology, Locked Bag 33, Clayton, Victoria 3168, Australia

$Hg_{1-x}Cd_xTe$ (MCT) is a ternary alloy with the cubic zincblende structure. It is currently receiving considerable attention because of its applications in areas such as infrared detection, optoelectronic devices and solar cells. Stevenson, Gao, Pain & Wieluński (1991) reported on structural aspects of six metal organic chemical vapour deposition (MOCVD)-grown $Hg_{1-x}Cd_xTe$ epitaxial layers (of order 1 to 2 μm thick) on novel GaAs substrates. GaAs is chosen as a substrate because of its inexpensiveness, excellent structural quality and the availability of large-area material. There is however, a large lattice mismatch between GaAs and $Hg_{1-x}Cd_xTe$. Large layer miscuts (the angle between the surface and the Bragg planes of the nominal orientation), of 4.3°, were reported for the samples of (311) and $(\overline{3}\overline{1}\overline{1})$ orientation, whereas the substrate miscuts were less than 1° (0.94° and 0.84° respectively). The substrate orientations are the same as for the corresponding layers. Double-crystal diffractometry has been used, employing the method described by Li Runshen & Zhu Nanchang (1990), to accurately determine the distorted unit cell of the $Hg_{1-x}Cd_xTe$ $(\overline{3}\overline{1}\overline{1})$ layer and its orientation relative to the unit cell of the GaAs $(\overline{3}\overline{1}\overline{1})$ substrate. Four-circle diffractometry is used to relate the disposition of the unit cells to the sample surface.

The effects of wavelength dispersion and asymmetric Bragg diffraction geometry on the double-crystal rocking curves collected will be discussed. The rocking curves also reveal an anisotropy in the $Hg_{1-x}Cd_xTe$ layer. The composition of the $Hg_{1-x}Cd_xTe$ layer (i.e. the Cd x fraction) is also determined.

Stevenson, A.W., Gao, D., Pain, G.N. & Wieluński, L.S. (1991). *Acta Cryst.* A47, 128-133.
Li Runshen & Zhu Nanchang. (1990). *Chin. J. Semiconductors*. 11, 759-767 (in Chinese).

EVALUATION OF THE ROUGHNESS OF CRYSTAL SURFACE BY X-RAY SCATTERING
— THEORETICAL CONSIDERATION —

J.Harada, Department of Applied Physics, Nagoya University, Chikusa-ku, Nagoya, 464-01, Japan

The relationship between the intensity distribution of the Crystal Truncation Rod (CTR) scattering and the surface roughness of a crystal is discussed by developing a kinematic theory for the CTR scattering. The intensity of the CTR scattering elongated from a Bragg point is shown to be reduced by a factor $|\Gamma(q)|^2$ for a surface possessing some roughness, where $\Gamma(q)$ is defined by a simple Fourier summation of γ_p , the relative area with the same step height p on a surface, ie

$$\Gamma(q) = \sum_{p=0}^{\infty} \gamma_p exp\{2\pi ip \cdot q\} \qquad with \ \sum_{p=0}^{\infty} \gamma_p = 1,$$

q being the distance in reciprocal space from the Bragg point along the CTR scattering. A pair correlation function between the steps can, therefore, be obtained by a simple Fourier integral of the Roughness Damping Factor $|\Gamma(q)|^2$.

$$< \gamma_0 \gamma_p >= 2 \int_0^{q_{max}} |\Gamma(q)|^2 exp\{2\pi ip \cdot q\} dq$$

where $< \gamma_0 \gamma_p >$ is the pair correlation function defined as

$$< \gamma_0 \gamma_p >= \sum_{p' \geq 0} \gamma_{p'} \gamma_{p'+p}$$

For the case where γ_p has a Gaussian distribution around the average step height, $|\Gamma(q)|^2$ is approximated by the well known Debye-Waller like factor, $exp\{-4\pi^2 \cdot < \Delta p^2 > \cdot q\}$, where $< \Delta p^2 >$ is the mean square deviation of step height in the units of lattice spacing.

Diffuse scattering arises also due to the existence of the irregularity of the surface. This term is given by Fourier summation of pair corrections between the steps separated by r_{mn} lattice on the surface. The relationship between the diffuse scattering and above $\Gamma(q)$ will also be given.

14Z–3

GRAZING-ANGLE X-RAY STANDING WAVE STUDY OF As-ADSORBED SILICON SURFACE

H. Kurashina, O. Sakata and H. Hashizume, Res. Laboratory of Engineering Materials, Tokyo Institute Technology, Yokohama 227, Japan

Monolayer As atoms chemisorbed to clean silicon (111) surface are known to remove the complex reconstruction of the silicon surface. An X-ray standing-wave study revealed the As atoms occupying the upper half of the silicon (111) double layer at a slightly increased vertical distance. Bond considerations favor the three-fold T sites for the As atoms but this has yet to be experimentally confirmed. We have attempted to use X-ray standing waves at grazing angles to tackle this problem. The Si (111) surface was cleaned by thermal evaporation of oxide layers at 850°C in ultrahigh vacuum. The substrate was then exposed to a beam of As molecules from an effusion cell for 25 min during which time the sample was cooled from 800 to 400°C. A sharp (1×1) RHEED pattern was observed after As deposition. The X-ray experiment was performed at the BL-14B workstation of the Photon Factory. Vertically polarized synchrotron X ray at 17.5 KeV photon energy made a small glancing angle to the surface and simultaneously satisfied the Bragg condition for the bulk ($2\bar{2}0$) planes. In this condition the coherent interference of the incident, the specular reflected and the Bragg diffracted beams generates X-ray standing wave field with an intensity modulation parallel to the surface. In Fig. 1 the observed intensity profiles of the specular reflected and the Bragg diffracted beams show features of the perfect-crystal rocking curves with half widths 50% larger than calculation. The valley-peak profile of As*K* emission signal is characteristic of a disordered surface structure. Exposure to air for four days destroyed the original registry of the As atoms to substrate Si atoms. This difficulty could be overcome by placing the sample in a UHV chamber with beryllium windows under commissioning. The sample is to be transported in a pumped vessel and transferred to the scattering chamber mounted on a high-precision rotary table at the Photon Factory workstation.

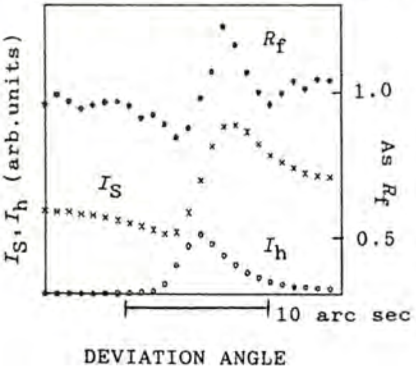

14Z–4

AXIAL SYMMETRY QUASICRYSTAL STRUCTURE IN SOME COATING THIN FILMS AND VEGETABLE FIBRES. ESR STUDY

Nguyen Van Tri, Pham The Vung and Le Hai Hung,
Institute of Technical Physics, Hanoi University of Technology.
PCHT, Truong Dai hoc Bach khoa Ha noi, Hanoi Vietnam.

The microstructure and related properties of oxidized silicon surface, special porcelain enamel and pineapple fibre have been studied. The normal diffraction and other methods showed that these materials can be referred to as amorphous or polycrystalline. However, a careful ESR study can give another result: distinct axial symmetry quasicrystal structures persist in these systems. Numerous exchange couple complexes and the respective bond lengths and bond angles were revealed and evaluated. Especially, the angular dependences of the g-values on the magnetic field direction were measured. These dependences possess a very prominent characteristic axial symmetry. In the case of the Si-SiO_2 system, the factor responsible for this axial symmetry is an ensemble included in the Si-SiO_2 interface layer with identical Zachariasen units whose planes are parallel to the silicon surface. In the case of special porcelain enamel, the responsible ensemble includes plane pentagonal units coupled by fivefold (2F-2M) complexes growing on the porcelain surface. In the case of pineapple fibre, there is a local structure in the physical network coupled by fivefold (2Fe-2S) rhombic complexes diagonally bonding a macromolecule chain with five neighbouring ones. This local structure is based on a pentagon created by five sulfur atoms whose plane is perpendicular to the axis of the fibre. The important roles of quasicrystal structures in specific features of these materials (such as the peculiar conductivity of the porcelain enamel and the strength, the tensility, the torsional module of natural fibres, etc.) have been partly discovered.

14Z-5

DOUBLE CRYSTAL X-RAY CHARACTERIZATION OF III-V MULTILAYERED SPECIMENS BY SELECTIVE ETCHING

S Swaminathan, School of Electrical and Electronic Engineering,
Nanyang Technological University, Singapore 2263

Double crystal experimental rocking curves of III-V multilayer specimens can provide valuable information about the lattice mismatch, crystallographic quality, compositional and thickness variations of the individual layers. Thick multilayer systems as in laser structures undergo interference effects resulting in oscillations in rocking curves (Chu & Tanner, 1986). In extreme cases, when the layers are thin, additional peaks are predicted that do not correspond to a Bragg peak (Halliwell et al, 1984). Rocking curves from multilayer structures thus generally have complex shapes and extractiing relevant information from the experimental curves is not straightforward. In order to isolate rocking curve characteristic of each layer in a heterostructure, a selective etching technique (Phatak & Kelner, 1979) has been used. Two specimens were chosen for this purpose, a DH laser and an edge emitting LED, grown by liquid phase epitaxy on (100) InP substrates. Each layer in the multilayer structure was etched off in sequence. A corresponding experimental double crystal rocking curve plotted.

The double crystal arrangement (Grasserbauer & Werner, 1991) was aligned for recording a (400) reflection at 1.54 Å wavelength, with a highly polished (100) InP crystal on the first axis. From a comparison of the different experimental rocking curves, it was possible to extract information about peak height, peak width, and lattice mismatch of individual layers. The method of selective etching has therefore made it possible to identify individual layer peaks in a multilayer structure. This mismatch data from selective etching was effectively used as initial input for simulating rocking curves for the multilayer specimens and an accurate estimate of the thickness and compositional variation in the individual layers was thus possible.

Chu, X. & Tanner, B.K. (1986). *Appl. Phys. Lett.*, **49**, 1773.

Grasserbauer, M. & Werner, H. W. (Eds) (1991). *Analysis of Microelectronic Materials*, John Wiley and Sons.

Halliwell, M.A.G. et al (1984). *J. Crystal Growth*, **68**, 523.

Phatak, S. B. & Kelner, G. (1979). *J. Electrochemical Soc.*, **126**, 287.

14P–01

CRYSTALLIZATION AND PRELIMINARY X-RAY CRYSTALLOGRAPHIC STUDY OF LYSOZYME PRODUCED *BY STREPTOMYCES GLOBISPORUS*

C.Uematsu, H. Naitoh, S.Harada, Y.Kai and N.Kasai
Department of Applied Chemistry, Faculty of Engineering
Osaka University, Suita, Osaka 565, Japan

Lysozyme is the enzyme which causes lysis of cell walls of bacteria by hydrolyzing the, β-(l→4)-glycosidic bonds of the polysaccharide backbone of the peptidoglycan. On the basis of the homology of amino acid sequence, lysozymes are classified into four distinct types: (l) chikin, (2) phage, (3) goose and (4) *Chalaropsis*. *Streptomyces globisporus* produces two kinds of lysozyme (M-l and M-2 lysozyme) and secretes them in the cultural broth. The molecular weights are about 20,000 and 11,000 for M-l and M-2 lysozyme, respectively. Analysis of the amino acid composition of M-l and M-2 lysozyme indicated that (1) M-l lysozyme belongs to the *Chalaropsis* type, and (2) M-2 lysozyme is similar to hen-egg white lysozyme but there was no cystein residue in this enzyme. M-l lysozyme from *Streptomyces globisporus* has been crystallized in a form suitable for X-ray crystallographic structure analysis. Crystallization was achieved by hanging-drop vapour diffusion and a seeding method using sodium citrate as a precipitant at room temperature.

Crystal data: tetragonal, space group $P4_12_12$ (or $P4_32_12$)
a=b=63.09, c=121.44Å

After the heavy atom derivative search, diffraction data sets were collected for native and two kinds of Hg derivative crystals using synchrotron radiation at the Photon Factory. Structure analysis using the SR data is in progress.

14P–02

PRELIMINARY CRYSTALLOGRAPHIC STUDY OF CYTOCHROME c' FROM *ACHROMOBACTER XYLOSOXIDANS* NCIB 11015

N. Shibata, T. Inoue, Y. Kai, S. Harada and N. Kasai, Department of Applied Chemistry, Faculty of Engineering, Osaka University, Suita, Osaka 565, Japan,
T. Kohzuma and S. Suzuki, Institute of Chemistry, College of General Education, Osaka University, Toyonaka, Osaka 560, Japan,
H. Iwasaki, Nagoya University of Foreign Studies, Nisshincho, Aichi 470-01, Japan and
S. Shidara, Department of Environmental Science, Faculty of Integrated Arts and Sciences, Hiroshima University, Naka-ku, Hiroshima, Hiroshima 730, Japan.

Cytochromes *c*', a class of *c*-type cytochrome found in photosynthetic and denitrifying bacteria, are noted for their unusual chemical and physical properties. These properties are derived from the ferric heme-ion ground state electronic configuration. The function of cytochrome *c'* is unknown, but cytochrome *c'* must contribute to denitrification, since a complex of cytochrome *c'* with nitrogen monoxide was found to exist in *Achromobacter xylosoxidans* NCIB 11015 by Yoshimura, Iwasaki, Shidara, Suzuki, Nakahara & Matsubara (1988). A preliminary crystallographic study on cytochrome *c'* from *Ach. xylosoxidans* NCIB 11015 has already been reported by Norris, Anderson, Baker & Rumball (1979), but successful structure determinations have never been reported. Consequently, to elucidate the heme environment and the mechanism of denitrification, cytochrome *c'* crystals suitable for X-ray crystal structure analysis have been prepared. The crystals belong to the hexagonal space group $P6_122$ (or $P6_522$). The unit cell dimensions are $a=b=54.9$Å, $c=181.3$Å. We have collected the native data with synchrotron radiation at 1.0Å. Data collection at the iron absorption edge and structure analysis by molecular replacement using model of cytochrome *c'* from *Rhodospirillum molischianum* are in progress.

Yoshimura T., Iwasaki H., Shidara S., Suzuki S., Nakahara, A. & Matsubara, T. *(1988). J. Biochem.* **103**, 1016-1019.
Norris, G. E., Anderson, B. F., Baker, E. N. & Rumball, S. V. (1979). *J. Mol. Biol.* **135**, 309-312.

14P–03

CRYSTAL STRUCTURE OF *STREPTOMYCES ERYTHRAEUS* TRYPSIN AT 2.7Å RESOLUTION

T. YAMANE, A. SUZUKI and T. ASHIDA, School of Engineering, Nagoya University, Nagoya 464-01, Japan, and Y. KAWATA and F. SAKIYAMA, Institute for Protein Research, Osaka University, Osaka 565, Japan

Streptomyces erythraeus trypsin(abbr. as SET) is a trypsin-like serine protease very similar to *St. griseus* trypsin (abbr. as SGT). SET consists of 227 amino-acid residues with three disulfide bridges, and has a molecular weight of 22,300. SET is stable between pH 5 and 10, and hardly autolyzes itself at all at its active pH range. SET was crystallized at its active pH of 7.0. The space group is $P3_221$ and the lattice constants are a=47.0 and c=178.9Å. An asymmetric unit contains one molecule with Vm=2.45Å^3/dalton. The structure was determined by the MIR method, using K_2PtCl_4, $(NH_4)_2Hg(SCN)_4$, and K_2HgI_4 derivatives. High resolution X-ray data of the native protein were collected with a screenless Weissenberg camera(Sakabe) at the BL6A$_2$ station at the Photon Factory. A total of 48,452 reflections were measured at 1.7Å resolution, of which 19,912 were independent, giving the merging R factor of 0.061. The model structure was made at 3.5Å resolution. Now the structure refinement using X-PLOR(Bruenger) is in progress. Comparison of the molecular structures among SET, *bovine* trypsin and SGT shows that: 1) the folding of the main chains of the three proteins is essentially the same though there are significant differences on the molecular surface; 2) the spatial arrangements of the catalytic triads in the three proteins are similar to each other.

Bruenger, A. T. (1990) X-PLOR Manual, Version 2.1, Yale Univ., New Haven, USA.

Sakabe, N. (1983) *J. Appl. Cryst.* **16**, 542-547.

14P–04

CRYSTAL STRUCTURE OF [2Fe-2S] FERRODOXIN I FROM THE *Equisetum arvense* AT 1.8Å RESOLUTION

M.Bando, Y.Morimoto, T.Tsukihara, Department of Biotechnology, The University of Tokushima, Tokushima, Japan,
S.Ikemizu, National Lab. for High Energy Physics, Tsukuba, Japan and
K.Fukuyama, Faculty of Science, Osaka University, Toyanaka, Japan.

The ferredoxin with two iron atoms and two inorganic sulfur atoms, [2Fe-2S], that have been isolated from a wide range of plans and algae have been named plant-type ferredoxin (Fd). The ferredoxin functions as redox components in photosynthetic system I and other metabolic system with low redox-potentials at about -400mV.

The [2Fe-2S] Fd I from *Equisetum arvense* consists of 95 amino acid residues and has a relative molecular mass of 10,263. The amino acid sequence of this protein differs from that of *Aphanothece sacrum* Fd by 58%. The crystal was monoclinic with space group $P2_1$ and unit cell parameters a=30.4, b=57.4, c=47.5 Å, and β=78.7°. It contains two molecules per asymmetric unit with a Vm of 1.98$Å^3$/Da. The structure of Fd I was solved by molecular replacement using the structure of the Fd I from the blue-green alga *Aphanothece sacrum*. The electron density map was so clear and unambiguous that main polypeptide chains could be easily traced. However N-terminal residues and 4 C-terminal residues of both independent molecules could not be traced in the map because of the poor electron density in these regions. An atomic model of the Fd I was constructed using the "FRODO" program on a Silicon Graphics IRIS graphics system. Crystallographic refinement was performed using the restrained least-squares refinement program of Hendrickson and Konnert. The occupancies of all atoms were fixed at 1.0. The final refinement cycle was carried out for 1420 non-hydrogen protein atoms and 183 water molecules, using 13,838 ($>1\sigma$) observed F_o data between 10.0 to 1.8Å spacing. The present crystallographic R factor for the refined model is 16.3% at 1.8Å resolution, with a root-mean-square (r.m.s.) deviation of 0.014Å from the ideal bond length.
The r.m.s. deviations for equivalent Cα atoms of two independent molecules superposed by the least squares method average 0.26Å. There are structural differences between them in the molecular surface. For example, Glul9 Cα atoms of two independent molecules are more than 0.4Å from each other, and the deviation was also lain on the residue of Ser61. The structural differences are presumably caused by hydrogen bonds between carbonyl oxygen atoms and water molecules.

14P–05

CRYSTAL STRUCTURE OF THE TFIID TATA BOX BINDING PROTEIN: A Novel DNA binding Motif that Recognizes the Minor Groove

D.B. Nikolov[†], S.-H. Hu[†%], J.P. Lin[†%], A. Gasch[†], A. Hoffmann[†], M. Horikoshi[†] N.-H. Chua[†], R.G. Roeder[†] and S.K. Burley[†%]
[†]Laboratories of The Rockefeller University and [%]Howard Hughes Medical Institute, 1230 York Avenue New York, NY 10021-6399 USA

The three-dimensional structure of the TATA-box binding protein, a central eukaryotic transcription factor, has been determined by multiple isomorphous replacement and refined at 2.6Å resolution. Eukaryotic organisms possess three distinct RNA polymerases (forms I, II, and III) that catalyze transcription of nuclear genes. Despite their considerable structural complexity, these multi-subunit enzymes require sets of auxiliary proteins known as general transcription factors to initiate specific transcription from corresponding class I, II, and III nuclear gene promoters. Recent studies have documented that a phylogenetically-conserved TATA-box binding protein (TBP or TFIIDτ), first identified as a component of the class II initiation factor TFIID, is required for transcription by all three nuclear RNA polymerases, making it the first universal transcription factor. In class II transcription, TBP functions by recognizing and binding DNA in the vicinity of the transcription start site (the TATA-box) and subsequently directing assembly of the transcription machinery prior to mRNA synthesis. The newly determined structure of TBP is that of a highly symmetric α/β protein representing a novel DNA-binding fold, which resembles a molecular "saddle" that sits astride the DNA. The DNA-binding surface is a curved, antiparallel β-sheet that can make specific contacts with the minor groove of DNA. When bound to DNA, the convex surface of the molecular "saddle" is presented for interaction with other transcription initiation factors and regulatory proteins.

14Q–06

CRYSTALLOGRAPHIC REFINEMENT OF TRICHOSANTHIN AT 1.9Å RESOLUTION

Lin YuJuan, Pan KeZhen, Fu ZhuJi,and Zhou KangJing, Fujian Institute of Research on the Structure of Matter, Chinese Academy of Sciences, Fuzhou Fujian 350002, P. R. China.

Trichosanthin is a protein extracted from a Chinese herb medicine. Recently, it has drawn great attention because of its application in medicine. As well as having an abortion function, it is a ribosome inactivating protein with a single chain, which can also combine with antibody to produce immunotoxin. A series of research studies of trichosanthin have been reported [1,2,3,4,].

A crystal suitable for X-ray diffraction at 1.9Å has been obtained. A set of data (32357 reflections with $Fo > 1\sigma\ (Fo)$) has been collected by synchrotron radiation with the help of researchers in EMBL. An initial model based on the results of refinement at 2.6 Å was refined with 1.9 Å data first by the molecular dynamics (XPLOR) in SGI station and then by restrained least squares (PROLSQ) on a VAX785 computer. After the initial model was refined by XPLOR, the *R*-factor decreased from 0.365 to 0.299, with RMS deviations of bond lengths and angles of 0.021 Å and 3.99° respectively, using 32119 reflections in the resolution range 8 to 1.9 Å with $|F_o| > 1\sigma(F_o)$.

The 2FoFc map was used to adjust the displacing protein atoms and the FoFc map to find solvent molecules. A total of 3828 protein atoms and 105 water molecules have been refined to an *R*-factor of 0.239 with RMS deviations of 0.040Å (1-2), 0.099 Å (1-3), and 0.125 Å (1-4).

The crystalline form of the protein ($Mr \approx 27{,}132$ Dalton) is monoclinic, space group *C*2, with unit cell parameters $a = 75.60$ Å, $b = 75.44$ Å, $c = 88.36$ Å $\beta = 99.50°$. There are two molecules in an asymmetric unit, each molecule containing 247 amino acids and 1914 non-hydrogen atoms. The polypeptide chain folds into 8α - helices and 13β - strands, forming two domains, the bigger one from N terminal to Pro 181, and the smaller one from Ser 182 to C terminal. Refinement of the structure is still in progress.

We are grateful to K.S. Wilson for help with data collection.

[1] Pan Kezhen et al.,(1982). *Scientia Sinica*, B**25** 730-737.
[2] Pan Kezhen et al.,(1985). *Scientia Sinica*, B**29** 26-32.
[3] Pan Kezhen et al.,(1987). *Scientia Sinica*, B**30** 386-394.
[4] Pan Kezhen et al.,(1992). *Scientia Sinica*, B**35** 29-39.

14Q–07

CRYSTAL STRUCTURES OF TWO BLUE COPPER PROTEINS

T. Inoue, Y. Kai, S. Harada, N. Kasai, Department of Applied Chemistry, Faculty of Engineering, Osaka University, Suita, Osaka 565, Japan,
S. Suzuki, T. Kohzuma, Institute of Chemistry, College of General Education, Osaka University, Toyonaka, Osaka 560, Japan,
J. Tobari, Department of Chemistry, College of Science, Rikkyo University, Nishi-ikebukuro, Tokyo 171, Japan,
S. Shidara, Department of Environmental Science, Hiroshima University, Naka-ku, Hiroshima 730, Japan, and
H. Iwasaki, Nagoya University of Foreign Studies, Nisshin-cho, Aichi 470-01, Japan.

The proteins containing type-I copper(II) turn deep blue in the oxidized state and their absorption intensities are about 10 to 50 times larger than those of non-blue copper proteins. Both pseudoazurin from *Methylobacterium extorquens* AM1 and azurin from *Achromobacter xylosoxidans* NCIB11015 are blue copper proteins.
Single crystals of these blue copper proteins have been obtained by the hanging-drop vapor diffusion method using ammonium sulfate as precipitant. Crystal data are

Pseudoazurin;	orthorhombic, space group $P2_12_12_1$(No.19) a=52.62, b=63.28, c=35.13Å
Azurin;	tetragonal, space group $P4_122$ (No.91) a=b=52.3, c=100.2Å

Intensity data were collected with SR radiation at 2.5 Gev. For pseudoazurin, native data up to 1.2Å were collected with two X-ray beams of 1.04 and 1.375Å, and for azurin, data up to 2.0Å with a 1.0Å beam. The locations of copper atom in the unit cell for each crystal were obtained by calculating the anomalous difference Patterson function.
The structure analyses have been carried out by molecular replacement using the copper-copper distances as translation parameters in MERLOT. The starting structure was obtained from pseudoazurin from *Alcaligenes faecalis* S-6 (homology 44%), and azurin from *Alcaligenes denitrificans* NCTC 8582 (homology 73%), respectively. By using XPLOR, the crystallographic R-factor has been reduced from 0.52 to 0.25 at 2.2Å resolution for pseudoazurin, and from 0.35 to 0.25 at 2.5 Å for azurin. The refinements including solvent molecules are now in progress.

14Q–08

HIGH RESOLUTION ELECTRON CRYSTALLOGRAPHY OF AN α - HELICAL COILED-COIL PROTEIN

P A Tulloch, Biomolecular Research Institute, 343 Royal Parade,
Parkville, 3052, Australia,
Y Fujiyoshi & Y Kimura, Protein Engineering Research Institute,
6-2-3,Furuedai, Suita-shi, Osaka, 565, Japan,
A W S Johnson, Centre for Microscopy & Microanalysis, University of
Western Australia, Nedlands 6009, Australia, and
P W Dyson and A E C Spargo, School of Physics, University of
Melbourne, Parkville 3052, Australia.

Our aim is the 3-dimensional structure determination of a fibrous protein at 3Å resolution, extending the poorer resolution projection analysis of Bullough and Tulloch (1990). The success of Henderson and his co-workers in determining the major part of the structure of the membrane protein bacteriorhodopsin in the dehydrated state by electron crystallographic methods, together with recent improvements in technique has shown that the problems of radiation damage and lack of structural stability can be overcome for a number of 2-dimensional protein crystals. A significant experimental advance has been the development of a highly stable super fluid helium temperature stage and cryo-transfer system in a dedicated high resolution microscope by Fujiyoshi et al (1991). This machine is used in the present study of α-helical coiled-coil protein in the form of natural micro-crystals extracted from the ootheca of the praying mantid. Further development of the vitreous ice embedding technique has resulted in the diffraction data being extended to 1 Å for untilted crystals and 2 to 3 Å for tilted crystals. The phases for the diffraction data will be determined from the FT of images to the resolution limit of the image of around 3 Å.

Tilting methods show the micro-crystals to be 200 to 300 Å thick with a repeat distance in the electron beam direction of 18Å. These values mean that for some orientations, considerable atomic overlap will exist and that the possibility of multiple scattering should be investigated. This has been done by dynamical calculation for a poly-alanine model of the structure based on the low resolution result of Bullough and Tulloch (1990). The results so far, in the untilted case, show the weak phase object approximation, upon which the phase determining method relies, will hold reasonably well for crystals of 200Å (Dyson, Spargo, Tulloch & Johnson, 1992).

Bullough, P A, & Tulloch, P A (1990). *J. Mol. Biol.* **215**, 161.
Dyson, P W, Spargo, A E C, Tulloch, P A, & Johnson, A W S, (1992).

Fujiyoshi, Y, et al (1991). *Ultramicroscopy* **38**, 241.

14Q–09

CRYSTALLOGRAPHIC STUDIES ON A DOUBLE SHELLED SPHERICAL VIRUS, RICE DWARF VIRUS (RDV) II.

Y.Morimoto, T.Tomizaki, T.Sato, T.Tsukihara, The University of Tokushima,Tokushima, Japan,
M.Koizumi, National Institute of Sericultural and Entomological Science, Tsukuba, Japan,
T.Omura, National Agriculture Research Center, Tsukuba, Japan, and
H.Kano and H.Mizuno, National Institute of Agrobiological Resources, Tsukuba, Japan.

Rice Dwarf Virus (RDV), a phytoreovirus, from *Nephotettix* species infects systemically rice and wheat plant and causes stunting or dwarfing of plant bodies. The virus is an icosahedral double-shelled particle approximately 700 Å in diameter. The particle molecular weight of the virus is 6.52×10^7. A total of 540 identical protein subunits are on the particle surface, suggesting $T=9$ icosahedral symmetry of the capsid. X-ray crystallographic analysis of the virus is a useful method for determining the double shelled structure of the virus, and for revealing the mechanism of symmetrical self-assembly of subunits. The virus has been crystallized in the cubic space group $I23$ with a=789Å. Two particles are located on positions of Wyckoff notation "a" in the unit cell.

Diffraction experiments were carried out with a macromolecular Weissenberg camera at BL-6A2 in the Photon Factory, Japan. The crystal to film distance was 573mm and the wavelength was 1.488Å. The incident beam, focused by double bent mirrors, was collimated to 0.lmmϕ. Oscillation speed 0.03°/sec, oscillation range 1.5°, coupling constant 100°/mm. Diffraction data were recorded on an Imaging-Plates (IP), and read out by the Fuji BA-100 system. Program "WEIS" was used to process the data. As the crystals deteriorated quickly when taken from the mother solution, they were kept in that solution during data collection. Therefore, modifying "WEIS" to determine the crystal orientation of without setting photographs, we searched ϕx, ϕy, ϕz values from -45° to 45° for each angle with step size of 1° on a Personal IRIS workstation. A total of 56096 reflections up to 10 Å was collected from one crystal, and the mean *R*merge of 10.51% for 29075 independent reflections was obtained by a scaling procedure. The self-rotation function calculated using the diffraction data indicated icosahedral symmetry. As very low angle reflections are important when using molecular replacement methods in the initial stage of structure analysis, they were observed by means of a small beam stopper attached just before the Imaging-Plate. We will report a non-crystallographic symmetry or self-assembly of the virus structure calculated from the diffraction data.

14Q-10

CRYSTAL STRUCTURE ANALYSES OF THE SPHERICAL VIRUSES, TOBACCO NECROSIS VIRUS (TNV) AND RICE DWARF VIRUS(RDV).

T. Tsukihara[1], Y. Morimoto[1], K. Fukuyama[2], M. Koizumi[3], T. Omura[4], K. Kano[5], H. Mizuno[5].

[1]Faculty of Engineering, The University of Tokushima.
[2]Faculty of Science, Osaka University
[3]National Institute of Sericultural and Entomological Science, Tsukuba
[4]National Agriculture Research Center, Tsukuba
[5]National Institute of Agrobiological Resources, Tsukuba, Japan.

Tobacco necrosis virus (TNV) is a typical spherical virus. Its coat protein contains 275 amino acids. TNV crystallizes in cubic space group $P4_232$ with $a=b=c=338$ Å. Its 3.86×10^7Å^3 unit cell contains two virus particles with molecular weight 6.7×10^6, and Vm value 2.9A3/dalton. The (T=3) symmetry of TNV capsid and subunit arrangement of *180* copies of its coat protein were determined previously. X-ray diffraction intensities for a $0.7\times0.7\times0.7$ mm^3 TNV crystal were measured at 5 Å resolution on a Weissenberg camera with cassette radius 430 mm, at the Photon Factory synchrotron. The merging *R*-factor is 0.115 for 90,251 reflections with $I>5\sigma(I)$. The 27,437 ($F>3\sigma(F)$) and 24,127($F>5\sigma(F)$) independent reflections were 94% and 83% of the theoretical number. The virus crystal's structure was determined by a 91 cycle iteration of molecular replacement averaging. The correlation coefficient between calculated and observed structure factors converged to 0.92, and *R*-factor 0.16. Secondary structures such as α-helices and β–structures were clearly assigned in the 5 Å resolution electron density map. The TNV virus resembles SBMV both in the orientation and folding of the coat protein subunits. The ordered part of that subunit is shorter by 12 and the longer disordered part by 27 residues than corresponding parts of SBMV.

Rice Dwarf Virus (RDV), a phytoreovirus, from *Nephotettix* species infects rice and wheat systemically, causing stunting or dwarfing of plant bodies. The molecular weight of the double-shelled virus particle, approximately 700 Å in diameter, is 6.52×10^7. Crystallographic analysis helped reveal the double shelled structure of the virus, and the mechanism of symmetrical self-assembly of its subunits. RDV crystallized in cubic space group *I*23 with a=789Å. Two particles are on Wyckoff "a" positions in the cell. For diffraction experiments on a macromolecular Weissenberg camera at BL-6A2 in the Photon Factory, the crystal to film distance was 573mm, and wavelength 1.488Å. The incident beam, focused by double bent mirrors, was collimated to 0.lmmϕ. 56096 reflections up to 10 Å were collected from one crystal The mean *R*merge for 29075 independent reflections was 10.51%. A self-rotation function indicates icosahedral symmetry for RDV.

14Q-11

THE STRUCTURE AND FUNCTION OF MOS KINASE

B.K. Sathyanarayana, Wayne Matten, Renping Zhou, Nelson Yew, Ira Daar, Terry Copeland, George F Vande Woude, John Erickson+ and Ronald Rubin

ABL-Basic Research Program, and +PRI-Dyncorp NCI-FCRDC,
Frederick, Maryland 21702.

The c-mos proto-oncogene product, $pp39^{mos}$, is a cellular threonine/ serine kinase which functions during oocyte maturation and is the active component of cytostatic factor (CSF).

Based on the three-dimensional structure of the related cyclic AMP dependent protein kinase catalytic domain (CPK), we have modelled the structures of the protein kinase domains of mos from several sources including human, mouse and Xenopus. The model structures were refined using energy minimization. Although the mos amino acid sequence form these species can differ in up to 48% of the residues, most changes are found on the surface of the 3D structure distal from the active site cleft. The modelled structures consist of two distinct domains; an amino terminal ATP binding domain consisting of residues 58-143 in the human c-mos sequence, and a larger carboxyl terminal peptide binding domain consisting of residues 144-346. The polypeptide chain linking these two domains contains the conserved mos sequence GTIIME, which is located at the initiation site for truncated forms of mos expressed in maturing mouse oocytes and transformed cells. The substrate binding cleft lies in a deep groove located between the two domains. The topology of the mos kinase active site cleft was used to model potential substrate/inhibitor peptides which maximize the electrostatic, hydrogen bonding and van der Waals interactions with residues in the active site cleft.

Research sponsored in part by the National Cancer Institute, DHHS, under contract No. NO1-CO-74101 with ABL.

14R–12

DRUG-PROTEIN INTERACTION: REFINEMENT AND MODELLING OF SULFONAMIDE DRUGS BOUND TO HUMAN CARBONIC ANHYDRASE I ENZYME

S. Chakravarty and K.K. Kannan, Solid State Physics Division, Bhabha Atomic Research Centre, Bombay 400 085, India.

Therapeutic effects of Sulfonamide compounds with unsubstituted sulfamido group is believed to be strongly correlated with the specific inhibition of Carbonic Anhydrase isozymes. Structures of three Sulfonamide drugs namely, Acetazolamide, Methazolamide and 3-Acetoxy Mercuri, 4-amino benezene sulfonamide (AmSulf) complexed to Human Carbonic Anhydrase I enzyme have been investigated. The structures have been refined by PROLSQ Package as implemented by us on a local RISC based parallel processing system. While the R-factor for Acetazolamide is 0.176 using 14303 reflections the corresponding R-factors for Methazolamide and AmSulf are 0.182 and 0.192 using 14201 and 13691 reflections respectively with good stereochemical models. Inspection of the $(|Fo|-|Fc|)$ *and* $(2|Fo|-|Fc|)$ *maps clearly shows the drug molecules bound in the active site of the enzyme. The Sulfamido group and the cyclic rings are located in approximately the same region around Zinc in all the three complexes. Besides, the Nitrogen atom of the Sulfamido group displaces a zinc coordinated solvent molecule of the native enzyme and the two Oxygens displace two other solvent molecules in the active site, one of which is a proposed fifth coordination site for the substrate* CO_2 *molecule. On comparing the spherical polar coordinates of the atoms of residues in the active site with Zinc at the origin, it is seen that LEU 198 shows the maximum change in both Acetazolamide and Methazolamide complexes as compared to the native, while His 200 shows the largest change in Amsulf. Eight residues in the active site which show significant changes have been identified and it is seen that amongst these, there are systematic differences in the interactions with the heterocyclic ring (Acetazolamide and Methazolamide) and benzene ring of AmSulf. These differences may govern the final orientation of the sulfamido group with respect to the Zinc ion and the binding of drug molecules in the active site thereby explaining the differences in the strength of inhibition. Based on the above location of the sulfamido group and the cyclic ring as found from experimental data, twenty sulfonamides containing heterocyclic and/or homocyclic rings were docked into the active site using IRIS-4D work station, and free energy minima determined using XPLOR. Details of interactions of these drugs with the protein residues including intramolecular Hydrogen bonding show systematic trends which may also be correlated to their strength of inhibition.*

14R–13

CRYSTAL STRUCTURE OF GLUTATHIONE SYNTHETASE WITH ADENOSINE(5')TETRAPHOSPHO(5')PYRIDOXAL

T. Hibi, H. Kato, T. Nishioka, and J. Oda, Institute for Chemical Research, Kyoto University, and H. Yamaguchi and Y. Katsube, Institute for Protein Research, Osaka University, Japan.

Glutathione synthetase from *E. coli* B was specifically modified with an ATP analog, adenosine(5')tetraphospho(5')pyridoxal (AP_4-PL). AP_4-PL was more tightly bound to the ATP-binding site of the enzyme than ATP, and was irreversibly attached to a lysyl residue (Lys-18) by reduction. In contrast, modification with AP_3-PL, an analog one phosphate shorter than AP_4-PL, was less specific because of unstable binding. To elucidate such behaviors of the reagents, the crystal structure of the enzyme complexed with AP_4-PL has been determined at 2.55 Å resolution.

The crystals of the AP_4-PL:enzyme reduced complex was isomorphous to the unliganded enzyme crystals ($P6_222$), with cell dimensions of $a = b =$ 87.8 Å and c = 164.8 Å. The adenosine moiety of bound AP_4-PL was sandwiched between two β-sheets, and this site corresponds to the ATP-binding site identified with D-Fourier method. Whereas, the pyridoxyl moiety of AP_4-PL was fixed at the entrance of the γ-Glu-Cys-binding crevice. The main body structure of the enzyme subunit was almost unchanged as compared with that of the unliganded enzyme. In addition, well-defined electron density was shown for a flexible loop region (residues 226-241), which is disordered in the unliganded enzyme. The model of the flexible loop had an Ω-loop-like structure and appeared to form a hydrogen bond between α-phosphate of AP_4-PL and NH atom of Ile-236. Closure of the loop assisted the formation of the Schiff base between Lys-18 of the enzyme and AP_4-PL. The resulting structure of the complex supports the ligand-induced conformational change of the loop, which is suggested by limited proteolysis of the loop (Tanaka et al. 1992). Refinement is in progress and the detail structure of the active site will be presented.

Tanaka, T. et al. (1992). *Biochemistry* 31, 2259-2265.

14R–14

ACTIVE SITE CONFORMATION OF CYTOPLASMIC CYCLOPHILIN OF *Eschrichia Coli* IN ASPECT OF STERIC HINDRANCE TO ATTACHMENT OF CYCLOSPOLIN A

M. Ito and M. Konno, Department of Chemistry, Faculty of Science, Ochanomizu University, Bunkyo-ku, Tokyo 112
T. Hayano, M. Suzuki, S. Sato and N. Takahashi, Corporate Research and Development Laboratory, Tonen K. K., Iruma-gun, Saitama 354, Japan

Cyclospolin A(CsA) inhibits signal transduction pathway to T-lymphocyte activity, commonly available to prevent graft rejection in clinical organ transplantation. Complexes between CsA and cyclophilins from yeast to human are abundant, whereas in *E. coli* cyclophilin little affinity to CsA was unexpectedly confirmed. The complex of CsA-cyclophilin blocks phosphatase activity of calcineurin required for transcription of interleukin 2 in T-cell. The complex of FK506 and FKBP (FK506 binding protein) (Van Duyne, et al. (1991)) also inhibits potently T-cell activity in the same manner as the complex of CsA-cyclophilin. Drastic conformational change of CsA follows attachment to cyclophilin(Kallen, et al.(l991); Spitzfaden, et al.(1992)). In *E. coli* little affinity is attributed to the conformational difference at the active site, where CsA will not attach. Our structure analysis aims to clarify the structural difference between prokaryotic and eukaryotic proteins.
Crystals of the *E. Coli* cyclophilin complex consisting of 164 residues and tripeptide succinyl-Ala-Pro-Ala-*p*-nitoanilide have space group $P2_12_12_1$, a=66.33(12), b=68.23 (9), c=40.03(5) Å. Intensity data for native and $HgCl_2$, K_2PtCl_4 and $SmCl_3$ derivatives were collected with a Weissenberg camera using 1.00 Å synchrotron radiation at KEK. After refinement, the mean figure of merit for MIR phases was 0.73 at 2.5 Å resolution. The electron density maps show the core of an eight-stranded anti-parallel, β-barrel as observed in human cyclophilin. Four hydrophobic residues Phe-48, Met-49, Phe-99 and Leu-108 at the active site have the same conformation as in human protein. Notable differences apparently found are l)A hydrogen bond links Asn-102 and MeBmt-l of CsA in human cyclophilin. By contrast, Arg-87 in *E. coli*, corresponding to Asn-102, is in no case fixed in a rigid loop. 2)*E. coli* has Phe-107 at the position corresponding to a conserved Trp-121 of human cyclophilin which hydrogen bonds to the MeLeu-9 carbonyl group of CsA. A 13 residues antiparallel β type loop is additionally inserted next to Phe-107.

We thank Prof. N. Sakabe, Dr. A. Nakagawa and Dr. S. Iwata at the Photon Factory KEK for kind help in data collection and model building.

Kallen, J., *et al.,* (1991). Nature, **353**, 276-279.
Spitzfaden, C., *et al.,* (1992). FEBS Lett., **300**, 286-290
Van Duyne, G. D., *et al.,* (1991). Science, **252**, 839-842.

14R–15

ALKALINE METAL ION BOUND IN HUMAN LYSOZYME

M. Matsushima, A. Pähler, K. Morikami and K. Inaka

Protein Engineering Research Institute, Furuedai, Suita, Osaka 565, Japan

The human lysozyme crystals were soaked in NaCl, LiCl, and KCl solutions. The x-ray diffraction intensity data were collected by use of Mo Kα radiation and an area detector. The crystal structures were refined at 1.50 Å resolution and the conventional R-factors were reduced to 0.145, 0.150, and 0.144, respectively. One of the solvent molecules in the crystal soaked in the NaCl solution had a low B factor and extensively interacted with the protein molecule. The solvent molecule was surrounded in an octahedral geometry by three main-chain carbonyl oxygen atoms of Ser 61, Cys 65, and Val 74, two water molecules and a methyl group of Ala 73. The distances to these oxygen atoms were 2.4 Å. On the other hand, the electron density of the solvent molecule was not found in the crystal structure soaked in the LiCl solution. Therefore, the solvent molecule was identified as a sodium ion. In addition to these results, the ion was substituted by a water molecule in the crystals soaked in the KCl solution and the peptide bond between Val 74 and Asn 75 was rotated in the structure. The water molecule donated the hydrogen bonds to the carbonyl oxygen atoms of Ser 61 and Cys 65, and accepted the bonds from the amido of the rotated peptide and a water molecule.

Since neither a potassium ion, nor a divalent metal ion, such as a calcium ion or a copper ion, was bound at the site, human lysozyme selectively bound a sodium ion, which was octahedrally coordinated by the three carbonyl oxygen atoms of the main-chain and the water molecules.

Inaka, K. et al. (1991) J. Biol. Chem. **266**, 20666-20671.

Blake, C.C.F. et al. (1983) J. Mol. Biol. **167**, 693-723.

14R–16

STRUCTURE OF *P.STUTZERI* G4-AMYLASE AND ITS COMPLEX WITH MALTOTETROSE

Y. Matsuura, Y. Morishita, Y. Yoshioka, M. Sato and Y. Katsube,
Institute for Protein Research, Osaka University, Suita, Osaka, Japan,
and M. Kubota, Hayashibara Biochem. Lab. Inc., Amase-minami, Okayama, Japan.

Maltotetraose forming α-amylase from *Pseudomonas stutzeri* is an exo-amylase which degrade starch from its non-reducing end. We have determined the crystal structure of this enzyme and its complex with maltotetraose at 2.2Å resolution.
The enzyme crystallizes in orthorhombic $P2_12_12_1$, a=65.6, b=170.5 and c=46.7 Å. The complexed crystal was obtained by co-crystallization of the E219Q mutant of this enzyme with maltopentaose, as orthorhombic $P2_12_12_1$, a=65.1, b=138.4 and c=50.7Å. Both crystals were obtained from the ammonium sulfate solution at pH7.5 by hanging drop vapor diffusion. Intensity data were collected on an imaging-plate diffractometer Rigaku RAXIS-IIc. The structure of the native enzyme was solved by MIR method using two heavy-atom derivatives, $K_3UO_2F_5$ and $SmCl_3$. The structure of the complexed crystal was solved by the molecular replacement method with the native structure as a search model by using the program AUTOMR[1]. The native crystal structure was refined to an R-factor 17.4% by using the programs XPLOR and PROFFT. A $C\alpha$-backbone model of the native enzyme is shown in the Figure. Two disulfide bonds and two calcium atoms were defined. A loop (66-72th) and the C-terminal (418-429th) region are not well-defined in the electron density map. A 2Fo-Fc map of the CORELS refined complexed crystal showed clearly the maltotetraose instead of pentaose and the loop which was invisible in the native crystal. Model building showed that the maltotetraose is bound essentially in the same manner with that proposed in Taka-amylase[2].

1) Y. Matsuura. (1991). *J. Appl. Cryst.* **24**, 1063-1066.
2) Y. Matsuura *et al.* (1984). *J. Biochem.* **95**, 697-702.

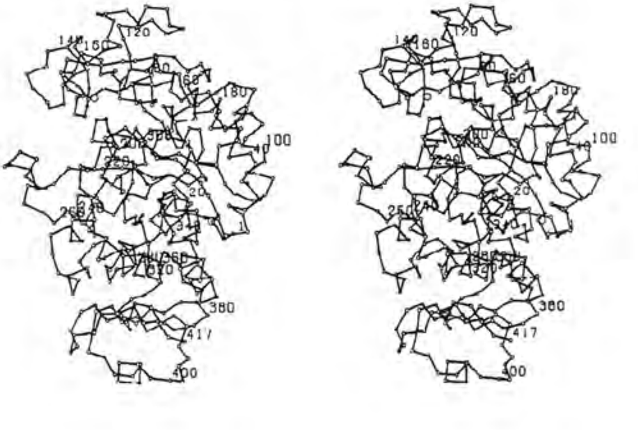

14R–17

STUDY OF CONFORMATIONAL DIFFERENCE BETWEEN A DIHYDROPYRIDINE CALCIUM CHANNEL ANTAGONIST AND A NON ANTAGONIST

Safia Mehdi and K. Ravi Kumar, X-ray Section, Indian Institute of Chemical Technology, Hyderabad - 500 007, AP, INDIA.

Crystal structure of 1,4-dihydro-2,6-dimethyl-4-(2,4-dichlorophenyl)-3,5-N-methyl carbamoyl pyridine (I) and 1,4-dihydro-2,6-dimethyl-4-(2,4-dichlorophenyl)-3,5-N-diethyl carbamoyl pyridine (II) have been determined and the important structural requirements for biological activity (Janis & Triggle, 1983) compared with those of twenty three other reported ones.

Crystal data of (I) is:- M_r=368.26, orthorhombic, $Pca2_1$, a=12.928 (3), b=14.506(3), c=9.740(2) Å, Z=4, (Mo $K\alpha$) = 0.71069Å, T=293K, R=0.0541 and R_w=0.0582.

Crystal data of II is:- M_r=470.4, monoclinic, $P2_1/n$, a=14.686(5), b=7.590(2), c=23.578(6) Å, β=107.47°(1), Z=4, (Mo $K\alpha$) = 0.71069Å, T=293K, R=0.051 and R_w=0.055.

The overall structure of both compounds is similar to that of the reported analogues. But the deviation from planarity in the dihydropyridine ring (defined as the sum of the numeric values of the six intra ring torsion angles) is 106°.15 for compound I and 75°.09 for II, it being 72°.1 for nifedipine, the most potent calcium channel antagonist (Triggle, Shefter and Triggle, 1980). The 2,4-dichlorophenyl ring in compound I is not normal to the DHP ring, whereas in compound II it is normal to this ring, which is the orientation preferred in all the phenyl substituted derivatives investigated. The presence of the water molecule in II provided a different type of hydrogen bonding pattern.

Janis, R.A. & Triggle, D.I. (1983). *J Med Chem* **26**, 775-785.
Triggle, A.M., Shefter E. & Triggle, D.Ju (1980). *J Med Chem* **23**, 1442-1445.

14R–18

CRYSTAL STRUCTURE OF THE COMPLEX BETWEEN PORCINE PANCREATIC ELASTASE AND MACROCYCLIC INHIBITOR

T. Tada and T. Yasuda, Analytical Research Laboratories, Fujisawa Pharmaceutical Co., Ltd., Osaka, Japan, and S. Harada, Y. Kai and N. Kasai, Department of Applied Chemistry, Faculty of Engineering, Osaka University, Osaka, Japan.

Elastase belongs to the serine protease family of enzymes which are capable of cleaving connective tissue components. Uncontrolled proteolysis by the elastase can cause some inflammatory diseases. The title compound was isolated from *Streptomyces resistomicificus*. The compound has a unique macrocyclic structure and exhibits potent inhibitory activity for elastase. To investigate the nature of the interaction of this novel class of inhibitor, X-ray structure analysis of the complex of porcine pancreatic elastase (PPE) with the inhibitor has been performed. Crystals of the complex were obtained using a solution of PPE and inhibitor in 0.08M sodium sulfate and 0.05M sodium acetate at pH 5.0 by vapor diffusion from 0.16M sodium sulfate and 0.1M sodium acetate solution over 20 days. The reflection data were collected to 1.7 Å resolution on the RIGAKU R-AXIS IIC Imaging Plate Area Detector using Cu-Kα radiation less than 2 days. All the data were measured on one crystal and a total of 23097 unique reflections ($I(\sigma) \geq \sigma$) were obtained (R-merge : 4.44%). The space group is $P2_12_12_1$ with cell dimensions a=51.67 Å, b=57.84 Å, and c=75.52 Å. The isomorphous native PPE coordinates were used for initial phasing of the reflections and calculation of a difference Fourier map to locate the inhibitor. Programs X-PLOR and PROLSQ were used for the refinements and the calculation of maps. The electron density map confirmed conclusively the location and orientation of the inhibitor molecule in the active site of PPE. Details of the structural features for the interaction mode between PPE and inhibitor will be reported.

14R–19

VARIATIONS ON THE SAME THEME — CRYSTAL STRUCTURE OF L-ASPARAGINASE AND THE UNIQUENESS OF ITS STRUCTURAL FOLD

J. K. Mohana Rao, Michael Gribskov, Dominique Housset,
Mariusz Jaskolski, Jacek Lubkowski, Maria Miller, B. K. Sathyanarayana,
Amy Swain and Alexander Wlodawer
ABL-BRP, NCI-FCRDC, P.O. Box B, Frederick, MD 21702, USA.

L-asparaginase (E.C.3.5.1.1), an enzyme encountered in the oxaloacetate pathway, catalyzes the hydrolysis of L-asparagine to L-aspartate and ammonia. It is used clinically in the treatment of acute lymphoblastic leukemia. The crystal structures of the type II tetrameric L-asparaginase from *Escherichia coli* (EcA), *Erwinia chrysanthemi* (ErA), and *Acenetobacter glutaminasificans* (AGA) have been solved in our laboratory using multiple isomorphous replacement and molecular replacement techniques. At present, the R-factors for the three crystal structures are respectively 0.14 for EcA at 2.3 Å, 0.16 for ErA at 1.8 Å, and, 0.17 for AGA at 2.9 Å resolution. These highly similar structures of enzymes with different activity profiles have also been compared among themselves. Each monomer of the tetramer (222 symmetry) has two distinct domains with unique topological features. The larger N-terminal domain has a mixed eight-stranded β sheet and four α-helices. The parallel α/β part of this domain has a flavodoxin-like fold. However, this region is characterized by a unique left-handed crossover, rarely seen in protein structures. The C-terminal domain has a four-stranded parallel β sheet flanked on either side by two α helices. From the topological features, the active site was first predicted and thereafter verified in the electron density maps. The active site lies between the N- and C- terminal domains belonging to different monomers. Details of various comparisons (among themselves and with other proteins) with the resulting similarities and differences will be discussed. Based on the crystal structure of the type II*E. coli* enzyme and its sequence alignment with the type I enzyme from *E. coli,* the structure of the type I enzyme has been modeled.

This research is sponsored by the National Cancer Institute (DHHS) contract NOl-CO-74101 with ABL.

14R–20

BINDING AND CATALYTIC ROLES OF THE ACTIVE SITE METAL IN ZINC PROTEINASES

G. Shoham. H. M. Greenblatt and H. Feinberg, Department of Inorganic Chemistry and The Laboratory of Structural Chemistry and Biology, The Hebrew University, Jerusalem 91904, Israel.

Several series of crystallographic studies have been performed to determine the yet unknown general mode of action of zinc proteinases. For detailed structural analysis we chose the digestive proteinase Carboxypeptidase A (CPA) which is often used to represent this enzyme family. In attempts to fully understand the role of zinc in CPA and other zinc proteinases, and in zinc enzymes in general, several metal derivatives have been prepared and their kinetic behaviour studied. These metal-substituted enzymes show very interesting patterns of activity towards various peptide and ester substrates. The catalytic activity changes dramatically with the particular metal substituted and with the specific substrate chosen. Although crystallographic studies of such zinc proteinase derivatives have been carried out previously, no satisfactory explanation has been given to the kinetic deviations observed. We have prepared apo-CPA (zinc removed) in which no trace of zinc remains, and have used the resulting enzyme to prepare a series of metallo-CPA derivatives. These derivatives were crystallized and their crystal structures were determined at high resolution. In addition to the detailed structures of the metallo-derivatives themselves, we have also analyzed structures of their complexes with a number of inhibitors and reaction coordinate analogues. The specific purpose of these studies was to ascertain whether the observed changes in the activities of metallo-derivatives of CPA (or zinc proteinases in general) are due to differences in the way in which the metal is bound to the enzyme, due to local changes in the conformation of the active site, or whether different metals affect the binding of substrates in various ways. Similar studies were also carried out on the apo-enzyme, in order to determine the effect of the zinc ion on the so called "Michaelis-Menten" complex, formed before any reaction takes place. We will present high resolution, refined structures of native-, apo-, and metallo-enzymes described above, both alone and in complex with various affectors, and describe the relevance of these data to the role of zinc in biological catalytic activity.

14S–31

USE OF ATOMIC FORCE MICROSCOPE IN THE DETERMINATION OF SPACE GROUPS BY X-RAY DIFFRACTION ANALYSIS OF CRYSTALS

N. Masaki and K. Machida, Fac. of Pharm. Sci., Kyoto Univ., Kyoto,
H. Kado, K.Yokoyama and T. Tohda, Central Res. Labs., Matsushita Elec. & Ind. Co.Ltd., Moriguchi, Osaka,
Y. Yoshimura, Fac. of Sci. & Eng., Ritsumeikan Univ., Kyoto, and
M. Kitamura, Fac. Sci., Kyoto Univ., Kyoto, Japan.

Space group determination is an important initial step in diffraction studies of crystals. Systematic absences of reflections are mainly used for this purpose. Identifying centers of symmetry, mirror planes or rotation axes which give no systematic absences requires subsidiary means such as intensity statistics and crystal morphology that are always not definitive. The final space group may be determined from possible ones after completing x-ray analyses by selecting that with the lowest R-factor. Even the proof of extinction spectra from a limited range of intensities observed under particular experimental conditions is often unclear.
An atomic force microscope AFM revealed atomic scale images of surfaces on (001) and (100) faces of aspirin crystals.[1,2] The (001) image satisfied the X-ray structure[3-5] but the (100) image did not. It did not revealed the c-glide plane expected for the accepted space group (a=11.430, b=6.591, c=l 1.395Å, β=95.68°, $P2_1/a$, Z=4)
Re-examination of h01 reflections from aspirin crystals in X-ray precession photographs confirmed the presence of weak but significant l=2n+1 reflections. In (0kl) and (hk0) photographs, 0k0 reflections for k=2n+1 were not detected. The space group for aspirin should therefore be $P2_1/m$ or $P2_1$ from the systematic absence data. Although we could not distinguish between them from systematic absences, the AFM images of (001) and (100) faces clearly show absence of mirror symmetry. The space group of aspirin crystals was uniquely determined as $P2_1$, Z=2.
The successful re-determination of the space group for aspirin confirms the power of AFM for determining space groups. AFM can easily detect mirror, glide plane or two fold axis symmetry if appropriate surfaces are prepared and are not reconstructed from the internal structure.

l) Masaki,N. etal.(1991) *Chem.Pharm.Bull.***39**,1899-1901.
2) Masaki, N. et al.(1992) *Ultramicroscopy* **41**, (5).
3) Nitta, I. & Watanabe,T. (l937) *Sci.Papers Inst Phys.Chem.Res.*(Tokyo) **31**,125-128.
4) Weatley, P.J. (1964) *J.Chem.Soc.* 1964, 6036-6048.
5) Kim,Y. et al.(1985) *Chem.Pharm.Bul1.* **33**, 2641-2647.

14S–32

ELECTRON MICROSCOPY AND DIFFRACTION STUDY OF THE DIRECT REACTION OF IRON AND CARBON AND THE FORMATION OF A NEW IRON CARBIDE

S. Nagakura and T. Komekyu, Department of Materials Engineering,
Waseda University, Shinjuku-ku, Tokyo 169,
M. Ando and S. Odawara, Department of Mechanical Engineering,
Nagaoka Univ. of Technology, Nagaoka, Niigata 940-21, Japan.

It has long been believed that iron and carbon do not react directly to produce carbides. Recently, however, the authors have found that direct reaction takes place when composite films of iron and carbon are heated in vacuum.

On amorphous carbon films, iron and carbon were successively vacuum deposited to produce C-Fe-C sandwich films. The deposited amounts of iron and carbon are 10-20 nm thick. AC vacuum-arc evaporation using iron and carbon electrodes was also applied to evaporate iron and carbon simultaneously to make Fe-C mixed films. The films produced were heated in a vacuum better than 2×10^{-4} Pa at various temperatures and for different periods of time.

In the as-deposited state, the sandwich films with iron thinner than 10 nm were structureless and gave halo rings, but those with iron thicker than 20 nm were made of finely dispersed iron particles embedded in amorphous carbon. The mixed films were always structureless giving halo rings. When they were heated, the direct reaction between iron and carbon occurred. No difference in the reaction products was found between the sandwich films and the mixed films.

(1) 700°C, 1 h: The reaction product is θ-Fe_3C (cementite) with particles about 30 nm in size dispersed in the film, as occurs in tempering of martensitic steel. High resolution observations did not reveal any structural defects in the particles. (2) 500°C, 3 h and 400°C, 48 h: The reaction product is θ'-particles, as in steel tempering, where thin (001) layers of θ-Fe_3C and thin (100) layers of χ-Fe_5C_2 are microsyntactically intergrown. (3) 400°C, 24 h ~200°C, 336 h: The reaction product was as large as 1 μm but very thin. Its diffraction pattern shows hexagonally arranged spots giving axial length a=0.5286 nm. The axial length c could not be measured because of crystal thinness. The products seems to be a new higher iron carbide. High temperature in situ observations showed that this carbide began to decompose at 400°C to form finely dispersed θ-Fe_3C particles 20-30 nm in size and without orientation.

14S–33

MODULATION MODES OF $Bi_2Sr_2(Ca_{1-x}Ln_x)Cu_2O_{8+\delta}$ CRYSTALS STUDIED BY HIGH–RESOLUTION REVERSE IMAGING

T. Onozuka
Institute for Materials Research, Tohoku University, Sendai 980, Japan.

Modulation modes of the $Bi_2Sr_2(Ca_{1-x}Ln_x)Cu_2O_{8+\delta}$ (Ln=Pr, Nd) compounds, of which the lattice is modulated by a longitudinal displacement wave of metal atoms along the *b* axis*, are analyzed on the basis of the microphotometric density distribution recorded directly from the negative film of [001] high-resolution reverse image and the simulations computed using three structure models of b=4.5b$_0$, 5b$_0$ and 4b$_0$. A microphotometric density distribution is shown in Fig.1 (the upper curve) together with its image, being equivalent to the one-dimensional contrast modulation in the image. The density distribution of the unit, 5b$_0$, has a single maximum peak at the middle. Those joining at both sides of the unit are that of the unit, 4.5b$_0$, which is distinguished from that of 5b$_0$ by the twin peaks in the middle. The pattern of density distribution is in good agreement with the simulation.

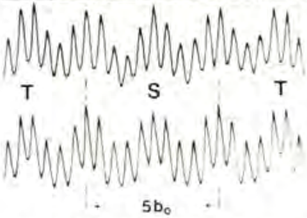

Fig 1. Microphotometric density distribution and its image, being compared with the simulations (the lower curve and the inset)

The density distributions of Fig.2 reveal the existence of the modulation modes of $(1,1)_5$ and (1,0) in the crystal.

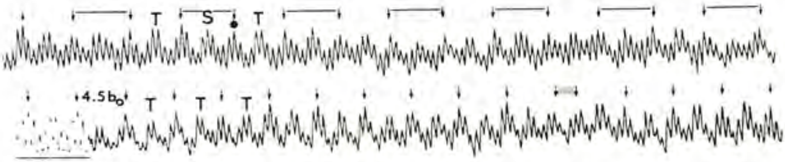

Fig. 2. Microphotometric density distributions obtained from specimens of x=0 (the upper curve) and the praseodymium concentration of x=0.32 (the lower curve).

*ONOZUKA, T., IWABUCHI, Y., FUKASE, T., SATO, H. & MITCHELL, T. (1991). Phys. Rev. B**43**, 13066-13072.

EELS STUDY OF THE TEMPERATURE DEPENDENCE OF THE VOLUME-PLASMON ENERGY IN ALUMINIUM

M.Terauchi, H.Abe, R.Kuzuo and M.Tanaka, Research Institute for Scientific Measurements, Tohoku University, Katahira 2-1-1, Aoba-ku, Sendai 980, Japan.

The temperature dependence of the volume-plasmon energy in aluminum had been measured using electron energy-loss spectrometers by several authors. The energy resolutions were about 2eV except for one report.[1] The temperature ranges examined were limited. The interpretation of the temperature dependence has not yet been clear because two different temperature dependences below room temperature were reported.[1,2]

The present authors have measured the volume-plasmon energy of aluminum over a wide temperature range between $-175°$C and $500°$C with energy resolutions of $0.10 \sim 0.27$eV. The high-resolution electron energy-loss spectroscopy (EELS) microscope used is equipped with two Wien filters as the monochrometer and the analyzer. The experimental results showed a smooth decrease of the volume-plasmon energy with increasing temperature. The theoretical temperature dependence was calculated based on the free-electron model, which takes account of the change in the density of the free electrons due to the thermal expansion of aluminum. The experimental temperature dependence agreed well with the theoretical one. Thus, it has been revealed that the temperature dependence of the volume-plasmon energy of aluminum is explained quantitatively by the thermal expansion of the material.

1) A.Imbusch and H.Niedrig : Phys. Lett. **32A**(1970)375.
2) L.B.Leder and L.Marton : Phys. Rev. **112**(1958)341.

14S-35

MODULATED STRUCTURES IN Fe–DOPED Bi-Sr-Cu-O SUPERCONDUCTORS STUDIED BY HIGH RESOLUTION TRANSMISSION ELECTRON MICROSCOPY

K. YANAGISAWA[1,*], Y. MATSUI[1], T. KOIZUMI[2] and T. HASEGAWA[2],
[1] National Institute for Research in Inorganic Materials *1-1 Namiki, Tsukuba 305, JAPAN,* [2] Showa Electric Wire & Cable Co., Ltd. *2-1-1 Odasakae, Kawasaki-ku, Kawasaki 210, JAPAN*, * *on leave from* Kobe Steel, Ltd. *1-5-5 Takatsukadai, Nishi-ku, Kobe 651-22, JAPAN.*

The effects of Fe-doping on the modulated structures in $Bi_{2.5}Sr_{1.5}CuO_y$(2.5/1.5-Phase), as well as $Bi_{2.2}Sr_{1.8}CuO_y$(2.2/1.8-Phase), are examined by electron diffraction and high-resolution electron microscopy. The Fe-free $Bi_{2.5}Sr_{1.5}CuO_y$[1], as well as the specimens doped with Fe up to 30% Cu in the initial ratio, crystallizes in an orthorhombic superlattice with modulation periodicity bs=4.5b(Fig.1-a). At 30% substitution, transition of the symmetry accompanied by a shortening of the modulation periodicity is observed. Specimens in the range of Fe from 30% to 50% have a monoclinic superlattice with bs=4.0b(Fig.1-b). The Fe-free $Bi_{2.2}Sr_{1.8}CuO_y$[2], on the other hand, has a monoclinic superlattice with bs=4.8b(Fig.2-a). Partial substitution of Cu with Fe in $Bi_{2.2}Sr_{1.8}CuO_y$ results in a slight decrease of the modulation periodicity down to bs=4.5b and also in a transition of the symmetry to an orthorhombic superlattice(Fig.2-b).

[1] Y. Ikeda, *et., al.* Physica C 159 (1989) 93. [2] Y. Matsui, *et., al.* Jpn. J. Appl. Phys. 27 (1988) L1873.

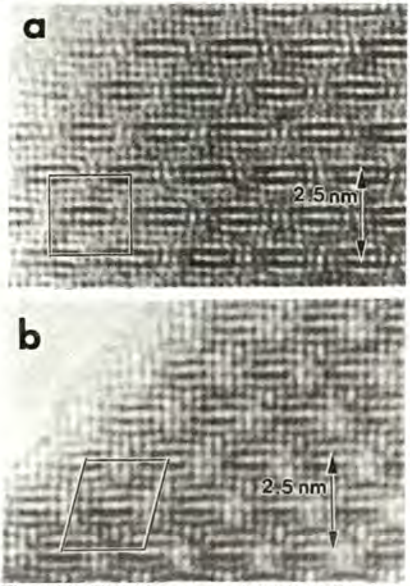

Fig.1 HRTEM images of 2.5/1.5-Phase doped with (a) 10% Fe and (b) 40% Fe.

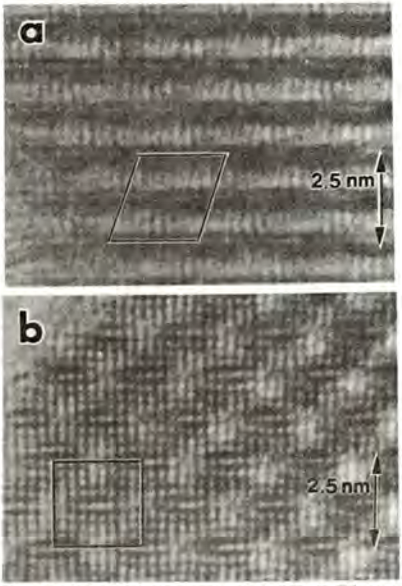

Fig.2 HRTEM images of 2.2/1.8-Phase doped with (a) 0% Fe and (b) 40% Fe.

14S–36

SEARCHING FOR THE CRYSTAL STRUCTURE OF A LONG-PERIOD TETRAGONAL Bi-Mn ALLOY AN EXAMPLE OF STRUCTURE ANALYSIS BY HIGH RESOLUTION ELECTRON MICROSCOPY

K. Yoshida, T. Kawai and K. Shimonishi, Faculty of Engineering, Kobe University, Rokkodai, Nada, Kobe 657, Japan.

Bi and Mn are difficult to mix atomically from the melt. However, the authors formed several new alloy phases by low temperature heating of their double layer composite films. Atomic arrangement of the most remarkable, a long-period tetragonal phase, is being investigated by high resolution electron microscopy and diffraction only, since we have no other means to analyse such thin and small crystallites.

Double layer thin films, consisting of a 300 Å Bi layer and a 200 Å Mn layer, were prepared by successive deposition in a vacuum of about 10^{-7} Torr. They were then heated for 50 to 200 hr in the same vacuum at 265° C, just below 271° C, the melting point of Bi. Solid state alloying occurred at the contacting interface for both layers, permitting some atomic ordering. As their total thickness is less than 500 Å, specimens could be observed directly under a JEM-200CX electron microscope.

Single crystal electron diffraction patterns were easily obtained. Some patterns consisted of closely spaced arrays. A three dimensional reciprocal lattice successfully constructed gave a tetragonal direct lattice, a = 17.26 Å, c = 10.21 Å.1) These cell dimensions are large (even assuming C-face-centering with a = 12.20 Å,c = 10.21 Å) compared with the Sigma-phase lattice constants, in some transition-transition binary metal alloys (e.g. a = 8.8 Å, c = 4.6 Å for Sigma phase Ni-Cr). However, Bi and Mn ions, were mixed in the above large unit cell with the Sigma-phase structure. Bi and Mn were assumed to have the Goldschmidt ionic radii, and the mixture assigned the arithmetic mean radius (1.82+1.12)/2 = 1.47 Å. The packing of these spheres in the Sigma-phase structure arranged in the above cell, is unexpectedly good. This structure was Fourier transformed and the result compared with the diffraction pattern. Some observed reflections satisfying the $h+k$=odd condition that should be extinct for the regular Sigma-phase structure are quite distinct. Thus 740 is too strong to be due to multiple diffraction. A structure with atoms displaced systematically from the regular structure, was Fourier transformed. Whereas the Sigma-phase space group is $P4_2/mnm$, the derived model may have $P4_2/n$. A few spots surrounding the originally extinct 740 reflection became relatively strong, but 740 remained weak, though not extinct. Simulated images of the structural model thus derived are now being being compared with high resolution electron micrographs.

1) K. Yoshida, T. Yamada and Y. Taniguchi, Acta Cryst. B45(1989) 40.

14T–38

CRYSTAL STRUCTURE OF A NEW TERNARY CHALCOGENIDE: Ta_2Ni_2 $(\mu_3\text{-}Se)_2(\mu_4\text{-}Se)_2(\mu_5\text{-}Se)$

S-X Liu, B Zhang, Z-M Wang and J-L Huang, Chemistry Department, Fuzhou University, Fuzhou, Fujian 350002, China; Fuzhou Laboratory of Structural Chemistry, Academia Sinica, Fuzhou, Fujian 350002, China.

Ta_2Ni_2 $(\mu_3\text{-}Se)_2$ $(\mu_4\text{-}Se)_2$ $(\mu_5\text{-}Se)$ was obtained by direct combination of the elements at high temperature. The title compound crystallizes with four formula units in the monoclinic space group C2/m in a cell with dimensions a=12.821(4) Å, b=3.4913(4) Å, c=16.444(2) Å, β=91.34(2)°, V=735.9 Å^3. The crystal structure was solved by the heavy atom method and refined by full matrix least square calculations. The final cycle of refinement included 56 variable parameters, R=0.048, R_W=0.059, goodness-of-fit=1.25, $w=1/\sigma^2(F_o)$. Max. shift/e.s.d. < 0.01, and the residual electron density was +4.02 (-9.29) eÅ^3, no chemically significant features.

The compound displays a new layered structure type. Every layer contains octahedral tantalum atoms, square pyramidal tantalum atoms, and tetrahedral nickel atoms each coordinated by selenium atoms. There is a van der Waals interaction between Se atoms from the neighbouring layers. There are two kinds of Ni atoms in a formula $Ta_2Ni_2Se_5$: one Ni atom is connected with other two Ni atoms and three Ta atoms in the same layer; the other Ni atom is connected with four Ta atoms in the same layer. Therefore metal chains are formed along the b axis in each layer. The one Ta atom in the formula has a square pyramidal geometry with Ta-Se bond lengths of 2.523-2.664 Å, while the other Ta atom in the formula is octahedrally coordinated with Ta-Se bond lengths of 2.548-2.661 Å. All Ni atoms are tetrahedrally coordinated by four Se atoms with Ni-Se bonds between 2.328 and 2.657 Å. These polyhedra which are distinctly irregular join via shared edges.

This search was supported by the National Natural Science Foundation of China.

14T–39

CRYSTAL STRUCTURES OF SOME TERNARY LAYERED TELLURIDES CONTAINING IRON ATOM

J-L Huang, S-X Liu and G-L Cal, Chemistry Department, Fuzhou University, Fuzhou, Fujian 350002, China; Fuzhou Laboratory of Structural Chemistry, Academia Sinica, Fuzhou, Fujian 350002, China.

Six ternary Fe-containing tellurides were prepared by high-temeprature reaction of the elements and characterized by the single crystal X-ray diffraction, shown in Table 1. The layered structure of these tellurides can be described as a series of sandwiches. Neighbouring sandwiches are held together by weak van der Waals interaction between Te atoms. In each sandwich, Fe atoms and Ta (or Nb) atoms are packed between layers of Te atoms. The Fe atoms in these compounds are in a distorted tetrahedral environment, Fe-Te bond lengths being between 2.478Å and 2.665Å. The Ta (or Nb) atoms in these tellurides have distorted octahedral, square-pyramidal and tetrahedral geometries, respectively.

The anisotropic resistivity and some other physical properties were measured for these layered compounds.

Table 1 Crystal Data

Compound	*a* (Å)	*b* (Å)	*c* (Å)	β (°)	Space Group	*R*
$FeTaTe_3$	7.407 (4)	3.625 (3)	9.966 (3)	109.16 (3)	$P2_1/m$	0.051
$FeNb_2Te_4$	12.412 (2)	3.8173 (9)	7.295 (2)		*Pmmn*	0.055
$FeTa_2Te_4$	12.377 (3)	3.7687 (7)	7.266 (2)		*Pmmn*	0.076
o-$Fe_2Nb_2Te_4$*	7.920 (3)	6.241 (3)	7.228 (4)		*Pma2*	0.076
m-$Fe_2Nb_2Te_4$+	7.301 (1)	6.313 (1)	8.002 (1)	92.46 (1)	$P2_1/c$	0.037
$FeTaTe_2$	7.873 (1)	7.2229 (6)	6.174 (1)		*Pmna*	0.083

*orthorhombic form of $Fe_2Nb_2Te_4$
+monoclinic form of $Fe_2Nb_2Te_4$

This research was supported by the National Natural Science Foundation of China.

14T–40

STRUCTURE OF $Na_4SrSi_3O_9$ AND ITS RELATIONSHIP TO OTHER COMPOUNDS OF FORMULA $M'_4M''(TO_3)_3$

R.P. Gunawardane, Department of Chemistry, University of Peradeniya, Peradeniya, Sri Lanka.

Single crystals of $Na_4SrSi_3O_9$ were grown from a melt of composition 75 mol% Na_2SiO_3: 25 mol% $SrSiO_3$ at 1035°C and the unit cell was determined using rotation and Weissenberg photographs. Crystal data: $Na_4SrSi_3O_9$ monoclinic, space group C2,

$$a = 10.706(2),\quad b=10.866(2),\ c = 6.509(1)\ \text{Å}$$
$$\beta = 144.14(2)^\circ,\ \ Z = 2.$$

The structure was determined using 411 independent reflections measured on a Nicolet P3 4-circle diffractometer. The atomic coordinates were refined to $R = 0.084$.

Bond lengths and angles are normal, although the Si-O-Si angle is nearly 180°; this rather large value is associated with large temperature factors for the bridging oxygen atoms.

The compound contains infinite SiO_3 chains of a conformation not described previously. The structure is built from a new type of zig-zag Si_3O_9 chain, parallel to (001), the conformation of which is quite different from the chain structure of calcium silicates such as wollastonite. Conformationally it more nearly resembles the infinite GeO_3 single chain found in $K_4BaGe_3O_9$. The structure of $Na_4SrSi_3O_9$ is compared with those of the other compounds of general formula $M'_4M''(TO_3)_3$ where M'=Na, K; M''=Ca,Sr, Ba and T=Si, Ge.

Gunawardane, R P and Glasser, F P (1975). Z Anorg Allg Chem **411**, 163-171.

14T-41

PLURALITY OF Si AND Co SITES IN Co ÅKERMANITE

K. Hagiya and M. Ohmasa, Department of Life Science, Himeji Institute
of Technology, Kanaji 1479-1, Kamigori, Akogun, Hyogo 678-12,
K. Iishi, Department of Mineralogical Science and Geology, Yamaguchi
University, Yoshida, Yamaguchi 753, Japan.

An incommensurate modulation in synthetic Co-åkermanite, $Ca_2CoSi_2O_7$, has been determined by five-dimensional refinement of the structure. The basic structure is tetragonal $P\bar{4}2_1m$, unit-cell dimensions a=7.8417(6), c=5.0249(3)Å, Z=2, D_m=3.307(4) g-cm^{-3} at 293K, D_x= 3.302 g-cm^{-3}. The modulated structure is also tetragonal $P^{P\bar{4}2_1m}_{p4mg}$, $\mathbf{k}_1$= 0.2913×($\mathbf{a}^*$+$\mathbf{b}^*$), $\mathbf{k}_2$=0.2913×(-$\mathbf{a}^*$+$\mathbf{b}^*$) where $\mathbf{k}_1$, $\mathbf{k}_2$ are wave vectors and $\mathbf{a}^*$, $\mathbf{b}^*$ are reciprocal lattice vectors of the basic structure. The modulation is caused by shifts of the constituent atoms and there was no evidence for anomalous occupancy at the metal sites. When distances longer than 3Å are excluded the coordination of oxygen around a Ca atom is 6 or 4+4. Since Ca-O distances at different sites change markedly, it is concluded that the SiO_4 tetrahedron does not behave as a rigid body. One of the four Si-O distances is almost constant along a direction of the modulation, while the rest vary markedly. This indicates that distortion of the Si-O tetrahedra in the crystal varies. The behaviour of the Co-O distances differs from that of the Si-O distances, since all four Co-O distances vary simultaneously in a sinusoidal manner. The distributions of the mean Si-O and Co-O distances evaluated from the modulation functions indicate that some mean distances occur more frequently than others in the structure. Splittings of peaks for tetrahedral cations in $Ca_2(Mg,Fe)Si_2O_7$ were observed by Merwin, Sebald and Seifert (1989) and by Seifert, Czank, Simons and Schmahl (1987) in spectroscopic studies. The plurality of tetrahedral bonds found in the present study may provide a reasonable interpretation of those spectra.

Merwin, L.H., Sebald, A. & Seifert, F. (1989). *Phys. Chem. Minerals* **16**, 752-756.

Seifert, F., Czank, M., Simons, B. & Schmahl, W. (1987). *Phys. Chem. Minerals* **14**, 26-35.

14T–42

CRYSTAL STRUCTURE OF DUFTITE POLYMORPHS

Kharisun and M. R. Taylor, School of Physical Sciences, The Flinders University of South Australia, G.P.O. Box 2100, Adelaide, SA 5001, Australia, and A. Pring, South Australian Museum, Adelaide, SA 5000, Australia.

The lead copper arsenate mineral, duftite, $PbCu(AsO_4)OH$ is found in nature in two polymorphs known as α-duftite and β-duftite. α-Duftite has the conichalcite, $CaCu(AsO_4)$, structure. Both polymorphs are believed to have essentially the same chemistry, however the relationship between the two structures has not yet been fully explored.

Single crystals of synthetic α-duftite have been prepared hydrothermally at 200 °C and 20 atmospheres from aqueous solutions which were 10^{-2} mol dm^{-3} in copper(II) acetate, lead(II) acetate and disodium hydrogen arsenate. The pHs of the solutions were adjusted to pH 3 using $HClO_4$. We are attempting to establish a synthetic route to β-duftite.

The crystal structures of the two polymorphs of duftite are believed to be closely related. Both structures consist of a network of AsO_4 tetrahedra, CuO_6 octahedra and Pb in square antiprisms. In α-duftite the copper-centred octahedron is regular, however, in β-duftite the octahedron is strongly distorted changing the space group from $Pnma$ to $P2_12_12_1$. A detailed comparison of the two structure types will be presented.

14T-43

POLARIZATION STUDY OF THE MAGNETIC X-RAY SCATTERING OF $(Ba,Sr)_2Zn_2Fe_{12}O_{22}$

E.Tsuji, S.Kumazawa, H.Katoh, N.Momozawa and K.Ishida, Science University of Tokyo, Noda-shi, Chiba 278, Japan,
K.Ohshima, University of Tsukuba, Tsukuba, Ibaraki 305, Japan,
J.Harada, Nagoya University, Chigusa-ku, Nagoya 464, Japan and
S.Kishimoto, Photon Factory, Oho-machi, Tsukuba, Ibaraki 305, Japan

The purpose of the present work is to study X-ray magnetic scattering of hexagonal ferrite $(Ba_{1-x},Sr_x)_2Zn_2Fe_{12}O_{22}$ with polarization analysis of the scattering peaks.

Single crystals of the hexagonal ferrite with x=0.748 were prepared by a flux growth method. The magnetic structure of the crystal is a proper helix below the Néel temperature 337K. The temperature dependence of the period of the helix was determined by neutron diffraction1). Since the period is incommensurate with the lattice, we attempt to observe weak peaks of magnetic X-ray scattering separately from intensive charge scattering. The X-ray experiment was carried out at BL4C in Photon Factory of KEK using a precise 4 axis goniometer with a variable-temperature cryostat. For the polarization analysis, we chose the wavelength, $\lambda = 1.15483$Å. Being of incommensurate nature, magnetic satellites such as 006^+, 009^+ were observed whereas 006^-, 009^- were not. The observed period of the helix at 5OK was in good agreement with that determined by neutron diffraction, but the angular resolution of the X-ray experiment is more than 20 times higher than that of the neutron experiment.

Polarization analysis was performed with a Ge(444) reflection whose Bragg angle is $\pi/4$ for $\lambda = 1.15483$A. The polarization planes for magnetic satellite peaks were rotated at right angle to that of the incident beam. The polarization analysis for weak diffraction peaks at the forbidden reflection angle of the crystal structure indicated that the peaks might be due to charge-magnetic interference scattering2).

1) N.Momozawa, (1986) *J. Phys. Soc. Jpn.*55, 4007-4013
2) M.Blume and D.Gibbs (1988) *Phys. Rev.* B**37**, 1779-1789

14T–44

SINGLE CRYSTAL X-RAY DIFFRACTION AND EXAFS STUDIES ON R_3TaO_7 (R=Ho,Y,Yb)

T. Tanaka, N. Ishizawa, M.Yoshimura, Research Laboratory of Engineering Materials, Tokyo Institute of Technology, Nagatsuta, Midori-ku, Yokohama, 227, Japan, K. Tanaka, Nagoya Institute of Technology, Gokiso-cho, showa-ku, Nagoya, 466, Japan, H. Oyanagi, Electrotechnical Laboratory, Umezono, Tsukuba, 305, Japan, and F. Marumo, College of Humanities and Science, Nihon University, Sakurajosui, Setagaya-ku, Tokyo, 156, Japan

The structure analysis of R_3TaO_7 (R=Ho,Y,Yb) have been carried out by means of single crystal X-ray diffraction and EXAFS spectroscopy. Although circular diffuse spots were observed in addition to the fundamental reflections based on the fluorite-type subcell for all compounds, the structural parameters were refined neglecting those diffuse spots and assuming the defect-fluorite-type structure with space group $Fm\bar{3}m$. Residual electron densities, which can be explained with the assumption of anharmonic thermal vibrations were, observed around the respective constituent atoms. Actually, refinement with anharmonic thermal parameters improved coincidence of observed and calculated structure factors significantly for Ho_3TaO_7 and Yb_3TaO_7. EXAFS spectra of these crystals were measured at Photon Factory, K.E.K, at absorption edges of Ta L_{III}, Ho L_{III}, Yb L_{III} and Y K, indicating that the R-O and Ta-O distances were generally slightly shorter than those given by the single crystal X-ray structure refinement.

14T-45

STRUCTURE ANALYSIS OF LEAD ORTHOVANADATE $Pb_3(VO_4)_2$ IN THE FERROELASTIC AND THE FERROELECTRIC PHASES

T. Umeki, H. Kasatani and H. Terauchi, School of Science, Kwansei-Gakuin University, Nishinomiya 662, Japan.

Lead orthovanadate $Pb3(VO_4)_2$ undergoes successive phase transitions at T_1=373K and T_2=273K. The crystal in the high-temperature phase ($T>T_1$) is trigonal with the space group of $R\bar{3}m$ (Z=1). The ferroelastic phase transition occurs at T_1 with decreasing temperature. The crystal in the ferroelastic phase ($T_1>T>T_2$) is monoclinic with a space group $P2_1/c$ (Z=2). The ferroelectric phase appears below T_2, where the crystal is monoclinic. A spontaneous polarization P_S takes place along the *b*-axis, the unique axis of the monoclinic system. Concerning the ferroelectric phase, there was a contradiction between the results of Salje and von Hodenberg (1977) and Garnier et al.(1984). The former authors reported that the ferroelectric phase belonged to $P2_1$ with the multiplications of the unit cell along the *a* and *c* axes. The latter authors, on the other hand, suggested that the space group of the ferroelectric phase was *A*2 without cell multiplication.

Here we determine the space group of the ferroelectric phase by means of X-ray diffraction using a mono-domain crystal. The space group of the ferroelectric phase was *A*2. The structure analyses were conducted at several temperatures from 300K to 14K. The R-factors were less than 0.060 in the ferroelastic phase and 0.045 in the ferroelectric phase. With a simple point-charge model, the spontaneous polarization was calculated from the atomic positions in the ferroelectric phase and compared with values observed using pyroelectric measurements by Midorikawa et al.(1980). The mechanism of the ferroelectric phase transition will be discussed in terms of the model of atomic displacements.

We wish to acknowledge Professor Y. Ishibashi of Nagoya University for supplying the $Pb_3(VO_4)_2$ crystal.

Salje, E. & von Hodenberg, R. (1977). *J. Appl. Crystallogr.* **10**, 132.

Garnier, P., Calvarin, G., Beran, J.F. & Weigel,D. (1984). *Mat. Res. Bull.* **19**, 407-414.

Midorikawa, M., Kashida, H., Sawada, A. & Ishibashi, Y. (1980). *J. Phys. Soc. Jpn.* **49**, 1095-1097.

14T-46

STRUCTURAL VARIABILITY IN GAMMA ALUMINA

B.K. Gan and B.H. O'Connor, Department of Applied Physics, Curtin University of Technology, GPO Box U1987, Perth, WA 6001, Australia and C.J. Howard, Ansto, Private Mail Bag 1, Menai, NSW 2234, Australia.

The extensive literature on γ-alumina (Al_2O_3) has established that the structure approximates to the spinel (AB_2O_4) form with either a cubic or tetragonally-distorted cell. The cubic structure for γ-alumina has the full complement of 32 close-packed oxygen ions found in spinel but only 21 $^1/_3$ Al^{3+} ions, i.e. there are 2 $^2/_3$ cation sites vacant. The arrangement of Al^{3+} ions is uncertain. Most reported structures describe a distribution of Al^{3+} ions between the octahedral and tetrahedral sites. Zhou (1988) reported some additional Al^{3+} occupation of a highly distorted octahedral site (32e). Analysis by the authors of γ-alumina x-ray powder patterns from three sources has indicated that the arrangement of cation vacancies may vary with synthesis conditions.

Comparisons were made using the gamma samples:-

1. Gamma alumina, Zhou (1988), obtained by heating boehmite (AlOOH) in air at 600 °C for 8 hours;
2. Gamma alumina produced by the authors from gibbsite $Al(OH)_3$, by heating in air at 700 °C for 8 hours;
3. Gamma alumina supplied by Johnson Matthey, Materials Technology, U.K.,consisting of a mixture of gamma and alpha (5%) alumina - synthesis procedure not known.

The measured patterns have been compared with a set of calculated patterns covering the range of possible vacancy distributions. The results indicate that the vacancy arrangements for these three specimens are markedly different. The differences are attributed to the distribution of Al^{3+} ions between the octahedral and tetrahedral sites. All still maintain the cubic spinel model.

Zhou, R-S (1988). Thesis for PhD in Ceramics, A Structural Study of the Transition Aluminas, Alfred University, New York, USA.

14T-47

A NEW FCC PHASE OF Y_2O_3

S. Katagiri and N. Ishizawa, Research Laboratory of Engineering Materials, Tokyo Institute of Technology 4259, Nagatsuda-cho, Midori-ku, Yokohama-shi, Japan and
F. Marumo, Department of Humanities and Sciences, Nihon University, Sakurajosui, Setagaya-ku, Tokyo 156, Japan.

A new high temperature form of Y_20_3 has been found to be attained with a laser beam heating technique. The new form has a fcc structure with a=5.2644(3)Å. The lanthanide sesquioxides are known to crystallize in either of three structures A, B and C, belonging to the hexagonal, monoclinic and cubic systems, respectively. The Y_20_3 crystals so far reported possess the C-type structure with the space group Ia3 and a=10.604Å. In the present study, Y_20_3 powder with 99.99 purity was pressed into a rod 4mm in diameter and 12mm in length. The upper part of this rod was heated at about 2220°C for 25min by making use of two YAG laser beams applied from symmetrically-placed positions. The powder diffraction pattern of the laser-processed part indicated that the lines typical of the C-type structure disappeared while those for the fluorite subcell remained. The space group of this crystal was found to be $Fm\overline{3}m$ or $Fm3$ from the precession photograph of a single crystal with a grain size of 30x40x2μm. The powder data are given in the Table 1. This new fcc form of Y_2O_3 appears to have a fluorite-type structure containing disordered oxygen vacancies.

Table 1. Powder diffraction data for Y_2O_3

h k 1	Iobs	dobs(Å)	dcalc(Å)
1 1 1	100	3.0346	3.0394
2 0 0	24	2.6318	2.6322
2 2 0	33	1.8615	1.8612
3 1 1	24	1.5870	1.5872
2 2 2	3	1.5200	1.5197
4 0 0	2	1.3161	1.3161
3 3 1	9	1.2079	1.2077
2 4 0	3	1.1771	1.1772

14U-48

CRYSTAL STRUCTURE AND LATTICE PARAMETERS OF $Zn_{1-x}Co_xS$, $Zn_{1-x}V_xS$ DILUTED MAGNETIC SEMICONDUCTORS

D. Gómez de Anderéz and S.A. López-Rivera, Facultad de Ciencias,
Universidad de Los Andes, Mérida, Venezuela and
W. Giriat, Centro de Fisica, IVIC, Aptdo 21827, Caracas 1020-A,
Venezuela.

Crystal structure of ternary alloys formed by substituting Co or V for the group II element in the $A^{II}B^{VI}$ lattice, are given in this paper. X-ray single crystal analysis of the new cobalt and vanadium diluted magnetic semiconductors $Zn_{1-x}Co_xS$ and $Zn_{1-x}V_xS$ are discussed for concentrations of x=0.01, 0.05, and 0.10. The diluted magnetic semiconductors retain the crystal structure of the "parent" hexagonal wurtzite ZnS structure for x=0.05 in $Zn_{1-x}Co_xS$ and for x=0.10 in $Zn_{1-x}V_xS$. For low (x=0.01) V concentration and for high (x=0.10) Co concentration, the structure is cubic. A complete crystal structure analysis of the compound $V_{0.1}Zn_{0.90}S$ will be presented. This the first time that single crystal X-ray analysis is reported for diluted magnetic semiconductors.

14U-49

STRUCTURE AND SYMMETRY OF PTCR PEROVSKITES

N.J. Calos, J.S. Forrester and T.J. White, Centre for Microscopy and Microanalysis, University of Queensland, St. Lucia, Australia, 4072 and S. Myhra, Division of Science and Technology, Griffith University, Nathan, Australia, 4111.

A number of perovskites show the unusual characteristic of higher resistivity with increasing temperature. Usually referred to as the positive temperature co-efficient of resistivity (PTCR), this property is finding application in thermistors and other temperature sensitive devices. In this investigation, PTCR characteristics are correlated with the crystal chemistry and microstructure for a number of titanate perovskites of the form $(Ca_{1-x}A_x)TiO_3$ where A= Sr, Pb, Ba, La. Average crystallographic features were determined by Rietveld analysis and Raman spectroscopy, while order-disorder phenomena and grain boundary structure were studied by convergent beam electron diffraction and high resolution electron microscopy.

The series $(Ca_{1-x}Pb_x)TiO_3$ typifies the results obtained. Using X-ray diffraction it was confirmed that in passing from the lead to calcium endmembers of the series, the symmetry changes from tetragonal (P4mm) to orthorhombic (Pnma), with the transition point occurring at x=0.4. This was confirmed by Raman spectroscopy where two broad bands between 200-500 cm^{-1} and 580-900cm^{-1} were preserved throughout the composition range, while the overlying fine structure changed markedly about the symmetry transition. The former bands are due to vibrational modes associated with the titanium and oxygen atoms (whose octahedral topology is essentially invariant) while the fine detail can be related to A-O bending and stretching which changes markedly throughout the series. In detail, the symmetry transition is quite complicated. For x=0.25 superlattices are observed by high resolution electron imaging and electron diffraction. These arise from Ca/Pb ordering which may be enhanced by long term, low temperature (<600°C) annealing. The influence of these complex structures on electrical resistance and other properties is now being evaluated.

14U-50

STRUCTURE OF $Ba_{6-3x}Sm_{8+2x}Ti_{16}O_{54}(0<x<1)$

H. Ohsato, T.Ohhashi and T.Okuda, Nagoya Institute of Technology,
Gokiso-cho Showa-ku Nagoya, 466 Japan.

The compound has excellent dielectric constant, low dielectric losses and low temperature coefficients of capacitance (Kolar et al. 1978). Recently, such dielectric ceramics have been used for microwave resonator. Ohsato et al.(1992) synthesized single crystals from the melts with composition $BaSm_2Ti_5O_{14}$, reported the dielectric properties and the crystal data, and found a superlattice with doubled *c*-axis lattice parameter.

Crystal data of fundamental lattice: Orthorhombic system, *Pba*2 (No.32) or *Pbam*(No.55), Z=l, a=12.142(4), b=22.300(6), c=3.827(2)Å.

The crystal analysis of the fundamental structure was performed based on the structure model of $Ba_{3.75}Pr_{9.5}Ti_{18}O_{54}$ reported by Matveeva et al.(1984). This compound has a tungsten bronze-like structure with perovskite-like columns, which have 2x2 perovskite unit cell dimensions. Because the TiO_6 octahedra connect with each other at apices, the atomic ratio of Ti to O is 1:3. There are three kinds of large cation sites, A_1, A_2 and C. A_1 has twelve fold coordination as in a perovskite structure. A_2 contains a pentagonal channel cavity among the perovskite-like columns as in the tungsten bronze structure. C has a triangle channel cavity which is vacant in this compound. The structural formula is described by $[(Ba_{2-2x}, Sm_{8+2x}) Ba_{4-x}]Ti_{18}O_{54}$.

The authors wish to thank K.Hiraiwa, M.Fujisawa & Y.Ishiguro.
This work was supported by Murata foundation for science development.

Kolar D., Stadler Z., Gaberscek S. & Suvorov, D.(1978). *Ber. Dt. Keram. Ges.* **55**, 346-348.

Matveeva R.G., Varfolomeev M.B. & Il'yushchenko L.S. (1984). *Zh. Neorg. Khim.* **29**, 31-34, transl.: *Russ. J. Inorg. Chem.* 29, 17-19.

Ohsato H., Nishigaki, S. & Okuda T. (1992), *JJAP*, in press.

MICROCRYSTALLINE KEATITE – A FIBROUS SiO_2-PHASE

B. Martin, Institute of Mineralogy, Ruhr-University, Universitätsstr.150, D-W4630 Bochum, Germany.

Keatite was first synthesized by Keat, 1954, who claimed to have obtained "single crystals". Shropshire et al.,1959, determined the structure and proclaimed an "idealized keatite-model". However, under the conditions given in Keat's paper the keatite synthesis is not reproducible.
For the first time microcrystalline, fibrous keatite, K, has been reproducibly crystallized from high purity silica glass HERALUX (>99.99 wt.% SiO_2) under hydrothermal conditions (400°C, 350 bar) in 0.01 mol $NaOH/H_2O$ solution (Martin & Röller,1990). This metastable silica transition phase is always associated with microcrystalline strongly stacking disordered cristobalite C_D in the beginning of its occurrence and with microcrystalline granular quartz before its fading out. The fibres are elongated parallel to <110> ($P\,4_12_1$-setting). The optical character of elongation is length-slow (KLS). KLS is crystallographically well characterized (Martin & Röller, 1990, Martin, 1991). A few milligram of keatite free of C_D, however, intergrown with quartz are used for X-ray diffraction analysis on a special automatic high-resolution Guinier-X-ray-diffractometer for small samples prepared without texture (method: Ihringer, 1982). Structure refinement was carried out with the WYRIET 2 of Schneider (1989).

Crystal data for keatite(micro-crystalline powder): space group $P4_12_12$ (or $P4_32_12$) a=7.479(7) c = 8.539(2)-8.540(7)Å V=477.6(9-14)Å^3,T = 298K X-rays:1.5406Å; 2θ range:14.0-60.0°; in 0.02° steps: 15 (overlapping!) reflections. R_{Bragg} (X-ray resolution 0.6 Å^{-1}) 15-32%

Comparison of the structural analysis of Shropshire et al. with "single-crystals" and the data for the new fibrous, microcrystalline material gives compatibility with the idealized keatite-model. Current investigations with neutron radiation will show whether the idealized structure model is a mean structure caused by right- and left-rotating a) domains or b) lamellae analogous to chalcedony, a natural microcrystalline fibrous quartz species (Martin,1991).

Keat, P.P.(1954). *Science* 120,328-330
Ihringer, J.(1982)*J.Appl.Cryst.* **15**,1-4
Martin, B. (1991)*Thesis Fakultät für Geowissenschaften,* Ruhr-University
Martin, B. & Roller, K.(1990). *N.Jb.Miner.Mh.***10**, 462-466.
Schneider, J. (1989). *IUCr Int.Workshop on the Rietveld method*, Petten.
Shropshire, J., Keat, P.P. & Vaughan, P.A. (1959).*Z.Krist.***112**, 400-413.

14U-52

THE INTERSITE DISTRIBUTION OF A SMALL AMOUNT OF Mn ION IN OLIVINE

Y. Ono, M. Tokonami and H. Horiuchi, Mineralogical Inst., Faculty of Sci., Univ. of Tokyo, Hongo,Tokyo 113,
N. Aikawa, Dept.of Geosciences, Faculty of Sci., Osaka City Univ., Sugimoto-cho, Osaka 459, and
S. Sasaki, Res. Lab. of Eng. Materials, Tokyo Inst. of Techn., Nagatsuta, Yokohama 227, Japan.

Olivine(M_2SiO_4) contains non-equivalent Ml and M2 sites and the inter-site distributions of cations are of importance in the geoscience of the upper mantle [l]. Large Mn^{2+} ions prefer larger M2 sites in Mg-Mn or Fe-Mn binary systems, but the distribution of very small amounts of Mn in the Mg-Fe-Mn ternary system has not been investigated.

Anomalous scattering with synchrotron radiation is effective for the determination of cation inter-site distributions, but in the case of a very small amounts of cation in ternary system, it remains very difficult. We now introduce order(O)-disorder(D) structural models and repeated data collection for statistical inspection. A new analysis of the inter-site distribution for only 1.4 mol% of Mn ion in $(Mg,Fe,Mn)_2SiO_4$ is described.

The sample was a natural crystal, shaped into a l00µm ellipsoid. Two wave lengths of 1.913Å and 1.903Å were used for the intensity measurements. The latter wavelength is very close to the Mn-absorption edge (1.8964Å). Accordingly the anomalous dispersion effect for the Mn ion is significant, whereas in the former case there is much less anomalous influence on the reflections. A set of seven reflections, which was measured repeatedly, was selected from two types of calculated structure factor. For three "standard" reflections, the difference between structure factors for the two wave length both in O and D models are almost zero, while in the other four, there are large differences only in the O-model.

From a comparison of the statistical coincidence factors with the O or D structural models at two wave lengths, Mn ions in the ternary systems seem to occupy the two non-equivalent sites randomly. The existence of many Mg^{2+} and Fe^{2+} ions, which tend to disordered distributions in their binary system, supposedly compensates for the energy gap between Ml-M2 sites for the Mn^{2+} ion.

[l] Aikawa N.,Kumazawa, M. & Tokonami, M. (1985). *Phys. Chem. Minerals* **12**, 1-8.

LOCAL CRYSTAL STRUCTURES OF AN ILVAITE SINGLE CRYSTAL

Y. Takéuchi, Y. Matsushita, H. Sawada and H. Taniguchi, Department of Earth Sciences, Nihon University, Tokyo 156, Japan.

Our eight structure refinements of ilvaite $CaFe^{2+}2Fe^{3+}Si_2O_7OOH$ from various localities in Japan have revealed that specimens from the Tochibora skarn, Kamioka mine, exhibit a notable feature (Takéuchi & Saga, 1990); the β versus order-parameter plots of those specimens deviate strongly from the correlation line proposed by Takéuchi, Haga & Bunno (1983). Using a single crystal of Tochibora ilvaite, about 1.5 cm wide and 4.5 cm long, we prepared X-ray specimens from three portions along *c*: (l) around the bottom, (2) middle, and (3) top (termination of the growth). Their MnO contents are around 3 wt%. Structural studies [$P2_1/a$; spherical specimens with radii 0.11~0.16 mm, AFC-SS, Mo$K\alpha$ $\lambda = 0.71073$ Å, 2θmax = 70° ~ 90°, No. of reflections 1486~2460, wt. scheme $1/\sigma^2$, $R = 0.030 \sim 0.035$, $wR = 0.041 \sim 0.047$] gave the following cell dimensions and approximate order parameters:

Specimen	*a*(Å)	*b*(Å)	*c*(Å)	β(°)	Order parameter(%)
(1)	13.040(1)	8.831(1)	5.8626(4)	90.012(7)	2
(2)	13.036(1)	8.829(1)	5.8610(4)	90.231(6)	36
(3)	13.019(4)	8.818(2)	5.855(1)	90.271(2)	47

Thus, the bottom portion, (1), is essentially orthorhombic while the other portions are monoclinic. This result contradicts the hypothesis that natural orthorhombic ilvaites were heated subsequent to their formation (Ghose, 1988). It thus appears to be worthwhile to consider the twinnings, disorders, along *c*, of the edge-sharing octahedral chains both suggested by Takéuchi et al. (1983) or partial oxidation to account for the natural occurrence of orthorhombic ilvaites.

Takéuchi Y. & Saga S.(l990). Abstr. 1990 *Annual Meet. Miner. Soc. Jpn*
Takéuchi Y. Haga N. & Bunno,T.(1983). Z. *Krist.* **163**, 267-283.
Ghose S.(1988). *Adv. in Phys. Geochem.* **7**, 141-161.

14U-54

LOCAL STRUCTURE OF INTERCALANTS IN THE LAYERED COMPOUND Cu_xTiS_2

K. Ohshima, R. Maruta and A. Makita, Institute of Applied Physics,
University of Tsukuba, Tsukuba 305, Japan.

X-ray measurements have been performed on the structure of the layered compound $Cu_{0.15}Ti_{1.08}S_2$ at room temperature. Both the intercalated copper atoms and self-intercalated titanium atoms are positioned at the octahedral sites in the van der Waals gap's layer. Weak diffuse scattering at 1/2 0 3/2, 0 1/2 3/2 and their equivalent positions is observed. This reveals that the intercalants are correlated with each other three-dimensionally and that stacking sequence $\alpha\beta\alpha\beta$ ... is deduced. By analyzing diffuse intensity, the short-range order (SRO) parameters were determined. 2x2 in-plane ordered structure is expected for the low temperature phase. The estimated in-plane and interlayer correlation lengths are about 12 Å, which correspond to about $4a_0$ and $2c_0$, respectively (a_0 and c_0 are unit cell parameters for a and c axes in the hexagonal lattice). In a computer-simulated arrangement of intercalants, based on the observed SRO parameters, it was noticed that the atoms have close to random positions with the above structural characteristics.

14U-55

THE Zr-N-F AND Y-O-F COMPOSITE MODULATED STRUCTURES

Siegbert Schmid, Ray L. Withers and John G. Thompson, Research School of Chemistry, The Australian National University, GPO Box 4, Canberra, ACT 2601, Australia

In both the YO_xF_{3-2x} ($0.78 \leq x \leq 0.87$) and ZrN_xF_{4-3x} ($0.906 \leq x \leq 0.936$) systems [1,2] there are reported to exist anion-excess, fluorite-related, non-stoichiometric solid solution fields in which each and every composition has its own unique (but closely related) structure. Such solid solution fields are best characterized as composite modulated structures. We report the results of a TEM and XRD study of the ZrN_xF_{4-3x} system. Yttrium oxide fluoride is difficult to study in the TEM because of beam damage. Isostructural ZrN_xF_{4-3x}, however, is 'beam-stable' and therefore various compositions of this material were synthesized by ammonolysis of ZrF_4 for study by TEM and XRD.

Composite modulated structures consist of two (or more) in general mutually incommensurable sub-structures each of which is characterized by its own 3-dimensional space group. The influence of the sub-structures upon each other leads to incommensurate modulation of the fractional coordinates of both. Structural characterization of such systems requires refinement of both parent sub-structures as well as of the Atomic Modulation Functions (AMF's) describing the above modulations. Approximations to the above parameters have been obtained via Fourier decomposition of the reported structures of $Y_7O_6F_9$, $Y_6O_5F_8$ and $Zr_{108}N_{98}F_{138}$ (obtained by using a superstructure approximation). Fourier decomposition of these reported structures gives both underlying sub-structures as well as the above AMF's. A modulated structure approach provides a much simpler parameterization and shows that superstructure refinements using independent atom-based parameters are grossly over-parameterized.

[1] Bevan, D. J. M., Mohyla, J., Hoskins, B. F. & Steen, R. J. (1990). *Eur. J. Solid State Inorg. Chem.* **27**, 451 - 465.

[2] Jung, W. & Juza, R. (1973). Z. *anorg. allg. Chem.* **399**,129 -147.

14U–56

X–RAY ANOMALOUS DISPERSION DETERMINATION OF $PbZrO_3$ SUPERSTRUCTURE

K.Nagino, M.Iida, Y.Itoh and Y.Soejima, Department of Physics, Kyushu University 812, Japan, and K.F.Fischer, Fachrichtung Kristallographie der Universität des Saarlandes, Saarbrücken, BRD.

The superstructure of $PbZrO_3$ has been investigated by using X-ray anomalous dispersion effect at both PbLIII and ZrK absorption edges. The method proposed by Soejima and Fischer (1988) was applied for determining displacements of Pb and Zr atoms along the Z direction. Intensity measurements of several superstructure reflections around both the absorption edges were made with synchrotron radiation. From changes in the intensity due to those in f' and f" we find the displacement vectors of Pb and Zr atoms in the superstructure. The results indicate that Zr atoms shift along z; this is in contradiction with the model given by Jona et al.(1975).

Jona,F., Shirane,G., Mazzi,F. & Pepinsky,R.(1975). Phys. Rev. 105,849-860.
Soejima,Y. & Fischer,K.F.(1988) Z.Kristallogr. 184,71-85.

14U–57

CHANGES IN MORPHOLOGY OF PERIODIC ANTIPHASE BOUNDARIES IN ONE-DIMENSIONAL LONG PERIOD SUPERSTRUCTURES

M. Itakura, N. Kuwano, S. Iwasaki, K. Kajiwara, A. Matsumoto and K. Oki, Department of Materials Science and Technology, Graduate School of Engineering Sciences, Kyushu University-39, Kasuga, Fukuoka 816, Japan.

Cu_3Pt and Pd_5Ce have one-dimensional long period superstructures (LPSs) where antiphase boundaries (APBs) are distributed periodically in the Ll_2 ordered structure. It is well known that Cu_3Pt has a state of a normal Ll_2 at low temperatures. Some of the present authors (Itakura et al., 1990) confirmed that in Pd_5Ce the LPS transforms to $L1_2$ at high temperature. In this study, the changes in morphology of periodic APBs in the alloys during the $LPS \rightarrow L1_2$ transition process have been investigated by electron microscopy. On the way to the transformation, a lot of hairpinshaped APBs are formed by linking adjacent periodic APBs. Some of the hairpin tips have a spear-like shape. High resolution images indicate that the order-structure is distributed in the region of the hairpin-tip, demonstrating that the hairpin-shaped APB recedes, dragging a small region of a low degree of order. It is found that the hairpin-shaped APBs tend to be arrayed to form "patchwork" of Ll_2- and LPS-regions. This texture shows that formation of a pair of hairpins induces another formations in the neighbourhood. A computer simulation of the transformation from LPS to Ll_2 has been performed using a time dependent Ginzburg-Landau model to successfully reproduce the formation process of hairpins. The kinetics of annihilation of periodic APBs have also been discussed in order to clarify the dependence of the stability of LPS on the shapes of the APBs.

Itakura, M., Kuwano, N., Yamamoto, K. & Oki, K. (1990). *J. Electron Microsc.* **39**, 1-6.

DIFFUSE SCATTERING IN AN YTTRIA–STABILISED CUBIC ZIRCONIA, ($Zr_{0.61}Y_{0.39}O_{1.805}$)

T.R.Welberry, R.L.Withers, J.G.Thompson & B.D.Butler. Research School of Chemistry, Australian National University, GPO Box 4, Canberra City, ACT 2601, Australia.

Details of the diffuse X-ray scattering distributions in a cubic yttria-stabilized zirconia, recorded using a position-sensitive detector (PSD) system, are presented in far greater deail than has hitherto been reported. In addition we present the results of some investigations using Monte Carlo simulation techniques to try to establish the origins of the various diffraction features that are observed in the experimental patterns.

The most significant feature of the experimental patterns that is observed is a set of dark planes normal to each of the six ⟨1 1 0⟩ directions and of a spacing equal to the reciprocal of the metal-metal interatomic vector. This feature is observable in yttria-doped zirconia as a result of the fact that the scattering factors for Y and Zr are very similar, and would probably be unobserved in systems displaying first order scattering effects which depend on the difference in the two scattering factors. We consider that this feature unequivocally demonstrates that lattice distortions due to variations of this fundamental metal-metal distance are the basis for understanding the whole diffraction pattern. The presence of such dark lines in this second-order scattering term (i.e. due to mean-square atomic displacements), is characteristic of atomic size-effect distortions. In the classical 'size-effect', local lattice relaxation results in neighbouring atoms moving in towards the smaller atoms of a binary mixture or away from the larger atoms, the strain field being propagated outward relatively large distances along rows of atoms. In the present case, however, a second feature of the pattern, in the form of characteristic 'bow-tie' shaped regions of scattering, displays a polarization and azimuthal variation that can only be explained if the distortions in two orthogonal directions (e.g. [1 1 0] and [1 -1 0]) are out of phase. That is to say, if an atom tends to push away a neighbour in the [1 1 0] direction, then the corresponding neighbour in the [1 -1 0] direction is drawn inwards, and vice-versa. We have demonstrated with a simple 2D model system that, with this thesis, each of the different diffraction effects noted in observed patterns can be obtained.

14V-59

X-RAY STUDY OF PHASE TRANSITION IN C_{60} SINGLE CRYSTAL

H.Kasatani & H. Terauchi, School of Science, Kwansei-Gakuin
University, Nishinomiya 662, Japan, and
Y. Hamanaka & S. Nakashima, Faculty of Engineering, Osaka University,
Suita 565, Japan.

The discovery of a C_{60} molecule (Kroto, Heath, O'Brien, Curl & Smalley, 1985) and a method for synthesizing solid C_{60} [buckminsterfullerene] (Kratschmer, Lamb, Fostiropouls & Rhuffman, 1990) has inspired many studies in the physical and chemical properties of this new form of carbon. At room temperature, the pure C_{60} crystal has a face-centered cubic (fcc) Bravais lattice with a high degree of rotational disorder. With decrease in temperature, this rotation slows down. High-resolution synchrotron X-ray powder diffraction experiments conducted by Heiney et al. (1991) showed that the C_{60} crystal undergoes a weak first-order phase transition at 249K, where the crystal is transformed from the fcc structure of the orientationally disordered state of C_{60} molecules to a simple cubic (sc) structure of the orientationally ordered state. The space group of the sc structure is $Pa3$ as commented by Sachidanandam & Harris (1991).

Here, we carried out X-ray diffraction experiments on single-crystal C_{60} at temperatures from 300K to 14K. A small jump in the lattice parameter was observed at the transition temperature T_c=260K, implying that this was a first order transition. The integrated intensity of new Bragg reflections observed below T_c, which corresponded to the order parameter transformed from the orientationally disordered state to the orientationally ordered state, was proportional to the anomalous part of the lattice parameter.

We wish to thank Professor H. Shinohara for providing us with purified C_{60}.

Kroto, H. W., Heath, J. R., O'Brien, S. C., Curl, R. F. & Smalley, R. E., (1985). *Nature (London)* **318**. 162-163.
Kratschmer, W., Lamb, L. D., Fostiropouls, K. & Huffman, D. R. (1990) *Nature (London)* **347**. 354-358.
Heiney, P. A., Fischer, J. E., McGhie, A. R., Romanow, W. J., Denenstein, A. M., McCauley, Jr., J. P., Smith, III, A. B. & Cox, D. E. (1991) *Phys. Rev. Lett.* **66**. 2911-2914.
Sachidanandam, R. & Harris, A. B. (1991) *Phys. Rev. Lett.* **67**. 1467.

14V–60

CRYSTALLINE STATE RACEMIZATION OF A BULKY CHIRAL GROUP

Y. Sakai and Y. Ohashi, Department of Chemistry, Tokyo Institute of Technology, O-okayama, Meguro-ku, Tokyo 152, Japan, Y. Arai and Y. Ohgo, Niigata College of Pharmacy, Kamishin-ei-cho, Niigata 950-21, Japan, and N. Kamiya and H. Iwasaki, The Institute of Physical and Chemical Research, Wako, Saitama 350-01, Japan

A new type of bulky chiral group, 1,2-dimethoxycarbonylethyl group, of two cobaloxime complex crystals has been found to be racemized on exposure to a Xe lamp without degradation of the crystallinity. For the complex with diphenylmethylphosphine as an axial base ligand, three-dimensional intensity data were rapidly collected several times irradiating the crystal with a Xe lamp on a new diffractometer (IPD-WAS). The analyzed structures clearly indicate that the racemization occurs step-by-step and that the unstable intermediate structure appears during the reaction (Fig.1.). For the complex with pyridine as an axial base ligand, similar stepwise racemization was observed although the reaction rate was very slow. For the complexes with (S)-1-phenylethylamine, (R)-1-phenylethylamine and 1-propylamine, such a crystalline-state racemization has not been observed. These crystal structures were compared with those of the above two reactive crystals. The cooperative motion of the two reactive groups in a crystal and enough size of the cavity for the reactive group seem to be essential for the racemization.

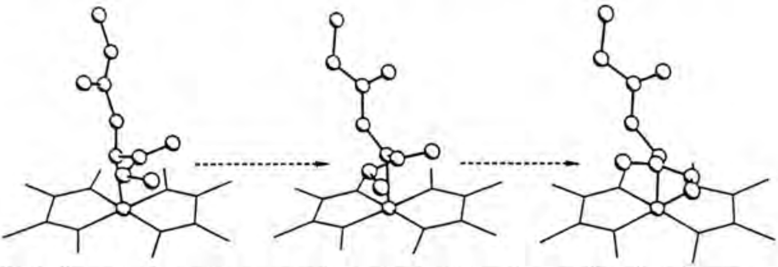

Fig.1. Stepwise inversion process of the chiral 1,2-dimethoxycarbonylethyl group

14V–61

X–RAY DIFFRACTION STUDY ON THE PHASE RELATION OF $BaZnGeO_4$

S. Takai, T. Atake, N. Ishizawa and F. Marumo, Res. Lab. Eng. Mater., Tokyo Inst. Tech., 4259 Nagatsuta-cho, Midori-ku, Yokohama, 227 Japan and A. Hamano, Sumitomo Metal Ind., Ltd. 1-3 Nishinagasu-Hondori, Amagasaki, 660 Japan.

Low temperature X-ray precession photography for $BaZnGeO_4$ of the crystal size of 0.2 – 0.8 mm in diameter has been carried out and a revised phase relation is proposed as shown in Fig. 1. The symmetry of phase VI, which appeared by holding the crystal larger than 0.2 mm in the temperature range 100 – 160 K for several hours (Hamano, Atake & Saito, 1989), was determined to be hexagonal with the lattice constants of $a = 5.32$ Å and $c = 8.73$ Å at 145 K. The diffraction pattern is essentially the same as that of phase I in the a_1^*-a_2^* plane, while the c-length is tripled. After holding the crystal in the temperature range 100 – 160 K for several weeks, the X-ray diffraction pattern at room temperature was found to be different from that of phase III. This new room temperature phase is considered to be hexagonal with the space group of $P6_3$ or $P6_3/m$, $a = 10.68$ Å and $c = 8.69$ Å at about 300 K. The a-length is doubled in comparison with phase I and the c-length is 1 % smaller than that of the sub-cell of phase III at 300 K. The new room temperature phase seems to be irrelevant to the sequence of the phases II-III-III'-IV-V, as they all have structures of tripled repetition along the ⟨110⟩ direction of phase I. The diffraction pattern of this new room temperature phase was retained even at 145K, whereas the crystal reversed to phase III by annealing at 1273 K.

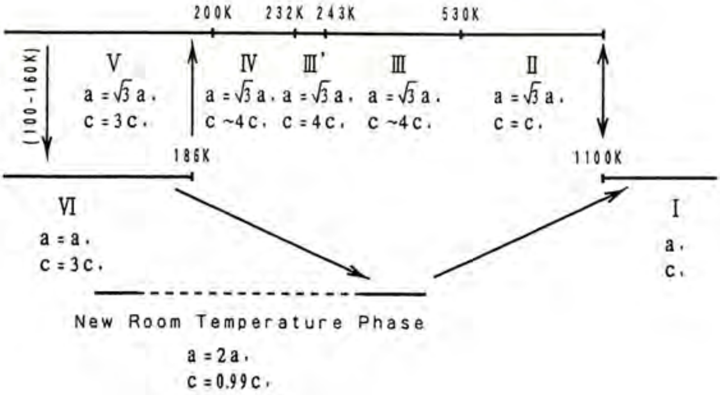

Fig. 1 Phase relation of $BaZnGeO_4$.

Hamano, A., Atake, T. & Saito Y. (1989). *Appl.Phys.* **A49**, 91-94.

14V-62

DETERMINATION OF DOMAIN DISTRIBUTIONS AROUND CUBIC-TETRAGONAL PHASE TRANSITIONS

T.Koga, N.Aomine, Z.Lu, Y.Soejima and A.Okazaki, Department of Physics, Kyushu Universlty 812, Japan.

In a single-crystal specimen of cubic crystals, three kind of domains appear when the crystal undergoes a cubic-to-tetragonal phase transition. Relative volumes of those domains can be determined, in principle, from the relative intensities at appropriate reciprocal-lattice points which are equivalent in the cubic phase. By high-resolution X-ray diffraction, we can separately observe relevant reflections which are overlapped in conventional measurements; we can then unambiguously determine the relative volumes. The only difficulty in a technique such as high-angle double-crystal X-ray diffractometry (HADOX) is limited freedom of motion of a specimen crystal. The problem is now solved by introducing into HADOX a combination of a four-circle goniometer and a refrigerator type of cryostat, and by taking advantage of the crystal symmetry. An application has been made to the 105 K transition in $SrTiO_3$: the reciprocal-lattice points 400, 040 and 004 in the cubic phase were successively traced around $\theta \approx 82$ with $FeK\alpha_1$ radiation. It is found that, when the temperature approaches the transition, the relative volumes of the domains varies so remarkably in some cases that one of the three kinds of domains nearly disappears. An anomalous variation of peak profiles observed in the previous HADOX experiment by Ohama et al. (1984) can be explained by the behaviour mentioned above.

Ohama, N., Sakashita, H. & Okazaki,A.(1984) *Phase Transitions* **4**, 81-90.

14V-63

CHIRAL-TO-RACEMIC TRANSFORMATION IN A COBALOXIME CRYSTAL ON EXPOSED TO VISIBLE LIGHT

Takashi Nemoto and Yuji Ohashi, Department of Chemistry, Tokyo
Institute of Technology, O-okayama, Meguro-ku, Tokyo 152, Japan

The crystal of (R-1-cyanoethyl)(piperidine)cobaloxime has space group $P2_12_12_1$ with two crystallographically independent molecules, A and B, in the asymmetric unit.1) The racemic crystal has a structure isomorphous to the chiral one, in which the cyanoethyl group of the B molecule (B ce group) has the opposite configuration to the A ce group. When both crystals, chiral and racemic, were exposed to visible light, the B ce group was gradually changed to the disordered racemates whereas the A molecule remained unaltered.2) This means that the racemic crystal was converted to the partly racemized one. In order to examine the disordering process of the B ce group more quantitatively, crystals with different R:S compositions were made.

As shown in Table 1, crystal 1 was obtained from a solution containing R and S complexes with the ratio of 50:50. Crystals 2 to 6 were also obtained from solutions with 56:44 to 100:0. Crystal structures of 2, 3 and 4 were determined. The ratio of R:S in each crystal differs slightly from that in solution. Table 1 also gives the cell dimensions for the six crystals. The *a* and *V* values of have maxima at the ratio of 75:25, which is the final stage if the chiral and racemic crystals were exposed to visible light. Each crystal has been exposed to a Xe lamp and crystal structure determination after irradiation is in progress.

Table 1.

sample	1	2	3	4	5	6
R:S/X-ray	—	55:45	66:34	75:25	—	—
/Solution	50:50	56:44	69:31	78:22	90:10	100:0
a/Å	11.682(4)	11.708(5)	11.733(2)	11.745(4)	11.733(4)	11.739(6)
b/Å	30.704(6)	30.684(5)	30.771(9)	30.844(4)	30.914(3)	31.055(4)
c/Å	11.395(6)	11.401(5)	11.412(4)	11.390(4)	11.340(3)	11.303(4)
V/Å^3	4087(3)	4096(2)	4120(3)	4126(2)	4105(4)	4120(3)
R	—	0.057	0.073	0.077	—	—

1) Osano, T.Y., Danno, M., Uchida, A., Ohashi, Y.(1991) *Nature* ***352***, 510-512
2) Osano, T.Y., Uchida, A., Ohashi, Y.(1991) *Acta Cryst.* ***B47***, 702-707.

14V–64

PHOTOISOMERIZATION RATES BEFORE AND AFTER REVERSIBLE THERMAL PHASE TRANSITIONS

Hiroaki Tatsuki, Akiko Sekine and Yuji Ohashi

Department of Chemistry, Tokyo Institute of Technology, O-okayama, Meguro-ku, Tokyo 152, Japan

It has been found that the 2-cyanoethyl (2-ce) group bonded to the cobalt atom is isomerized to 1-cyanoethyl (1-ce) group in some cobaloxime complexes on exposure to visible light in the solid state. Many cobaloxime crystals with the 2-ce group were prepared replacing the axial base ligand with the other amines or phosphines. The isomerization rates of the crystals were well explained by the reaction cavity for the 2-ce group. Among the crystals, the complex with 4-methylpyridine as an axial base ligand, exhibits a reversible single crystal-to-single crystal thermal phase transition at 343K. In order to examine whether or not the reaction rates and the cavity volumes before and after the phase transition are different to each other, the structure determination and measurement of the isomerization rate were performed at 341 and 346K. Table 1 shows the crystal data at 341 and 346K. Figure 1 shows the crystal structures at the two temperatures. The cavity volumes are 9.58 and 12.80Å^3 for at 341K, and 13.32Å^3 for at 346K. The measurement of the isomerization rate is now in progress.

Table 1. Crystal data

	341K	346K
Formula	$C_{17}N_6O_4H_{25}Co$	$C_{17}N_6O_4H_{25}Co$
F.W.	436.36	436.36
a/Å	30.18(2)	32.152(4)
b/Å	9.058(5)	8.918(5)
c/Å	17.16(1)	8.866(4)
β/°	124.21(4)	126.23(2)
V/Å^3	4007(5)	2051(2)
Z	8	4
S.G.	$P2_1/a$	$P2_1/a$
Dx/g cm^{-3}	1.447	1.413

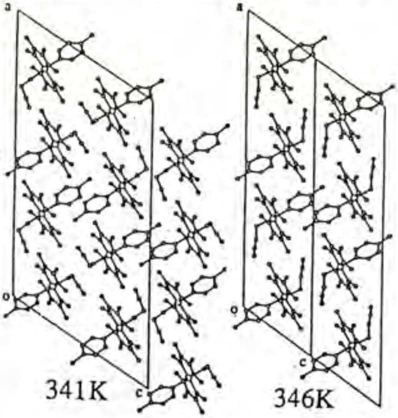

Figure 1. Crystal structures viewed along b axes

14W-66

STRUCTURAL FEATURES IN SOME RAPIDLY SOLIDIFIED ALUMINIUM ALLOYS

Lecong Dzuong, Ha Thanh Binh, Le Duc Lap, Nguyen Thanh Do,
Materials Science Center, Hanoi Technical University, Truong
DHBK Hanoi, Vietnam.

The influence of rapid solidification with moderate cooling rates of 10^2 ...10^4 K.s^{-1} on microstructure was studied for A-Mg and A-Cu based alloys containing a considerable amount of manganese. The microsegregation, the specific morphology of secondary phases, and the high density of lattice defects were important factors in as cast structure of the alloys. The precipitation process of the supersaturated solid solution occurred in a complicated manner.

14W–67

GROWTH OF PURE CADMIUM IODIDE CRYSTALS AND STUDY OF LASER INDUCED CRACKS IN THEM

S.K.Chaudhary, University College, M.D.University,
Rohtak-124001 (INDIA).

The single crystal cadmium iodide is characterized by a marked polytypism i.e. the ability of a substance to crystallize in various polytypic modifications. The crystal lattice of these polytypes is formed by structurally identical, yet translationally non-equivalent layer packets. Each layer packet forms a sandwich structure that consists of three monolayers of atoms I-Cd-I. The bonding in an I-Cd-I layer is largely ionic while that between the sandwich is predominantly Vander Waals.

For the purification of material and growth of CdI_2 crystals, a zone-refining system has been fabricated in our laboratory. The process of refinement was carried out in the atmosphere of argon which helped to prevent any oxidation of the material. Complete purification necessitated 10 Zone-passes. The atomic absorption-spectroscopic technique was exploited to check the purity. Crystals measuring nearly 1 inch in length have been grown successfully. The XRD oscillation photographs were employed for structure identification. A pulsed Nitrogen laser was used to irradiate the crystals at room temperature. The development of cracks when exposed to laser beam have been discussed on the basis of structural considerations of CdI_2.

14W-68

VAPOUR GROWTH AND CHARACTERIZATION OF CADMIUM CHLORIDE DOPED CRYSTALS OF CADMIUM IODIDE

Ritu Dhingra and G.C. Trigunayat, Department of Physics and Astrophysics, University of Delhi, Delhi - 110007, INDIA.

Horizontal zone refining technique has been employed for the purification of cadmium iodide. Single crystals of cadmium chloride doped cadmium iodide have been grown from the vapour phase. The crystals have been characterized by X-ray diffraction methods. The doped crystals have shown the formation of rhombohedral polytype 12R along with the common polytype 4H of CdI_2 in about 40% of the cases. This is in sharp contrast with the earlier findings of undoped crystals of cadmium iodide (grown by vapour deposition) which contained the 4H polytype exclusively. Streaking also occurs in three fourths of the oscillation photographs, with arcing in 30% of the cases. These observations are explained on the basis of thermodynamic considerations and the kinetics of crystal growth.

14W-69

GROWTH AND CHARACTERIZATION OF $CdBr_2$ DOPED GROWTH AND CHARACTERIZATION OF $CdBr_2$ DENDRITIC SINGLE CRYSTALS OF CdI_2

Binay Kumar and G L Bhalla, Sri Ram Institute for Industrial Research,
19 University Road, Delhi-7 and
G C Trigunayat, Dept. of Physics and Astrophysics, University of Delhi,
Delhi-110007, India.

Dendritic single crystals of $CdBr_2$ doped cadium iodide have been grown in vacuum. X-ray diffraction methods have been employed to characterise the dendrites for their polytypism and related behaviour. The surface growth features have been studied by optical and scanning electron microscopy. The crystals are fairly transparent and of lateral size up to 6*3mm. The X-ray diffraction studies have shown the occurrence of 4H(thermodynamically stable structure of CdI_2) and 12 layered rhombohedral polytype 12R. The microtopographic studies have revealed many interesting features on the crystal surface. It is observed that the growth is by two dimensional nucleation and not by spiral growth. The observed polytypes and related phenomena like streaking and arcing have been discussed in terms of various faults developed in the host structure by cadmium bromide doping.

14W-70

EPITAXIAL $BaTiO_3$ CRYSTALS I ON $SrTiO_3$ SUBSTRATES

H.Terauchi, Y.Yoneda, Y.Watanabe, H.Kasatani & K.Kamigaki, Dept of
Physics, Kwansei-Gakuin University, Nishinomiya 662,
Y.Yano, Research Institute of Production Development, Kyoto 606,
T.Terashima and Y.Bando, Institute for Chemical Research,
Kyoto University, Uji 661, Japan.

The polarization of small ferroelectric particles or thin film behaves differently compared to that in bulk crystals. Recently the preparation of high-quality thin films has been achieved (Terashima et al. 1990). Here we report results of an X-ray study of ultra-thin $BaTiO_3$ films with thickness ranging from 60A to 1500A. The films were grown on $SrTiO_3$ substrates using the activated reactive evaporation method. The ultra-thin crystal shows a large contraction along the a-direction and a large expansion along the c-direction due to a strong epitaxial effect. The lattice parameter a increases and the parameter c decreases with increasing thickness t of the thin crystal. The tetragonality, $\Delta = c/a - 1$, is found to be

$$\Delta = \Delta_0 \exp[\,-t/t_0\,], \qquad t_0 = 87.1\ \text{Å}\ .$$

Below t_0, the lattice parameter a becomes too small to fit that of the $SrTiO_3$ substrate. The mismatch between $BaTiO_3$ and $SrTiO_3$ is taken up in the strain of thin $BaTiO_3$. The temperature dependence of the lattice parameters was examined in order to clarify the nature of the phase transitions in our thin crystals, but there were no evidence of phase transitions in the temperature range 15K to 670K, where the $BaTiO_3$ lattice remained tetragonal or nearly cubic (Terauchi et al. 1992). This anomalous behaviour of our thin ferroelectric films will be discussed in term of a surface layer effect, as well as an effect of ionic or electric space charge.

Terashima, T., Bando, Y., Iijima, K., Yamamoto, K., Hirata, K., Hayashi, K., Kamigaki, K. & Terauchi, H. (1990) *Phys. Rev. Lett.* **65**, 2687-2690.
Terauchi, H., Watanabe, Y., Kasatani, H., Kamigaki, K., Yano, Y., Terashima, T. & Bando, Y. (1992) *J. Phys. Soc. Jpn.* **61** No.7.

14W-71

EPITAXIAL BaTiO3 CRYSTALS II ON [Pt/MgO] SUBSTRATES

Y.Yoneda, H.Yabuno, H.Kasatani & H.Terauchi, Department of Physics, Kwansei-Gakuin University, Nishinomiya 662 Y.Yano, Kyoto 606,
T.Terashima and Y.Bando, Institute for Chemical Research, Kyoto University, Uji 661, Japan.

$BaTiO_3$ film will show phase transitions differing from those in the bulk. Because of the effect of substrates interesting phase transitions will occur in films. Thin films were grown on MgO substrates. X-ray diffraction patterns in $BaTiO_3$ films were measured to clarify their properties such as the temperature dependence of the lattice parameter. At room temperature the lattice parameter a of bulk $BaTiO_3$ is 4.034Å and the parameter c is 3.993Å, and the lattice constant of MgO is 4.211Å. The mismatch is about 4 %. The epitaxial relation is MgO(1 0 0)// $BaTiO_3$(1 0 0).

In the case of MgO(1 0 0) substrates we use Pt (lattice constant = 3.933Å) as a buffer. Good quality $BaTiO_3$ thin films were grown on the Pt-coated substrates (Iijima et al. 1990). $BaTiO_3$ thin films on [Pt/MgO] were prepared by activated reactive evaporation method with several thicknesses from 66Å to 4000Å (Iijima et al.), in which we made certain that films were grown as single crystals. From X-ray measurements of lattice parameters of $BaTiO_3$ films, it is found that $BaTiO_3$ shows thermal expansion changes with film thickness in the temperature range room temperature to 800K. The results indicate that thin films have some bulk $BaTiO_3$ properties because of the effect of the Pt buffer layer. We will report experimental results of $BaTiO_3$ single-crystal-films on [Pt/MgO(1 0 0)] substrates.

Iijima, K., Terashima, T., Yamamoto, K., Hirata, K. & Bando, Y. (1990) *Appl. Phys. Lett.* **56**. 527-529.
Iijima, K., Terashimaj T., Bando, Y., Kamigaki, K. & Terauchi, H. J. *Appl. Phys.* (to be published)

14W-72

CHARACTERIZATION OF BARIUM TITANATE POWDER PREPARED BY CHEMICAL PRECIPITATION

T. Tunkasiri and G. Rujijanaqul., Department of Physics, Faculty of Science Chiang Mai University, Chiang Mai. 50002. Thailand.

Barium titanate powder was prepared by chemical precipitation. A solution of barium chloride and titanium tetrachloride in 1N hydrochloric acid was slowly added to aqueous oxalic acid (heated to 80 - 85 C). Barium titanyl oxalate tetrahydrate precipitated. This was filtered, dried and then annealed to yield barium titanate powder. Annealing was carried out for one hour. The effects of various temperatures, from 700 C to 1400 C in steps of 100 C, were examined by X-ray diffraction and differential thermal analysis. The ratios of lattice parameters, *c*/*a*, were determined by least squares methods. Results showed that for annealing temperatures less than 1100 C, the barium titanate formed in a cubic perovskite phase. However for temperatures above 1100 C, the product formed in a tetragonal phase. Microstrain was reduced by increasing the annealing temperature. The crystallite size was found to increase with the annealing temperature.

1. Wagner, C.N.J. (1966). *"Local atomic arrangements by X-ray Diffraction"* Gordon & Breach, New York.
2. Fu-Sen, Chen T. Chang, and Yen-Hwei Chang. (1990). *J. Am. Cerm. Soc.*, **73**[11] 3422-27

14W-73

HYDROTHERMAL SYNTHESIS AND STRUCTURAL CHARACTERIZATION OF $A_{0.5}VOPO_4.yH_2O$ (A-ALKALI, ALKALINE EARTH, AND TRANSITION METALS)

K. H. Lii, Institute of Chemistry, Academia Sinica, Taipei, and H. Y. Kang and S. L. Wang, Department of Chemistry, National Tsing Hua University, Hsinchu, Taiwan, Republic of China

In 1983, Johnson and Jacobson prepared a series of compounds $A_xVOPO_4 \cdot yH_2O$ by redox intercalation reactions of $VOPO_4 \cdot 2H_2O$ with metal iodides in aqueous solution. These are the first intercalation reactions in which the charge transfer proceeds chemically but not electrochemically. Further investigation on these interesting compounds appeared in several other reports. On the basis of powder X-ray diffraction, it was reported that the basic tetragonal structure of $VOPO_4 \cdot 2H_2O$ was essentially maintained and cations were incorporated into the interlayer spaces. Detailed structural information has been unavailable due to the lack of suitable single crystals for X-ray analysis. We have now found that crystals of $A_{0.5}VOPO_4 \cdot yH_2O$ can be grown under hydrothermal conditions. In this paper, we report the hydrothermal synthesis and structural characterization of six vanadyl phosphate hydrates $A_{0.5}VOPO_4 \cdot yH_2O$ (A = Na, Ca, Sr, Co, y = 2; A = K, Ni, y = 1.5). Their structural relationships will also be discussed.

14W-74

THE DEFECT SUBSTRUCTURES AND MECHANICAL PROPERTIES OF MULLITE PREPARED BY COPRECIPITATION

Shu-Cheng Yu* and Jiann-Shing Lee**
* Department of Earth Sciences
** Institute of Mining, Metallurgy and Materials Science National Cheng Kung University, Tainan, Taiwan 70101 Republic of China

Mullite and ZrO_2-mullite were prepared using co-precipitation with $ZrO(NO_3)_2$, $Al(N0_3)_3$ and silica sol as precursor materials. With two-beam conditions in an electron microscopy study, dislocations of ZrO_2-mullite(15wt%ZrO_2) with Burgers vectors in [001] and [213] directions were observed. The former dislocation is much more abundant in defect density than the latter. The prevailing dislocations with Burgers vector parallel to the *c*-axis in mullite is consistent with the fact that [001] is a prominent direction for chains of AlO_6 octahedra and double chains of $(Al,Si)O_4$ tetrahedra in mullite structures.

Mechanical property measurements on mullite with various ZrO_2 concentrations were also made. The result indicates that Vickers hardness, flexure strength and flexure toughness are all significantly improved for ZrO_2-mullite. With ZrO_2 content in mullite increased from O to 30%, Vickers hardness was found to increase from 11.1 to 13.2 GPa; flexure strength from 346 to 551 MPa and flexure toughness from 1.88 to 3.92 MPa-$m^{-1.5}$. In contrast, the Young's modulus was decreased from 190 to 168 GPa with increasing ZrO_2 content in mullite. Measurements on mechanical properties for mullite without ZrO_2 but with different $A1_2O_3/SiO_2$ ratios were also carried out. The data show that both flexure strength and flexure toughness were independent of the $A1_2O_3$ concentration in mullite.

14W-75

METHOD TO CONTROL MICROSTRUCTURE BY MEANS OF THE ELECTRON CHANNELING PATTERN (ECP) IN THE PRESENCE OF SUPPRESSING CONTRAST FORMING MECHANISMS

A.N. Efimov, A.F. Ioffe Physical-Technical Institute, Sankt-Peterburg, 194021, Russia

Microstructural characterization of crystalline objects by ECP provides a unique possibility for obtaining information about symmetry, crystallographic orientation and lattice parameters. High spatial resolution (10 nm) and non-destructive control of the crystallographic parameters makes this technique extremely convenient for micro-structural characterization. However, when objects with inhomogeneous structures are investigated, contrast necessarily occurs due to effects arise other than diffraction contrast.

In this study the diffraction component of the contrast was extracted by slightly varying the electron wavelength. The formation of the difference signal allowed us to reduce the contribution to the final signal of components not concerned with the crystalline perfection of the structure significantly. This is possible due to the fact that only diffraction angles depend significantly on the electron wavelength, leading to the displacement of ECP. The system of registration is based on the lock-in technique. The resulting difference signal is fed to the visual display unit.

Investigation of various objects with inhomogeneous structures showed high efficiency of the selective diffraction contrast formation.

14W-76

LATTICE METRIC MATCH AT HETEROEPITAXY: CASE OF NON-CUBIC CRYSTALS

A.N. Efimov, A.O. Lebedev, A.F. Ioffe Physical-Technical Institute,
Sankt-Petersburg, 194021, Russia

Traditionally active materials for microelectronics crystallize in the cubic system. For a cubic substrate, strict coincidence of lattice parameters is needed to create the transient region without defects. This should be possible by choosing the correct substrate or by using solid solutions when the dependence "composition - lattice parameter" is utilized. Both lattice parameter correspondence and coincidence of thermal expansion coefficients are possible for multi-component solid solutions.

Unfortunately, active materials used in modern functional (opto-, acousto-, HTSC-)electronics belong to both cubic and non-cubic systems. In the general case the modified lattice metric match is:

$$a_1=a_2,\ b_1=b_2,\ c_1=c_2,\ \alpha_1=\alpha_2,\ \beta_1=\beta_2, \gamma_1=\gamma_2 \qquad (1)$$

where $a,b,c,\alpha,\beta,\gamma$ are unit cell parameters; subscript $_1$ denotes epilayer, $_2$ denotes substrate.

It is impossible to find pairs of compounds satisfying all conditions (1) in practice. Altering solid solution composition makes feasible only one condition. The right choice of substrate orientation allows the inter-facial region "layer-substrate" to be created without topological defects if the following two conditions are fulfilled:

$d=ABC+2DEF-BE^2-CD^2-AF^2=0$ (2) ; $j=AB+BC+CA-D^2-E^2-F^2\leq 0$ (3)

where: $A=a_2^1-a_2^2$; $B=b_2^1-b_2^2$ $C=c_2^1-c_2^2$;

$D=a_1b_1\cos\gamma_1-a_2b_2\cos\gamma_2$;$E=c_1a_1\cos\beta_1-c_2a_2\cos\beta_2$; $F=b_1c_1\cos\alpha_1-b_2c_2\cos\gamma_2$

Angles and bond lengths for inter-facial atoms vary, but the changes are small if the difference between metrics of layer and substrate is small too. It should be pointed out that only condition (3) must be carried out strictly. Inequality (2) is a condition that enables the number of possible crystal combinations to be reduced.

So, if conditions (2,3) are fulfilled for a particular composition for a two-component solid solution, the defect-free interface can be created. Additionally, for any given pair of crystals the probability of satisfying is (2) and (3) is much higher than that for the six conditions (1).

Recommendations on the choice of metrically-matched substrate for HTSC-material growth based on the above statements will be presented.

15A–1

HIGH-RESOLUTION ELECTRON MICROSCOPY

K. Hiraga, Institute for Materials Research, Tohoku University,
Katahira, Aoba-ku, Sendai 980, Japan

The use of high-resolution electron microscopy has been extended to a wide range of natural sciences with the development of the resolving power of electron microscopes in the last two decades. In this paper, I will illustrate the capability of high-resolution electron microscopy for crystal structure analysis using results for high-Tc superconducting oxides (Hiraga, Shindo, Hirabayashi, Kikuchi, Kobayashi and Syono, 1988) and for quasicrystals (Hiraga and Sun, 1992). High-resolution images of the high-T_c superconductors, taken with an electron microscope having a resolution of 0.17 nm, make it possible to determine atomic arrangements of heavy atoms directly, atom positions to an accuracy of 0.0lnm, and positions of oxygen vacancies. Some materials with unknown structures, which are hard to prepare as single phases and single crystals, have been studied successfully. For quasicrystals with nonperiodic arrangements of atoms, high-resolution images show that the structures of the quasicrystals are formed by aggregation of atom clusters, enabling us to determine not only long-range correlations of the atom clusters in wide regions, but also the atomic arrangements in the atom clusters.

I will demonstrate that high-resolution electron microscopy exhibits its full power for crystal structure analysis when combined with diffraction methods.

Hiraga, K., Shindo, D., Hirabayashi, M., Kikuchi, M., Kobayashi, N. & Syono, Y. (1988). *Jpn. J. Appl. Phys.* **27**, L1848-Ll851 .

Hiraga, K. & Sun, W. (1992). *Philo. Mag. Lett.* in press.

15A–2

X-RAY AND ELECTRON DIFFRACTION FROM TWISTED QUARTZ CRYSTALS

M. Fehlmann, Institute of Crystallography, Swiss Federal Institute of Technology, ETH-Zentrum, CH-8092 Zurich, Switzerland, and A.F. Moodie, Department of Applied Physics, Royal Melbourne Institute of Technology, Melbourne, VIC 3001, Australia.

For over one hundred years, crystallographers and mineralogists have wondered about the origin of the twisting in 'Quindelquartzes'. It has been ascribed to twinning as well as to screw dislocations.
With conventional X-ray Laue diffraction, we have been able to confirm that the microscopic twisting corresponds to the macroscopically observed twists. White beam synchrotron radiation topography indicates that neither dislocations nor twinning can be responsible for the twisting. A suggestion by Kozlova & Belov (1981) that Brazilian type micro-twinning be the cause of the twisting must be rejected for several reasons (Laue diffraction, topography, electron microscopy, optical activity).
Using electron microscopy we have inspected a number of different samples. So far, we have observed a single twin boundary and occasionally a dislocation. But judging by the very low density of these defects we must conclude that they are not responsible for the bending, the more so because the crystals are uniformly bent in defect-free regions. 'Selected Area Diffraction' (SAD) does not reveal any clues as to the origin of the twists. We cannot observe any defects in 'Large Angle Convergent Beam' micrographs either. Conventional 'Convergent Beam Electron Diffraction' (CBED) pictures, however, show that the symmetry of the crystal (see *e.g.* Johnson, 1972) is indeed trigonal. The likelihood that crystal bending will influence the CBED patterns is less than in SAD patterns, because the volume of specimen contributing to it is so much smaller.

Kozlova, O.G. & Belov, N.V. (1981) *Sov. Phys. Dokl.* **26**, 805.
Johnson, A.W. (1972), *Acta Cryst.* **A28**, 89-91.

15A–3

ELECTRON MICROSCOPE STUDY OF INCOMMENSURATE LATTICE MODULATION IN LAYERED COMPOSITE CRYSTAL PbS-VS_2

N. Yamamoto, K. Akiyama and K. Yagi, Tokyo Institute of Technology,
Oh-okayama, Tokyo 152, Japan, and
Y.Gotoh and Y. Oosawa, National Chemical Lab. for Industry
Tsukuba, Ibaraki 305, Japan

PbS-VS_2 is a composite crystal which is made up of alternative stacking of NaCl-type PbS layers and CdI_2-type VS_2 layers. The PbS and VS_2 layers have common lattice parameters along the *a* and *c* axes, but different ones along the *b* axis, i.e., $b_1/b_2=1.74$. The interaction forces between the two layers cause atomic displacements with a lattice period in the neighbouring layer, which result in an incommensurately modulated lattice in each layer (Onoda (1990)). From an analyses of the extinction of diffraction spots and convergent beam electron diffraction patterns, a super-spacegroup of the crystal is determined to be $P^{C2}_{\;1}$. In order to avoid multiple diffraction from the fundamental reflections to the satellite ones, a diffraction pattern in the (100) orientation is compared with a calculation by the multi-slice method. We propose a new model for the lattice modulation which gives a good fitting with the observed intensity distribution for the satellite reflections.

Onoda, M Kato, K. Gotoh, Y. & Oosawa, Y.(1990) Acta Cryst B**46**, 487-492.

15A–4

HIGH–RESOLUTION EELS STUDY OF THE ELECTRONIC STRUCTURES OF SEMICONDUCTORS CONTAINING LATTICE DEFECTS

M.Terauchi and M.Tanaka, Research Institute for Scientific Measurements, Tohoku University, Katahira 2-1-1, Aoba-ku, Sendai 980, Japan.

We have studied the effect of lattice defects on the electronic structures of Si and GaAS using the high-resolution electron energy-loss spectroscopy (EELS) microscope, which is equipped with two Wien filters as the monochrometer and the analyzer.

The energy-loss spectra were obtained from specified specimen areas of 1800Å in diameter of Si containing dislocations with an energy resolution of 90meV. The spectra showed three features different from the spectra obtained from perfect specimen areas. Firstly, there exist the additional energy-loss peaks originated from dislocations below the onset energy (band-gap energy) of perfect Si. Secondly, high intensity was observed in an energy region between about 1eV (onset energy) and about 2eV, whereas the spectra of perfect Si did not show such high intensity because the direct interband-transition does not exist in this energy region. Thirdly, two of nine peaks due to the interband transitions, which were observed at the shoulder of the broad volume-plasmon peak, were shifted to the lower energy side from those of perfect Si, other peaks being not shifted. These results clearly showed the influence of dislocations on the electronic structure of Si.

The energy-loss spectra of as grown GaAs were obtained with an energy resolution of 58meV. The spectra showed a lower onset energy of the interband transition than a band gap energy of 1.4eV and exhibited a specific structure near the onset energy. Those features may be due to the anti site defects of EL2.

Those spectra obtained from Si and GaAs will be discussed with the strain fields and the energy-band structures.

15B-1

CRYSTAL STRUCTURE ANALYSES OF THE SPHERICAL VIRUSES, TOBACCO NECROSIS VIRUS (TNV) AND RICE DWARF VIRUS(RDV).

T. Tsukihara[1], Y. Morimoto[1], K. Fukuyama[2], M. Koizumi[3], T. Omura[4], K. Kano[5], H. Mizuno[5].
[1]Faculty of Engineering, The University of Tokushima.
[2]Faculty of Science, Osaka University
[3]National Institute of Sericultural and Entomological Science, Tsukuba
[4]National Agriculture Research Center, Tsukuba
[5]National Institute of Agrobiological Resources, Tsukuba, Japan.

Tobacco necrosis virus (TNV) is a typical spherical virus. Its coat protein contains 275 amino acids. TNV crystallizes in cubic space group $P4_232$ with $a=b=c=338$ Å. Its 3.86×10^7Å^3 unit cell contains two virus particles with molecular weight 6.7×10^6, and Vm value 2.9A3/dalton. The (T=3) symmetry of TNV capsid and subunit arrangement of *180* copies of its coat protein were determined previously. X-ray diffraction intensities for a $0.7\times0.7\times0.7$ mm^3 TNV crystal were measured at 5 Å resolution on a Weissenberg camera with cassette radius 430 mm, at the Photon Factory synchrotron. The merging *R*-factor is 0.115 for 90,251 reflections with $I>5\sigma(I)$. The 27,437 ($F>3\sigma(F)$) and 24,127($F>5\sigma(F)$) independent reflections were 94% and 83% of the theoretical number. The virus crystal's structure was determined by a 91 cycle iteration of molecular replacement averaging. The correlation coefficient between calculated and observed structure factors converged to 0.92, and *R*-factor 0.16. Secondary structures such as α-helices and β–structures were clearly assigned in the 5 Å resolution electron density map. The TNV virus resembles SBMV both in the orientation and folding of the coat protein subunits. The ordered part of that subunit is shorter by 12 and the longer disordered part by 27 residues than corresponding parts of SBMV.

Rice Dwarf Virus (RDV), a phytoreovirus, from *Nephotettix* species infects rice and wheat systemically, causing stunting or dwarfing of plant bodies. The molecular weight of the double-shelled virus particle, approximately 700 Å in diameter, is 6.52×10^7. Crystallographic analysis helped reveal the double shelled structure of the virus, and the mechanism of symmetrical self-assembly of its subunits. RDV crystallized in cubic space group *I*23 with a=789Å. Two particles are on Wyckoff "a" positions in the cell. For diffraction experiments on a macromolecular Weissenberg camera at BL-6A2 in the Photon Factory, the crystal to film distance was 573mm, and wavelength 1.488Å. The incident beam, focused by double bent mirrors, was collimated to 0.lmmφ. 56096 reflections up to 10 Å were collected from one crystal The mean *R*merge for 29075 independent reflections was 10.51%. A self-rotation function indicates icosahedral symmetry for RDV.

THE CRYSTAL STRUCTURE OF NC41 ANTI-NEURAMINIDASE FAB IN ITS UNCOMPLEXED FORM

M. C. Lawrence, R. Malby, A. Kortt, V. Staton and P. M. Colman, CSIRO Division of Biomolecular Engineering / Biomolecular Research Institute, 343 Royal Parade, Parkville 3052, Victoria, Australia, and R. G. Webster, St Judes Childrens Research Hospital, Memphis, Tennessee 38101, USA.

The structure of the uncomplexed NC41 anti-neuraminidase Fab has been solved by molecular replacement from diffraction data collected at the Photon Factory, with the aim of determining what structural changes occur in the Fab on binding antigen. This work complements structural studies of the NC41 Fab in complex with influenza-virus neuraminidase (Colman *et al.*, 1987, Tulip *et al.*, 1992).

The structure of the uncomplexed Fab is surprising in that the complementarity-determining regions (CDR's) of the two molecules in the asymmetric unit abut each other across a psuedo-diad. The interface is comparable in size (*ca* 900$\mathring{A}^2$) and complementarity of fit to that observed in the complex. The interface area is considerably larger than that typical of crystal contacts, and would tend to imply dimerization and self-complementarity of the Fab in solution.

The earlier study of the Fab-antigen complex suggested that significant movement of the heavy-chain variable domain with respect to the light-chain variable domain on antigen binding. Analysis of the uncomplexed structure indicates slight differences in domain pairing compared to the complexed structure. However the extensive interaction between the Fab's in the uncomplexed crystal structure could imply that this structure is not a good representation of that found in solution.

Colman, P.M., Laver, W.G., Varghese, J.N., Baker, A.T., Air, G.M. & Webster, R.G. (1987) *Nature* **326**, 358-363.
Tulip, W.R., Varghese, J.N., Laver, W.G., Webster, R.G. and Colman, P.M. (1992) *J. Mol. Biol.* (in press).

15B–3

STUDIES ON THE STRUCTURES OF INSULIN ANALOGUES AND THE BINDING INTERACTION OF INSULIN MOLECULE WITH ITS RECEPTOR

W. R. Chang and D. C. Liang
National Laboratory of Biomacromolecules, Institute of Biophysics, Chinese Academy of Sciences, Beijing, 100101 China.

Extensive conformational comparisons among the structures determined for different species and crystal forms of insulin and its derivatives were performed using least-squares superimposition and graphics techniques. The investigation showed that the structure of molecule I in 2Zn insulin was closer to that in the natural monomer. The conformational difference between two molecules that emerged during dimerization was further improved and stabilized during the hexamerization and packing of hexamers in crystals Through the hinge peptides, such as A10, B4, B8, B24, B20 and B23, there was flexible relative motion among the structural segments in the insulin molecule. The residues at the B-chain C-terminal might shift more than 10Å. The mobility for each residue side-chain was very different due to the changed environment.

The structures of DPI, 2Zn insulin and some other derivatives of insulin were compared after investigation in detail. The binding interaction with the receptor molecule should take place mainly on an amphipathic surface of the insulin molecule. In the middle, there is a hydrophobic surface with an area of about 150Å^2 consisting of many hydrophobic residues. The polar or charged groups distributed around the hydrophobic surface construct a hydrophilic zone. The hydrophobic surface is usually covered by the extended B-chain C-terminal peptides with great mobility and is thus protected from the solvent molecules. The angle between the amphipathic surface and the surface of dimerization is about 20 degrees. The detailed structural comparison of Al-(L-Trp) insulin with Al-(D-Trp) insulin has provided a very good explanation for the great difference in their biological activities, confirming our proposed binding interaction model of the insulin molecule with its receptor.

15B–4

ENZYME SUBSTRATE INTERACTIONS: REFINED STRUCTURE OF HUMAN CARBONIC ANHYDRASE I (HCAI)-HCO_3^- COMPLEX

Vinay Kumar and K.K. Kannan, Solid State Physics Division, Bhabha Atomic Research Centre, Bombay-400085, India.

HCO_3^- anion, the substrate for reverse reaction catalyzed by Carbonic anhydrase (CA) isoenzymes, inhibits the enzyme at higher pH. The single crystal diffraction data for the complex at pH 8.7, extending to 1.6Å resolution, was collected using synchrotron radiation at the Photon Factory, Japan (Kannan et al., 1989) with R_{merge} of 8.13%. Treating the refined HCAI model (Kannan et al., 1984) without solvent molecules as the initial model the structure of the complex was refined by alternating PROLSQ cycles and model building against 'OMIT' Fourier maps on IRIS-4D graphics using TOM. The data was extended during refinement in steps from 3Å to 1.6Å resolution. The added solvent molecules and inhibitor were refined for occupancy in addition to positional and thermal parameters. The R-factor for the final model with 2023 non-hydrogen protein atoms, one HCO_3^- anion and 279 solvent molecules, against 24967 F_{obs} in the resolution shell of 10-1.6Å, is 17.3%. The rms shift for positional parameters in the final PROLSQ cycle was 0.023Å. In contrast to the initial Fourier maps, the refined structure suggests [4+1] coordination for the essential Zn(II) ion. The HCO_3^- anion binds in the vicinity of the Zn(II) ion. In addition, the imidazole ring of the H200 residue is marginally displaced in the complex structure compared to that in native HCAI. The Fourier maps computed with refined phases also reveal an alternate partially occupied binding site for the HCO_3^- anion.

The details of binding mode and interactions of the HCO_3^- anion in the active site of HCAI will be presented.

Kannan, K.K., Ramanadham, M & Jones, T.A., (1984). Ann. N.Y. Acad. Sci., **429**, 49-60.

Kannan, K.K., Vinay Kumar., Chakravarty, S & Sathyamurthi, P. (1989). Photon Factory Activity Report, Japan, **7**, 112-113.

15Y–1

ENHANCED PHASE EFFECT IN FOUR-BEAM X-RAY DIFFRACTION – DETERMINATION OF TRIPLET PHASE FROM FOUR-BEAM DIFFRACTION

Y. S. Tsai, M. T. Huang, and S. L. Chang, Department of Physics, National Tsing Hua University, Hsinchu, Taiwan, 30043, R. O. C.

Coherent interaction in multiple diffraction of x-rays is known as a clue to phase determination of structure-factor multiplets. For a three-beam (O, G, L) diffraction with a weak reflection G, the phase effect on the multiply diffracted intensity I(G) is so weak that it may not be suited for phase determination for non-centrosymmetric crystals. In this paper, we report that a strong triplet phase dependence of I(G) is observed for four-beam (O, G, L, M) cases in which M is an additional reflection to the three-beam (O, G, L) diffraction. Theoretically, the dynamical and the kinematical theories are employed to account for this observation. It is found that the intensity variation in I(G) due to the three-wave interference in the weak four-beam cases is at least an order of magnitude stronger than that in the three-beam diffraction. The origin of this enhanced phase effect on weak four-beam diffraction will be discussed in the light of dynamical theory.

15Y–2

PHASE DETERMINATION AND REFINEMENT BY DENSITY MODIFICATION – LOW DENSITY ELIMINATION

M Shiono, Department of Physics, Faculty of Science, Kyushu University, Higashi-ku, Fukuoka, 812, Japan.

A density modification technique for phase determination and refinement, which replaces all density less than one-fifth of the average peak height by zero, is presented. Its effectiveness is demonstrated by applications to small proteins. 36-amino acid Avian Pancreatic Polypeptide (App) which has 302 independent atoms has been solved with this Low Density Elimination procedure (LDE) starting from random phase sets. The method was successfully applied to phase refinement for Ribonuclease Pl: A phase set with a 74° mean phase error was refined. The final mean phase error was 50.2° after 293 cycles.

Since the procedure includes two Fourier Transforms in one cycle, it is very expensive in computation time. In order to speed up the procedure, we square the electron density instead of Low Density Elimination in the early stage of phase determination. We will also discuss possible combinations with conventional reciprocal-space direct methods.

Shiono, M. and Woolfson M. M. (1992). *Acta Cryst.* A**48** (In press).

15Y–3

RESTORING THE ORIGINAL ELECTRON DISTRIBUTION OF LIPID BILAYERS - A SIMULATION STUDY

S.Yamamura, M.Takata, M.Sakata, H.Takahashi and I.Hatta
Department of Applied Physics, Nagoya University, Furo-cho,
Chikusa-ku, Nagoya, 464-01, Japan

X-ray diffraction studies have identified a characteristic feature of lipid bilayers, i.e. both sides of each bilayer are composed of high electron density polar headgroups (PH). There are hydrocarbon chains (HC) with low electron density inside the layer. Biomembrane structure is often studied by Fourier reconstruction of the electron density from X-ray diffraction data. In most cases, only a one dimensional distribution, perpendicular to the lipid bilayer, is considered. A typical model structure and electron density for such a bilayer is shown in Fig. 1. The electron density evaluated by Fourier transformation shows rather severe termination effects because the number of measurable reflections is normally less than 10. It is of prime importance to establish better methods for reconstructing electron density distributions in biomembranes. To assist that objective, restoration of the original one dimensional electron density shown in Fig.1 from a limited number of diffraction measurements was simulated.
A Maximum Entropy Method (MEM) density evaluated initially was almost identical with that from Fourier transformation. As the map resolution is much worse than atomic scale, an MEM constraint that the density is positive everywhere does not play an important role. The MEM density improves when the method is modified to permit densities positive or negative compared to the flat density of the hydrocarbon chain – an approach resembling that used to cope with negative scattering density in neutron diffraction. It worked effectively, being able to restore the original model density with reasonable accuracy using 10 reflections as shown in Fig.2. Practical applications are under consideration.

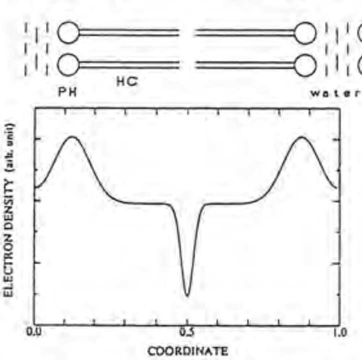

Fig.1 Model Structure and Density

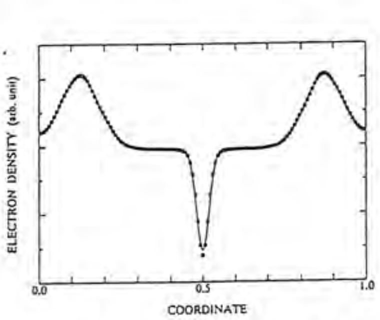

Fig.2 Reconstruction of Electron Density

15Y–4

THE ROLE OF ANOMALOUS DISPERSION IN THE COMPARATIVE REFINEMENT OF MODULATED CRYSTAL STRUCTURES

A. David Rae, School of Chemistry, University of New South Wales, Kensington 2033, Australia.

A modulated crystal structure is conveniently described as a perturbation away from an idealised parent structure. This idealised parent structure may consist of more than one coexisting substructure, each with its own unit cell and space group. The perturbations may be described as modulation waves associated with vectors in the Brillouin zones of the substructures and correspond to extra observed reflections. Options for the relative phases of modulation waves exist and these need not necessarily correspond simply to choice of origin and orientation. In real crystals some waves may be continuous throughout the crystal while others may not. This allows the possibility of stacking faults, twinning and intergrowths of components of different overall symmetry and this alters the scale of some of the various symmetrised components of the observed intensity. A hierarchical approach to refinement is necessary and an understanding of the distribution of information content is essential.

Anomalous dispersion creates correlations between modulation waves and can be used to resolve questions involving modulation wave amplitude, disorder and twinning as well as distinguishing between Friedel related reflections. These correlations may be used to initiate refinement of modulation waves starting from a zero amplitude approximation and to accentuate differences in comparative refinement statistics for alternative stable refinement minima.

Application to the refinement of the Aurivillius phase compounds Bi_2WO_6, $Bi_4Ti_3O_{12}$ and $Bi_2SrTa_2O_9$ will be outlined and a comparison of the X-ray structure of Bi_2WO_6 and the powder neutron diffraction structure of γ-Bi_2MoO_6 will be made.

15Y–5

OPTICAL TRANSFORMS

T.R.Welberry. Research School of Chemistry, Australian National University, GPO Box 4, Canberra City, ACT 2601, Australia.

The idea of using optical analogues (or Optical Transforms) to aid in the interpretation of X-ray diffraction patterns originated with Sir Lawrence Bragg round about 1938, and the method has developed considerably since that time. Prior to the advent of digital computers calculation of the diffraction pattern of even a fairly simple crystal structure was an enormous task, and use of optical diffraction from a model had obvious benefits, particularly for testing trial structures. With the advent of computers the task of obtaining a calculated diffraction pattern of an ordered crystal structure for comparison with observed measurements became a rather trivial exercise and use of the optical method for this purpose began to fall into disuse. On the other hand for the structural elucidation of disordered structures, amorphous materials and even liquids the transform method has continued to be used even though the diffraction pattern of even the most complex structural model can in principle be calculated quite readily with modern computers.

Optical Transforms are particularly useful in a teaching context where the student is able to verify for him/herself the relationship between a real-space object and its diffraction pattern. In this demonstration we present examples of optical diffraction masks, the structural details of which can be inspected with the use of an ordinary micro-fiche viewer or 35mm slide projector, and whose diffraction patterns can be observed using only simple apparatus. A varied selection of masks will be available to demonstrate the diversity of diffraction effects which may be achieved by the technique.

In recent years we have sought to develop methods to allow the routine production of optical diffraction masks (or screens) for use as aids in the interpretation of X-ray or electron diffraction patterns. We are now able to produce, rapidly and easily, an optical diffaction mask which is a good representation of almost any real diffraction problem encountered with X-rays or electrons. Among the diverse range of problems that we have studied with the aid of such diffraction masks are: short-range order in molecular crystals; size-effect distortions in alloys; thermal and disorder diffuse scattering in minerals; small-angle scattering in microemulsions; fluctuations of local order in liquids; quasi-crystals.

15C–1

COMPUTER SIMULATION OF THE STRUCTURAL AND PHYSICAL PROPERTIES OF THE $MgSiO_3$ POLYMORPHS

Masanori Matsui, Department of Earth and Planetary Sciences, Faculty of Science, Kyushu University, Hakozaki, Fukuoka 812, Japan

There are six known $MgSiO_3$ polymorphs. Of these, both enstatite (Pbca) and clinoenstatite($P2_1/c$) occur naturally. Protoenstatite(Pbcn) is stable above 1273 K at ambient pressure. The garnet($I4_1/a$), ilmenite ($R\bar{3}$), and perovskite(Pbnm) phases occur at high pressures. The purpose of the present investigation is to simulate the structural and physical properties of the six $MgSiO_3$ polymorphs using molecular dynamics(MD) method with quantum corrections to the simulated properties.

The potential energy of the crystal is approximated as the sum of Coulomb, dispersion, and repulsion interactions between atoms (Matsui & Price, 1992). Energy parameters are taken from our previous investigation. The simulated crystal structures, bulk moduli, volume thermal expansivities, and enthalpy trends are in good agreement with those observed. In addition, the simulation is successfully used to reproduce the measured (or estimated) density of the $MgSiO_3$ melt at 2000 K and 0 pressure, and its temperature and pressure derivatives.

The MD technique is further applied to the investigation of the possible existence of a post-protoenstatite phase at high temperature and another pyroxene phase with space group C2/c at high pressure, both of which have previously been inferred from experiment.

Matsui, M. & Price, G. D.(1992). Phys. Chem. Minerals 18, 365-372.

15C–2

PHOTOREFRACTIVE KNSBN CRYSTALS WITH A-SITES UNFULFILLED TUNGSTEN-BRONZE STRUCTURE

H. C. Chen, D. L. Sun and Q. Z. Jiang, Institute of Crystal Materials,
Shandong University, Jinan 250100, P R China.

This paper describes studies of new compositions of photorefractive crystals of potassium sodium strontium barium niobate (abbreviated KNSBN) which have the tungsten-bronze structure. By changing the A-site occupation with IA ions of the periodic table in the structure and doping with the ions of the first transition metal series in B-sites, the ferroelectric and photorefractive parameters of the crystals are considerably modified. Cu-doped crystals are typical examples, exhibiting excellent polarization stabilities with two-wave coupling gain coefficients as large as 20^{-1}cm. The PR sensitivity is in the order of 10^{-3}cm^2/J and the "cat" self-pumped conjugation reflectivity up to 65% with a response time of ten seconds can be reached.

15C–3

A MODULATION WAVE APPROACH TO THE STRUCTURAL PARAMETERIZATION AND RIETVELD REFINEMENT OF THE C9 – CRISTOBALITE RELATED, LOW CARNEGIEITE STRUCTURE

R.L.Withers and J.G.Thompson, Research School of Chemistry, Australian National University, GPO Box 4, Canberra, ACT, 2601, Australia.

Carnegeite, $NaAlSiO_4$, is one of a large family of materials topologically closely related to the so-called C9 structure type. Its parent crystal structure can be described as a "stuffed" derivative of the C9 structure type in which half of the cavities in the corner-connected, tetrahedral $AlSiO_4$ framework are filled with sodium atoms. The crystal structure of low carnegeite has not been solved. Indeed even its unit cell and space group symmetry have proved difficult to determine owing to the extremely sluggish kinetics of formation of fully-ordered, single-phase low carnegeite from the component oxides. Powder XRD and TEM give an orthorhombic unit cell a' = 10.261, b' = 14.030 and c' = 5.1566Å with space group symmetry of $Pb2_1a$.

Given this resultant space group symmetry, there are potentially (14 + 2) x 3 = 48 displacive degrees of freedom plus 8 compositional degrees of freedom to be refined in order to determine the structure of low carnegeite - far too many to be refined via an unconstrained Rietveld refinement. Therefore it is essential to be able to derive a plausible starting model for the structure before beginning a Rietveld refinement. In this contribution, a group theoretical or modulation wave approach is used in order to parameterize the structural deviation of low carnegeite from its underlying C9 aristotype. Appropriate crystal chemical constraints are then applied in order to provide what turns out to be two distinct plausible starting models for subsequent Rietveld refinement. The chemical plausibility of both starting models is checked via the use of the bond length-bond valence formalism and Rietveld refinement used to distinguish between the two possibilities and to give a final refined structure.

LOW CARNEGIEITE - WHY PREVIOUS ATTEMPTS TO SOLVE ITS STRUCTURE WERE UNSUCCESSFUL

J. G. Thompson and R. L. Withers, Research School of Chemistry, Australian National University, GPO Box 4, Canberra, ACT 2601, Australia, A. K. Whittaker, Centre for Magnetic Resonance, University of Queensland, QLD 4072, Australia, R. M. Traill, Department of Chemistry, Monash University, Clayton VIC 3168, Australia.

Single crystals of low-carnegieite, $NaAlSiO_4$, have not been attainable due primarily to a phase transition at ~ 940 K. Consequently it has been necessary to study powder specimens. We have reinvestigated the crystal structure of low-carnegieite by a combination of X-ray powder diffraction, transmission electron microscopy, solid-state ^{29}Si and ^{27}Al MAS NMR spectroscopy, and electron microprobe analysis. With sufficient homogenisation of component oxides and annealling at 1673 K it was possible to obtain a single crystalline phase which could be indexed to an orthorhombic unit cell: $Pb2_1a$, $a = 10.261(1)$, $b = 14.030(2)$, $c = 5.1566(6)$ Å. Electron microprobe analysis confirmed the stoichiometry to be $NaAlSiO_4$. ^{29}Si and ^{27}Al NMR spectroscopy verified the perfect Si:Al ordering.

It is now clear from the present work that previous attempts to synthesize low-carnegieite all suffered from incomplete reaction and the presence of multiple phases. Having for the first time synthesized low-carnegieite as the only crystalline phase it has been possible, using the constraints provided by group theory and bond-valence requirements, to determine the Na ordering and to refine the crystal structure using X-ray powder diffraction data.

15Z–1

HOLOGRAPHIC STUDIES OF THE SOLID-LIQUID INTERFACE BOUNDARY LAYER IN FLUX CRYSTAL GROWTH

Xiling Yu, Youchen Liu and Xuefeng Yue, National Laboratory of Crystal Materials, Shandong University, Jinan, 250100, P R China.

As compared with low temperature solutions, high temperature solutions have relatively large viscosity, small diffusion coefficient and low transparency. Moreover, during crystal growth, flux may have the disadvantages of being volatile, corrosive or poisonous, which brings about experimental difficulties in research on crystal growth. Special single crystal growth equipment designed by us not only satisfies the conditions for stable crystal growth, but is also convenient for real-time observation and measurement by optical methods. Potassium Titanium Oxide Phosphate (DTP) crystal which has extensive applications, has been grown with this equipment. The growth temperature usually ranges from 800 to 1000°C. We have investigated regular variations of the solid-liquid interface boundary layer in KTP crystal growth and dissolution by holographic phase-contrast interferometric microphotography. The experiments demonstrate that the relation between the thickness of the boundary layer and the supersaturation is linear under free convection conditions. The variation of refractive index caused by the change of solute concentration in the boundary layer has a logarithmic relation to the distance from a crystal face.

15Z–2

GROWTH AND CHARACTERIZATION OF Bi-Sr-Ca-Cu-O SINGLE CRYSTALS

Alka Jain and G.C. Trigunayat, Department of Physics and Astrophysics,
University of Delhi, Delhi - 110 007, India.

Single crystals of $Bi_2Sr_2CaCu_2O_x$ (2:2:1:2) have been grown by a flux growth technique. The crystals prepared so far are thin and have small lateral sizes, measuring approximately 2 mm x 1 mm x 0.1 mm. Examination by X-ray diffraction has confirmed their single crystal character. Their surface growth features have also been studied, both through optical microscopy and scanning electron microscopy. Typically, a crystal surface displays parallel domains of different widths, with each domain consisting of parallel steps oriented at approximately 60° with respect to the length of the domain. It is conjectured that the surface features observed are related to the formation of polytypes in the crystals.

15Z-3

PRESSURE DEPENDENCE OF CELL DIMENSIONS IN NiS_2 CRYSTALS GROWN UNDER DIFFERENT SULFUR VAPOUR PRESSURES

Takashi Komori and Nobuo Ishizawa, Research Laboratory of Engineering Materials,Tokyo Institute of Technology, and Fumiyuki Marumo, Department of Earth Sciences,Nihon University, and Yasutoshi Noda, Department of Materials Science,Tohoku University, Japan

Crystals of NiS_2 have a pyrite-type structure with the cubic space group of Pa3 and are known to show insulator-metal transition at about 46 kbar. There is no drastic structural changes at the phase transition pressure. The authors have already examined changes of the cell dimension and the x parameter of the sulfur atom (the only positional parameter in the pyrite-type structure) with pressure on several NiS_2 crystals grown with different method, and found that the pressure dependence of cell dimension is not identical in the crystals prepared by chemical vapour transport with chlorine with those in the crystal grown by the sublimation method. The origin of the difference was supposed to lie in the degree of imperfections of the crystals. To verify this speculation, cell-dimension measurements were carried out up to 55 kbar on two types of crystals grown with the sublimation method under the sulfur vapour pressure (Ps) of about 2.0 atm and 0.5 atm, respectively.

The diffraction angles of 50 reflections ranging from 40 to 70° were measured with the single-crystal method on a four-circle diffractometer on the respective types of crystals at various pressures by making use of Ag $K\alpha_1$ radiation and a diamond-anvil high-pressure device. At the ambient pressure, the crystal grown under Ps=0.5 atm has a cell dimension slightly longer (0.0014 A) than that grown under Ps=2.0 atm. However, the cell dimension of the former crystal decreases more slowly than that of the latter crystal with increasing pressure, and the difference increases to 0.0086 A at 45 kbar. Both crystals undergo the phase transition at around 46 kbar, showing discontinuous diminutions of the cell dimensions. The discontinuity at the transition point is larger in the former crystal than in the latter. After the phase transition, the cell dimension of the former crystal also decreases more slowly with increasing pressure than that of the latter. Since the crystals grown under lower Ps are supposed to have higher defect densities than the crystals grown under higher Ps, the results of the present study indicate that an NiS_2 crystal with a higher defect density decreases the cell dimension more slowly and shows a larger jump of the cell dimension at the transition point than that with a lower defect density.

15Z–4

THE SYNTHESIS AND STRUCTURE OF $Cu_3Bi_4V_2O_{14}$.

Glen B. Deacon, Bryan M. Gatehouse and Gregory N. Ward.
Chemistry Department, Monash University, Clayton 3168, Victoria, Australia.

Crystals of Namibite ($CuBi_2VO_6$)[1] in a mineral sample[2] from the Iron Monarch mine in South Australia were unsuitable for single-crystal data collection . The title compound was produced during unsuccessful attempts to synthesize Namibite by solid state reaction.

Crystal data. $Cu_3Bi_4V_2O_{14}$, Mr = 1352.4 $gmol^{-1}$, triclinic P-1 (#2), a = 5.317(2), b = 7.916(4), c = 8.095(5) Å , $\alpha = 74.58(5)^o$,$\beta = 89.38(4)^o$,$\gamma = 70.39(3)^o$. Z = 1, D_m not measured, $D_c = 7.286$ Mg m^{-3}. U = 308.2(3) $Å^3$. R = 0.0398 , R_w = 0.0576 for 1382 observed reflections ($F > 6.0\ \sigma$ (F)). Single crystal data were collected on a Nicolet four-circle diffractometer and solved by direct methods using the SHELXTL-plus software.

The structure consists of an infinite three-dimensional metal oxygen array in which the two independent copper(II) atoms are square-planar (Cu(1) has one, and Cu(2) has two, longer contacts), the two independent bismuth(III) atoms are eight-coordinate (4,4 bicapped trigonal pyramidal[3]) and vanadium(V) is four-coordinate (tetrahedral). Mean bond distances are Bi-O 2.57(31)Å, Cu-O 1.956(27)Å (square planes), 2.64(10)Å for the three long contacts, and V-O 1.713(29)Å; the shortest Cu-O distance is 3,063(3)Å. The Bi-O and Cu-O distances compare favourably with those in Francisite ($Cu_3Bi(SeO_3)_2O_2Cl$), a recently determined structure[4].

Further attempts to synthesise Namibite hydrothermally, which coincidently has a cell volume of 309.7Å[1], or an erbium substituted compound $CuEr_2VO_6$, failed to yield crystals of suitable size for X-ray structure determination.

References.

1. Knorring, O. V. & Sahama, Th. G. (1981), Schweiz. Mineral. Petrogr. Mitt.. (1981), 61, 7-12.

2. Birch, W. D. & Pring, A. Private Communication.

3. King, R. B.(1969). J. Am. Chem. Soc., 91, 7211-7216.

4. Birch, W. D., Gatehouse, B. M. & Pring, A. (1990), Amer. Mineralogist, 75, 1421-1425.

15Z–5

SYNTHESIS AND CHARACTERIZATION OF Ni_3S_2 (HEAZLEWOODITE) CRYSTALS

S. M. Dharmaprakash, Department of Physics, Mangalore University, Mangalagangotri 574199 Mangalore, India.

The growth of Ni_3S_2 (Heazlewoodite) single crystals is described. Heazlewoodite crystals were synthesized by chemical vapour transport, using iodine as a transporting agent. The size and quality of the grown crystals were influenced by the growth conditions. Optimum conditions to grow large size and defect free single crystals were determined. Single crystals up to 2 - 3 mm on edge were grown in 10 – 12 days under the conditions used.

The Ni_3S_2 crystals were characterized utilizing chemical analysis, atomic absorption spectral analysis, x-ray diffraction and differential thermal analysis.

Ni_3S_2 crystals are rhombohedral with unit cell parameters a - 5.7522Å, $c = 7.1405$Å, $\alpha = 89.99°$. Ni_3S_2 crystals melt at 1043 K.

P-00

THE AUSTRALIAN NATIONAL BEAMLINE FACILITY

R.F. Garrett, J.W. Boldeman, D.J. Cookson, G. Foran, Australian Nuclear Science and Technology Organisation, PMB 1, Menai NSW, 2234; D.C. Creagh, F. Johnson, University College, University of New South Wales, Campbell ACT, 2600; and S. Janky, S. W. Wilkins, CSIRO Department of Materials Science and Technology, Locked Mailbag 33, Clayton VIC, 3168.

The Australian National Beamline Facility is a cooperative project involving several Australian research organisations, Universities and government funding agencies. A multi-purpose X-ray beamline is being constructed at the Photon Factory, Tsukuba, Japan. The aim of the project is to provide Australian scientists with routine access to synchrotron radiation in the hard X-ray region.

The beamline will deliver either monochromatic light, in the 5-20 keV range, or white light to the experimental hutch. The main experimental instrument will be a multi-configuration vacuum diffractometer which combines a two-circle goniometer with a large Weissenberg mode Imaging Plate camera. The diffractometer is optimised for protein crystallography, high resolution powder diffraction, small angle scattering and single crystal diffraction. In addition, the white or monochromatic beam can pass through the diffractometer to a secondary table-top station, where experiments such as reflectometry, EXAFS, a fluorescence microprobe, and other white beam techniques can be performed. This secondary station will be available in late 1992 for white beam experiments.

Details of the beamline, monochromator and diffractometer design and performance will be presented, and preliminary results from the first white beam experiments will be reported.

15P–02

PROPOSED SYNCHROTRON X-RAY STUDIES OF MONOLAYERS AT THE PHOTON FACTORY

Geoffrey T. Barnes and Colin H.L. Kennard
The University of Queensland, Brisbane, Q4072, Australia

Studies of monolayers on water surfaces help in understanding amphiphile structure and behaviour, evaporation control, modelling biological membranes and modelling of some industrial processes.

Monolayers are formed on the water surface in a film balance, enabling the monolayer to be compressed and expanded, much as gas is compressed and expanded in a cylinder and piston apparatus. A very small amount of compound in a volatile solvent is carefully placed on a cleaned water surface with a microsyringe. The balance contains a trough and movable barrier. Surface pressures are measured by a Wilhelmy plate suspended from a strain gauge. As the barrier is moved, molecules align in a perpendicular orientation, forming a monolayer with hydrophilic ends of molecules pointing towards the water, and hydrophobic ends away. This is followed in the film balance by measuring surface pressure as a function of monolayer area. At a critical stage, the fully compressed monolayer behaves like a crystal with regular order which may be studied by diffraction techniques. On further reduction of area, the monolayer collapses.

A high resolution powder diffractometer is being designed by others under Australian Government auspices for installation on an X-ray beam line at the Tsukuba Photon Factory in Japan. It is proposed to mount the film balance on a second platform behind the powder diffractometer, to study monolayers on water surfaces. A system that should allow users to gain experience involves phosphotungstic acid and uranyl acetate as stains in electron microscopy. At low pH use of the film balance indicates that there are changes in the structures of stained animal cell wall materials, such as phospholipid monolayers. For better understanding, it is planned to study the structure of the material by X-ray reflectivity/diffraction techniques.

In **specular reflectivity,** the reflected beam at a low angle of less than 0.1 of a degree is scanned directly (Q_x scans) with a scintillation counter. This may be interpreted to give the density profile of the interface with the total count representing the integral of the scattered intensity along the Bragg rod. However, additional information is obtained using **grazing incidence diffraction.** Then for a given Q_x peak, Q_z scans using Soller slits and a position sensitive detector are carried out by varying the Bragg angle.

It is possible with the film balance to obtain a phase diagram. By selecting the appropriate surface pressure at a given temperature, a particular state may be selected. Analysing the results, it is possible to get an idea of the structure of this monolayer.

15P–03

AN INSTRUMENT FOR X-RAY SURFACE STUDIES

G. Barnes and C. Kennard, Department of Chemistry, University of Queensland, St Lucia, Qld, 4072, D. Creagh and I. Jamie, Department of Physics, University College, University of New South Wales, Campbell, ACT, 2600 and J. White, Research School of Chemistry, Australian National University, Canberra, ACT, 2601

While traditionally the bulk properties and structure of materials have received an overwhelming proportion of attention in materials studies, it is becoming increasingly obvious that an understanding of the surface science is very important. The main barrier to investigation of surfaces in standard X-ray techniques has been the lack of sufficient intensity to produce measureable scattering from the very small proportion of material in the surface region, compared to that in the bulk volume. Synchrotron radiation has provided the required intensity and there has been an increasing number of surface studies undertaken in recent years.

This paper will present an overview of the Australian National Beamline Facility. It will also discuss in more detail a refractometer that is currently under construction, which will be used for high resolution surface studies at the ANBF. The reflectometer will allow the surfaces to be studied through Critical External Reflection, Grazing Angle Diffraction, Total Reflection X-Ray Fluorescence and Surface Extended X-ray Absorption Fine Structure spectroscopy. Some of the initial experiments to be undertaken will be the investigation of the structure of Langmuir films of phospholipids and cholesterol (Barnes (1986), Barnes *et. al* (1980), Gorwyn and Barnes (1989)), and the investigation of phase transitions in crystalline fatty acids (Kenn *et. al* (1990)) and polymer (Dai *et. al* (1989)) monolayers.

Barnes, G., (1986) *Adv. Colloid Interface Sci.*, **25**, 89

Barnes, G., Bacon, K. and Ash, J., (1980), *J. Colloid Interface Sci.*, **76**, 263

Gorwyn, D, and Barnes, G., (1990), Langmuir, **27**, 113

Kenn, R.M., Bilbo, A.M., Peterson, I.R., Mohwald, H., Kjaer, K., and Als-Nielsen, J., (1990), Physics Department Annual Progress Report, 1 Jan - 31 Dec, 1990, Risø National Laboratory. Risø-R-582

Dai, L., White, J.W., Kerr, J., Thomas, B.K., Penfold, P. and Aldissi, M., (1989), *Synth. Metals*, **28**, D69 - D89

15P-04

X-RAY EVALUATION OF A LAPPED Si SINGLE CRYSTAL

Hideaki Shiwaku[1], Masami Ando[2], Kazuyuki Hyodo[2],Xiao-Jing Wu[3]
and Shigeo Horiuchi[4]

1. Japan Atomic Energy Research Institute, Tokai, Naka, Ibaraki, 319-11, JAPAN
2. Photon Factory, KEK, Ohol-l, Tsukuba, Ibaraki, 305, JAPAN
3. Mitsubishi Gas Chemical Co. Ltd., Tsukuba Ibaraki, 30s, JAPAN
4. National Institute Research in Inorganic Materials, Tsukuba, Ibaraki, 30s, JAPAN

Development of a K-edge subtraction imaging system with synchrotron radiation, for non-invasive coronary angiography is under way at the Photon Factory, KEK. It needs a large monochromatic x-ray beam with high integrated intensity, and energy resolution better than 150 eV. Single crystals lapped by abrasives were characterized by their integrated intensity, reflectivity and full-width at half maximum (FWHM). The effect of abrasives was studied for a range of abrasive particle sizes and for some semiconductor materials via the shape of the rocking curve. The effect of Bragg plane asymmetry relative to the crystal surface was also studied. For example, at photon energy 33.17 keV a Si 311 single crystal with an asymmetry angle α of 5° has good (70%) reflectivity in spite of lapping of the surfaces by 10μm abrasive particles. This photon energy corresponds to the K absorption edge of iodine, a commonly used contrast material in angiography. Its FWHM becomes 10 to 15 times that of a mechanochemically polished crystal, implying that the integrated intensity becomes 15 to 20 times larger. This confirms that a lapped asymmetrical Si single crystal can be used as a monochromator for coronary imaging with synchrotron radiation.(1,2)

Fitting of rocking curve, by a mixture of Gaussian and Cauchy functions of the form $f(x)=A\ e^{-px^2} + B/(1+qx^2)$, where x is the deviation angle from the Bragg angle and A, B, p, q are constants, has been attempted. The Figure 1 example shows FWHMs of resolved Gaussian and Cauchy components for Si 311 with $\alpha = 5°$ lapped by abrasives. The Gaussian and Cauchy components from the fitted curves were found from this analysis. The FWHMs and integrated intensities were then related to the abrasive material's particle size. Cross-sectional observations by transmission electron microscopy shows many cracks and grains generated on the surface by the lapping process.(3) Construction of a diffraction model to elucidate these data is under discussion.

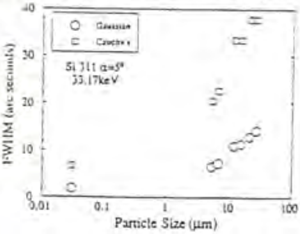

1) H Shiwaku et al, Jpn J. Appl. Phys. **30**(12A) L2065 (1991)
2) H Shiwaku et al, Rev. Sci. Instrum. **63** 1201 (1992)
3) X.-J.Wu et al, Jpn J. Appl. Phys. **31**(6B) L803 (1992)

15P-05

INTENSITY ENHANCEMENT IN ASYMMETRIC DIFFRACTION WITH PARALLEL-BEAM SYNCHROTRON RADIATION

H. Toraya, Ceramics Research Laboratory, Nagoya Institute of Technology, Asahigaoka, Tajimi 507, JAPAN
T.C. Huang and Y. Wu, IBM Research Division, Almaden Research Center, 650 Harry Road, San Jose, CA95120-6099, USA

Recently, there has been considerable interest in the use of parallel-beam X-ray optics in powder diffraction. In this paper, intensity enhancement in asymmetric diffraction with a fixed incident angle a was studied using parallel-beam synchrotron radiation. Vertical-scan powder diffractometers having horizontal parallel-slits with an aperture of 0.05° and parallel-beam synchrotron radiation with λ of 1.54Å and α of 5° and 10° were used to collect the diffraction patterns of Si, CeO_2, and ZrO_2 powders. Experiments were conducted for Si and CeO_2 at the Photon Factory (PF) in Tsukuba and for ZrO_2 at both PF and Stanford Synchrotron Radiation Laboratory. The experimental data for Si and CeO_2 were analyzed by the individual profile fitting technique and those of ZrO_2 by the whole-powder-pattern fitting technique. Experimental intensities were corrected for the incident beam decay by using monitor counts collected between the monochromator and specimen. As expected, significantly higher intensities were obtained from the asymmetric diffraction. Intensity enhancement in asymmetric diffraction was measured as a ratio R of the integrated intensity obtained in asymmetric 2θ scanning to that of the corresponding reflection in symmetric θ-2θ scanning. The observed ratios R had values between 1 and 2 in the range $2\theta > 2\alpha$, and its variation with 2θ was well in accord with that expected from the intensity formula derived in the case of asymmetric diffraction. The change in profile shape was very small between the two cases obtained by 2θ (α fixed) and θ-2θ scannings, as expected from the previous experiment 1) The shift in peak maximum position was also very small for a sufficiently large incident angle as in the present experiment. These results showed that the diffracted intensity from a stationary sample could be enhanced without degrading the profile shape in asymmetric diffraction.

1) H. Toraya, T.C. Huang, and Y. Wu, Denver X-ray Conference, Aug. 1992, Colorado Springs, Colorado.

15P-06

STRUCTURE REFINEMENT OF SUBMICROMETER-SIZED TWINNED DOMAINS BY USING SYNCHROTRON RADIATION WITH THE LAÜE METHOD

K Ohsumi, PF-KEK, K Hagiya, HIT, T Takase, Univ Tokyo,
Y Shimizugawa, NIRIM, M Ohmasa, HIT and M Miyamoto, Univ Tokyo

It is essential to analyze the structure and/or texture of submicrometer-sized specimens to understand the phase compositions of these materials more completely. A system developed for this purpose has been applied to some inorganic materials at the Photon Factory(PF), KEK, using synchrotron radiation(SR) with the Laüe method.

In analyzing submicrometer-sized specimens, it is important to reduce background to the lowest possible level. Use of a strong X-ray source such as SR is essential for such an experiment. To reduce the time needed to collect diffracted intensities from such small samples, it was decided to use the Laüe method with an imaging plate (Fuji Co, Ltd) – a storage phosphor detector. A new optical system has been developed and installed in the Laue camera to reduce the background caused by interaction of the polychromatic SR beam with the slit systems. Software for Laüe reflection data reduction and for structure refinement has been developed at the PF to support this new experimental program.

This has been applied to study a twinned molybdenum sphere 0.8 μm in diameter, and a truncated icosahedral chemical vapour deposited(CVD) diamond, 5 μm in diameter.

Molybdenum Sphere

The Mo sphere was found to be twinned. The volume ratio of the twinned domains was determined from 14 Laüe reflections. The isotropic temperature factor (B) of 0.08(6)$Å^2$ compares with a value of 0.04$Å^2$ obtained by the same method for another Mo sphere of the same size and with 0.07(4)$Å^2$ determined for the same powdered chemical by powder diffraction. The refined volume of the smaller domain, 0.02mm^3, is beyond the resolution limit of an optical microscope. The estimated number of molybdenum atoms within that domain is around 5×10^8.

Icosahedral CVD Diamond

A truncated icosahedral CVD diamond was found to consist of 17 domains. The presence of a spinel twin type was confirmed in sixteen of those domains. The isotropic temperature factor (B) was determined to be 0.2(1)$Å^2$ by analysing a twin-free domain with an 0.08mm^3 volume.

These results demonstrate that crystal structure refinement of twinned samples can succeed even under these extremely difficult conditions.

15P-07

ULTRAMICRO-SINGLE-CRYSTAL DIFFRACTION STUDY ON BARIUM TITANATE USING SR

M. Kataoka, K. Suda, N. Ishizawa, Research Laboratory of Engineering Materials, Tokyo Institute of Technology, Nagatsuta, Midori-ku, Yokohama 227, Japan, F. Marumo, College of Humanities and Science, Nihon University, Sakurajosui, Setagaya-ku, Tokyo 156, Japan, Y. Shimizugawa, National Institute for Research in Inorganic Materials, Namiki, Tsukuba 305, Japan, and K. Ohsumi, National Laboratory for High Energy Physics, Oho, Tsukuba 305, Japan

The effect of crystal size on the tetragonal-cubic phase transition of barium titanate, $BaTiO_3$, has been studied by means of ultramicro-single-crystal diffraction using SR. Crystals of $BaTiO_3$ were synthesized by the flux method. Laue photographs were taken at the beam line 4B of the Photon Factory, KEK, on crystals with dimensions ranging from 10 μm to 0.25 μm. The imaging plate was used as an X-ray detector. The exposure time was varied from 1 s to 4 h depending on the size of specimen. The crystal to film distance was fixed at 66.5mm. Splitting of diffraction spots due to the twinning of the tetragonal form was clearly observed for crystals with dimensions of 10μm-0.56 μm. The splitting seemed to become smaller as the crystal size decreases, and the crystal with dimension of 0.25 μm gave no clear splitting. This crystal has the least volume among the crystals from which Laue photographs have ever been taken. A detailed analysis on the change of c/a ratio with crystal size is now in progress and will provide a clearer understanding on the critical size of the tetragonal-cubic phase transition of $BaTiO_3$.

15P-08

DIFFRACTION FROM COMPOSITE CRYSTAL $Nd_{13}Fe_{46}B_{41}$ BY SYNCHROTRON RADIATION

T. Ohba, Department of Materials Science and Engineering, Teikyo University, Utsunomiya 320, JAPAN, S. Sasaki, Tokyo Institute of Technology, Nagatsuda, Yokohama 227, JAPAN, M. Takata, Department of Applied Physics, University of Nagoya, Furoucho, Nagoya 464-01, JAPAN, and Y. Komura, Hiroshima Institute of Technology, Saeki-ku, Hiroshima 730-51, JAPAN.

$Nd_{13}Fe_{46}B_{41}$ is a composite crystal which is constructed by two subsystems interpenetrating each other in a crystal, i. e. Nd and Fe subsystems. We observed electron diffraction patterns using several kinds of heat treated samples to examine a correlation between a periodicity of the composite crystal and those of Nd and Fe subsystems. Recently, a structural study of the composite crystal has been done by multi-dimensional analysis by many authors. However, it is not easy to understand the structure for this method. Structural study of the composite crystal using a synchrotron radiation was made for examining a contribution of each subsystem. X-ray diffraction profiles along 20ℓ line was measured with Nd and Fe absorption edges by synchrotron radiation at BL-10A at Photon Factory in KEK.
A ratio of intensity I(Nd)/I(Fe) along 20ℓ was shown in Fig. 1. The ratio at $\ell=18$ becomes stronger than the back ground and that of $\ell=20$ is weaker than the back ground. It is obvious that an effect of two subsystems contribute differently.

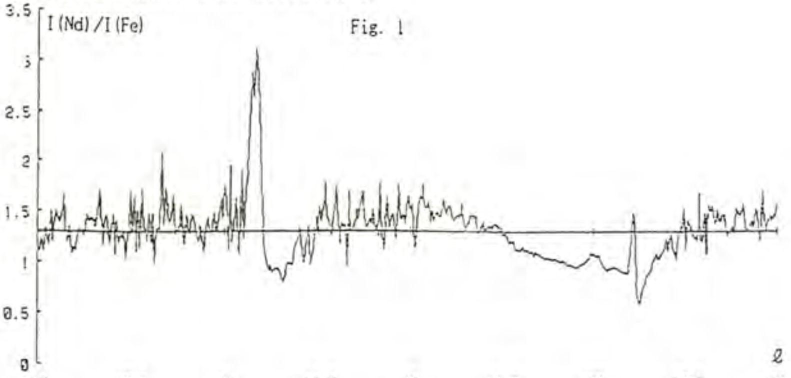
Fig. 1

15Q-09

MICRO-AREA X-RAY DIFFRACTION: ITS APPLICATION TO CRYSTALLOGRAPHIC ANALYSES OF MINERAL TEXTURES AND TINY SINGLE CRYSTALS

H. Horiuchi, M. Tanaka*, S. Nojima, T. Mitsuki, Mineralogical Institute,
University of Tokyo, Hongo, Bunkyo Tokyo 113, Japan and
I.Minato, JEOL Ltd., Application Laboratory Musashino, Akishima,
Tokyo 196, Japan.

A new method was developed in order to analyze lattice constants and lattice orientation relationships among the crystalline substances which comprise textured minerals or inorganic materials. Analysis can proceed without special sample separation, using conventional X-ray sources such as Cu$K\alpha$ radiation from a shielded tube operating at 35KV, 25mA. When a crystalline fragment of synthetic rare-earth aluminate with diameter around 30μm was examined, it was found that the fragment was composed of several individual crystals. We succeeded in analyzing lattice constants for each crystal. It was finally deduced that some of these crystals were related to each other by twinning. In the case of a single crystal specimen of synthetic $CaNiSi_2O_6$ of about $10^3\mu m^3$ volume, a data set of integrated intensities strong enough for structure analysis was obtained. Thus, in the case of analyzing lattice constants and lattice orientations for crystalline phases in mineral textures, the minimum size of a crystal which can be studied individually is $10^3\mu m^3$ or less.

Equipment originally developed by JEOL as a micro-area powder X-ray diffraction apparatus (DX-MAP2), was utilized as a single crystal diffractometer for this work. A curved one dimensional position sensitive proportional counter was used as a detector and this provides an effective record of the intensities of the diffracted beams. The distance from the X-ray source through the specimen to the detector is 220mm. The X-ray beam is collimated by holes of 10, 30, 50 or 100μmϕ. Specimen orientations can be controlled by three axes θ, χ and ϕ as for a 4-circle goniometer. Software systems for data collection and for analyses of lattices and their orientations were developed in this investigation.

*) Present address: Photon Factory, National Laboratory for High Energy Physics, Tsukuba, Ibaraki 305, Japan.

15Q-10

MICROSTRUCTURE AND CRYSTALLINITY OF LUMINESCENT POROUS SILICON STUDIED BY DIFFRACTION TECHNIQUES

Kuniko Takemoto, Yoshio Nakamura and Osamu Nittono
Department of Metallurgical Engineering, Tokyo Institute of Technology,
2-12-1, Oh-okayama, Meguro-ku, Tokyo 152, Japan.

Porous Silicon (PS) layer is obtained by anodic oxidation of a monocrystal silicon wafer in concentrated hydrofluoric acid (HF) solution. It consists of a great number of micro pores and fine silicon parts. The silicon parts have intricate 3-dimensional micro systems and a huge specific surface area depending on the wafer type and formation conditions. Using these characteristics, applications of PS layer to electronic materials were expected and have actually been achieved.

In 1990, Canham reported a demonstration of visible photo-luminescence (PL) from highly porosity PS layer. Silicon normally emits only extremely weak infrared PL because of the relatively small and indirect band gap. Then this phenomenon was explained by quantum size effects in silicon parts such as quantum wires. Now red, orange, yellow and green visible light emissions have been reported. Many studies of luminescent characteristic of PS layer have been performed, but few studies discuss the possibility of quantum size effect from the view points of microstructure, size and morphology, and the crystallinity of silicon parts.

In this study, we investigated microstructure and crystallinity of PS layers produced on p- and n-type degenerate silicon (100) wafers by high resolution SEM (HRSEM) observations and by X-ray multi-crystal diffractometry. Anodization was carried out with current densities ranging from 10 to 300 mA/cm^2 in a constant electrolyte solution of HF: C_2H_5OH: H_2O = 1: 2: 1. In addition, visible light emission excited by He-Cd laser was confirmed for several PS layers.

The main results are: 1) p-type silicon: When a PS layer was anodized below 200mA/cm^2, the lattice distortion of the PS layer increased, depending on the forming current density. Its crystallinity was as good as that of the substrate. Above 250mA/cm^2, the lattice distortion decreased and the crystallinity was considerably worse than that of the substrate. 2) n-type silicon: The lattice distortion decreased depending on the forming current density. Especially at low current densities, its variation was remarkable.

The relationship between crystallinity and the visible light emission will be discussed on the basis of experimental results.

15Q-11

DESIGN OF NEW TYPE FOUR CIRCLE DIFFRACTOMETER WITH MOVABLE ROTATING ANODE X-RAY SOURCE

J. Harada, 1. Takahashi, T. Shimura, T. Miyazaki,
*K Yamada, and K Masuda**

*Department of Applied Physics, Nagoya University, Chikusa-ku, Nagoya 464, Japan. * Department of Product Development, Rigaku Co., 3-9-12, Matsubara-cho, Akishima-shi, Tokyo 196, Japan.*

A new type of multi-purpose four circle diffractometer system has been constructed by developing a movable rotating anode X-ray source. It enables us to collect X-ray scattering data from a single crystal or liquid surface by keeping the sample stage horizontal. It provides rotation around the φ axis normal to the horizontal plane. The mechanism of this goniometer is such that, with the sample stage fixed horizontally, a rotating anode X-ray generator(18kW: 40kV, 450mA for a Cu target) is driven to change the grazing incidence angle α. A conventional scintillation counter can be set to any scattering angle by rotating it through an angle η around the φ axis and by a tilting angle χ from the horizontal plane. The goniometer movements, shown schematically in the figure, are driven by computer controlled stepping motors.

The goniometer proves to be effective, especially for measurement of surface scattering with the grazing incidence in vacuum, and also for solutions or for samples which dissolve or melt at high temperature. It would be the well suited to measurement of the critical scattering for phase transitions from solid to liquid, using single crystals.

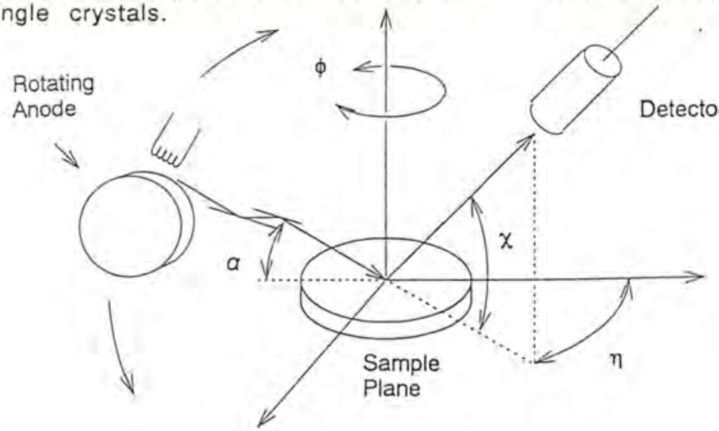

15Q-12

FUNDAMENTAL STUDY OF A TIME-RESOLVED LAÜE METHOD FOR PROTEIN CRYSTALLOGRAPHY

N.Watanabe and N.Sakabe, Photon Factory, KEK, Tsukuba, Ibaraki 305, T.Higashi, Rigaku Corporation, Akishimashi, Tokyo 196, and K.Sakabe, Nagoya University, Nagoya 305, Japan.

White synchrotron X ray can be used to obtain the integrated intensity from a single crystal in Laue geometry. In spite of many inherent limitations, the use of the technique is believed to have a great potential in time-resolved structural studies on macromolecules within the time scale of milliseconds or less. We have constructed a Laue camera to investigate the dynamical change of molecular structure in a single crystal. The camera system combines a multi-slit rotation shutter with a linearly streakable Imaging Plate (IP) cassette. It can record the diffraction pattern after the reaction initiation into continual spots as a function of time. Eight IP's can be put on the largest cassette with a total size of 800mm×800mm. A large area is required in order to record the continual spots without spatial overlap. The shortest width of the X ray pulse achieved by the shutter is 125μsec. The preliminary test of the camera was performed at a bending magnet beamline BL-6A2 and at the vertical wiggler beamline BL-14C of the Photon Factory with protein crystals of ω-amino acid:pyruvate aminotransferase (ω-APT), myoglobin, hemoglobin, actin, and L-lactate dehydrogenase. A bent plane fused quartz focussing mirror was installed at 6A2 and no focussing optics were used at 14C. A typical one-shot exposure time using an IP with a crystal of ω-APT (the size of crystals are about 0.7 × 0.8 × 2.0mm) was 10msec at 6A2 and 100msec at 14C, when the storage ring was operated with 2.5GeV 350mA. The quality of the Laue data was compared with the monochromatic (Weissenberg) data using crystals of ω-APT. Time-resolved experiments on ω-APT crystal and some organic crystals were performed using a Q-switched Nd:YAG laser as a trigger. Intensity variations of reflection spots were observed with a time resolution of submilliseconds to milliseconds. Results of this work will be presented.

15Q-13

HIGH RESOLUTION DATA COLLECTION FROM PROTEIN CRYSTALS ON R-AXIS IIC DIFFRACTOMETER

T. Sato and T. Higashi, Rigaku Corporation, 3-9-12 Matsubara-cho, Akishima-shi, Tokyo 196, Japan, and T. Tada, Fujisawa Pharmaceutical Co. Ltd., 2-1-6 Kashima, Yodogawa-ku, Osaka 532, Japan

The Rigaku R-AXIS IIC diffractometer was designed for automatic data collection from protein crystals using the Fuji Imaging Plate (IP) as an X-ray detector. The size of the flat-plate IP is $200\times200mm^2$ and the minimum crystal to IP distance is 55mm, hence the maximum resolution limit is ca. 1.6Å for CuKα radiation.

Elastase-inhibitor complex crystals (orthorhombic, $P2_12_12_1$, a=57.8, b=74.5, c=51.7Å) diffract up to 1.3Å resolution and were used for the present test of high resolution data collection on the R-AXIS IIC.

Using CuKα radiation, diffraction data were collected up to the resolution limit of 1.6Å in a routine manner (40KV 100mA, crystal to IP 59mm, 2°/frame, 30min/2°, total oscillation angle 86°). Using MoKα radiation, on the other hand, similar data collection was performed to obtain higher-angle data (50KV 90mA, crystal to IP 160mm, 2°/frame, 40min/2°, total oscillation range 80°).

The R-merge of 3.4% for Cu dataset (1.6Å resolution and 75% completeness) indicates that reasonable data quality is obtainable to the mechanical resolution limit of the machine. The Mo dataset (1.3Å resolution and 77% completeness) was of rather poor quality, with R-merge 7.5%, partly due to crystal decay and inevitably weak intensities (averaged intensity was only 22% of Cu case).

The present experiment shows the capability for high resolution data collection from protein crystals on the R-AXIS IIC. A detailed comparison of Cu and Mo datasets will be presented.

15Q-14

STRUCTURE DETERMINATION OF ORGANIC COMPOUNDS BY A RAPID X-RAY MEASUREMENT SYSTEM

E. Iwasaki, M. Sakuratani and M. Yasui, Dept. of Applied Physics and Chemistry, The Univ. of Electro-Communications, Chofu-shi, Tokyo 182, Japan and N. Kamiya and H. Iwasaki, The Institute of Physical and Chemical Research (RIKEN), Wako-shi, Saitama 351-01, Japan.

Rapid collection of X-ray intensity data is especially important for determining structures of unstable compounds. In order to get structural information from a single crystal within several hours, a new type of X-ray diffractometer has been developed (Iwasaki & Kamiya, 1992). This equipment is a Weissenberg camera type with multi-screens, two cylindrical imaging plates (IP; the two IP's are used alternately to reduce effective readout time) and rotating laser optics designed for the readout of the cylindrical IP. Diffraction intensities of two stable compounds (I and II) and two unstable compounds (III and IV) were measured using this equipment with MoKα radiation (50kV, 200mA, $2\theta_{max}$=45°). Total time for measurement is 2 or 3 hours for each compound. The structures were solved successfully by conventional direct methods and the Patterson method. For I and II intensities were also measured with a 4-circle diffractometer using the same specimens. The agreement between the two sets of structural geometry, obtained from the IP and the 4-circle diffratometers, was quite satisfactory. Accurate intensities of the unstable III and IV could not been obtained by the 4-circle diffractometer.

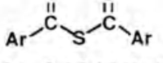

Ar = 2,4,6-tri-Me-Ph

I

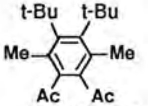

Ac = COOMe

II

$(Me\text{-}Ph)_3BiCl_2$

III

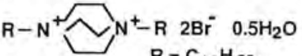

R = $C_{14}H_{29}$

IV

	Sp. gr.	a/Å	b/Å	c/Å	β/°	V/Å^3	Z	Refs.	R
I	$P2_1/c$	8.520(2)	12.434(2)	18.790(3)	100.91(2)	1954.7(6)	4	1995	0.054
II	$P2_1/n$	10.855(1)	10.169(1)	17.597(2)	104.82(1)	1883.1(3)	4	2360	0.050
III	$C2/c$	15.429	19.729	16.036	121.36	4123.6	8	2502	0.067
IV	$P2_1/c$	8.720(1)	8.789(2)	49.298(8)	93.83(2)	3770(1)	4	3667	0.063

Iwasaki, H. and Kamiya, N. (1992). to be published.

15Q-15

FULLY AUTOMATIC STRUCTURE ELUCIDATION

Kentaro Yamaguchi, Emi Yasudome and Go Matsumura,
School of Pharmaceutical Sciences, Showa University,
1-5-8 Hatanodai, Shinagawa-ku, Tokyo 142, Japan.

A fully automatic procedure for solving crystal structures of organic small molecules has been devised. Automatic decisions at each critical point of the analysis in which the user intervention used to be required are provided, based on empirical considerations. The procedure named *FASE* (*Fully Automatic Structure Elucidation*) has been mainly implemented into the packages *RCRYSTAN* and *SAPI85*. It is able to solve structures without any user intervention. The user simply inputs "*FASE*" to carry out this procedure. The complete structure is solved and displayed in most cases. This procedure has been applied to 137 crystaline organic compounds and 112 chemically significant structures were derived. The highest molecular weight was 848 throughout these analyses, indicating its capability to be applied to organic structures generally. The shortest computing time of 3 minutes for the whole calculation suggests quick analysis. *R* values refined without missing atoms using isotropic refinement are normally in the range 0.15-0.30. Some results using this procedure will be shown.

15Q-16

XTAL 3.2: A NEW SYSTEM RELEASE.

E. Blanc, U. Lausanne, D.M. Collins, N.R.L. Washington DC, D.D. Dexter, Middlebury College, D.A. Grossie, Wright State U., H.D .Flack, U. Geneva, S.R. Hall, U. Western Australia, G.S.D. King, U. Leuven, B.G. Kruger, Rand Africaans U., R. Olthof-Hazekamp, U. Utrecht, D. Schwarzenbach, U. Lausanne, J.M. Stewart, U. Maryland and K.D. Watenpaugh, Upjohn Co. Kalamazoo.

Version 3.2 of the *Xtal* System was released in September 1992. The prime difference with version 3.0 is the inclusion of the new programs summarised below. Other system changes simplify implementation: these include macro switches to specify f77 compilers types and an automatic implementation script for Unix OS's. The ability to process CIF's is an important aspect of *Xtal*. and these may be generated for archiving and submission to *Acta Crystallographica* and the *Cambridge Data Centre*.

New programs in *Xtal3.2* are: (a) *ADDPAT* to input powder intensity patterns into *Xtal*; (b) *CREDUC* is an adaption of the Le Page cell reduction approach augmented with the calculation of (psuedo)-merohedral twin laws; (c) *LSABS* applies absorption corrections which lead to refineable crystal dimensions; (d) *LSLS* is a SF least-squares refinement with restraints dealing with raw observed intensities and innovative error calculation; (e) *LSRES* is a restraint loader; (f) *MIND* generates site data for the graphics program *MindTool* (Tirado-Rives & Blake); (g) *MOLVU* generates site data for the graphics program *MolView* (Cense); (h) *NEWCEL* transforms cell data; (i) *REFCAL* reduces and analyses raw data intensities; (j) *RIETVD* refines structures from multi-phase powder samples by the Rietveld method; and (k) *XTINCT* estimates an extinction coefficient from measured intensities.

ELECTRON IRRADIATION DEFECT STUDIES ON QUARTZ CRYSTALS AT CONSTANT ELECTRON ENERGY (200kV)

B . Martin, Institute of Mineralogy
Ruhr-University, Universitätsstr. 150, D-W4630 Bochum, Germany .

Electron irradiation damage in quartz single crystals and the induced transformation of crystalline areas to non-crystalline were studied by McLaren & Phakey, 1965 . Later Gopal Das & Mitchell,1974, Hobbs & Pascussi,1980, Pascussi et al. ,1983, Haliburton,1985, Vance et al. ,1986 and Inui et al.,1990 examined particular aspects of this phenomenon.

Because electron irradiation has a complex action we studied only well characterized, homogeneous areas of synthetic single crystals with fewer structural defects than those in natural quartz. In view of results by McLaren & Phakey, 1965, we examined samples with different concentrations of Li, Al, K, Fe, H only in two growth sectors (<c>, <z>). The proton concentration and defect types were influenced by heat pre-treatment.

We used crystallographically oriented cantilever thin sections (30 µm) for parallel light-microscope, REM, TEM and FTIR-, Ramanspectrometer studies. The electron irradiation defect, in a circular isotropic volume area (IVA) with damage decreasing from the inner to outer zones, was carried out in TEM at constant electron energy and varying temperatures (Florke et al.,1990).

Damaged areas, when characterized by the methods cited above, show that the electron irradiation defects are independent of ion etching method and nearly independent of proton concentration for a given sample orientation. The damage induced depends on thin section orientation and temperature pre-treatment. This is evident in light-microscope, bright-field mode in TEM, REM after slight HF-etching of the sample, diffraction mode in TEM and in Raman spectra.

Electron diffraction patterns show variable streaking for certain Bragg reflections, dependent on the volume studied in the IVA which means a measuring point in the structurally disordered IVA. These observations can also be verified by studying the strong quartz Raman signals scanning the sample from the non-damaged outer crystalline zones representing structural ordered quartz to the inner non-crystalline center of IVA.

McLaren, A . C . & Phakey, P . P ., Aust . J . Phys . (1965) **18**, 135.
Gopal Das & Mitchel, T . E ., Radiation Effects (1974) **23**, 49.
Hobbs, L . W . & Pascussi, M.R.,J.Phys.,C**6** No.7,Tome (1980) 41,237.
Pascussi, M.R., Hutchison, J.L. & Hobbs, L.W.,Radiation Effects (1983)**74**,219.
Halliburton, L.E.,Cryst.Latt.Def. and Amorph. Mat. (1985)**12**,163.
Vance, E.R., Cann, C.D. & Richardson, P.G. ,Radiation Effects (1986)**98**,71.
Florke, O.W., Martin, B., Roller, K. & Wirth, R. ,15th General Meeting of the Int. Min. ASS. (1990), Abstracts Vol.I,425.
Florke, O.W., Martin, B., Roller, K. & Wirth, R., Proc. of the XII th Int. Congress for Electron Microscopy,Material Sciences, (1990), VOL.IV,826.

15R-18

POLARITY OF THERMAL CONDUCTIVITY IN $LiNbO_3$ AND $LiTaO_3$

M.Tokonami, O.Tachikwa, Y.Ono and T.Suetsugu, Mineralogical Inst.,
Faculty of & i., Univ. of Tokyo, Hongo,Tokyo 113, Japan,
S.Kan, Daiso Co.,Ltd., Otakasu-cho, Amagasaki 660, Japan
K.Yamamoto and J.Hikita, R&D Center
Toshiba Ceramics Co. Ltd., Soya, Hadano 257, Japan.

Thermal conductivity is believed to be a second-rank symmetrical tensor property, showing no difference for any given direction and the reverse. To study the hypothesis that conductivity may reflect the polarity of materials, we measured thermal diffusivity of polar crystals by a laser flash method, observing significant differences between (+) and (-) directions along a polar *c*-axis.

$LiNbO_3$ and $LiTaO_3$ were selected for study from a variety of polar crystals, since their polarity is hard to reverse at room temperature, and homogeneous synthetic crystals are readily obtained.

Preparation of oriented specimens: Single crystals were grown by CZ techniques taking care with poling procedures. Discs, 3.5mm thick and 9.5mm in diameter, were cutperpendicular to the*c*-axis from single domain samples of $LiNbO_3$ and $LiTaO_3$.

Thermal diffusivities were measured with an ULVAC TC-3000 flash-type thermal constant analyzer. Data measurement in a disc was repeated 10 times for each direction along the *c* axis. The table shows sample number, average value(mm^2/s), standard deviation and temperature (°C) for three $LiNbO_3$(N) and one $LiTaO_3$(T) samples.

No.	$\langle\alpha\rangle$	s	Temp.
Nl+	1.65	.18	21
N1-	1.51	.12	20
N2+	1.70	.10	21
N2-	1.59	.10	21
N3+	1.63	.07	20
N3-	1.53	.11	19
N1-	1.65	.05	22
Nl+	1.70	.05	22
T1-	1.81	.05	22
Tl+	1.95	.08	23

The diffusivity with the (+) direction is significantly larger than one with the (-) direction in all five data sets. The difference of the diffusivity in $LiTaO_3$ is larger than that for $LiNbO_3$. It is concluded that thermal conductivity, which is product of diffusivity, specific heat and the density, is also a polar property.

15R-19

SMECTIC LAYER STRUCTURE OF FERROCENE CONTAINING LIQUID CRYSTALS

N. Nakamura, T. Hanasaki, and H. Onoi, Department of Chemistry,
Faculty of Science and Engineering, Ritsumeikan University,
Kita-ku, Kyoto 603, Japan.

The liquid crystallinity of the ferrocene derivatives, [4-[ω-cholesteryloxycarbonyl)alkoxy carbonyl]phenyl]ferrocene, was studied by Nakamura, Hanasaki, and Onoi(1992) using a polarizing microscope and differential scanning calorimeter. Liquid crystallinity was observed in the ferrocene derivatives containing 2, 4, 6, 10 and 11 carbon atoms in the flexible alkyl spacer. Small angle X-ray measurements on these compounds were carried out using a position sensitive proportional counter(PSPC). The temperature of the samples was controlled by a nitrogen gas blow system. Results obtained in the liquid crystal phase for these samples are listed in Table 1.

Table 1.. long spacing

n	(Å)	
2	61.3	
4	62.0	
6	64.4	
10	38.0	
11	37.4	50.6

n is the carbon atom number in the flexible alkyl spacer

The results suggest that the ferrocene derivatives containing 2, 4, 6 carbon atoms in the flexible alkyl spacer have double-layer structures and the others are mono-layer structures. The derivative with 11 carbon atoms is intermediate between the double-layer and the mono-layer structures.

Nakamura, N., Hanasaki, T. & Onoi, H. (1992). *Mol. Cryst. Liq. Cryst.*, in press.

15R-20

CUMULATIVE DISTRIBUTION FUNCTIONS OF NORMALIZED INTENSITY, ALLOWING FOR ATOMS IN SPECIAL POSITIONS IN THE UNIT CELL

B. Pal and G. D. Nigam, Department of Physics, Indian Institute of Technology, Kharagpur 721 302, India.

The effect of atoms, located in fixed and variable special positions, on the cumulative distribution function of the normalized intensity has been investigated, under the assumption that the heavy atoms are surrounded by inaccessible volumes (parallel strips surrounding the mirror planes and cylinders surrounding the axis of symmetry), which exclude light atoms occupying general Wyckoff positions in the unit cell. The shape transform of the inaccessible volume modulates the intensity in the reciprocal space, which changes the cumulative distribution function of intensity significantly from the usual Wilson type for $P1$ and $P\bar{1}$. A detailed numerical study has been made. It is noted that the effect of heavy scatterers, located in special positions in triclinic, monoclinic and orthorhombic space groups investigated, is very marked and should be considered in cases of space-group ambiguity.

The theoretical results have been tested on sets of diffraction data available for a few compounds. It was observed that the theory is capable of resolving space group ambiguities in such cases.

15S-32

REFINEMENT OF THE CRYSTAL STRUCTURES OF Cu_6O_9InCl AND $Cu_6O_9Cu_2Cl$ BY NEUTRON AND X-RAY POWDER DIFFRACTION

H. Hayakawa, E. Akiba and S. Ono, National Chemical Laboratory for Industry, Tsukuba, Ibaraki 305, Japan,
H. Ihara, Electrotechnical Laboratory, Tsukuba, Ibaraki 305, Japan,
F. Izumi, National Institute for Research in Inorganic Materials, Tsukuba, Ibaraki 305, Japan and
H. Asano, University of Tsukuba, Tsukuba, Ibaraki 305, Japan.

A new group of Cu oxide compounds $Cu_6O_8M_mX$ (M=Cu,In,Y,Ln,Pb etc.; X=halogen, NO_3 etc.) are electrical conductors. Two typical compounds with different structures have been synthesized and their crystal structures refined by the Rietveld method using neutron (NPD) and X-ray powder diffraction (XRD) data. A Rigaku RAX diffractometer was used for XRD measurements. NPD measurements were carried out using a time-of-flight diffractometer, HRP, at KENS, KEK. A Rietveld program, RIETAN, was used for both XRD and NPD analyses.

Cu_6O_8InCl is stoichiometric, with a murdochite-like structure (Dubler, 1983). Crystallographic data are space group: $Fm\bar{3}m$, a =9.1555(2)Å, d_o=5.69 g/cm^3, Z=4. R_{wp} =4.74%. [Cu_6O_8] blocks form a 3-dimensional network of 26 polyhedra composed of [CuO_4] planes sharing oxygen atoms (Cu-O:1.908Å). Another block is a network of [InO_8] cubes sharing oxygens with the 26 polyhedra at the corners (In-O:2.257Å). The centers of each block are occupied by Cl and In, respectively. The O and Cl sites (32f and 4b) are fully occupied. It is concluded that the compound has the ordered structure Cu_6O_8InCl.

The Cl sites for $Cu_6O_8Cu_2Cl$ were partly substituted by NO_3. Crystallographic data are space group: $Fm\bar{3}m$, a =9.3806(4)Å, d_o=4.95 g/cm^3, Z=4. R_{wp} 4.09 %. The $Cu_6O_8Cu_2Cl$ unit cell is larger than that of Cu_6O_8InCl, as the former contains large NO_3 anions instead of Cl atoms. The crystal structure is essentially the same as that of Cu_6O_8InCl except for Cu sites corresponding to In sites. The Cu atoms are located, not at the In sites (2b), but distributed among 6 equivalent sites (24e) around the center of the oxygen cubes with occupation factor about 29%. A Cu atom from the cubes is coordinated with 4 oxygens forming a distorted [CuO_4] plane (Cu-O:1.916Å). The cubes and the 26 polyhedra share the [CuO_4] planes and form the 3-dimensional network. This type of compound can therefore be expressed as $Cu_{6-m}O_8{\bullet}Cu_{2-n}Cl_{0.7}(NO_3)_{0.3}$ where m+n = 0.4. For the sample in this work, m was 0.1.

15S-33

A NEUTRON DIFFRACTION STUDY OF DEUTERATED BENZENE FROM 4K TO THE MELTING POINT

C.J. Craven, P.D. Hatton, and G.S. Pawley, Department of Physics, University of Edinburgh, Scotland and C.J. Howard, Australian Nuclear Science and Technology Organisation, Australia.

Benzene (C_6H_6) is one of the basic compounds of organic chemistry, and for this reason there have been numerous experimental and theoretical investigations of this material. In many respects, the benzene molecule is now very well understood. There are, however, several reports of unusual behaviour of benzene in its solid form. These include the suggestion of a discontinuous variation of lattice parameters with temperature below 140 K and reports of anomalies near the melting point (280 K) in nmr determined rotation rates and in X-ray intensities and lattice parameters.

We have completed a neutron powder diffraction investigation of deuterated benzene (C_6D_6) from 4 K to the melting point[1]. The data were refined to provide estimates of lattice parameters and data on the orientation of the benzene molecule as a function of temperature. The lattice parameters obtained are in excellent agreement with those recorded (at a limited number of temperatures) in previous work on the deuterated compound, and they varied smoothly across the whole temperature range. The most spectacular "anomaly" was the occurrence of crystal growth a few degrees below melting; we believe this has been responsible for the effects seen, for example, in the X-ray work. There remained an increase in the expansion of the *b* parameter and some anomalous changes in orientation of the benzene molecule just below melting. These are thought to be the first indications of a structural phase transition which is, however, preceded by melting[2].

References

[1] C.J. Craven, P.D. Hatton, C.J. Howard and G.S. Pawley. To appear in *J. Chem. Phys.*

[2] C.J. Craven, P.D. Hatton and G.S. Pawley. Submitted to *J. Chem. Phys.*

15S-34

A NEUTRON X-RAY/DIFFRACTION STUDY OF SIMULATED RADIATION-WASTE ELEMENT SUBSTITUTION IN SYNROC

W. Kalceff, E.A. Xuereb and D.N. Argyriou, Department of Applied Physics, University of Technology, Sydney, P.O. Box 123, Broadway, N.S.W. 2007, Australia.

This paper decribes a study aimed at revealing the mechanism of incorporation of waste elements into the various phases of SYNROC. Seven SYNROC samples, with simulated-waste loadings ranging from 0% (SYNROC-B) to 30% (SYNROC-C) at increments of 5% were fabricated using the alkoxide route and Pw-4b-D waste. Preliminary characterisation studies were carried out on each sample, including density and open porosity measurements, scanning electron microscopy studies and leach rate and chemical analyses. The x-ray and neutron TOF diffraction data was then simultaneously refined using the GSAS program (Larsen and Vondreele, 1986).

The hollandite phase was found to exist in two forms, monoclinic and tetragonal, depending on the waste loading. There is conclusive evidence for the substitution of Cs into Ba sites in the tetragonal material. It is also clear that Sr substitutes for Ca in the perovskite phase. However, substitutions into other phases could not be determined as reliably, due to the complexity of the data.

Larsen, A.C. and Von Dreele, R.B. (1986), *GSAS, General Structure Analysis System*, LAUR 86-748, Los Alamos National Laboratory.

INFLUENCE OF ^{13}C CONCENTRATION ON THE STRUCTURE OF DIAMOND

T.Yamanaka1), S.Morimoto1), H.Kanzaki2) and S.Sasaki3)
1)College of General Education, Osaka University, 1-1 Machikaneyama Toyonaka, Osaka 560
2)Nat. Inst. Res. Inorganic Materials, 1-1 Namiki Tsukuba Ibaraki 305
3) Res. Lab. Engineering Mater. Tokyo Inst. Tech. 4259 Nagatsuda Midoriku Yokohama 227, Japan

Differences in lattice constant between 3He and 4He, 20Ne and 22Ne, 12C and 13C, 74Ge and 72.6Ge have been reported. The thermal conductivity of diamond is extremely sensitive to 13C isotope concentration. The influence of 13C concentration on the structure of diamond was therefore investigated by X-ray diffraction. Diamond single-crystals with various 13C concentrations were synthesized using a flat-belt high pressure apparatus. The 13C concentration for all synthesized specimens, verified by secondary ion mass spectroscopy (SIMS) was 18.3±1.1, 48.1±1.0, 67.3±1.1 and 98.5± 0.4wt%. Specimens about 20 μm in diameter were used for diffraction studies.

Lattice constants of these and a natural sample were determined from 25~30 independent 2θ values measured at 26±0.5°C on a four-circle diffractometer using positron synchrotron radiation at the Photon Factory, Tsukuba. The wavelength λ for the incident X-ray beam, finely monochromated by a Si (111) plate, was 0.697148±0.000028Å, confirmed by reference to a silicon crystal with lattice constant a=5.430940±0.000003Å. Diffraction intensities were measured in ω-2θ scan mode with scan speed 0.01° /sec in 2θ.

The influence of 13C concentration on the diamond lattice constant can be expressed by the binary equation $a(\text{Å}) = 3.56712 - 0.00155X + 0.00066X^2$ where X=13C/(12C+13C). The difference of the lattice constant Δa between natural diamond and 13C diamond a0.0l - a0.99 is 0.00086Å. Holloway et al (1991) previously reported the linear equation $a(\text{Å}) = 3.56715 - 0.00053X$ for isotope dependency. The linear function is, however, puzzling in view of the effect of lattice vibrations.

Thermal parameters for natural (1%) and 13C diamond (99%) were refined to elucidate the isotope dependence of the anharmonic thermal vibrations. Anharmonic temperature factors for 12C and 13C were evaluated by the cumulant expansion (Johnson, 1969). The one-particle potential V(u) (Wills, 1969) was also calculated. Raman peak shifts show that the lattice vibration varies with the atomic mass difference between 12C and 13C. Thus the lattice vibrations affects the atomic displacements.

H. Holloway, K.C. Hass and M.A. Tamor *Phys. Rev. B*. **44**, 7133 (1991)
C. K. Johnson *Acta Cryst.* A**25**, 187 (1969)
B.T.M. Willis *Acta Cryst.* A**25**, 277 (1969)

15T-37

SINGLE-CRYSTAL X-RAY STUDY ON *fcc* and *hcp* C_{60}

T. Kitamoto, S. Sasaki, H. Hashizume, T. Atake, T. Tanaka, and H. Kawaji, Research Laboratory of Engineering Materials, Tokyo Institute of Technology, 4259 Nagatsuta, Midori-ku, Yokohama 227, Japan and K. Kikuchi, K. Saito, S. Suzuki, Y. Achiba, and I. Ikemoto, Department of Chemistry, Tokyo Metropolitan University, Hachioji, Tokyo 192-03.

The crystal structure of pure C_{60} has been determined using single-crystal x-ray diffraction methods. Some crystals examined in this study gave single-crystal diffraction patterns, but the intensities were very weak at a laboratory source. Precession photographs and synchrotron x-ray measurements showed for the first time that face-centered cubic (*fcc*) and hexagonal close-packed (*hcp*) crystals coexist in a single sample.

The samples of C_{60} were prepared by arc-heating of graphite rod in a helium atmosphere and purified using the liquid chromatography with benzene solvent. The benzene residue in the crystal, determined by thermogravimetry, was less than 1 wt %. Single crystals of planar shape, $0.1 \times 0.1 \times 0.01$-$0.03$ mm, were selected from the polycrystalline aggregate. Unit cells and space groups of the two phases were determined from precession photographs and synchrotron x-ray measurements with a vertical-type four-circle diffractometer ($\lambda = 0.7$ Å; BL-10A, Photon Factory). The maximum observed peak intensity was 2 kcps. The *fcc* phase at 267 K has a cell with $a = 14.13(2)$ Å; the space group is $Fm\overline{3}m$. The crystal structure was refined with 13 independent reflections of 57 measured up to $2\theta = 20°$, where a fullerene form factor of the molecular radius 3.55 Å was assumed ($R = 0.06$, $wR = 0.04$). The isotropic temperature factor of the C_{60} fullerene is 10(2) Å^2. The cell dimensions of the *hcp* phase at 299 K are $a = 9.98(2)$ and $c = 16.30(5)$ Å; the space group is $P6_3/mmc$. The intensity data up to $2\theta = 40°$ were measured but no significant peak was observed at 2θ's higher than 20° because of strong thermal vibration. Fifteen independent reflections of 934 measured are being used in refinements of the *hcp* phase. Low-temperature studies within 100 - 260 K are in progress.

15T-38

AN X-RAY STUDY OF A TWINNED n-TETRACOSANE CRYSTAL

S.C. Nyburg & A. R. Gerson,
Department of Chemistry, King's College, London
University, Strand, London WC2R 2LS, England.

n-Tetracosane (*n*-$C_{24}H_{50}$) crystals appear commonly to be twinned. The method for structure analysis of a twinned *n*-$C_{24}H_{50}$ crystal is described. The crystal consisted of a number of crystallites related by a 180° rotation about c*. On recording diffraction data (2θ scans) a high degree of overlap between the two x-ray diffraction sets was observed as manifested by extremely uneven background measurements. In order to correct the two sets of diffraction intensities for overlap and perform an ab-initio structure determination an iterative routine was devised. From the orientation matrices of the twins and a model of the reflection intensity profile it is possible to approximate the degree of overlap between reflections. Analysis of each data set corrected for overlap is carried out to give rise to a new structural model which is in turn used to calculate a new set of diffraction intensities and a more accurate definition of the overlap between neighbouring reflections.

Crystal data: *n*-$C_{24}H_{50}$, triclinic, Z=1, space group $P\bar{1}$ (No. 2) a 4.282(6), b 4.828(6), c 32.56(2)Å, α 86.20(8), β 68.83(9), γ 72.3(1)°

From this analysis it was possible to show that *n*-$C_{24}H_{50}$ is isostructural with the shorter even *n*-alkanes (eg $C_{20}H_{42}$, Nyburg & Gerson, 1992, $C_{18}H_{38}$, Nyburg & Potworowski, 1973).

Gerson, A. R. & Nyburg, S. C. (1992). *Acta. Cryst.* **B48**, 103-106.
Nyburg, S. C. & Potworowski, J. A. (1973). *Acta. Cryst.* **B29**, 347-352.

15T-39

MOLECULAR AGGREGATION OF CATIONIC SURFACTANTS AND AROMATIC COMPOUNDS

Tatsuo Kitamura, Hidehiro Uekusa, and Yuji Ohashi, Department of Chemistry, Tokyo Institute of Technology, 2-12-1, O-okayama, Meguro-ku, Tokyo 152, Japan, and Hirotaka Hirata, Niigata College of Pharmacy, 2-13-5 Kamishin' eicho, Niigata, 950-21, Japan

It has been found that some cationic surfactants such as cethyl-, myristyl- and decyltrimethylammoniumbromide (CTAB, MTAB and DTAB, respectively) exhibit very high viscoelasticity even in very dilute solutions when some aromatic compounds are added to the solution. The electron microscopic study revealed that such high viscoelasticity is caused by the entanglement of enormously elongated rod-like micelles. Recently single crystals were obtained from the solution containing the surfactant and aromatic compound. The obtained crystals are CTAB only[I], CTAB/m-cyanophenol[II], CTAB/p-cresol[III], CTAB/acridine[IV], CTAB/o-iodophenol[V], MTAB/o-iodophenol[VI] and DTAB/o-iodophenol[VII]. In order to analyse the rod-like micelles, the crystal structures of the above crystals were determined.

Crystal data are summarized in Table 1. In all the crystals the surfactant molecules are packed to form a head-to-tail ribbon. The ribbons are aligned in an antiparallel fashion to form a layer.The aromatic molecules are situated between the surfactant cations and bromide ions. Such a characteristic structure seems to be closely related to the structure of the micelles.

Table 1. Crystal data   *; 238K

	a/Å	b/Å	c/Å	β/°	V/Å^3		Z
I	5.638(1)	7.260(2)	52.072(7)	93.78(1)	2128.8(8)	$P2_1/c$	4
II	33.767(3)	7.470(1)	5.575(1)	107.076(7)	1344.2(6)	$P2_1$	2
III	32.303(3)	7.4737(5)	5.5743(5)	92.19(1)	1344.8(3)	$P2_1$	2
IV	32.066(2)	7.4014(7)	5.5898(4)	91.602(8)	1326.1(2)	$P2_1$	2
V	17.482(4)	8.409(3)	40.052(5)	90.0	5888(2)	$Pna2_1$	8
V*	17.231(2)	8.5132(6)	39.167(4)	90.0	5745(1)	$Pna2_1$	8
VI*	17.288(3)	8.292(6)	37.34(1)	90.0	5351(1)	$Pca2_1$	8
VII*	17.21	8.271	35.319	90.0	5027	-----	--

15T-40

LATTICE INSTABILITY COUPLED WITH MOLECULAR INTERNAL DEGREES OF FREEDOM IN BIPHENYL AND BIS(4–CHLOROPHENYL)SULFONE

T. Atake, T. Tanaka and H. Kawaji, Res. Lab. Eng. Mater., Tokyo Institute of Technology, Yokohama, 227 Japan, and K. Saito, K. Kikuchi and I. Ikemoto, Department of Chemistry, Faculty of Science, Tokyo Metropolitan University, Tokyo, 192-03 Japan.

Biphenyl and bis(4-chlorophenyl)sulfone(BCPS) are typical examples of a group of crystals which undergo a structural phase transition closely related to the molecular flexibility. The heat capacity of BCPS was measured by adiabatic calorimetry between 10 and 300 K, and an anomaly caused by the normal-incommensurate transition was found at 148 K. No anomaly was detected concerning a possible lock-in transition at about 115 K. The role of internal twistings of phenyl groups in BCPS was studied through a calculation of simple lattice dynamics. Only three internal degrees of freedom, *i.e.*, two internal rotations of chlorophenyl rings around the C-S axes and the ∠C-S-C bending, were taken into account for the calculation. The internal rotation of the B species of the molecular point group C_2 strongly couples with acoustic phonon modes. The coupling probably induces a normal-incommensurate phase transition associated with a soft mode. The detailed comparison between the present result of the calculation and that on biphenyl (Plakida *et al.*, 1983) reveals an interesting difference in a role of the molecular flexibility in the structural phase transition in biphenyl and BCPS. Although the lattice modulation in the low temperature phase of biphenyl is essentially due to the molecular twisting, the flexibility of BCPS molecule merely enhances the intrinsic lattice instability and the lattice modulation in crystalline BCPS is probably a complex combination of all the possible degrees of freedom allowed by the symmetry properties. In this respect, biphenyl and BCPS should be regarded as two limiting examples that show two types of coupling of molecular internal degrees of freedom with lattice properties.

Plakida, N.M., Belushkin, A.V., Natkaniec, I. & Wasiutynski, T. (1983). Phys. Status Solidi b 118, 129-138.

15T-41

DIRECTED HETEROMOLECULAR HYDROGEN BOND INTERACTIONS IN CARBOXYLIC ACID COCRYSTALS

Daniel E. Lynch and Graham Smith, Centre for Instrumental and Developmental Chemistry, School of Chemistry, Queensland University of Technology, Brisbane, and Colin H. L. Kennard, Department of Chemistry, The University of Queensland, Brisbane.

Directed hydrogen bonding has recently been used as a means to design acentric organic materials for non-linear optical purposes. Formation occurs between chemically different carboxylic acids as the result of a difference in pKa values. Important biological interactions between an acid and a base occur, more often than not, because of zwitterion formation. A series of simple model compounds that demonstrate different modes of directed hydrogen bonding have been prepared and characterized using X-ray diffraction. The series shows eight examples ranging from an O-H···O dimer (Fig.1) to an O···H–N dimer (Fig.2). The different modes of interaction are also detectable in the infrared spectra. Some of the molecules used have important herbicidal properties.

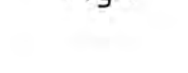

Fig.1

Fig.2

15T-42

CRYSTAL AND MOLECULAR STRUCTURES AND THERMAL PROPERTIES OF MESOGENIC 2,5-BIS(4-ETHYLBENZOYL)OXYSTYRENE AND 2,5-BIS(4-METHOXYBENZOYL)OXYBENZALDEHYDE

Yang Qingchuan Dai Sheng Zhou Hongbing Zhou Qifeng Tang Youqi
(Department of Chemistry , Peking University, Beijing 100871, China)

The crystal and molecular structures of the mesogenic 2,5-bis-(4-ethylbenzoyl)oxystyrene (I) and 2,5-bis(4-methoxybenzoyl)oxybenzaldehyde (II) have been determined by single crystal X-ray diffraction methods. Both compound I and compound II are liquid crystalline.

Crystal data:
Compound I, $C_2H_5 \cdot C_6H_4 \cdot COO \cdot C_6H_3(CH{:}CH_2) \cdot OOC \cdot C_6H_4 \cdot C_2H_5$, triclinic, space group $P\bar{1}$(No. 2), a=9.356(6), b=9.842(6), c=13.357(8) Å, α =108.68(5)°, β =105.67(5)°, γ =96.36(5)°, Z=2;
Compound II, $H_3CO \cdot C_6H_4 \cdot COO \cdot C_6H_3(CHO) \cdot OOC \cdot C_6H_4 \cdot OCH_3$, monoclinic, space group P n(No. 7), a=9.109(2), b=9.187(3), c=23.166(8) Å, β =93.93(2)°, Z=4.

In both crystals, the molecules take fully extended form with the long molecular axes of 22.7 Å for compound I and of 22.2 Å for compound II. The molecules of these two compounds are not plate-like but rather rod-like. The middle phenyl rings of the molecules rotate from the other two phenyl rings by 86.3° and 135.8° for compound I; and by 84.9° and 84.7° for compound II. All molecules are arranged parallel along their long axes in the crystals.

Compound I is a polymerizable monomer, it easily forms high molecular weight polymer upon heating without any initiators at about 140°C. Its high polymerizability might be explained by the fact that the molecules are packed such that the lateral vinyl groups of neighbouring molecules are closely correlated with a distance of only 4.7-5.6 Å and the energy-favorable parallel molecular arrangement, which is similar to the arrangement of the mesogens in its polymer.

[1] Zhou, Q. F., Li, H. M., Feng, X. D., Macromolecules, 1987, 20, 233.
[2] Zhu, X. L., Yang, Q. C., Zhou, Q. F., Chinese J. of Polymer Science, 1992, 10, 187.

15T-43

UNUSUALLY SHORT ETHYLENE BOND LENGTH AND LARGE AMPLITUDE TORSIONAL MOTION OF (*E*)-STILBENES IN CRYSTALS

K. Ogawa, S. Yoshimura, and Y. Takéuchi, Department of Chemistry, The College of Arts and Sciences, The University of Tokyo, Komaba, Meguro-ku, Tokyo, 153, Japan T. Sano, Mitsubishi Oil Co. Ltd., Ohgimachi, Kawasaki-ku, Kawasaki, 210 Japan and K. Toriumi, Dept. of Material Science, Faculty of Science, Himeji Institute of Technology, Harima Science Park City, Kamigori, Hyogo, 678-12 Japan.

This paper answers a long standing problem on the X-ray structures of (*E*)-stilbene (Ogawa, Sano, Yoshimura, Takéuchi & Toriumi, 1992). X-ray diffraction analyses of (*E*)-stilbenes **1** - **6** revealed that the X-ray structures of these compounds commonly show an unusually short bond length for the ethylene bond and strong temperature dependence of the molecular structure. No confirmation of these anomalies could be detected in solution NMR or UV spectroscopy. It is concluded that the short ethylene bond is an artifact of dynamic averaging originating in large amplitude torsional vibration of the C-Ph bonds during which the movements of the benzene rings are restrained minima. The observed temperature dependence of the molecular structure is ascribed to the slight energy difference between conformers that are interconverted by the torsional vibration.

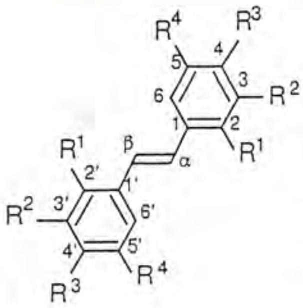

	R^1	R^2	R^3	R^4
1	H	H	H	H
2	Me	H	H	H
3	Me	H	Me	H
4	Me	H	H	Me
5	Me	H	Me	Me
6	Me	Me	H	H

Reference

Ogawa, K., Sano, T., Yoshimura, S., Takéuchi, Y. & Toriumi, K. (1992). J. *Am. Chem. Soc.* **114**,1041-1051.

15T-44

UNUSUAL STRUCTURE OF PENTAFLUORONITROSOBENZENE

H.G. Ang, W.L. Kwik, K.K. Ong and W.Y. Leong, Department of Chemistry, National University of Singapore, Lower Kent Ridge Road, Singapore 0511.

The title compound was prepared from oxidation of pentafluoroaniline (28 mmole) by 90% hydrogen peroxide (5 ml) and 90% formic acid (20 ml) in dichloromethane (125 ml) under reflux. The product was purified by vacuum fractionation to afford a volatile blue fraction in dichloromethane and a less volatile brownish green fraction. Blue and green variations of C_6F_5NO crystallised out from the respective fractions. Interestingly, structure determination of blue pentafluoronitrosobenzene (I) at 218K by single-crystal X-ray diffraction methods revealed the co-packing of hexafluorobenzene molecules and cis-dimeric units of C_6F_5NO.

Crystal data: $[C_6F_5NO]_2[C_6F_6]$ monoclinic, space group $P2_1/c$
a 9.132(2), b 16.993(5), c 11.387(3) Å, β 110.96(3)°.

The N-N distance [1.335(7) Å] in the cis-dimer [cis-azo(pentafluorobenzene)dioxide] does not differ significantly from those in the analogous nitrosobenzene cis-dimer and nitrosomethane cis-dimer, but is 0.09 Å longer than the N-N distances in trans-azobenzene and trans-p-azotoluene.

The pentafluorophenyl rings are essentially planar. As with nitrosobenzene and α-nitrosonaphthalene, no trans-dimer has been detected in the solid state for I.

15U-46

THE CRYSTAL STRUCTURE OF [ISOTHIOCYANATO(1,4,8,12-TETRAAZACYCLOPENTADECANE)COPPER(II)] THIOCYANATE

[1]Tsong-Jen Lee, [1]C.-T. Tsai, [2]Wei-Jen Lan & [2]Chung-Sun Chung
[1]Department of Physics, [2]Department of Chemistry, National Tsing Hua University

$[Cu(C_{11}H_{26}N_4)(NCS)](SCN)$, Mr = 394.06, Monoclinic $P2_1/c$, a = 9.058(1), b = 14.729(1), c = 14.443(2) Å, β = 107.24(1)°, U = 1840.4 $Å^3$, Z=4, D_x = 1.41 $Mg{\cdot}m^{-3}$, λ(Mokα)= 0.71073 Å, μ=1.41mm^{-1}, F(000) = 828, room temperature (300±5 k), final R=0.056, WR =0.055 for 2085 observed reflections. The coordination about Cu(II) is a distorted square pyramid with tetraamine equatorial and the N atom of the isothiocyanato group axial. The four donor N atoms of the macrocyclic ligand lie almost in a plane with maximum displacement of 0.038 Å. The copper(II) atom is 0.207 Å out of the basal plane of the four nitrogens toward the isothiocyanato group. The axial Cu(II)-N bond distance 2.201(5)Å is significantly longer than the equatorial Cu(II)-N bond distances, 2.035(6)-2.062(6) Å. The isothiocyanato ion is almost in a straight line,(angle N(5)-C(12)-S(1)= 179.1°). This bond angle and the bond lengths suggest that the resonance structure M-N=C=S is predominant in this crystal. The configuration of the four chiral nitrogen centers is (1RS, 4RS, 8SR, 12RS).The figure shows a perspective view of the molecule, with the displacements of Cu and N atoms indicated.

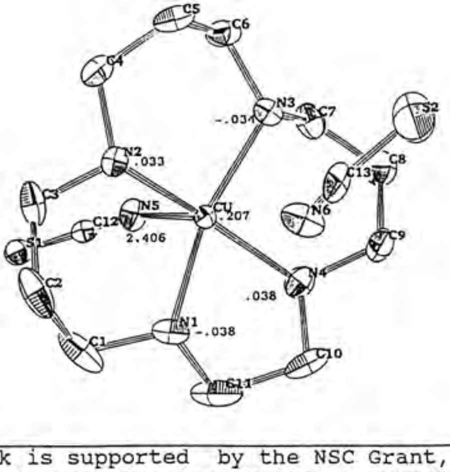

---

*This work is supported by the NSC Grant, ROC, under the contract number NSC81-0228-M-007-44 and NSC-81-208-M007-86.

15U-47

STRUCTURE OF A HEXANUCLEAR BIMETALLIC CLUSTER (μ–H)$Os_5Cu(CO)_{18}PPh_3$

H.G. Ang, W.L. Kwik, K.H. Ng, Department of Chemistry, National University of Singapore, Lower Kent Ridge Road, Singapore 0511, Republic of Singapore.

The hexanuclear bimetallic cluster (μ-H)$Os_5Cu(CO)_{18}PPh_3$ (**I**), was prepared from the reaction of (μ-H)$_2Os_3(CO)_{10}$ and (CF_3COOCu)PPh_3. (**I**) was shown by X-ray analysis to consist of a pentaosmium framework with a copper atom bridging four of the osmium atoms to form a puckered "ladder-like" arrangement based on four triangular units. The dihedral angles are: Os(1)Os(2)Os(3) and Os(2)Os(3)Cu(1), 20.7°; Os(2)Os(3)Cu(1) and Os(3)Os(4)Cu(1), 26.5°; Os(3)Os(4)Cu(1) and Os(4)Os(5)Cu(1), 25.1°. It is interesting to note that the bond distances between Cu(1) and the four Os atoms are almost equal, being 2.589(2), 2.673(2), 2.663(2) and 2.663(2) Å. The three longer Cu-bridged Os-Os bonds are also of similar length, being 3.000(1), 3.041(1), 3.069(1) Å. A bridging hydride was detected to be either bridging Os(4)-Os(5), Os(5)-Cu(1) or Os(4)-Os(5)-Cu(1).

Crystal data : (μ-H)$Os_5Cu(CO)_{18}PPh_3$ (**I**) , monoclinic, space group $P2_1/n$, $a = 16.072(4)$, $b = 14.834(2)$, $c = 18.032(4)$Å, $\beta = 100.97(2)°$ and $Z = 8$.

15U-48

STRUCTURAL STUDIES OF THE COMPLEXES OF COPPER(I) HALIDES WITH ETHYLENE THIOUREA AND *sym*-DIPHENYLTHIOUREA

P. Thavornyutikarn, Department of Chemistry, Chiangmai University, Chiangmai 50002, Thailand, and Y. Wattanakanjana and C.Pakawatchai, Department of Chemistry, Prince of Songkla University, Hat Yai 90112, Thailand, and B. W. Skelton and A. H. White, School of Chemistry, University of Western Australia, Nedlands, WA 6009, Australia.

Complexes of ethylene thiourea(etu) and *sym*- diphenylthiourea (*s*- dptu) with copper(I) halides (X=Cl,Br,I) were synthesized by varying the mole ratio of copper halides and ligands in appropriate solvents; water, ethanol or acetone. Qualitative elementary analysis was performed using X-ray fluorescence spectrometry. The percentage of copper and of sulphur of these complexes were determined by titrimetric methods. These complexes form different stoichiometries and geometries which are expected to be $[(etu)_2CuCl]_2$, $(etu)_3CuBr$, $[(etu)_2CuI]_2$, $(s\text{- }dptu)_2CuCl.H_2O$, $(s\text{- }dptu)_2CuBr$ and $(s\text{- }dptu)_2CuI$. Crystal structures of the complexes $[(etu)_2CuCl]_2$ and $(s\text{- }dptu)_2CuCl.H_2O$ determined by single crystal X-ray diffraction methods revealed the former complex to be dimeric with two different geometries of Cu(I) and the latter complex to be monomeric solvated by a water molecule with trigonal Cu(I) geometry. In both complexes the ligands coordinate to Cu atoms via S atoms.

Crystal data: $[(etu)_2CuCl]_2$ monoclinic, space group $P2_1/c$ (No. 14)
a 7.516(4), *b* 18.686(6), *c* 16.376(6) Å, β 94.73(4)°
$(s\text{- }dptu)_2CuCl.H_2O$ triclinic, space group $P\bar{1}$ (No. 2)
a 12.747(8), *b* 12.118(7), *c* 9.609(6) Å, α 68.96(5),
β 73.28(5), γ 88.46(5)°.

15U-49

THE ROLE OF NCS$^-$ ION IN Cu(II) COMPLEXES WITH DEPROTONATED DIAZADIOXIMES AND TETRAAMINES

Tahir H.Tahirov, Tian-Huey Lu, Yun-Long Hsieh & Chung-Sun Chung
National Tsing Hua University, Hsinchu, Taiwan 300, ROC

How can the linear NCS$^-$ ion enter into the coordination sphere of the named type of Cu(II) complexes, with N or S, or both atoms simultaneously? To solve this question we studied the structures of (A) Thiocyanato[3,9-dimethyl-4,8-diaza-3,8undecadiene-2,10-dione dioximato(1-)]copper(II), Cu(NCS) ($O_2N_4C_{11}H_{19}$), triclinic, *a*=7.275(3), *b*=7.7110(7), *c*=14.293(1) Å, α=90.152(7), β=98.77(1), γ=100.49(2)°, sp. gr. *P*1, Z=2, 4193 refl., *R*=0.062; (B) Isothiocyanato[3,10-diethyl-4,9-diaza-3,9-dodecadiene-2,11-dione dioximato(1-)]copper(II) (Tahirov, Lu, Luh & Chung, ACA meeting, 1992); (C) Isothiocyanato{u-thiocyanato-di-[N,N'-bis(3-aminopropyl-ethylenediamine)]}copper(II) dithiocyanate hydrate, $[Cu(NCS)(N_4C_8H_{22})]_2\ (SCN)_2 \cdot H_2O$, monoclinic, *a*=9.932(3), *b*=13.934(7), *c*=12.137(2) Å, β=98.35(2)°, sp. gr. *Pn*, Z=2, 2120 refl., *R*=0.031.

The number n of CH2 links in the poly-ethylene N,N' bridge in complexes (A) and (B) essentially influences the Cu coordination with the NCS$^-$ group. The geometry about the Cu atom in both (A) and (B) is distorted square-pyramidal with four N atoms of the diazadioxime equatorial, but the axial positions in (A) and (B) involve different atoms of the NCS$^-$ group. In (A) with n=3 the axial position is occupied by the thiocyanate S atom, the Cu-S distance being 2.520(2)Å. In (B) with n=4 the axial position is occupied by the isothiocyanate N atom with Cu-N distance 2.147(4)Å. Unlike (A) and (B), the crystal structure of (C) consists of not one but two crystallographically independent molecules (C1) and (C2) bonded with the interaction Cu...S 3.059(3)Å. The coordination geometry about Cu in (C1) is square-pyramidal with the tetraamine N atoms equatorial and the isothiocyanate N atom axial. But in (C2) the S atom from the bridging NCS$^-$ group in another axial position has square-bipyramidal geometry. The axial distances Cu-N for (C1) and (C2) are 2.261(8) and 2.372(9)Å respectively.

This work was supported by the National Science Council, ROC, under grants NSC81-0208-M007-110 and NSC81-0208-M007-86.

15U-50

MAGNETO-STRUCTURAL CORRELATIONS OF DIMERIC COPPER(II) TRICHLOROACETATES

Hidehiro Uekusa, Department of Chemistry, Tokyo Institute of Technology, Tokyo 152, Japan, Shigeru Ohba, Department of Chemistry, Keio University, Yokohama 223.

The structures of sixteen copper(II) trichloroacetate dimers have been determined by single-crystal X-ray diffraction in order to establish the correlations between the $-2J$ values, a singlet-triplet energy separation due to anti-ferromagnetic spin-exchange interaction, and the deformations of the cage structure.* In the crystals of the compounds which have small $-2J$ values, less than 200 cm^{-1}, the coordination geometry around the Cu atom is deformed from square-pyramidal (SP) to trigonal-bipyramidal (TBP)(Fig. 1), and the Cu···Cu interatomic distance is elongated (3.112(3) – 3.261(1) Å). The tendency that the longer is the Cu···Cu distance, the smaller is the $-2J$ value is observed (Fig. 2). This indicates that the spin super-exchange interaction is weaker in the TBP than in the SP structure. The reason may be as follows; The magnetic orbitals in the TBP structure mainly consist of the copper d_{z^2} orbitals, which are directed perpendicularly to each other at the two Cu atoms, and overlap only slightly with each other on the bridging carboxylate ligands. Therefore the spin-super exchange interactions are suppressed by the TBP deformation.

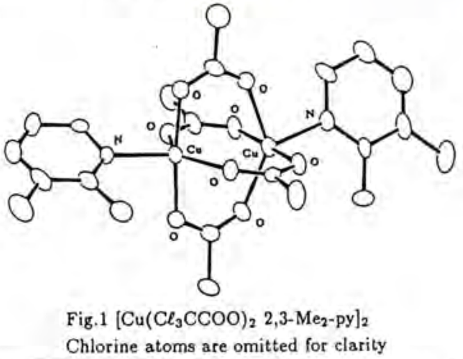

Fig.1 $[Cu(C\ell_3CCOO)_2\ 2,3\text{-}Me_2\text{-}py]_2$
Chlorine atoms are omitted for clarity

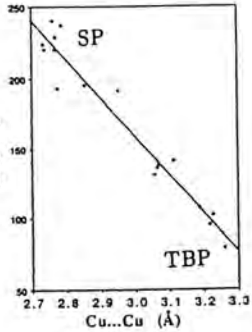

Fig.2

---

*Uekusa, H., Ohba, S., Tokii, T., Muto, Y., Kato, M., Husebye, S., Steward, O. W., Chang, S.-C., Rose, J. P., Pletcher, J. F. & Suzuki, I. (1992).*Acta Cryst.* B48, in press.

15U–51

THE STRUCTURAL CHARACTERIZATION OF $[(cy)_3PIAgpyAgIP(cy)_3]$

Effendy, and Allan H. White, Department of Physical and Inorganic Chemistry, University of Western Australia, Nedlands, W. A. 6009.

1:1 Complexes of silver (I) chloride and bromide with the bulky phosphine ligand L = $P(cy)_3$ (cy = cyclohexyl) have been structurally characterized as centrosymmetric dimers, $LAgX_2AgL$, suitable crystals being obtained from acetonitrile or pyridine.[1] The iodide complex was obtained in a satisfactorily crystalline form only from pyridine, as a hemisolvate. Surprisingly, this complex provides an example of "crevice" coordination of pyridine ligand, a previously recorded example being $[(MoO)_2(C_8H_9PS_2)_4(OS)_2py]$.[2] Crystal data monoclinic, $C2/c$, $a = 9.313(7)$Å, $b = 17.03(3)$Å, $c = 28.23(1)$Å, $\beta = 93.17(5)°$, $Z = 4$. Two projections of the molecule are shown, a two-fold axis passing through the pyridine.

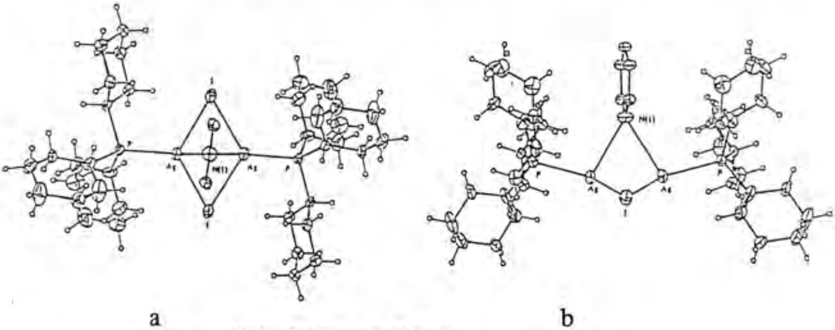

$[(cy)_3PIAgpyAgIP(cy)_3]$,
projected (a) down the two-fold axis; (b) normal to the two-fold axis

Interatomic distances and angles

Primed atom lies at (l-x, y, 1/2-z)

Atoms	distance(Å)	Atoms	angle(°)
Ag - I	2.822(1)	I - Ag - I'	106.43(5)
Ag - I'	2.857(2)	I - Ag - P	128.56(8)
Ag - P	2.415(3)	I'- Ag - P	122.43(8)
Ag - N(l)	2.76(1)	I - Ag - N(l)	88.1(1)
Ag .. Ag'	2.977(2)	I'- Ag - N(l)	87.4(1)
I .. I'	4.548(3)	P - Ag - N(1)	107.9(2)
		Ag- I - Ag'	63.24(4)
		Ag-N(1)- Ag'	65.3(3)

1. Effendy and A. H. White, Unpublished work.
2. M. G. B. Drew, P. C. H. Mitchell and A. R. Read, J. *Chem. Soc., Chem. Commun.*, 1982, 239.

15U-52

NOVEL INTERPENETRATING MOLECULAR FRAMEWORKS DERIVED FROM AgTCM

Stuart R. Batten, Bernard F. Hoskins, and Richard Robson.
Inorganic Section, School of Chemistry, University of Melbourne, Parkville, Vic 3052, Australia.

The construction of large, open frameworks with unusual structural properties has been the focus of recent research. One consequence of assembling such structures is the interpenetration of two or more identical frameworks.

The recrystallisation of AgTCM (TCM = tricyanomethanide, $C(CN)_3^-$) from acetonitrile, yields the compound AgTCM(MeCN). The structure of this compound is very similar to AgTCM. AgTCM consists of layers of two infinite, corrugated, interwoven hexagonal "chicken-wire" sheets stacked one on top of the other. The corrugation of the sheets, which allows the interpenetrating, is produced by the Ag having a distorted trigonal geometry. In AgTCM(MeCN), this is replaced by a tetrahedral Ag, which is also three-coordinate with respect to the sheets, but has a fourth bond to acetonitrile, which projects into the space between the layers.

Reaction of AgTCM in acetonitrile with a number of linear bridging ligands gives a new type of structure possessing a five coordinate silver. This time the framework consists of layers of *planar* infinite, hexagonal "chicken-wire" sheets linked to each other by the bridges connected to the axial positions of the trigonal bipyramidal silver. The structure then consists of two of these frameworks interpenetrating each other, such that the bridges of one framework pass through the centre of the hexagonal rings in the sheets of the other.

While this structure is found for the pyrazine and dabco bridges, the 4,4'-bipyridine (bipy) bridge is found to behave slightly differently. In this structure the bridge connects the layers at an angle of about 70°.

15U-53

Ag(I) AS(III) COMPLEXES WITH α-HYDROXY ACIDS: STRUCTURES OF ISOMORPHOUS COMPLEXES $\{Ag_5As_4(C_4H_2O_6)4(H_2O)_5(X)\}_n$ $\{C_4H_2O_6$ = (+)TARTRATE(4-) AND $X=NO_3^-,ClO_4^-\}$ WITH Ag-As BONDS

Graham Smith, Raymond C. Bott and Dalius S. Sagatys, Centre for Instrumental and Developmental Chemistry, School of Chemistry, Queensland University of Technology, Brisbane, 4000, Australia.

Silver(I) has proved to be a considerable utility in the stabilization of crystalline complexes of antimony(III) with hydroxy acids (Sagatys et al., 1991: Hartley et al., 1991). As an extension of this project in our laboratories, to include complexes of other Group 15 metal ions with carboxylic acids, the isomorphous silver(I) arsenic(III) complexes with tartaric acid, having formula $\{Ag_5As_4(C_4H_2O_6)_4(H_2O)_5(X)\}_n$, $[(C_4H_2O_6)$ = tartrate(4-); $X = NO_3^-$ (1) and ClO_4^- (2)] have been prepared and characterized by X-ray diffraction. Crystals are monoclinic, space group $P2_1$ with $Z = 2$ in cells of dimensions $a = 12.057(3)$, $b = 10.651(1)$, $c = 12.496(3)$, $\beta = 93.37(2)°$, (1) and $a = 12.170(5)$, $b = 10.570(1)$, $c = 12.634(4)$Å, $\beta = 92.74(2)°$, (2). The two complexes have polymer framework structures based upon two configurationally identical $[As_2(C_4H_2O_6)_2]^{2-}$ dimer anions, analogous to these in the tartar emetic structure [As-O(hydroxyl): 1.790(7) - 1.804(8)Å (1); 1.767(4) - 1.818(4)Å (2). As-O(carboxyl): 1.966(8) - 2.118(8)Å(1); 1.940(5) -2.127(5)Å (2)]. However, an arsenic of one of the dimers forms a short bond to a silver atom [As-Ag, 2.729(2)Å (1) and 2.728(1)Å (2)], completing a trigonal bipyramidal coordination about arsenic. The arsenic dimers are in turn linked by a chain of five silver cation centres via both carboxyl and hydroxyl oxygens which also form intra-chain links. All five water molecules are bonded to silver ions, with three of them bridging silver centres. The main difference between the two structures arises from the isomorphous replacement of the nitrate group in structure (1) by a perchlorate in structure (2).

Sagatys, D.S., Smith, G., Lynch, D.E. & Kennard, C.H.L., (1991), *J. Chem. Soc. Dalton Trans.*, 361-364.

Hartley, D.W., Smith, G., Sagatys, D.S. & Kennard, C.H.L., (1991), *J. Chem. Soc. Dalton Trans.*, 2735-2739.

15U-54

THE CRYSTAL STRUCTURE OF $Au(PPh_3)_2(PhCS_2)$

Ju-Chun Wang, Department of Chemistry, Soochow University, Taipei, Taiwan 11102, REP OF CHINA

The title compound have been synthesized by reacting $Au(PhCS_2)$ with excess triphenylphosphine in DCM solution. The dark reddish brown crystals suitable for X-ray analysis were grown from DCM/Et_2O mixed solvent system. The crystal structure has been determined at room temperature. The Au-P distances are 2.328(2) and 2.317(2)Å, respectively. The Au-S distances are 2.627(2) and 2.859(2)Å, which are slightly longer than the sum of the covalent radii, 2.37Å, of these two atoms. The bonding interaction in between the dithiobenzoate ligand and the Au atoms is significant. This significant bonding interaction is also reflected on the non-linear angle of P1-Au-P2, which is 136.66(6)°. Thus, the coordination number about Au center is 4, and the coordination geometry about Au center is distorted tetrahedron.

Crystal Data: $Au(PPh_3)_2(PhCS_2)$ is monoclinic, $a=9.190(2)$, $b=19.561(6)$, $c=20.734(3)$Å, $\beta=98.54(1)°$, $V=3685.7(15)Å^3$, $Z=4$, space group $P2_1/n$ (NO 14). Final R values are $R=0.044$, $R_w=0.057$ and $S=1.607$ for 4359 observed reflections and 223 parameters.

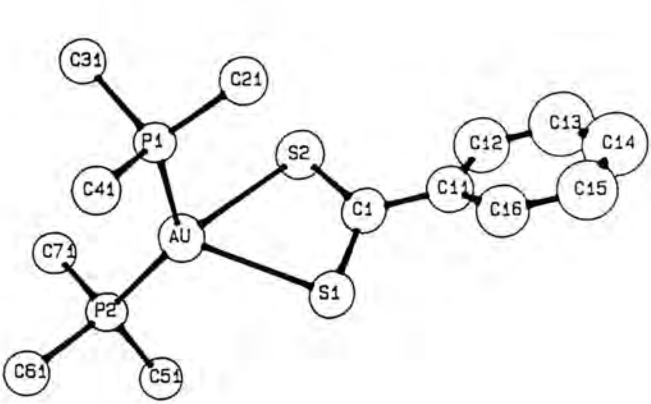

15U-55

THE CRYSTAL STRUCTURE OF A PLATINUM(II) COMPLEX OF L-METHIONYL-GLYCINE

D. Shi, T.W. Hambley & H.C. Freeman, School of Chemistry, University of Sydney, Sydney, NSW 2006, Australia.

The investigation of the interactions of platinum(II) with amino acids, peptides and related ligands is interesting for two reasons. (i) It contributes to a better understanding of the various reactions that platinum(II) undergoes in the body including those which contribute to the toxic side effects of cisplatin and to its deactivation. (ii) Platinum(II) has been used extensively to prepare isomorphous heavy-atom derivatives for protein structure analysis. The present research is aimed at providing models for the interaction of platinum(II) with proteins.

The discovery that the $[PtCl_4]^{2-}$ complex ion binds preferentially to the methionine (Met) residues in proteins, especially when these are located at the surface of the protein molecule, aroused an interest in the platinum(II)-methionine compound. It has also been reported that methionine and its metallic complexes show some antiviral and carcinostatic properties. Here the complex dichloro-L-methionyl-glycineplatinum(II) monohydrate [Pt(L-Met-Gly)Cl_2].H_2O has been prepared by the direct interaction of $PtCl_4^{2-}$ with the free ligand in aqueous solution, followed by recrystallization from dilute HCL.

Crystal Data: [Pt(L-Met-Gly)Cl_2].H_2O, orthorhombic, space group $P2_12_12_1$, Z 4, a 5.004(2), b 6.761(2), c 39.159(7) Å. The crystal structure has been determined by single-crystal X-ray diffraction methods and refined to a conventional residual ,R of 0.037.

The structure of the complex may be described as a platinum atom surrounded in a square-planar configuration by two chlorine atoms and a L-methionyl-glycine ligand. The latter is coordinated to platinum(II) atom via the N(amino) and S(thioether) atoms to form a six-membered chelate ring. The protonated peptide N, the peptide O and protonated carboxyl group are not coordinated. The conformation of the six-membered chelate ring is a 'chair' conformation with the peptide group and the S-CH_3 in equatorial positions.

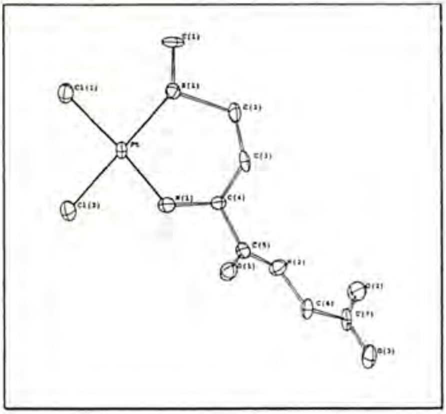

15U-56

CRYSTAL STRUCTURE OF POTASSIUM THEOBROMINIUM TETRAKIS(THIOCYANATO)PALLADATE(II)

T. Giraldi and M. R. Taylor, School of Physical Sciences, The Flinders University of South Australia, G.P.O. Box 2100, Adelaide 5001, Australia, and M. I. Moreno-Vida, J. Ruiz-Sanchez, J. M. Salas-Peregrín and E. Colacio, Departmento de Quimica Inorganica, Facultad de Ciencias, Universidad de Granada, 18071 Granada, Spain.

In the course of attempting to prepare palladium complexes of xanthine derivatives, red crystals were obtained from a mixture of (10 ml) K_2PdCl_4 (0.33 g, 1 mmol), KSCN (0.97 g, 10 mmol) and a suspension of 2 mmol of theobromine refluxed in 100 ml ethanol. X-ray crystal structure analysis has shown that the solid is the potassium theobrominium salt of tetrakisthiocyanatopalladate(II). Theobromine is protonated at N1. The tetrakisthiocyanatopalladate(II) ion is very nearly planar with thiocyanato groups making a swastika pattern around the palladium.

A search of the Cambridge Structural Database has shown that this is the first example of the tetrakisthiocyanatopalladate(II) anion whose structure has been determined, at least in structures containing organic carbon. The planar anions and the theobrominium cations lie parallel to each other in the structure and are stacked alternately. Potassium ions have a distorted 7-fold co-ordination.

Crystal Data: $KC_7H_8N_4O_2Pd(SCN)_4.H_2O$ monoclinic, spacegroup $P2_1/c$ (No.14)
a 15.172(2), b 7.173(1), c 18.619(2) Å, $\beta = 95.98(1)°$.

The Pd-S distances do not differ significantly and average 2.338(2) Å. The anion has very close to C_{4h} symmetry although this is not required crystallographically. The anion and base cation will be compared with similar species in other structures.

15U-57

PLATINUM, PALLADIUM AND RHODIUM COMPLEXES WITH METALAPENTALENE FRAMEWORK

M. Yasui, S. Yoshida and F. Iwasaki, Dept. of Applied Physics and Chemistry, The Univ. of Electro-Communications, Chofu, Tokyo 182, Japan

6a-Thiatetraazapentalene derivative (**1**) which contains the hypervalent sulfur atom (Iwasaki *et al.*) was found to give novel carbene complexes treating with $Pt(PPh_3)_4$, $Pd(PPh_3)_4$ and $Rh(PPh_3)_3Cl$. X-ray investigations have revealed that the central sulfur atom in **1** was substituted by a metal atom and the thioamide group on one or both sides was rotated to have the metal-sulfur bond in the resulted metalapentalene framework. The molecular structures of platinum (**2**) and palladium (**3**) complexes were very similar. Each metal atom is coordinated by S, S, C and P atoms in a square planar geometry. The M-S (2.28-2.29 Å), M-C distances (2.01 Å) and S-M-S (169°), P-M-C angles (177) in **2** agree well with those in **3**. The rhodium complex (**4**) has S-Rh-N bonds in contrast to Pt or Pd complexes that have S-M-S bonds. The Rh atom is coordinated by six atoms in the distorted octahedron with Cl, N, S, and C atoms in an equatorial plane and two triphenylphosphine groups in apical positions. A pseudo mirror relating two PPh_3 groups is lying on the metalapentalene plane. Rh-S 2.34, Rh-C 1.94Å and P-Rh-P 174, Cl-Rh-C 174 and S-Rh-N 162° were found. The steric hindrance due to two PPh_3 led this asymmetric S-Rh-N bond. On the other hand, Pt and Pd complexes with S-M-N bonds were found in solution, which transformed gradually to S-M-S structure.

Crystal data:

	space group	*a*	*b*	*c* /Å	β/°	No of observed	R
2	$P2_1/a$	16.419(4)	10.415(2)	16.748(4)	112.72(2)	4114	0.043
3	$P2_1/a$	17.667(5)	11.001(2)	15.658(4)	112.26(2)	5005	0.068
4	$P2_1/n$	10.302(2)	36.241(5)	11.958(2)	101.04(2)	6175	0.074

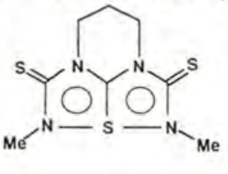

1

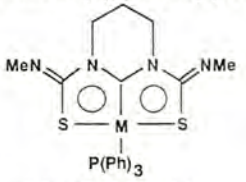

2 M=Pt;3 M=Pd

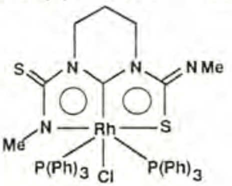

4

Iwasaki, F., Murakami, H., Yamazaki, N., Yasui, M., Tomura, M. and Matsumura, N. (1991)*Acta Cryst.* **C47**, 998-1003

15U-58

THALLIUM-CONTAINING PLATINUM SULPHUR COMPLEXES: CRYSTAL STRUCTURE OF $TlS_2Pt_2(PPh_3)_4PF_6$

M S Zhou, L L Koh, Y Xu*, T S A Hor, P H Leung and K F Mok
Dept of Chemistry, National University of Singapore, S(0511)

A main group element, thallium(Tl^+) was, for the first time, successfully introduced into platinum-sulphur complexes. The resulting compound forms yellowish, diamond-shape crystalS. The structure has been determined using X-ray diffraction.

Crystal data: $TlS_2Pt_2(PPh_3)_4PF_6$, Monoclinic, Space group *P2/n*, *Z*=2
a=18.128(2)Å, *b*=10.544(3}Å *c*=18.348(5)Å
α=γ=90.00° β=107.37(4)°
R=0.0470 for 3634 observed reflections

The crystal structure (Fig 1) shows that the $TlS_2Pt_2(PPh_3)_4PF_6$ moiety has a hat-like geometry. Tl^+ sits on top of the 2-fold axis passing through the complex. Tl^+ is strongly bound to two, 2-fold axis related, S atoms with T1-S=2.764Å and S-T1-S=68.9°. There is secondary interaction between Tl^+ and two 2-fold axis related Pt atoms with Tl-Pt=3.379Å and Pt-Tl-Pt=58.3°, suggesting substantial covalency in the Tl-Pt bonding. The geometry of the Tl, Pt and S cluster allows stabilization of this one centre(Tl^+) platinum-sulphur complexe, differentiating it from transition metal analogues, through electron delocalization. It is interesting to note that the PF_6^- counter ions are far from the positive charge centre Tl^+, which again supports the delocalization function of the cluster. Pt, coordinating with two S and two P, forms a plane with average Pt-P=2.304Å, Pt-S=2.380Å, P-Pt-P=97.0°, P-Pt-S=87.4°, S-Pt-S=82° and S-Pt-P=92°.

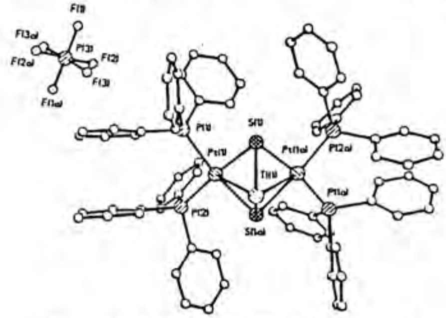

Figure 1 Crystal structure of $TlS_2Pt_2(PPh_3)_4PF_6$

15U-59

STUDY OF SYMMETRY AXIS OF THE VANADYL COMPLEX IN VO^{2+} DOPED $Cd(C_4H_2O_4).2H_2O$ SINGLE CRYSTALS

R S Bansal and V P Seth, Dept of Physics, M.D. University Rohtak, Hryana, India.

Single crystals of $Cd(C_4H_2O_4)$ doped with VO^{2+} were grown at room temperature (300K). The transparent crystals grew as prisms approximately rectangular in shape and slightly elongated along the a-axis with the (011) faces well developed, $Cd(C_4H_2O_4).2H_2O$ is monoclinic with space group $P2_{1/c}$[1]. the EPR spectra were recorded along a-axis and c*-axis of the crystal at RT and LNT. Angular variation of the hyperfine lines recorded at RT in different planes indicate that VO^{2+} ion occupies a single site in the lattice. The hyperfine tensor A and the g-tensor are found to be axially symmetric and co-axial for the VO^{2+} complex. The V-O bond direction determined from angular variation is $\theta=85°$ and $\phi=46°$ which shows the distorted octahedron around V^+ (See Figure). It is evident that this octahedron is quite distorted and the higher symmetry (axial, C_{4V}) of the vanadyl complex as indicated by the EPR results demands a local relaxation around the impurity metal ion to create the observed axial symmetry of the vanadyl complex.

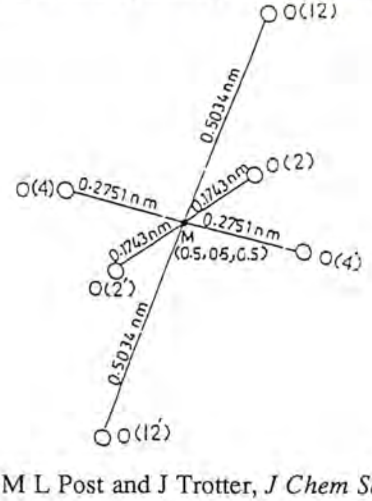

Reference: 1. M L Post and J Trotter, *J Chem Soc* (Dalton) (1974) 674.

15U-60

UNPRECEDENTED FRAMEWORK STRUCTURES: NEW DERIVATIVES OF $Cd(CN)_2$

Brendan F. Abrahams; Michaele J. Hardie; Bernard F. Hoskins and Richard Robson, School of Chemistry, University of Melbourne, Parkville, Victoria, 3052, Australia, and Geoffrey A. Williams, Australian Radiation Laboratory, Lower Plenty Road, Yallambie, Victoria, 3085, Australia.

Cadmium cyanide and its derivatives have provided a diverse range of 3D-polymeric framework structures, which may lead to prototypical structures important for industrial processes such as heterogeneous catalysis and molecular sieving. Although the structure of the parent $Cd(CN)_2$ involves two independent interpenetrating diamond-related frameworks, newly discovered geometrical arrangements involving $Cd(CN)_2$ frameworks are based on either a single diamond-like lattice, linked 2D grids or a honeycomb-like arrangement.

Crystal structures of new cadmium cyanide derivatives obtained by the reacting $Cd(CN)_2$ with N-donor ligands will be presented. The different coordination numbers available to cadmium and the flexibility shown by the usually rigid M-cyanide-M linkages have resulted in novel variations of the known structural types of $Cd(CN)_2$. The framework structure of crystals of $Cd(CN)_2.1/2$[4,4'-bipyridine], for instance, consists of an approximately trigonal bipyramidal Cd environment with bridging cyanides bent so that the $Cd(CN)_2$ framework forms a distorted diamond-like arrangement. Each rod-like bipyridine links two Cd centres in two adjacent adamantane-shaped cavities of the diamond-like framework and passes through the shared cyclohexane-like window. The $Cd(CN)_2$ pyrazine structure consists of a single framework of pyrazine linked $Cd(CN)_2$ grids and exhibits self-catenation, and $Cd(CN)_2.2/3CH_3OH.1/3$tetramethylpyrazine has a deformed honeycomb-like $Cd(CN)_2$ arrangement.

Solvated species of $Cd(CN)_2$ exist as either diamond or honeycomb related systems. The study of vapour-phase solvent exchange within such crystals will also be presented. This study has demonstrated that solvent exchange can be accompanied by an extensive topological reorganization of the $Cd(CN)_2$ framework where crystallinity, and even the single nature of the crystals involved, is preserved.

15V-62

BONDING DEFORMATION AND SUPERPOSITION EFFECTS IN THE ELECTRON DENSITY

I. Olovsson, G.J. McIntyre * & H. Ptasiewicz-Bak**

Institute of Chemistry, University of Uppsala, Box 531,
S-751 21 Uppsala, Sweden

* Permanent address: Institut Laue-Langevin,
156X, 380 42 Grenoble CEDEX, France.

** Permanent address: Institute of Nuclear Chemistry and Technology,
Dorodna 16, 03-195 Warsaw, Poland

There appears to be conflicting experimental evidence on the redistribution of the electron density in the lone-pair and other regions of a molecule due to the interaction with its nearest neigbours. In some experimental as well as theoretical deformation density maps a decrease in the lone-pair density has been reported, whereas in other cases an increase has been found. It appears that two major, counteracting factors are responsible for these differences (apart from experimental errors in the diffraction studies and limited accuracy in the theoretical calculations): an increase in the lone-pair density is expected due to the polarizing influence of the neighbours, whereas simple superposition of the isolated monomer deformation densities will lead to an apparent decrease due to the overlap with the negative contours of the neighbouring atom. Depending on which of these factors is the dominant one, an increase or decrease may thus be observed.

These facts will be illustrated by recent results on nickel sulfate hexahydrate and some other hydrogen-bonded compounds. The electron density in $NiSO_4 \cdot 6\ H_2O$ has been determined at room temperature and 25K by multipole refinement against single-crystal X-ray intensity data. The electron density based on the fitted deformation functions of all atoms in the structure is compared with the individual densities calculated from deformation functions of only Ni or the separate water molecules. In this way the effects of simple superposition of the individual densities were studied, and a partitioning of the electrostatic and polarization contributions to the hydrogen bonds and relatively weak Ni ··· O bonds attempted. When the effects of superposition are removed the deformation density around Ni shows just the features expected for Ni in a weak ideally-octahedral ligand field. The individual deformation of the three crystallographically independent water molecules show that their interaction with the environment is largely electrostatic. However, some polarization of the lone-pair densities according to the coordination of the water molecules is clearly evident.

The spin density of $NiSO_4 \cdot 6H_2O$ has also recently been studied at 1.5K and a comparison is made with the charge deformation density.

CORRECTIONS FOR EXTINCTION FROM EQUIVALENT REFLECTION INTENSITIES

E.N. Maslen & N. Spadaccini, Crystallography Centre, University of Western Australia, Nedlands, WA 6009, Australia.

Alternative procedures for correcting diffraction intensities for extinction are based on different models of crystal micro-structure. Reliable corrections require a correct theory of extinction, accurate intensity measurements, and valid statistical procedures when deriving parameter values. The widely known Zachariasen (1967) theory contains parameters defining a mosaic distribution of micro-domains, which determine the extinction corrections. Such parameters can minimize a weighted sum of squares of differences between observed and calculated structure factors, but if a modest change to the weight of a strong reflection changes extinction corrections by amounts which standard tests indicate to be significant when correcting for extinction as part of a structure refinement, the validity conditions for least squares processes are unlikely to be satisfied. Extinction corrections evaluated from diffraction intensities for equivalent reflections with different path lengths provide an independent check on values which minimize differences between observed and calculated structure factors. The former technique eliminates correlation between extinction corrections and bonding electron contributions to X-ray structure factors. The principles are not restricted to any particular form of extinction formula. For X-ray studies on several small ionic crystals corrections with the Zachariasen theory from comparison of equivalent reflections are markedly less than those which minimize differences between observed and calculated structure factors. Discrepancies originating in extinction parameter bias are exacerbated by the unfavourable statistical distribution function of the residuals when minimizing differences between observed and calculated structure factors. Analysis of intensities for equivalent reflections, although more demanding experimentally, provides least squares residuals closer to the normal distribution required for reliable non-linear least squares processes.

Zachariasen, W. H. (1967). *Acta Cryst.* A**23**, 558-564.

15V-64

ELECTRON DENSITY DISTRIBUTION OF A HIGH MELTING SUBSTANCE, TiN.

M. J. Kisono, Y. Kubota, M. Takata, and M. Sakata
Department of Applied Physics,Nagoya University, Nagoya, Japan

Titanium nitride TiN, has a NaCl type crystal structure, a high melting temperature(~3200°C), great hardness(1770kg/mm^2), and high electric conductivity (22-30μΩcm). It would be reasonable to expect very strong chemical bonding in this substance. There have been several investigations of the bonding in TiN, by both experimental and theoretical approaches. It is often considered that chemical bonding in TiN combines ionic, covalent, and metallic contributions in a rather complicated bonding state. The purpose of this paper is to study bonding in this high melting substance via a precise electron density distribution which should be obtained by the Maximum Entropy Method(MEM).

MEM provides an electron density distribution, consistent with the observed structure factors, which has least bias with respect to unmeasured structure factors. For a simple structure like TiN it is now possible to derive a high resolution distribution from X-ray powder diffraction data. The sample for this work was prepared by gas evaporation. Before measuring integrated intensities, the sample was checked by ω-scan observations and by electron microscopy, to ensure its suitability for X-ray powder diffraction. The micrograph showed that the TiN particles are about 0.1μm cubed, and the ω−scan profile was very smooth, indicating that the sample was suitable for intensity measurements by powder diffraction.

Intensities were measured with Cu$K\alpha$ radiation, and using synchrotron radiation with λ=0.9Å at the Photon Factory. Line profiles were broadened slightly, because of the small particle size. Only 10 structure factors were measured from the Cu$K\alpha$ experiment, and 22 with the synchrotron. The resultant MEM density maps show no covalent bond electrons between Ti and N atoms. The electron distributions around both atoms are slightly non-spherical. In order to estimate ionic bonding contributions, charges for Ti and N were calculated by integrating the electron density within a sphere around the Ti and N sites. The results shows that both ions are positively charged, by about +2 for Ti and slightly for N. The electron density between Ti and N is rather high, i.e. 0.56(e/Å^3) at the mid-point along the [100] direction. This strongly suggests that metallic bonding predominates in TiN. The result is preliminary because the limited number of reflections measured and coarse pixel size (32x32x32 pixels per cell) may not justify final conclusions. In order to improve the MEM map, an experiment using Mo$K\alpha$ radiation is in progress. Results will be presented at the meeting.

15V-65

ELECTRON DISTRIBUTION IN A CRYSTAL OF $NiS_{2-x}Se_x$

U. Tanaka, N. Ishizawa, Research Laboratory of Engineering Materials,
Tokyo Inst. of Technology, Nagatsuta, Midori-ku, Yokohama 227
F. Marumo, Department of Earth Sciences, Nihon University,
Sakurajosui, Setagaya-ku, Tokyo 156, and
T. Miyadai, Faculty of Science, Hokkaido University, Kita-ku, Sapporo
060, Japan.

Crystals of NiS_2 are known to show the insulator-metal transition on replacing S with Se or applying pressure. The transition occurs around $x \approx 0.55$ in the $NiS_{2-x}Se_x$ solid solution[1]. In order to investigate the changes of the electron density distribution in this solid solution system, structure refinement was carried out on an $NiS_{2-x}Se_x$ single crystal with $x \approx 0.37$.

Crystals were grown by the chemical vapour transport method using Cl_2 carrier gas. Intensities were measured on a 4-circle diffractometer with Mo$K\alpha$ radiation monochromatized with pyrolytic graphite. On the residual electron density maps, eight positive peaks corresponding to the filled dε orbitals of the Ni atom were found on the threefold axis and on three pseudo-threefold axes of the NiS_6 octahedron. Among them, six peaks on the latter axes are located further from the two on the former axis. This is slightly different from the electron distribution observed in NiS_2[2], where the eight positive peaks around Ni atom were located at almost equal distances. The structural distortion of $NiS_{2-x}Se_x$ ($x \approx 0.37$) is similar to that for NiS_2 under high pressures[3]. Therefore, replacement of S with Se in NiS^2 will have an effect similar to that of increasing pressure.

[1] Bouchard. R. J. et al., *Mat.Res.Bull.* **8**, 489-496 (1973).
[2] Sato. S & Noda. Y., *Abstract of the 38th Annual Meeting of Phys. Soc. Jpn.*, **164** (1983).
[3] T. Tsuchida, T. Komori & F. Marumo, *unpublished work*.

15V-66

ELECTRON DENSITY DISTRIBUTION IN CRYSTAL OF DIPOTASSIUM TETRAFLUORONICKELATE, K_2NiF_4

S.K. Yeh, S.Y. Wu and Yu Wang, Department of Chemistry, National Taiwan University, Taipei, Taiwan, R.O.C.

Dipotassium tetrafluoronickelate(II), Mr=212.90 tetragonal, $I\frac{4}{m}mm$, $Z=2$, $a=4.0130(6)$, $c= 13.088(2)$Å,$V=210.78(4)$ Å^3, T=300K, $Dx=3.36$ Mg.m^{-3}, Mo$K\alpha$, λ =0.7107Å , μ = 6.56cm^{-1}, F(000)=204, final R=0.018 for 698 unique reflections. The charge asphericity around the Ni atom caused by the splitting of 3d orbitals is clearly observed in the deformation density. Although the Ni site symmetry is D_{4h}, the geometry around Ni is practically O_h, with Ni-F distances of 2.0065(3), 2.0062(8)Å. The d-orbital occupancies derived from the multipole coefficients are in accord with the prediction of simple crystal field theory. The splitting of the d-orbitals in D_{4h} is e_g, b_{2g} (from t_{2g} orbitals in Oh), and b_{1g}, a_{1g} (from e_g in O_h). The occupancies of all these orbitals are nearly equal with e_g the largest (1.57), b_{1g}, and b_{2g} the second (1.54), and a_{1g} the smallest (1.51). Although the differences in occupancies are minimal, the asphericity around M can still be observed in the deformation density distribution: Positive deformation density corresponding to e_g (d_{xz}, d_{yz}) orbitals, negative troughs corresponding to a_{1g} (d_z2) orbitals and slightly negative density corresponding to b_{1g} ($d_x2_{-y}2$) and b_{2g} (d_{xy}) orbitals are manifested around the Ni atom. The effect of extinction on the deformation density will be discussed.

15V-67

SYNCHROTRON RADIATION VIBRATION AMPLITUDES AND $\Delta\rho$ MAPS FOR K_2SiF_6 AND K_2PdCl_4

J. R. Hester, E.N. Maslen & N. Spadaccini, Crystallography Centre, University of Western Australia, Nedlands, WA 6009, Australia
N. Ishizawa, Research Lab. of Engineering Materials, Tokyo Institute of Technology, 4259 Nagatsuta, Midori-Ku, Yokohama 227, Japan
and Y. Satow, Faculty of Pharmaceutical Sciences,
University of Tokyo, Hongo 7-3-1, Bunkyo-ku, Tokyo 113, Japan.

The value of synchrotron radiation in accurate electron density studies is confirmed by the agreement between $\Delta\rho$ maps measured with $\lambda = 0.9$Å and 0.7Å. High angle Fourier coefficients contribute less strongly to synchrotron maps than to maps for Mo $K\alpha$ radiation.
Low noise in the 0.9Å $\Delta\rho$ maps for K_2SiF_6 justifies confidence that physical properties predicted from the one-electron density should be reliable. Atomic charges for K, Si and F from all three data sets are close to zero. The redistribution of electrons indicated by the $\Delta\rho$ maps mainly reflects exchange interactions, and does not support simple ionic and orbital models for the bonding in K_2PdCl_4.
Vibration parameters from least squares refinements on the three K_2PdCl_4 data sets agree closely. The $\Delta\rho$ maps for the synchrotron data are consistent, and agree approximately with the Mo $K\alpha$ map away from the Pd nucleus. There is marked depletion of electrons near the Pd core, and substantial movement of electron density near the structural cavities. Whereas the Pd charge approximates +2, the K charge is significantly negative. These charges reflect transfers of electron density from tightly packed to open regions of the structure, which do not necessarily reflect atomic electronegativities.

Potassium hexafluorosilicate, K_2SiF_6, $Fm\overline{3}m$, cubic, $M_r = 220.27$, $a = 8.1419(3)$Å, $V = 539.73(3)$Å^3, $Z = 4$, $D_x = 2.711$Mg m^{-3}, $\mu_{0.9} = 39.19$, $\mu_{0.7} = 19.09$, $\mu_{\mathrm{Mo}\ K\alpha} = 20.07$ cm^{-1}, $F(000) = 424$; $T = 293$ K, $R = 0.021$, $wR = 0.018$, $S = 4.519$ for 155 unique reflections measured with 0.9Å data.
Potassium tetrachloropalladate, K_2PdCl_4, $P4/mmm$, tetragonal $M_r = 326.4$, $a = 7.0750(5)$, $c = 4.1158(5)$Å, $V = 206.02(4)$Å^3, $Z = 1$, $D_x = 2.631$Mg m^{-3}, $\mu_{0.7} = 41.874$, $\mu_{0.9} = 86.075$cm^{-1}, $F(000)=152$, $T = 293$K, $R = 0.021$, $wR = 0.020$, $S = 3.96$ for 710 unique reflections measured with 0.7Å data.

SYNCHROTRON X-RAY STUDY OF THE ELECTRON DENSITY IN CORUNDUM α–Al_2O_3

E. N. Maslen and V. A. Streltsov, Crystallography Centre, University of Western Australia, Nedlands, 6009, Australia, and N. Ishizawa, Research Laboratory of Engineering Materials, Tokyo Institute of Technology, 4259 Nagatsuta, Midori-Ku, Yokohama 227, Japan, and Y. Satow, Faculty of Pharmaceutical Sciences, University of Tokyo, Hongo 7-3-1, Bunkyo-ku, Tokyo 113, Japan.

The corundum α-Al_2O_3 structure can be classified as defining an archetypal special class within the important perovskite ABX_3 series. A detailed understanding of its structural properties and electron density is an essential prerequisite to any classification of the physical property/structure relationships for the perovskite series as a whole.

Over the past decade the electron density in single crystals of α-Al_2O_3 has been measured in X-ray diffraction analyses several times using a range of experimental techniques and crystal specimens. While these studies have much in common, there are significant discrepancies between the deformation density maps reported. This motivated us to carry out further independent studies, aimed at identifying the source of the differences between the published analyses.

The problem may originate in the common practice of determining extinction corrections as part of the least squares minimizing of differences between observed and calculated structure factors.

Deformation electron densities for corundum α-Al_2O_3 have been measured using 0.7Å and 0.9Å synchrotron radiation as well as Mo $K\alpha$ (λ=0.71069Å) radiation. Two small specimens with natural faces and dimensions 20 x 38 x 38 x 38 μm for crystal 1 and 20 x 44 x 44 x 44 μm for crystal 2 were prepared by flux growth methods. Structure factors from two sets of synchrotron and three sets of Mo *Ka* tube data for the two crystals are remarkably consistent. An isotropic extinction parameter refinement was compared with results from the method of Maslen and Spadaccini (1992). The difference electron densities exhibit approximate symmetry related more closely to the Al-Al contacts than to the nearest neighbour Al-O interactions.

Maslen, E.N. & Spadaccini, N. (1992). *Acta Cryst.* Submitted.

15V-69

A SYNCHROTRON X-RAY STUDY OF Δρ IN Y_2BaCuO_5

R. M. Hsu and E. N. Maslen, Crystallography Centre, The University of Western Australia, Nedlands, WA 6009, Australia.

Diyttrium barium copper (II) pentoxide, Y_2BaCuO_5, $M_r = 458.7$, *Pnma*, orthorhombic, $Z = 4$, $a = 12.1793$ (7), $b = 5.6591$ (5), $c = 7.1323$ (4) Å, $V = 491.58$ (6) Å^3, $D_x = 6.197$ Mg m^{-3}, $\lambda = 0.9$ Å, $\mu = 28.893$ mm^{-1}, $F(000) = 812$, $T = 295$ K. $R = 0.020$, $\omega R = 0.022$ for 16154 unique reflections measured at the Tsukuba Photon Factory. Seven O atoms are bonded to each Y atom. Each Ba atom is surrounded by eleven O atoms. Five O atoms coordinate pyramidally to the Cu atom. Bond lengths: Y-O 2.275(2)—2.379(1), Ba-O 2.611(2)—2.8312(3) and Cu-O 1.974(1)—2.016(1). The Δρ map in (010) plane, $y/b = 0.25$, on which two Y, one Ba and one O atoms are packed tightly is strongly depleted near the metal nuclei. This reflects the depleting effect of exchange on closed sub-shell density. The depleted region around each metal atom has two hollous symmetrically dispersed along the *a*-axis as shown. The depletion of electron density is reflected in charges of 2.8(1), 2.1(1), 1.6(1), 2.4(1), and -1.6(1), -1.8(1) -1.8(1) *e* for Y1, Y2, Ba, Cu and O1, O2, O3 determined by projecting the Δρ function onto atomic density basis functions. The orientation of the depleted regions provides significant evidence for second nearest neighbours interactions between Y, Ba and Cu atoms, because the density is strongly depleted along the line of the metal-metal vectors.

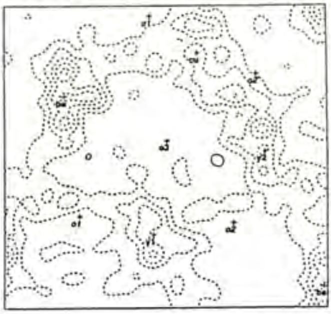

15V-70

STRUCTURE AND ELECTRON-DENSITY STUDIES OF A $Tl_2CaBa_2Cu_2O_8$ SUPERCONDUCTOR BY SYNCHROTRON X-RAYS

Satoshi Sasaki, Res. Lab. Engineering Materials, Tokyo Institute of Technology, Nagatsuta, Midori-ku, Yokohama 227, and Takeharu Mori, Photon Factory, Nat'l Lab. High Energy Physics, Oho, Tsukuba 305, and Kenichi Kawaguchi and Masao Nakao, Sanyo Tsukuba Res. Center, Koyadai, Tsukuba 305, Japan.

We have examined a high-T_c oxide superconductor of a $Tl_2CaBa_2Cu_2O_8$ phase, based on the accurate X-ray intensity data above and below the critical temperature T_c. The SQUID magnetometer measurement for the single crystal showed diamagnetism below 108 K.

Single crystals were grown from an oxide melt by a slow-cooling method from 1233 K. Using spherical single crystals of 80 and 120 μm ϕ, integrated intensity data up to $\sin\theta/\lambda = 1.37$ were collected at 296 K (Mo $K\alpha$) and 104 K ($\lambda = 0.6$ Å; BL-10A, Photon Factory). Final R and wR values in the least-squares refinements (RADY) are 0.015 and 0.014 at 296 K and 0.014 and 0.016 at 104 K, respectively. Cell dimensions and isotropic thermal parameters become smaller at lower temperature, but little structural changes were observed (Table 1). Refinements with anharmonic Gram-Charlier thermal parameters showed large c_{113} and d_{1111} for both Tl and Ba atoms, suggesting dominant anharmonicity in the <110> and <111> directions, and different values for d_{1111} and d_{1133} at two temperatures. Because the existence of electron-pairing is strongly suggested for high-T_c oxides and Cu^{2+} ions have partially filled $3d$ orbitals, electron density distributions around Cu atoms are discussed based on the difference-Fourier maps obtained from intensity data at two temperatures.

Table 1. Structural parameters of $Tl_2CaBa_2Cu_2O_8$ with anharmonic thermal parameters (x10^6).

			296 K	104 K
a (Å)			3.8471(6)	3.814(1)
c (Å)			29.397(5)	29.06(1)
V (Å^3)			435.1(1)	422.7
Tl	$4e$	z	0.213209(5)	0.21324(2)
		B_{eq}	1.342(2)	0.896(9)
Ca	$2a$	B_{eq}	0.547(6)	0.272(5)
Ba	$4e$	z	0.120818(6)	0.12075(2)
		B_{eq}	0.671(2)	0.307(6)
Cu	$4e$	z	0.05345(1)	0.05338(2)
		B_{eq}	0.514(2)	0.227(4)
O(1)	$8g$	z	0.05263(6)	0.05246(6)
		B_{eq}	0.73(3)	0.41(5)
O(2)	$4e$	z	0.14508(9)	0.1455(1)
		B_{eq}	1.02(4)	0.42(2)
O(3)	$4e$	z	0.2822(2)	0.2823(3)
		B_{eq}	5.4(2)	4.9(2)
Tl		c_{113}	2.20(9)	2.2(1)
		c_{333}	0.004(1)	-0.006(3)
		d_{1111}	2.01(8)	0.27(1)
		d_{1133}	0.027(2)	-0.001(3)
		d_{3333}	0.00011(2)	-0.00016(3)
Ba		c_{113}	0.15(7)	0.5(1)
		c_{333}	0.006(1)	0.006(2)
		d_{1111}	0.25(3)	-0.11(7)
		d_{1133}	0.012(2)	-0.012(3)
		d_{3333}	0.00012(3)	0.00004(5)

15V-71

A HYDROGEN BONDING STUDY WITH CHARGE DENSITY DISTRIBUTION AND INTERACTION ENERGY

Kuan-Jiuh Lin and Yu Wang*,
Department of Chemistry, National Taiwan University, Taipei, Taiwan, R.O.C.

Dimethylammonium hydrobis(hydrogen squarate), $(H_2NMe_2)^+$ $[H(HC_4O_4)_2]^-$, was chosen for a hydrogen bonding study since it contains both a symmetric (O···H···O distance 2.4320(6)Å) and an asymmetric (O···H···O distance 2.5646(6)Å) H-bond in the crystal structure. The compound crystallizes in the orthorhombic space group *Pccn*. The cell parameters are a=15.614(3), b=6.0537(7), c=11.691(2)Å, and Z=4 at 136K. Accurate X-ray diffraction data were measured with the Mo $K\alpha$ radiation up to 2θ of 100°.

Deformation density distributions are illustrated in terms of $\Delta\rho_{X-X}$, $\Delta\rho_{M-A}$ and $\Delta\rho_{theo}$; the former two are calculated from experimental data with the spherical and multipole atomic model respectively, and the latter one derived from ab initio calculation using a 3-21G+ basis set with the geometry obtained from the crystal structure. All these deformation density distributions give consistent agreement. The ring strain of the four-membered squarate ring is nicely demonstrated in the deformation density map with the bonding electron density maximum directed outwards from the C-C interatomic axis (exocyclic). The bonding electron density maximum gives an angle of 110°, which is much larger than the C-C-C angle of 90.80(4)°.

The H-bonds of both symmetric and asymmetric types are illustrated in the deformation density map. Their difference are quite obvious, with the deformation density much more evenly distributed around the symmetric H-bond. In addition, the calculated interaction energies of the hydrogen bonding after BSSE(basis set superposition error) correction are -58.22 and -6.62 kcal/mole for the symmetric and asymmetric types respectively. According to the energy decomposition analysis, the charge transfer and the mutual polarization play important roles in stabilizing the linear hydrogen bonding system.

15V-72

SPIN AND CHARGE TRANSFER THROUGH HYDROGEN BONDING IN $[Co(NH_3)_5(OH_2)][Cr(CN_6)]$

Brian N. Figgis, Department of Chemistry, University of Western Australia, Nedlands, WA 6009, Australia, Edward S. Kucharski, CSIRO Division of Geomechanics, 39 Fairway, Nedlands, WA 6009, Australia, and Mary Vrtis, Institut Laue-Langevin, Grenoble 38042, France.

The results of a polarised neutron diffraction (pnd) experiment on $[Co(NH_3)_5(OH_2)][Cr(CN)_6]$ carried out at 1.5 K and a magnetic field of 4.6 T with two crystal orientations are reported. Surprisingly, the experiment shows the presence of substantial amounts of spin in the cation, located on both the cobalt atom and the ammine protons. The net spin population of the cation is about one third of the total of the 3.0 unpaired electrons which arise from the $S={}^3/_2$ d^3 system of the Cr^{3+} ion. As well as the net spin transfer to the cation, there is strong spin polarisation, so that regions of negative spin, where the direction is opposite to that of the majority spin, are seen, including the cobalt atom. The $[Cr(CN)_6]^{3-}$ ion is strongly perturbed, relative to that in the salt $Cs_2KCr(CN)_6$ (Figgis, Forsyth & Reynolds (1987)).

Crystal data: $[Co(NH_3)_5(OH_2)][Cr(CN)_6]$ rhombohedral, space group $R\overline{3}$ $a = 7.282(2)$Å, $\alpha = 97.71(2)$, $V = 374.6(2)$Å^3, $Z = 1$.

Local density functional (ldf) calculations on models containing the $[Co(NH_3)_6]^{3+}$ cation and one or two $[Cr(CN)_6]^{3-}$ anions show broad agreement with the pnd results in giving considerable spin transfer to the cation, with a strong involvement of the protons in the hydrogen bonds, and large spin polarisation effects. These models contain the major features of the hydrogen bonding interactions in the crystal. However, there are many points of disagreement in detail, at least partly due to the fact that a simple model to reproduce the complex hydrogen bonding arrangements of the crystal is not possible.

Figgis, B.N., Forsyth, J.B. & Reynolds, P.A. (1987) *Inorg. Chem.*, **26**, 101-105.

15V-73

THE ELECTRON DISTRIBUTION IN $Nd_2Fe_{14}B$

D. du Boulay and E. N. Maslen, Department of Physics,
University of Western Australia, Nedlands, WA, 6009, Australia.

$Nd_2Fe_{14}B$ is ferromagnetic with a tetragonal structure, $P4_2/mnm$, $Z = 4$, a=8.816(5) and c=12.229(6) at 295 K, R=.044, ωR=.032 from 2936 unique reflections. The locally antisymmetric distribution of density near the B atom in the x-ray difference density is consistent with sp^2 bonding of B to the Nd atoms. The $4f$ and $3d$ electrons for Nd and Fe atoms are extensively redistributed. The topography indicates that the Nd and Fe sublattices are in parallel alignment. The densities near the two crystallographically independent Nd atoms show evidence of uniaxial anisotropy (see fig 1. below). The asymmetry is related to the structural geometry and the vibrational motion. Although the principal axes for the $\Delta\rho$ maps near the crystallographically independent Nd(1) and Nd(2) maps are parallel the magnitudes of the $\Delta\rho$ map features differ significantly. That presumably reflects differing contributions to the intensity of magnetization in the material by those atoms.

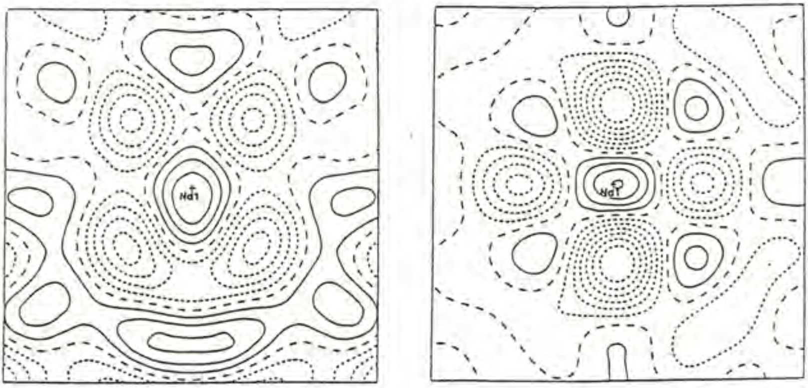

(i) z = 0 plane

(ii) Section perpendicular to (i)

Fig 1. $\Delta\rho$ near Nd(1). Map borders 2.0 x 2.0 Å^2, contour interval 1.0 e/Å^3

15V-74

ELECTRON DISTRIBUTION IN AlN FROM POWDER X-RAY DATA BY THE MAXIMUM ENTROPY METHOD

K. Nakahigashi, H. Ishibashi, S. Minamigawa and M. Kogachi, Department of Materials Science, University of Osaka Prefecture, Gakuen-cho, Sakai 593, Japan.

AlN is a tetrahedrally coordinated Ⅲ-V compound, forming a hexagonal wurtzite structure which is regarded as partially ionic and partially covalent. Gabe *et al.* (1981) determined the valence electron density in AlN by single crystal X-ray diffraction and deduced that the bonding was probably more ionic than covalent. In the present study, two kinds of AlN powder were used for powder X-ray diffraction analysis. One was ultrafine particles prepared by a "nitrogen plasma-metal" reaction method and the other was powder with an average particle size of $1.2\mu m$ offered by Tokuyama Soda Co., Ltd. The former contains about 70% aluminum. Integrated intensities were estimated from profile fits by the computer program WPPD with split Pearson Ⅶ function. The scale factor was determined by an ordinary least-squares analysis using the POWLS computer program. Adoption of this refinement method means that the phase problem can be solved by this process. Sakata *et al.* (1990) have reported that the maximum-entropy-method (MEM) has advantages for evaluating high-quality electron-density maps from X-ray powder data. As a last step, the MEM was used to obtain an electron-density-distribution for AlN. The maps for the two kinds of the powder agree well with results from single crystal X-ray diffraction which indicate the lack of a distinct bond charge. An example of the maps at the lower electron density regions for the (110) plane of AlN obtained by MEM is shown in the figure.

(110) PLANE, SINGLE UNIT CELL

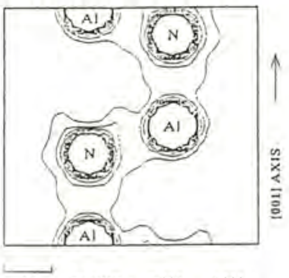

RANGE = 0.000 - 4.000,
STEP = 0.4000 $e\text{A}^{-3}$

Gabe, E., Page, Y. L & Mair, S. L. (1981). Phys. Rev. 24, 5634-5641.
Sakata, M., Mori, R., Kumazawa, S., Takata, M. & Toraya, H. (1990). J. Appl. Phys. 23, 526-534.

15V-75

ELECTRON DISTRIBUTIONS IN PURE METALS BY THE MAXIMUM ENTROPY METHOD

Y. Kubota, M. Takata and M. Sakata. Department of Applied Physics, Nagoya University, Chikusa-ku, Nagoya, 464-01, Japan.

We have already reported electron density distributions for FCC and HCP metals, such as Al, Cu and Be, Mg and Zn in the annual meetings of CSJ [1),2)] and other meeting [3),4)]. It was found that HCP metals have characteristic electron densities, with excess electrons around T sites, while there was no such features for FCC metals. FCC metals can therefore be described as metals having nearly free electrons. On the other hand, it was understood that HCP metals form electronic layers by these excess and core electrons. The structure of electronic layers in the basal plane was honeycomb shaped. These conclusions were obtained directly from the electron density distributions drawn by the Maximum Entropy Method (MEM) which could be obtained by analyzing X-ray powder diffraction data using no structural models. The purpose here is to extend this work to the electron density distributions of BCC metals, such as, W and Mo as part of a series of studies on the structure of pure metals at the electron level. Both W and Mo have rather high melting points which may reflect strong chemical bonding.

Because of the short lattice parameters of the specimens, e.g. 3.1650Å for W and 3.1470Å for Mo, a very limited number of structure factors, less than 10, could be measured if Cu$K\alpha$ radiation was used. This is not sufficient to provide reliable electron density maps by the MEM. The whole powder pattern of W was therefore collected by Mo$K\alpha$ radiation with 0.01° steps in 2θ. The collection time was 20 sec. Preliminary results show that there is no particular chemical bonding in the BCC metals, W, which is similar to FCC metals. The remarkable difference between FCC and BCC metals is that the electron densities between atomic sites is much higher in the BCC metal than that in the FCC metal. Such high electron densities around non-atomic sites could be regarded as non-directional bonding and seem to be consistent with the high melting points.

In the meeting, the results for W and Mo from much higher counting statistics data will be presented.

References
1) Y. Kubota, M. Takata, & M. Sakata. (1990) Annual meeting of CSJ.
2) M. Takata, Y. Kubota, & M. Sakata. (1991) Annual meeting of CSJ.
3) M. Takata, M. Yamada, Y. Kubota, & M. Sakata.
to be published in Advances in X-ray Analysis, Vol.**35**, (1991).
4) M. Sakata, M. Takata, Y. Kubota, T. Uno, S. Kumazawa, & C.J. Howard.
to be published in Advances in X-ray Analysis, Vol.**35**, (1991).

15V-76

ON THE REPRODUCIBILITY OF ELECTRON DENSITY MAPS FOR IDEAL PEROVSKITES

E. N. Maslen and N. R. Streltsova, Crystallography Centre, University of Western Australia, Nedlands, 6009, Australia

Assessment of the significance of differences between theoretical and experimental measurements becomes increasingly more difficult as the precision that is claimed improves. It becomes correspondingly more important to check the reproducibility of theory and of the experiments. The IUCr's Commission on Charge,Spin and Momentum Density is undertaking an international project to assess the reproducibility by comparing results obtained in different laboratories. In the case of experimental measurements reliable corrections for extinction are especially important if a quantitative comparison is required.

The use of small crystals can reduce the severity of extinction as a factor limiting the precision of the measurements. However,small crystal size limits statistical precision if a conventional tube source is used for the measurements. This difficulty can be alleviated by using synchrotron radiation. Measurements at two wavelengths provide additional information on extinction, while simultaneously providing a check on the reproducibility of the measured electron densities.

The compounds selected for the study are perovskites with the general formula ABX_3, with the ideal cubic $KZnF_3$ used as a standard, for calibrational purposes. $KCoF_3$ has a closely similar structure. Single crystals of $KZnF_3$ and $KCoF_3$ grown by slow diffusion from aqueous solution exhibited mainly {100} and {111} faces. The dimensions of specimens selected for investigation, with sizes ranging from 15 to 75 μm were measured using an Philips 505 electron microscope. In a preliminary investigation to check their suitability for the project, data sets for $KZnF_3$ and $KCoF_3$ crystals with maximum dimensions 49 and 66 μm were measured on a Syntex $P2_1$ diffractometer. After correcting the intensities for Lorentz factor, polarization and absorbtion analytically, an isotropic extinction parameter was determined by comparing intensities of equivalent reflections with different path lengths. The results are broadly consistent with earlier studies, but differ in details of electron density studies.

16A-1

NEUTRON SOURCES AND THEIR CRYSTALLOGRAPHIC APPLICATIONS

R. Chidambaram, Solid State Physics Division, Bhabha Atomic Research Centre, Trombay, Bombay - 400 085, India.

Most of the current research in neutron diffraction is being done with research reactors having thermal neutron fluxes in the range of 10^{14}~10^{15} neutrons/cm^2/sec. Some intense pulsed neutron source with higher fluxes are also available. Several medium flux reactors incorporating improved design features have recently become available in the Asian countries. For example, the new indigenously developed 100 MW Dhruva reactor at Trombay, India, has several new design features like tangential beam tubes, through-tubes, neutron guides, etc. There are also state-of-the-art instruments like computer controlled single crystal diffractometers and powder diffractometers using position sensitive detectors relating to crystallographic investigations.

The applications range from structure refinements based on profile analysis of powder patterns, studies of molecules of biological interest using single crystals and low resolution studies using small angle scattering. The scope of neutron powder diffraction studies has been considerably enhanced by recent advances in the application of the Rietveld profile refinement technique. It is now fairly straightforward to refine structures having more than 10 atoms/basis using medium resolution instruments at medium flux reactors. For example, the structures of a large number of high-T_c superconductors have been investigated at Trombay in the last few years. Some results of these studies will be highlighted.

The visualisation and interpretation of the H-bond interaction in protein structures deduced by X-ray diffraction can be assisted to a large extent by neutron diffraction studies of small biomolecules. An analysis specifically addressing experimentally observed H-bond populations associated with individual donor and acceptor groups in terms of bond length - bond strength correlations will be presented.

16A-2

SCATTERING LENGTH VARIATION IN NEUTRON DIFFRACTION

J.W. White, Research School of Chemistry, Australian National University, Canberra, Australia.

The variation of scattering contrast in neutron diffraction by substitution of one isotope for another, particularly deuterium for hydrogen [1] but also, for example, in the study of the structure of solutions by the use of nickel isotopes,[2] has had a major impact on structural studies of polymers, biological molecules and colloids and ionic solutions.
Examples will be drawn from:-

1. The structure of virus and ribosome.
2. Template induced nucleation of zeolite crystallisation from gels.[3]
3. Neutron reflectivity and the structure of thin films.

The growing interest in the use of neutron spin polarisation and polarised nuclei [4,5] for scattering length variation and the induction of contrast in crystals and biological systems with it will also be discussed.

[1] J.W. White The Continuing Promise of Neutron Scattering in Chemistry, Physics and Biology, *Trans Amer. Cryst. Assoc.*, **23**, 1-16 (1987).

[2] J. E. Enderby In "Neutron Scattering in Biology, Chemistry and Physics", Eds. R. Mason, E.W.J.Mitchell and J.W. White, Royal Society, London, 1980. Also *Phil. Trans. R. Soc. Lond. B*, **290**, 553-566 (1980).

[3] T.O. Brun, J.E. Epperson, S.J. Henderson, L.E. Iton, F. Trouw and J.W. White Small-Angle Neutron Scattering Studies of the Template-Mediated Crystallization of ZSM-S Type Zeolite. *Langmuir,* (1992).

[4] J.B. Hayter, G.T. Jenkin and J.W. White
Polarized Neutron Diffraction from Spin Polarized Protons: A Tool in Structure Determination? *Phys. Rev. Lett.*, **33**, 696-699 (1974).

[5] S. Cox, J.B. Hayter, G.T. Jenkin, M. Leslie, G. Warner and J.W. White
Precise Location of Hydrogen Atoms in Complicated Structures by Diffraction of Polarised Neutrons from Dynamically Polarized Nuclei. *Phil. Trans. R. Soc. Lond. B,* **290**, 497-503(1980).

16A-3

STRUCTURAL ANALYSIS OF ORTHORHOMBIC HfO_2 BY NEUTRON POWDER DIFFRACTION

O. Ohtaka, T. Yamanaka,College of General Education, Osaka University, Toyonaka, 560 Japan, N. Hara, H. Asano, Institute of Materials Science, University of Tsukuba, Tsukuba, Ibaraki 305 Japan, and F. Izumi, National Institute for Research in Inorganic Material Tsukuba, Ibaraki 305 Japan

A time-of-flight neutron diffraction experiment was undertaken on a powder sample of orthorhombic HfO_2 synthesized at 6 GPa and 600 ℃ for 30 min. The Rietveld analysis for the diffraction data shows that the space group of this phase is Pbca and that the crystal structure is the same as that of orthorhombic ZrO_2. The refined lattice parameters are a=1.00177, b=0.52276, and c=0.50599 nm. The feature of the structure is derived from a distorted fluorite (CaF_2) structure by the b-glide parallel to the a axis. The hafnium atom is in seven-fold coordination, with Hf-O distances ranging from 0.20496 to 0.22020nm. The oxygen-1 atom is coordinated by three hafnium atoms in an approximately coplanar configuration, whereas the oxygen-2 atom has a nearly tetrahedral coordination.

By means of neutron diffraction, controversy on the crystal structure of orthorhombic HfO_2 and ZrO_2 (high pressure form) has been terminated.

Orthorhombic HfO_2 Space group: Pbca

Atom	Position	g^a	x	y	z	$B(nm^2)^b$
Hf	8e	1.0	0.3845(1)^c	0.0338(2)	0.2439(4)	2.0(2)*10-3
O1	8e	1.0	0.2902(2)	0.3716(4)	0.3720(4)	5.4(3)*10-3
O2	8e	1.0	0.0227(1)	0.2431(6)	0.0004(5)	3.5(2)*10-3

Rwp=4.77 Rp=3.57 R_E=4.24 R_I=3.44 R_F=1.68

a Site occupancies

b Isotropic thermal parameters

c The figures in parentheses indicate estimated standard deviations of the last significant digit.

Ohtaka,O., Yamanaka,T., Kume S., Hara N., Asano H. and Izumi, F.(1990) Proc. Jpn. Acad. 66 Ser.B 193-196

Ohtaka,O., Yamanaka,T., and Kume, S.(1991) J. Ceram. Soc. Jpn. 99 826-827.

16A-4

BRAGG AND DIFFUSE NEUTRON SCATTERING STUDIES OF CUBIC ZIRCONIA

D.N. Argyriou, and M.M. Elcombe, Australian Nuclear Science and Technology Organisation, Private Mail Bag 1, Menai 2234, Australia

A number of models have been proposed for the defect structure of cubic zirconia (typically a fluorite structure), which include displacements of the O atom either along [100] or [111], or positioning the O atoms on a combination of sites. It has also been suggested that the Zr atom is displaced along [110] (1-4). In $Zr_{0.81}Y_{0.19}O_{1.905}$, $Zr_{0.875}Ca_{0.125}O_{1.875}$ and $Zr_{0.610}Y_{0.390}O_{1.805}$ we have measured acoustic phonon dispersion curves, as well as neutron elastic diffuse scattering, and we are in the process of collecting single crystal TOF neutron diffraction data.

Measurements of diffuse intensity in the 110 plane of these crystals shows a gradual shift of intensity from diffuse peaks at 112, 114, 116 and 332 (forbidden reflection for fluorite, but allowed for tetragonal zirconia) to diffuse features on the zone boundary faces, perpendicular to the [111] direction, with increasing vacancy concentration. Measured acoustic phonons in $Zr_{0.81}Y_{0.19}O_{1.905}$ and $Zr_{0.875}Ca_{0.125}O_{1.875}$ crystals are anomalously broad, so measurement as the zone boundary is approached is difficult. In contrast in the $Zr_{0.610}Y_{0.390}O_{1.805}$ crystal, phonons are better defined and both the TA and LA modes are significantly higher than in the previous two crystals. Results of the single crystal studies will be discussed with reference to current studies of diffuse and inelastic neutron scattering, as well as proposed models for the defect structure of cubic zirconia (5,6).

1. D. Steele and B.E.F. Fender, 1974. *J.Phys. C*, **7**, 1.
2. J.Jr. Faber, M.H. Mueller, B.R. Cooper 1978. *Phys. Rev.* B, **17**, 4884.
3. M. Morinaga, J.B. Cohen, J.Jr Faber 1979. *Acta Cryst.* **A35**, 789.
4. H. Horiuchi, A.J. Schultz, P.C.W. Leung, and J.M. Williams, *Acta Cryst.* **B40**, 372.
5. R.B.Nader, F.Frey, and H.Schulz, 1990. *Acta Cryst.,* **A46**, 799.
6. J.G. Allpress and H.J. Rossel, 1975. *J.Sol.St.Chem.,* **15**, 68.

16X-1

NITRO-NITRITO LINKAGE PHOTOISOMERIZATION IN CRYSTAL OF NITROPENTAAMINECOBALT (III) DICHLORIDE

S. Ohba. Department of Chemistry, Faculty of Science and Technology, Keio University, Hiyoshi 3, Kohoku-ku, Yokohama 223, Japan.

Crystals of linkage isomers, $[Co(NH_3)_5 NO_2]Cl_2$ (**I**; monoclinic *C*2/*c*. Z=4) and $[Co(NH_3)_5 ONO]Cl_2$ (**II**; orthorhombic *P*2$_1$*nb*, Z=4) can be obtained. The nitro coordination (Co- NO_2) is thermodynamically favoured and nitrito(Co-ONO) to nitro isomerization occurs in (**II**) and a phase transition follows. On the other hand, nitro to nitrito isomerization occurs in (**I**) as a result of irradiation by light. Because the crystals gradually cracked during irradiation, the initial stage of the reaction was investigated(Kubota &Ohba, 1992). Crystal of (**I**) was cooled by a cold nitrogen stream in order to protect it against degradation by heat during irradiation and to prevent the thermodynamical nitrito to nitro back reaction. Crystal structures before illumination with a Xe-lamp, (**Ia**), after illumination for 40 min, (**Ib**), and for 150 min, (**Ic**), have been analyzed. Nitrito coordination, caused by photochemical reaction, was detected on electron density maps and the populations were refined to (Ib) 8.9(5) % and (Ic) 14.5(8) %. Thermodynamical linkage isomerization in (**II**) was reinvestigated based on the X-ray intensity data measured by Grenthe and Nordin(1979). Linkage isomerization occurs in the original plane of NO_2^- in (**I**). However, the nitro plane is inclined during the isomerization of (**II**) because of steric hindrance to rotation of NO_2^- in the original plane.

Kubota, M. & Ohba, S. (1992). *Acta Cryst.* B**48**. In the press.
Grenthe, I. & Nordin, E. (1979). *Inorg. Chem.* **18**,1869-1874.

16X-2

CRYSTALLINE-STATE PHOTOISOMERIZATION OF COBALOXIME COMPLEXES

Akiko SEKINE and Yuji OHASHI , Department of Chemistry, Tokyo Institute of Technology, O-okayama, Meguro-ku, Tokyo 152, Japan

It has been found that the β-cyanoethyl (β-ce) group in cobaloxime complexes is transformed to α-cyanoethyl (α-ce) group when the complex is exposed to visible light in the solid state. Among the complexes with various base ligands, (β-ce)(3-methylpyridine)-cobaloxime forms mixed crystals with the photoproduct α-ce complex in any composition. A crystal of the β-ce complex was mounted on a Rigaku AFC-5R diffractometer and was irradiated with a Xe lamp. The lattice constants, measured by the diffractometer at a constant interval, showed gradual change. After about 75h exposure, the three-dimensional intensity data were collected. The analysed structure revealed the disordered form of the cyanoethyl group with the β-ce group and the α-ce ones. This clearly indicates that the β-ce group is isomerized to the α-ce group keeping a single crystal form on exposure to visible light. Such a crystalline-state photoisomerization has been observed for the crystals of the β-ce complexes with 3-chloropyridine and 3-bromopyridine as axial base ligands.

16X-3

PHASE TRANSITION AND CRYSTAL STRUCTURES IN 1-Br-ADAMANTANE

H.Takakura, N.Achiwa and M.Shiono, Department of Physics, Faculty of Science Kyushu University, Higashi-ku, Fukuoka, 812, Japan.

Structures of the plastic disordered, semi-ordered and ordered phases of 1-Br-adamantane ($C_{10}H_{15}Br$) were studied by X-ray diffraction and diffuse scattering analyses. The plastic phase crystallizes in the cubic space group ($Fm\overline{3}m$, $a= 10.079(1)$Å, at 340K). Its structure was well interpreted by random populated orientations of the Br-C molecular principal axis parallel to the six equivalent $< 100 >$ directions. Diffuse scattering analyses, however, suggest that the molecule has comparatively large and nearly isotropic motion. The ordered phase crystallizes in the monoclinic space group ($P2_1/c$, $a=$ 10.134(1)Å, $b=$ 6.868(1)Å, $c=$ 13.315(2)Å, β=90.05(1)°, at 244K) and the Br-C axis orients alternatively in (011) and ($0\overline{1}1$) directions propagating along the c-axis. The semi-ordered phase crystallizes in the orthorombic space group ($Pmcn$, $a=$ 10.120(2)Å, $b=$ 6.902(1)Å, $c=$ 13.626(2)Å, at 297K) where tumbling motion of molecules around the molecular principal axis is expected to occur. In all cases there are 4 molecules per unit cell. The temperature dependence of lattice parameters in three phases is described. Remarkable anomalies were seen at two transition points. We will also report structural refinements for the plastic disorderd and the semi-ordered phases based on the rigid molecular model.

16X-4

X-RAY STUDY OF THE FERRIDISTORTIVE PHASE TRANSITION IN $\{N(CH_3)_4\}_2CoBr_4$

Y. Nishihata and A. Sawada, Faculty of Science, Okayama University, Okayama 700, Japan, and H. Kasatani and H. Terauchi, School of Science, Kwansei Gakuin University, Nishinomiya 662, Japan.

Tetramethylammonium tetrabromocobaltate, $\{N(CH_3)_4\}_2CoBr_4$, undergoes a second order phase transition at about 287 K from Pmcn in the normal phase to $P12_1/c1$ in the ferroelastic phase. The deviation $\Delta\beta$ of the monoclinic angle from 90° behaves anomalously as reported by Hasebe *et al.* The behaviour suggests that it does not represent the primary order parameter of the phase transition. Ferridistortive crystals are defined by Sawada as crystals whose spontaneous strains consist of two kinds of sublattice strains with opposite signs and different magnitudes. The purpose of the present work is to clarify the microscopic origin of sublattice strains in this crystal.

A four-circle automatic diffractometer with a large χ-cradle, Rigaku AFC off-center type, was used with Mo-Kα radiation. The specimen temperature was changed by using a closed-cycle He-gas refrigerator. Structure determination of $\{N(CH_3)_4\}_2CoBr_4$ at 300 K by single-crystal X-ray diffraction methods revealed a disordered array of tetrahedral molecules. The unit cell contains three kinds of sublattices; two nonequivalent for $N(CH_3)_4$ molecules and one for $CoBr_4$ molecules. Electron density contour maps represent the disorder character as mirror reflection for all C atoms. In the low temperature phase, the crystal structure was studied at 175, 126, 76 and 46 K. Tentative results show that the occupation probability for the two configurations of $CoBr_4$ molecules tends to be saturated faster than that of $N(CH_3)_4$ molecules with decreasing temperature. The three kinds of tetrahedral molecule rotate with different temperature dependences.

Hasebe, K., Mashiyama, H., Tanisaki, S. & Gesi, K. (1984). J. Phys. Soc. Jpn. 53, 1866-1868.

Sawada, A. (1991). J. Phys. Soc. Jpn. 60, 3593-3595.

16X-5

PHASE TRANSITIONS OF THE HALOGEN BRIDGED M(II)-X-M(IV) MIXED-VALENCE COMPLEXES. STRUCTURAL STUDIES OF HIGH- AND LOW-TEMPERATURE PHASES OF $[Pt(en)_2][PtBr_2(en)_2](ClO_4)_4$

K. Toriumi, Dept of Material Science, Himeji Inst of Tech, Harima Science Park City, Hyogo 678-12, Jpn, M. Yamashita, Dept of Chem, College of General Edu, Nagoya Univ, Nagoya 464, Jpn, S. Kurita, Lab of Applied Phys, Yokohama National Univ, Yokohama 240, Jpn, I. Murase, College of General Edu, Kyushu Univ, Fukuoka 810, Jpn, and T. Ito, Dept of Chem, Tohoku Univ, Sendai 980, Jpn

Halogen-bridged M^{II}-X-M^{IV} mixed-valence complexes of $[M(en)_2]$-$[MX_2(en)_2](ClO_4)_4$ (M=Pt, Pd; X=Cl, Br; en=ethylenediamine) with linear-chain structures exhibit first-order phase transitions at temperature range of -4°C ~ 25°C. Crystal structures of the orthorhombic **1** (high-temperature) and monoclinic **2** (low-temperature) phases of $[Pt(en)_2]$-$[PtBr_2(en)_2](ClO_4)_4$ have been determined by X-ray diffraction method at room temperature. Both the structures consist of infinite linear chains with repeating unit of ($\cdots Pt^{II}\cdots Br—Pt^{IV}—Br\cdots$) along the b axes. It has been revealed that conformations of the ethylenediamine chelate rings of $Pt(en)_2$ moieties are changed from $\lambda\lambda$ ($\delta\delta$) in **1** to $\delta\lambda$ ($\lambda\delta$) in **2**. A change of the molecular symmetry owing to the conformational change is just corresponding to the change of site symmetry at the Pt complex from 222 to $\bar{1}$. Structural differences can be well expressed by sequences of the chelate ring conformations in the chains with repeating units of $[(\lambda\lambda)(\delta\delta)]$ for **1** and $[(\delta\lambda)(\lambda\delta)]$ for **2**, the conformations being coupled with each other through intra- and inter-chain hydrogen bond of NH$\cdots$O(perchlorate)$\cdots$HN. The hydrogen bond network is also changed due to the conformational change from three-dimensional **1** to two-dimensional **2**. X-ray structure analyses have also revealed that both the $Pt^{IV}—Br$ and $Pt^{II}\cdots Br$ distances in **2** are significantly elongated as compared with those in **1**, which correspond to the negative thermal expansion phenomena observed at the transition temperatures.

Crystal data: for **1**, orthorhombic, Icma, a=13.563(2), b=10.939(3), c=9.664(2) Å, Z=2, at 25°C; for **2**, monoclinic, $P2_1/m$, a=8.544(1), b=10.973(1), c=7.972(1) Å, β=109.39(1)°, Z=1, at 25°C.

16B-1

DNA CONFORMATION IN CRYSTALS

M. Sundaralingam, Department of Chemistry and Biotechnology Center, Laboratory of Biological Macromolecular Structure, The Ohio State University, 012 Rightmire Hall, 1060 Carmack Road, Columbus, Ohio 43210-1002 U.S.A.

The number of deoxyoligonucleotide crystal structures available is expanding. The main reason for X-ray structural studies of DNA crystals is to understand the structural and conformational properties of the DNA governed by their base sequences. There is new information indicating that the conformation of the DNA is determined by the base sequence. The order of the bases determines the binding characteristics of the DNA segments for the recognition enzymes. Unfortunately, in the crystal lattice, the intermolecular interactions between symmetry-related molecules seem to impart significant perturbations, not only on the DNA structure but also on the types of association between the constituent nucleotides. From the X-ray structural studies conducted in my laboratory on DNA octamers, decamers and dodecamers, I will show various instances where changes in the DNA structures have been induced by the close packing contacts. This packing effect complicates the interpretation and understanding of base sequence on DNA structure.

Research supported by NIH grant GM17378.

16B-2

PROBING THE INTERACTION BETWEEN PLATINUM ANTI-CANCER DRUGS AND DNA

T.W. Hambley, G.W. Allen, R.R. Fenton, E.C.H. Ling & K. Patser, School of Chemistry, University of Sydney, Sydney, NSW 2006, Australia.

Platinum based anti-cancer drugs such as *cisplatin* (*cis*-$[Pt\{NH_3\}_2Cl_2]$) bind tightly to DNA and interfere with replication. It is generally accepted that these events are responsible for cell death, however, it is yet to be unequivocally established which of the adducts *cisplatin* forms with DNA are responsible for the cytotoxic action (Pinto & Lippard, 1985). The inactivity of compounds only able to form monofunctional adducts has been taken to mean that one or more of the bifunctional adducts are responsible (Lippard, Ushay, Merkel & Poirier, 1983). The major bifunctional adducts fall into two classes; (i) intrastrand, i.e. GpG (60%), ApG (25%) and GNG (<10%) and (ii) interstrand linking two guanines (<10%) {Eastman, 1983}. Our approach to establishing which of these adducts effects the cytotoxic activity is to design compounds which should have a strong preference for forming only one class of adduct. We use the techniques of molecular mechanics and computer graphics to construct and investigate models of each of the *cisplatin*/DNA adducts and to design compounds which will bind stereospecifically. These compounds are then prepared, structurally characterised, their interactions with DNA measured and their *in vitro* and *in vivo* anti-tumour activities are determined.

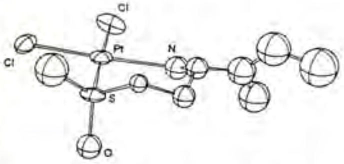

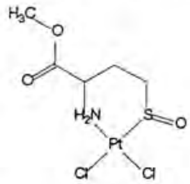

For example we have designed a series of compounds to bind to GpA sequences of DNA in preference to GpG or ApG sequences (*cisplatin* does not bind to GpA sequences {Eastman, 1983}). An ORTEP plot and a schematic diagram of one of these compounds, 2*S*, *S*S-dichloro-methionine-methylester-sulfoxide-platinum(II) are shown here. The basis of the design is our hypothesis that *cisplatin* does not bind to GpA sequences because of repulsions between an NH_3 ligand and the exocyclic NH_2 group of the adenine (Hambley, 1991). The compound shown here has a sulfoxide group in place of one NH_3 ligand and the O atom of the sulfoxide is correctly oriented to H-bond to the adenine NH_2 group.

Results will also be presented for compounds designed to bind enantiospecifically to GpG or ApG sequences and for compounds designed to bind interstrand in preference to intrastrand.

Eastman, A. (1983) *Biochemistry* 22, 3120.
Hambley, T.W. (1991) *Inorg. Chem.* 30, 937.
Lippard, S.J., Ushay, H.M., Merkel, C.M. & Poirier, M.C. (1983) *Biochemistry* 22, 5165.
Pinto, A.L. & Lippard, S.J. (1985) *Biochim. Biophys. Acta* 780, 167.

ELECTROSTATIC POTENTIAL IN tRNA^{Asp} RECOGNITION BY ASPARTYL-tRNA SYNTHETASE

A. Takenaka, Faculty of Bioscience and Biotechnology,Tokyo Institute of Technology, Yokohama 227, Japan, and
Jean Cavarelli, Jean Craude Thierry and Dino Moras, Institut de Biologie Moleculaire et Cellulaire du CNRS, 67084 Strasbourg, France.

For high fidelity transfer of genetic information, aminoacyl-tRNA synthetases recognize tRNA anticodon bases, catalyzing specific amino acid attachment to a tRNA's CCA terminus. Although diverse in size, sequence, and quarternary structure, they form only two classes with a consensus sequence motif corresponding to the aminoacylation site. X-ray structures are available for two aminoacyl-tRNA synthetase complexes (in different classes) with their cognate tRNA's[Rould, Perona, Soll & Steitz (1989), Rould, Perona & Steitz (1991), Ruff, et al. (1991)]. To help help understand recognition specificity we calculated electrostatic potentials of aspartyl-tRNA synthetase (yeast) with tRNA^{Asp} (yeast) and its mutants.

Using recently refined atomic coordinates(R=0.25 at 2.8Å resolution), nine point-mutant tRNA's were derived by replacing one base at the anticodon, assuming a conformation as in the wild type. Net charges from a CNDO/2 calculation for every amino acid and nucleotide residue were assigned to all the atoms. Electrostatic potentials were computed by solving the Poisson-Boltzmann equation with a finite differential method, using a modified program DELPHI (B. Honig et al.).

There is reasonable electrostatic complementarity of the phosphate group of tRNA with the protein's basic amino acid residues. The free tRNA molecule is surrounded by an extened negative potential that drives its approach to the synthetase molecule. There are negative minima at the O atoms in each phosphate, unless the group charge is positive. The base pairs form negative columns at the central parts in the stems. The positive potential localized on H atoms attached to C and N atoms extruding laterally from the bases compensates the negative sites on the synthetase. The nine point-mutants show how crucial local adaptation of electrostatic interaction is to specific recognition. Mis-matching of electrostatic fields occurs in any substitution replacing the anticodon base. Although the anticodon loop is flexibile, it is hard to fine tune interactions by moving the mutated base after overall matching between the two molecules is accomplished. Mis-matching at the anticodon binding site causes an unfavourable situation at the reaction site or binding itself is weakened. The next question is "how is small mis-matching transduced to and magnified in the distant reaction site of the other domain?"

Rould, M.A., Perona, J.J., Soll, D. & Steitz, T.A. (1989). Sci. **246**, 1135-1141.
Rould, M.A., Perona, J.J. & Steitz, T.A. (1991). Nature **352**, 213-218.
Ruff, M., Krishnaswamy, S., Boeglin, M., Poterszman, A., Mitschler, A., Podjarny, A., Rees, B., Thierry, J.C. & Moras, D. (1991). Sci. **252**, 1682-1689.

16B-4

BIOPHYSICAL AND CRYSTALLOGRAPHIC STUDY OF DNA RECOGNITION BY A BASIC-HELIX-LOOP-HELIX ZIPPER PROTEIN

A.R. Ferré-D'Amaré[+], P. Pognonec[@], R.G. Roeder[@] & S.K. Burley[+%]
[+] Laboratories of Molecular Biophysics,
[@]Laboratory of Biochemistry and Molecular Biology and
[%]Howard Hughes Medical Institute
The Rockefeller University, 1230 York Avenue, New York, NY 10021
USA

Upstream Stimulatory Factor (USF) is an eukaryotic transcription factor that belongs to a family of DNA binding proteins containing a basic region (B), thought directly to contact the DNA, and two putative dimerization motifs: the helix-loop-helix (HLH) and the leucine zipper (Z). In addition to full-size USF, constructs comprising the full DNA binding domain (BHLHZ) or the DNA binding domain minus the leucine zipper (BHLH) were overexpressed, purified to homogeneity, and shown to bind DNA specifically. Circular dichroism spectroscopy indicated that all three proteins undergo a similar coil-to-helix folding transition upon specific DNA binding, the increase in helical content being consistent with the basic region becoming fully α-helical when the proteins are bound to DNA. Photon correlation spectroscopic measurements of the hydrodynamic masses of the protein-DNA complexes at physiologic concentration showed that while the BHLH-DNA complex consists of a protein dimer bound to a single piece of DNA, the leucine zipper containing BHLHZ-DNA complex is a protein tetramer simultaneously bound to two pieces of DNA. Co-crystals of BHLH bound to an oligonucleotide containing its cognate recognition site have been obtained and structure determination is underway. Recent results will be presented.

16Y-1

THE EXACT SOLUTION OF DYNAMICAL DIFFRACTION IN A DISTORTED CRYSTAL AND ITS APPLICATIONS

Norio Kato, Department of Physics,
Faculty of Science and Technology, Meijo University, Nagoya, Japan

The exact solution of the dynamical diffraction was obtained (Kato, 1990) for a one-dimensional lattice expansion, in which the reflection vector is given in the form $[g(x) = g + D_o \tanh(x/H)]$, x being the coordinate normal to the crystal surface. One can represent various forms of strain by choosing suitable parameters D_o, H and x_e (e: the suffix denoting the entrance surface). This paper presents the following two applications based on this solution.

(l) Darwin-Prins rocking curves: The expression is given by

$$R(E) = |C_a|^2 \left| \frac{F(i\bar{v}+q,\ 1 - i\bar{v} + q;\ 1 + p + q;\ \frac{1}{2}(1 + \xi_e))}{F(-i\bar{v}+q, 1+i\bar{v}+q; 1+p+q;\ \frac{1}{2}(1+\xi_e))} \right|^2$$

where $|C_a|^2$ is the reflectivity for the perfect crystal, F is hypergeometric function and the parameters involved are determined by D_o, H, E (the deviation from the Bragg condition), A (absorption parameter) and $\xi_e = \tanh(x_e/H)$ etc. In cases of no absorption (neutron diffraction), R(E) has a singular behaviour -- total reflection for any distortion. The higher angular side of the main Bragg peak, under a special condition, shows an oscillation which can be interpreted by a simple theory as an interference of modified Bloch waves propagating in ± x directions. Various numerical examples will be presented systematically .

(2) Standing waves: In surface crystallography, the standing wave method is widely used. In most of the literature it has been assumed that the base crystal is ideally perfect. It can be shown that, if the crystal is deformed, an extra phase is introduced to each O and G waves in a different manner, so that the spatial positions of the standing wave are somehow different from those expected for the perfect crystal. Therefore, erroneous conclusions could be drawn about the atomic positions in unfortunate cases. Some numerical examples will be presented, demonstrating this effect.

Kato, N. (1990). *Acta Cryst.* A**46**, 672-681.

16Y-2

EXPERIMENTAL TEST OF THE DYNAMICAL THEORY OF DIFFRACTION

T. Takama and T. Kihara, Department of Applied Physics, Faculty of Engineering, Hokkaido University, Kita-ku, Sapporo 060, Japan.

Kato has developed an extinction theory (1980,1991) in which the local displacement field within a crystal is treated as variable. It is free from the traditional treatment of the mosaic idea. The theory is expected to cover the full range of diffraction from perfect to imperfect crystals. Few experiments, however, have been made to verify the theory. In our previous test (1990), we studied the influence of randomly distributed small defects on the Pendellösung beats of X-ray on the wavelength scale. The results showed good agreement with the theory on the assumption that the correlation length Γ of the amplitude of the wave-field is constant for a reflection of sample. In the present work, a similar study was performed for a crystal with a higher degree of distortion.

The samples used were three wafers 485 μm thick of Si single crystal with dislocation density ρ of 1×10^4 to $2\times10^5/\mathrm{cm}^2$ and one 588 μm with $5\times10^2/\mathrm{cm}^2$. The integrated intensities on the symmetrical Laue case were measured by a solid state detector in an X-ray wavelength range from 0.2 to 0.8 A. It was shown that the diffracted intensities increased with dislocation density. The degree of increase was dependent on the wavelength and the indices of the reflection plane. The Pendellösung beats were observed only for the sample with $\rho=5\times10^2/\mathrm{cm}^2$. The period of the beat somewhat expanded as predicted by the theory. The experimental results except for the lowest dislocation density were compared with Kato's theory(1980). The comparison was made for two functional forms of Γ ; one is proportional to the extinction distance and the other is constant for a reflection. The R factors obtained were 1% for the (220), 2% for the (422) and 4% for the (440). In contrast to the previous study, there was no significant difference between two functional forms. The increase of the R factor with index of reflection indicates that diffuse scattering is important to describe the diffraction from heavily distorted crystals.

Kato,N. (1980).*Acta Cryst.*A36,763-769 ,770-778.
Kato,N. (1991).*Acta Cryst.*A47,1-11.
Takama,T., Harima,H. & Sato,S.(1990)*Acta Cryst.*A46,C412.

16Y-3

A GENERAL THEORY OF EXTINCTION IN CRYSTALS

T. M. Sabine, Advanced Materials Program, ANSTO, Menai, NSW 2234, Australia.

The starting point for crystal structure analysis is a set of relative structure factor magnitudes for Bragg reflections from a crystal.The structure factor magnitudes ($|F_H|$) are found from measurements of the integrated intensities (I_H) of scattered radiation as the crystal is rotated through the Bragg position.A knowledge of the exact relationship between $|F_H|$ and I_H for each reflection is essential for the accurate determination of $|F_H|$. Theories of extinction are designed to provide this relationship.

In the earliest theory of X-ray diffraction from crystals, which is called the kinematic theory,the result I_H proportional to $|F_H|^2$ is obtained for all reflections. The dynamical theory, which takes into account interactions between the incident and diffracted beams during their passage through the crystal,leads to I_H proportional to $|F_H|$ for strong reflections in large crystals and to a power between 1 and 2 for weaker reflections or smaller crystals.

By convention departure from agreement with the kinematic theory is called extinction, and an extinction factor is defined by the equation $I_H^{obs} = E\, I_H^{kin}$ in which I_H^{obs} is the observed intensity and I_H^{kin} is the intensity expected for the reflection from the kinematic theory.The factor E is a function of the mosaic block size,the relative orientations of the mosaic blocks in the crystal, the strength of the reflection and the degree of absorption.

A theory has been proposed (Sabine, 1992) from which a single extinction factor incorporating all these quantities can be calculated. The expressions are rapidly convergent for use in least squares refinement methods, and apply at all angles of scattering. It is further shown (Sabine and Blair, 1992) that the theoretical methods used, namely the Hamilton-Darwin energy transfer equations (Darwin,1922;Hamilton,1957), lead to the exact Ewald and Darwin limits of the dynamical theory.

The application of this theory to practical cases will be discussed.

Darwin,C.G.(1922) Philos. Mag. 43 800-829
Hamilton,W.C.(1957) Acta Cryst. 10 629-634
Sabine, T.M. (1992) Int. Tables for Crystallography Vol C.
Sabine, T.M. and Blair, D.G. (1992) Acta Cryst. A48 98-103.

16Y-4

A NEUTRON DIFFRACTION STUDY OF KCl: A TEST OF THE SABINE EXTINCTION FORMALISM

S. Maheswaran and T. M. Sabine, Advanced Materials Program,
Australian Nuclear Science and Technology Organization, Private
Mail Bag 1, Menai, NSW 2234, Australia and
H. Klapper, Mineralogisches Institut, University of Bonn, W-5300
Bonn 1, Germany

Integrated intensities have been collected for the Bragg reflections of neutrons by a single crystal of KCl at room temperature. Measurements were made at a single neutron wavelength, 1.235 A°. The experimental data were analysed in terms of extinction formalism given by Sabine (1992). Good agreement was obtained between observed and calculated structure factors. Values obtained for the harmonic thermal parameters agree closely with previously published values. The results were compared with an analysis of the same data using the extinction formalism of Becker and Coppens (1974a, b) which is now commonly used by crystallographers. Correlations among the refined parameters are smaller with the Sabine extinction formalism compared to that of Becker and Coppens, otherwise the results (including the *R*-factor) are essentially identical.

Earlier, the crystal was characterised by Lang topography and measurements of rocking curves. The results predicted that the crystal is almost ideally imperfect. The refined values of mosaic block size (l) and mosaic spread parameter (g) obtained with both the extinction formalisms supports this prediction.

Sabine, T. M. (1992) *Int. Tables for Crystallography, Vol. C,* pp 530-533. Kluwer Academic publishers.
Becker, P. J. and Coppens, P. (1974a). *Acta Cryst.* **A30**, 129-147.
Becker, P. J. and Coppens, P. (1974b). *Acta Cryst.* **A30**, 148-153.

16Y-5

X-RAY 5*d*-ORBITAL ANALYSIS OF PtP_2 AND MULTIPLE DIFFRACTION FREE INTENSITY MEASUREMENT

K. Tanaka, S. Kumazawa* and S. Maruno*, Departments of Chemistry and Electrical and Computer Engineering*, Nagoya Institute of Technology, Nagoya, Japan, and
Ichimin Shirotani, Department of Electronic Engineering, Muroran Institute of Technology, Mizumoto-cho 27-1, Muroran Hokkaido 050, Japan.

Multiple diffraction(MD) free measurement was carried out for PtP_2 crystals with very high absorption (μ=780.8cm^{-1}). Two reflections are rarely located on the reflection sphere exactly at the same time, but MD occurs frequently if a little time lag between the two reflections is permitted. The R-factors were 0.0131 for 985 reflections and 0.165 for 936 reflections measured with and without avoiding MD, respectively. The deformation density calculated from the MD-free reflection data shows clear 5*d*-electron peaks, while the other one has additional large peaks which cannot be explained by further analysis.

In general *d*-orbitals are expressed in terms of the five real basis functions $\phi(r)$ as,

$$\Psi(\kappa_i r)=\Sigma c_{im}\phi_m(\kappa_i r), \qquad i=1,2,..5$$

where κ_i allows expansion($\kappa_i<0$) and contraction($\kappa_i>0$) of the *d*-orbitals calculated by the Hartree-Fock SCF method. The Pt *d*-orbitals in the ligand field C_{3i}-3 in Table 1 were obtained by X-ray *d*-orbital analysis (Tanaka, 1988). The deformation density from the spherical model and that calculated with these 5*d*-orbitals agreed well.

Table 1. 5*d*-orbitals of Pt in PtP_2

i	n_i	κ_i	$d_{x^2-y^2}$	d_{z^2}	d_{yz}	d_{zx}	d_{xy}
1	1.24(7)	1.18(3)	0.78(4)	0.0	-0.63(5)	-0.06(3)	0.0
2	1.24(7)	1.18(3)	0.0	0.0	-0.06(3)	0.63(5)	-0.78(4)
3	1.95(15)	0.94(6)	-0.06(3)	0.0	0.0	-0.78(4)	-0.63(5)
4	1.95(15)	0.94(6)	0.63(5)	0.0	0.78(4)	0.0	-0.06(3)
5	2.0	0.85(13)	0.0	1.0	0.0	0.0	0.0

n_i is number of electrons on the i-th orbital.

Tanaka, K. (1988). *Acta Cryst.* A**44**, 1002-1008

DIRECT OBSERVATION OF ANOMALOUS TRANSMISSION OF X-RAYS THROUGH THIN NATURAL DIAMOND CRYSTALS HAVING VARYING DEGREES OF CRYSTAL PERFECTION

Krishan Lal, S. Niranjana N. Goswami and Ajit Ram Verma, National Physical Laboratory, Dr. K.S. Krishnan Road, New Delhi - 110012, India.

We have succeeded in direct observation and study of anomalous transmission of X-rays through diamond crystals even when these were quite thin ($\mu t << 1$) and rather imperfect. Specimen diamond crystals were (111) platelets of Type I as well as Type II variety with thicknesses varying in the range : 1.24 mm - 1.63 mm corresponding to μt values : 0.28 - 0.37. These were borrowed from the famous collection of Late Prof. C.V. Raman. A five crystal X-ray diffractometer developed in our group has been employed in a three crystal configuration with (+,-,+) geometry. A highly monochromated and collimated MoK_{α_1} beam with very small width in the plane of diffraction was the exploring beam. A new technique for masking of residual direct beam and isolating bulk of the forward diffracted beam has been introduced. Type I diamond crystals were nearly perfect with diffraction curve half widths in the range : 10 arc sec - 20 arc sec (for $(\bar{2}20)$ diffracting planes). Contrast in the topographs also confirmed the high quality of these crystals. Type II diamonds were quite imperfect with diffraction curve half widths for $(\bar{2}20)$ diffracting planes in the range : 100 arc sec - 280 arc sec. Diffraction curves of the forward diffracted beam showed well defined peaks as expected when anomalous transmission of X-rays takes place. This phenomenon could be observed even when the specimen thicknesses corresponded to μt values of ~ 0.3. Crystals of low degree of perfection (Type II) also exhibited anomalous transmission. However, the intensity of the forward diffracted beam decreased with the fall in the level of perfection. These results cannot be understood in terms of the dynamical theory of X-ray diffraction.

16C-2

A SINGLE CRYSTAL DIFFRACTOMETER ON AN OPEN TUBE X-RAY GENERATOR WITH MAXIMUM TUBE VOLTAGE 200KV

F.P. Okamura and K. Yukino, National Institute for Research in Inorganic Materials, 1-1 Namiki, Tsukuba, Ibaraki 305,
K. Yamamoto, Institute of Applied Physics, University of Tsukuba, Tsukuba, Ibaraki 305,
T. Hori, S. Yoshimachi, R. Yokoyama, H. Kawasaki, K. Tsukamoto and
H. Izawa, Rigaku Corporation, 3-9-12 Matsubara-cho, Akishima, Tokyo 196, Japan.

An X-ray single crystal diffraction system suitable for high resolution electron distribution analysis has been designed and manufactured. The system is equipped with an open tube type X-ray generator which can be operated at a maximum tube voltage of 200kV. Detailed specifications for the system are as follows:

Generator	
tube voltage:	20-200kV
tube current:	2-15mA
power:	2kW
target/filter:	**Cu/Ni, Mo/Zr, Ag/Rh, W/Yb**
Goniometer:	off-centered four circle(Huber 512)
Collimator:	inner diameter = 0.2, 0.5, 1.0, 2.0 mm
Detector:	Tl—doped NaI scintillation counter

Specimen Temperature: R.T.–10K(cryostat=Cryogenics Inc.,DE202)

Reflection data for a spherical Si crystal were collected using Mo, Ag and W $K\alpha$ radiation, respectively After correction for the Lorentz factor, polarization, absorption and extinction, they were used for electron distribution analysis. The final residual R is 0.01.

16C-3

TEXTURE ANALYSIS FOR POLY-CRYSTALLINE MATERIALS ON A FOUR CIRCLE GONIOMETER

A.ul Haq and A.Q. Khan, Metallurgy Division, Dr. A.Q. Khan Research Laboratories, Kahuta, P.O. Box 502, Rawalpindi, Pakistan

Texture, i.e. non-random orientation of crystallites, is the main, if not exclusive, cause of anisotropy of the physical properties of polycrystalline materials. If a material consists of several phases the knowledge of texture becomes still more important as each phase has its own texture, which in turn leads to different anisotropy.

The texture can be determined by pole figure measurements. In this case a mathematical pole figure inversion is necessary, for which four methods have been published. Symmetry elements with inversion character in the crystal as well as in the sample lead to partial extinction of the orientation distribution function. In special cases the extinguished part can, nevertheless, be determined. In polycrystalline materials non-conventional sample symmetries, which require black-white symmetry groups for complete description, can occur. Textures may also be inhomogeneous.

Experimental texture determination is characterized by the development of step-motor operated and computerized four circle texture goniometers. Besides X-ray diffraction, neutron diffraction and electron diffraction are increasingly used. Angular dispersive methods are supplemented by energy dispersive ones. Position sensitive counters provide increased angular resolving power as well as short time measurements in order to study the kinetics of texture formation. In special cases on-line-measurements are used to control technological production processes.

Some actual applications of textures and texture measurements, especially in duplex steels, are to be presented.

16C-4

A SYSTEM FOR ANALYZING THIN FILM STRUCTURE BY GRAZING INCIDENCE DIFFRACTION: I. GRAZING INCIDENCE DIFFRACTOMETER

H. Toraya and T. Ochiai, Ceramics Research Laboratory,
Nagoya Institute of Technology, Asahigaoka, Tajimi 507, Japan.

There has been growing interest in the use of grazing incidence diffraction for analyzing thin single- and multi- film structures. This paper describes a study of part of a total system for thin-film structure analysis, consisting of a grazing incidence diffractometer and computer software for analyzing specular reflection patterns.
The hardware has been constructed from a Rigaku RINT system. Its optical system is based on the parallel-beam geometry proposed by the Parrish group for the study by reflectometry of thin-films 1). A Si (111) channel monochromator was mounted on the incident beam side at a distance of 150mm from the X-ray source, to remove the $K\alpha_2$ component and to collimate the beam. In the present study, a slit system with double-sliding mechanism was specially designed, and used after the monochromator for easy cutting of the $K\alpha_2$ component and alignment of the optical system. The thin film specimen, placed 220mm from the center of the monochromator, can be rotated in the plane of specimen surface to the desired angle by a pulse-driven motor. On the diffracted beam side, a Si (111) channel-cut crystal, mounted as an analyzer crystal 185mm from the specimen, can be removed when higher resolution is not required.

A scintillation counter was used as a detector. In order to compensate for loss of intensity due to monochromatization, the goniometer was installed on a (Cu target) rotating anode generator, which could be operated at a maximum load of 18 kW. The 111 reflection from an Si wafer was used to test the hardware system. It gave a virtually symmetric profile of nearly Gaussian shape, with a very narrow full-width at half-maximum of 0.02° and a high count rate of more than 7×10^4 cps, demonstrating high performance of the optical system as a grazing incidence diffractometer.

Several thin film samples are now under investigation using this system.

This work is supported by a Japanese Government Grant-in-Aid for General Scientific Research No. 03452293.

1) W. Parrish, C. Erickson, T.C. Huang, M. Hart, B. Gilles, and H. Toraya, *Mat. Res. Soc. Symp. Proc.*,**208**, 327-337 (1991).

16C-5

MEASUREMENT OF RADII OF CURVATURE OF SLIGHTLY BENT CRYSTALS USING A RETICON DETECTOR

Dachao Gao, Stephen W. Wilkins and Andrew W. Stevenson
CSIRO Division of Materials Science and Technology, Locked Bag 33, Clayton, Victoria 3168, Australia

A new experimental geometry for simultaneously mapping the rocking curves of a sample over a one- or two- dimensional array of points on the sample has been developed by Gao, Davis and Wilkins (1992). A monolithic channel-cut Si monochromator has been used. The calculated angular spread of the resulting (out-going) beam is of the order of 0.1″ and the expansion factor of the monochromator is 144. A cryogenically cooled Reticon linear photodiode array with 25 µm spatial resolution was used for the one-dimensional detector. When a wide incident beam in the form of pseudo-plane waves (such as is used here) irradiates a bent specimen, the Bragg diffraction conditions cannot be simultaneously satisfied at each point on the sample. However, by rotating the sample in incremental steps, the Bragg diffraction conditions could be satisfied point by point, for misorientation in the plane of diffraction. Then, the Reticon detector collects X-ray diffraction rocking curve data from a horizontal (plane of diffraction) linear segment of the sample. Due to the extremely parallel incident X-ray beam, there is a one-to-one correspondence between a point in the cross section of the diffracted-beam and a point on the sample giving rise to it. Therefore, the radius of the curvature of the sample is precisely determined from the contour map of X-ray rocking curves. This method is much more sensitive than the commonly used double-crystal diffractometry (Kα doublet) method (Cohen & Focht, 1970).

The measurements of radii of curvature of several samples (CdTe/GaAs, AlGaAs/GaAs, GaAs/Si, InSb and GaAs) have been obtained using this method. The results for the radii of curvature vary from 11.3 to 554 m., including both concave and convex cases. The detectable limit of radius of curvature could be greater than 1000 m. The uniformity and the local variation of the radii of curvature over the sample is easily revealed and precisely determined from the contour map.

Gao, D., Davis, T.J. & Wilkins, S.W. (1992). 1st European Symposium on X-ray Topography and High Resolution Diffraction, 8-10 July, 1992, Marseilles, France.
Cohen, B.G. & Focht, M.W. (1970). *Solid State Elec.* 13, 105-112.

THE WORLD DIRECTORY OF CRYSTALLOGRAPHERS, ELECTRONIC MAIL, AND COMMUNICATION WITH CRYSTALLOGRAPHERS IN THE ASIAN REGION

H. Hashizume, Res. Laboratory of Engineering Materials, Tokyo Institute Technology, Yokohama 227, Japan, and
Y. Epelboin, Lab. Miner. Crist., Univ. P-M Curie and CNRS, Paris 75252, France

During the organization of this conference the organizers were particularly sensitive to the need for good, fast communication in our region. This motivated them to propose AsCA ComNet, a communication network which collects current fax numbers and electronic mail addresses for Asian crystallographers[1]. Syd Hall collaborated in defining an information format which is simple and brief to expedite the collection task and future updating. Fifteen sub-editors were nominated in the Asia-Pacific region and data collection work started in April 1992.

Independently of the AsCA ComNet project, the International Union of Crystallography decided to create a database of crystallographers and other relevant information. The idea is to maintain that database at Chester, allowing crystallographers all over the world to enter and retrieve information, accessing it through computer networks. The database will be used to produce the 9th edition of World Directory of Crystallographers, and for other purposes like establishing mail lists of information exchange in special fields of crystallography. The stored information will be in STAR format[2] using only ASCII letters. It will include name, title, institution, postal address, year of birth, qualification, position, telephone and fax numbers, e-mail address and keywords[3]. The database will be regularly updated by national and regional sub-editors who are given the right to do so. An official invitation was issued to the sub-editors to gather the information in July 1992. A first demonstration is planned at the next IUCr meeting at Beijing, August 1993.

E-mail addresses of crystallographers can be found in the Boston database, compiled and maintained by Martha Teeter of Boston College. On request, the whole body of the database is sent to the user by e-mail. This database includes, however, only e-mail addresses and institution names. There are very few entries from Asian countries. It will eventually be integrated into the IUCr database together with AsCA ComNet, to produce a more complete database.

[1] H. Hashizume (1992) *J. Cryst. Soc. Japan* **34**, No. 2.
[2] S.R. Hall (1991) *J. Chem. Info. Comp. Sci.*, **31**, 326-333.
[3] Y. Epelboin (1992) *Acta Cryst.* A**48**, 5, 785.

16Z-2

CIFtbx: FORTRAN ROUTINES FOR MANIPULATING CIF's

S.R. Hall, Crystallography Centre, University of Western Australia,
Nedlands 6009, Australia.

CIFtbx is a subroutine library which provides for simple commands to read and write a Crystallographic Information File (CIF: Hall, Allen & Brown, 1991). The *CIF (software) tool box* routines may be added to any Fortran application manipulating CIF data. *CIFtbx* is public domain software which may be implemented on any computer.

CIFtbx was developed to assist programmers developing software for accessing and generating CIF's. It is proposed that this software makes access to data stored in CIF format *easier than for any other format.* Some important attributes of these tools are as follows:

- their application requires only a rudimentary knowledge of the CIF syntax.
- provides for automatic checking of the input and output CIF data structure.
- single commands are used to put and get CIF data to and from assigned Fortran variables. No knowledge is required of where the passed data item is in the CIF.
- the processing of repeated data or text lines or looped text packets is completely under the control of the programmer.
- data may be validated against one or more CIF dictionaries. This is convenient for checking global definitions (using standard dictionaries such as `cifdic.C91`) or for local customised applications such as *CIFIO* (Hall, 1992).

Hall, S.R. (1992) *CIFIO: Xtal3.2 System*. Ed.s Hall and Stewart. University of Western Australia and University of Maryland.

Hall, S.R., Allen, F.H., and Brown, I.D. (1991) *Acta Cryst.* **A47**, 655-685.

16Z-3

XAFS: CAN THIS IMPORTANT TECHNIQUE ACHIEVE RESPECTABILITY?

D.C. Creagh, Department of Physics, University College, The University of New South Wales, Northcott Drive, Campbell, ACT 2603, Australia.

Extended X ray Absorption Fine Structure (XAFS) is a technique which has the potential to elucidate facets of atomic environments in materials not observable using other techniques. It is, however, a technique which has been both improperly applied and imperfectly understood for at least the past two decades.

In the X ray Attenuation Project conducted under the auspices of the IUCr (Creagh & Hubbell (1987, 1990)) several thousand XAFS experiments were evaluated. Of these only a few hundred were not open to severe criticism, because of experimental deficiencies, incorrect analyses, or both.

Because of concerns about the ill-repute into which the study of materials using XAFS had fallen a committee was created at the XAFS V Conference in Seattle to discover how best to raise the standard of XAFS papers submitted to scientific journals.

The "Standards and Criteria Committee" has had three major workshops since its creation. Details concerning developments in the theory, apparatus, experimental procedures, data reduction, experimental and data analysis were addressed, and the results were reported (Lytle et al (1989), Bunker et al (1991)). Further, an XAFS data base, accessible by all XAFS users, was established at the National Nuclear Data Centre at the Brookhaven National Laboratory.

The response of XAFS users to these initiatives has been slow. Because of this a recent workshop addressed the problem of user education. A short course of XAFS instruction has been created with a view to making an XAFS education package available to all synchrotron radiation sources, and indeed to all interested parties.

This paper will describe the "Short Course in XAFS" and discuss its applicability to the solution of problems faced in the use of XAFS by crystallographers.

Creagh, D.C. & Hubbell, J.H. (1987), *Acta Cryst.* A43, 102-112.
Creagh, D.C. & Hubbell, J.H. (1990), *Acta Cryst.* A46, 402-408.
Lytle, F.W., Sayers, D.E. & Stern, E.A. (1989), *Physics B*, 158, 701-722.
Bunker, G., Hasnain, S. & Sayers, D.E. (1991), in *X ray Absorption Fine Structure*, eds S. Samar Hasnain & Ellis Horwood, (London), 751-771.

16Z-4

SHELXL-92 A NEW LEAST-SQUARES REFINEMENT PROGRAM FOR USE WITH SINGLE CRYSTAL DIFFRACTION DATA

George M. Sheldrick, Institut für Anorganische Chemie, der Universität, Göttingen, Germany, and Ward T. Robinson, Department of Chemistry, University of Canterbury, Christchurch, New Zealand.

SHELXL-92 is a FORTRAN-77 program for the refinement of crystal structures from X-ray or neutron diffraction data, and is primarily designed for single crystal data from small structures (1-1000 unique atoms) at atomic resolution. It is intended to be easy to install and use on a wide variety of computers, and replaces the structure-refining part of SHELX-76.

SHELXL-92 is general and efficient for all space groups in all settings and there are no arbitrary limits to the size of problems which can be handled, except for the total memory available to the program. All instructions are in machine independent free format, with extensive use of default settings to minimize the amount of input required from the user. Instructions and data are taken from two standard (ASCII) text files, so that input files can easily be transferred between different computers. SHELXL-92 is a PUBLIC DOMAIN progam; it is provided in source form, also as a precompiled version which has been optimized for Pc's. There are no restrictions on its use or distribution anywhere in the world for non-commercial purposes.

The program produces all the information required for efficient development of a complete structural model from a partially correct one derived using separate direct or vector methods programs such as SHELXS86. It contains many options for fully automatic handling of constraints on positional and thermal parameters and for placement of hydrogen atoms. Structural models can also be restrained to conform with chemically reasonable expectations for interatomic distances and thermal displacement parameters. These similarity restraints can be particularly useful in refinements of macromolecular structure. The atom designation rules, which accommodate standard practices, help minimize the instructions required to invoke constraints and restraints. All tables necessary for electronic mail submission to both Acta Cryst. (C) and the CSD are provided in CIF format and a companion program CIFTAB can produce hard copy in formats suitable for other journals.

16Z-5

AN INTEGRATED X-RAY MEASUREMENT AND COMPUTATION SYSTEM FOR PROTEIN CRYSTALLOGRAPHY

N. Yasuoka, Y. Higuchi, S. Misaki, Y. Morimoto* and I. Fujii**, Department of Life Science, Himeji Institute of Technology, Kanaji 1479-1, Hyogo 678-12, *Department of Bio-technology, Tokushima University, **Department of Biological Science and Technology, Tokai University

As workstations have become more popular in crystallography laboratories, powerful X-ray analysis systems can now be operated via local area networks. Here we describe an integrated system for measuring X-ray intensities, transferring the diffraction data to workstations, computing for structure analysis and displaying the molecular structure.

For the X-ray measurements, we have a four-circle diffractometer and an oscillation camera equipped with an imaging-plate. The machines are controlled with a personal computer, and measured data can be transferred via Ethernet to workstations. A block diagram of the system is illustrated in the Figure. The older graphics workstation is a TITAN with 2CPU (16MIPS x 2) and 64 megabytes of memory. A new one recently installed is a Silicon Graphics IRIS Indigo Elan. A DIP100 imaging plate X-ray diffraction apparatus is a kind of area detector. It has a disk 20cm in diameter. X-ray intensities are measured in 125 x 125 micrometer pixels, and the data are transferred to the TITAN by Ethernet to give observed structure factors. A four-circle diffractometer is also connected to the local area network and measured structure factors can be transferred to any workstation. Structure analysis packages such as XTAL, PROTEIN, XPLOR, PROLSQ and so on, are installed on these workstations. The performance of this system will be reported.

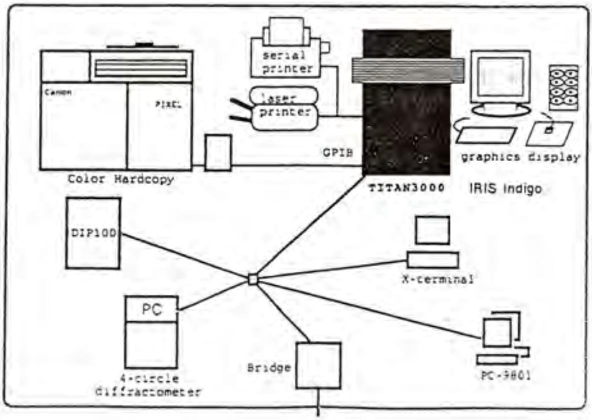

16P-01

MORPHOLOGICAL INVESTIGATION OF THE (0001) SURFACE OF ICE I_h CRYSTAL BY X-RAY CRYSTAL TRUNCATION ROD SCATTERING

A.Goto and K.Akiya, Department of Applied Physics, Hokkaido University, Sapporo 060, Japan, T.Shimura, I.Takahashi and J.Harada, Department of Applied Physics, Nagoya University, Nagoya 464-01, Japan, Y.Furukawa and T.Hondoh, Institute of Low Temperature Science, Hokkaido University, Sapporo 060, Japan.

An attempt was made to characterize the surface state of a single crystal of ice I_h on a molecular level by the X-ray crystal truncation rod (CTR) scattering technique[1]. As a result, it was found that very well-defined CTR scattering, elongated from the 0002 Bragg point along the surface normal direction of [0001], can be observed at 7℃ below the melting point, when the surface was sublimated for approximately 1 h in a cold room after making the surface mechanically flat by using a Japanese plane. Estimated from the divergence of the CTR scattering, it is suggested that the (0001) surface of the ice we investigated is very smoothly undulated like a sand dune. The result was compared with the theoretical prediction on the growth kinetics of ice surface from the vapour phase, discussed by Kuroda and Lacmann[2].

1) Goto,A., Akiya,K., Hondoh,T., Furukawa,Y., Shimura,T., Takahashi,I. and Harada,J.(1992),J.Crystal Growth, in press.
2) Kuroda,T. and Racmann,R.(1982).J.Crystal Growth,56,189-205.

16P-02

$CaSrF_2$/GaAs AND CaF_2/S/GaAs INTERFACE STRUCTURES REVEALED BY X-RAY STANDING WAVES AND CRYSTAL TRUNCATION RODS

H. Hashizume, T. Niwa, M. Sugiyama (*), O. Sakata and S. Maeyama (*),
Res. Laboratory of Engineering Materials, Tokyo Institute Technology,
Yokohama 227, Japan. (*) NTT Interdisciplinary Laboratories.

Fluoride epilayers on GaAs substrates are useful materials for insulator/semiconductor structures. Their electronic properties are affected by the stoichiometry and structure at the epilayer-substrate interface, which has been studied here using X-ray standing waves (XSW) and crystal truncation rods (CTR) at synchrotron radiation site Photon Factory, KEK Japan. Lattice-matched $CaSrF_2$ thin films were grown on the As-terminated (111) surface of GaAs by molecular beam epitaxy. XSW data collected using the (111) planes show a 0.7% expanded fluoride epilayer spacing relative to the bulk GaAs (111) planes and the first (Ca, Sr) layer lying at 2.38Å (= d_{IF}) above the top substrate (111) plane. The CTR data near the 111 Bragg point support the observed very short vertical distance d_{IF}, suggesting one or both of a F and As layer missing at the $CaSrF_2$/GaAs interface. Emission data obtained using the 220 and 113 reflections locate the Sr atoms midway between the *T* and *T4* sites on GaAs(111) surface [1]. This puzzling Sr position is studied by recording CTR intensity distributions near the 331 Bragg point. The observed oscillation profile is far from that expected from the (Ca, Sr) atoms occupying the *T4* sites but close to the one calculated for the (Ca, Sr) at the *T* sites. Mixed-site models can only explain the data with a marginal fraction of the metal atoms at the *T4* sites. Least-squares fits assuming the (Ca, Sr) atoms at the *T* sites favor missing top substrate As atoms over shifted As atoms at the *H3* sites.

We also studied CaF_2 epilayers grown on S-passivated GaAs (111) surface at 440°C using XSW and CTR. Our previous study suggest that on the As-terminated GaAs(111) surface the top layer As atoms are substituted by S atoms [2]. The present XSW data confirm this result with much more neatly fitted data. Well contrasted oscillations of the CTR profile near the 111 Bragg peak indicate ordered CaF_2 layers. Least-squares fits show a 1% contracted layer spacing relative to bulk CaF_2. The first Ca layer lies 2.4Å above the top substrate (111) plane, suggesting a missing F layer at the CaF_2/S interface either.

[1] H. Hashizume *et al.* (1991) *Rev. Sci. Instr.* 63, 1142.
[2] M. Sugiyama *et al.* (1991) *Appl. Phys. Letter* in press.

16P-03

X-RAY DIFFRACTION STUDY OF THE AIR CLEAVED NaCl(001) SURFACE

I. Takahashi, T. Kakiuchi, T. Shimura, and J. Harada
Department of Applied Physics, Nagoya University,
Chikusa-ku, 464, Nagoya, Japan.

In an attempt to study the morphology of a real crystal surface and the microscopic mechanism for sublimation, an air cleaved NaCl(001) surface was investigated by X-ray CTR scattering at several different temperatures.
Samples cleaved with a razor blade were put in a vacuum chamber installed on a diffractometer. The temperature was controlled to within 2K from room temperature to 900K. The degree of vacuum, 10^{-8} torr, was maintained throughout the experiment.
The CTR scattering around the (000) and (002) points at room temperature and at 400K was almost identical, while differing from data obtained from a surface cleaved in vacuum*. However, after the sample was heated to 570K, the CTR scattering changed and became similar to that from the vacuum-cleaved surface. This suggests that the surface cleaved in air is covered with absorbed molecules, such as water, that remain on the substrate until the temperature is increased to 570K.
Damping of CTR scattering is observed at 670K, indicating that the dynamical surface roughening due to sublimation occurs when the sample is heated further. Subsequent least squares fitting confirms this interpretation, and also indicates that CTR scattering is one of the powerful methods available for the study of adsorption and desorption on crystal surfaces.

* Y. Kashihara, S. Kimura, and J. Harada: *Surface Science.* **214**, (1989) 477-492.

16P-04

STRUCTURAL ANALYSIS OF Ag/Cu AND Ag/Pb MULTILAYERED FILMS BY X-RAY DIFFRACTION

K. Hazama, J. Kozaki, S. Ando and O. Nittono
Department of Metallurgical Engineering, Tokyo Institute of Technology, Meguro-ku, Tokyo 152, Japan.

In most cases, the structures of metallic multilayered films are analyzed by comparing observed X-ray diffraction profiles with calculated profiles based on models of layer stacking. This procedure, however, is troublesome when a real layer stacking deviates markedly from a model based on an ideally designed superlattice structure. Furthermore, metallic multilayered films have been prepared by various methods. In previous studies films constructed with the same constituent metals have not been investigated in detail by the same analytical technique.

In this study, we seek a practical and reliable procedure for precise structural analysis of metallic multilayered films. First, in order to see if a film's structure depends on the preparation method, we prepared Ag/Cu films by evaporation and by sputtering, and characterized their natures. Secondly, we developed a method for evaluating X-ray profiles using an analytical model modified by both interface roughness and fluctuation of layer thickness. This model was used to characterize the structures of Ag/Pb multilayered films.

The results are: (1) X-ray diffraction profiles from Ag/Cu films showed artificial layer periods, realized by both methods. Therefore, we first adopted an ideal model: compositional modulation is expressed in terms of a periodic rectangular concentration of the constituent element. It was shown that, as a result, the interplanar lattice spacing of each element was not the same as that of the bulk material, especially for small layer periods. The deviation of interplanar spacing appears slightly larger for dc-sputtering than for evaporation. (2) Our analytical procedure is essentially based on a model that a multilayered film is composed of many grains with large dimension parallel to the substrate. Fluctuations in the number of atomic planes and their relative positions were introduced to determine the layer period. Features of observed X-ray profiles were well explained by these parameters. The present model and the introduction of such parameters will be applicable to the analysis of the structural features for various kinds of metallic multilayered films.

16P-05

EPITAXIAL GROWTH OF (110) Ag THIN FILMS ON CLEAVED NaCl CRYSTAL IN A KNUDSEN GAS OF Ar

I. Ogura, College of Engineering, Nihon University, Koriyama 963, Japan

Since 1985, it has been reported that Ag thin films of (001) and/or (100) orientation are formed on (001) NaCl crystal at room temperature if the Ag atoms and clusters are deposited onto the substrate in a Knudsen gas of Ar. [1] Recently, the Ag flow in the Ar gas was calculated to obtain deposition parameters. In this case, the free path length ℓ of the Ag atom is postulated to be distributed as $dn/d\ell=\exp(-\ell/\bar{\ell})/\bar{\ell}$. [2] The calculated temperature T of the Ar gas is ~900 K during deposition, and the mean free path $\bar{\ell}$=~2.6mm. The deposition rate $d\delta/dt$ of ~0.3nm/s agrees with the experimental values. The number density n_2 of the Ag-Ag dimer is $3\times10^{-2}n_1$, where n_1 is that of the Ag monomer.

The growth of (110) Ag thin films on cold NaCl in the atmosphere of Ar is explained in this report. The substrate is maintained at room temperature. [3] The surface 2-dimensional gas of Ag monomers and dimers is more active than that in the case of vacuum deposition, because the high temperature Ar gas stimulates them by collision of Ar molecules with the surface-migrating Ag monomers and dimers. Ag deposits grow epitaxially on cold NaCl substrates. A cleaved NaCl substrate has a complicated structure, as shown by surface topographs. In some regions deformed by multiple slip, {110} planes tilted by 45° from the (001) cleaved surface are widely exposed, although the mean surface plane tilts within a few degrees. In these regions of multiple slip, the (110) orientation of the Ag deposits appears to grow.

[1] Hoshi, I. & Ogura, I. (1985). Jpn. J. Appl. L297-298.
[2] Ogura, I., Suzuki, S. & Nagashima, S. (1992) in print.
[3] Ogura, I., Hayashi, S. & Yomogita, K. (1986), J. Surf. Sci. Soc. Jpn. **8**, 192-196.

16Q-06

CRYSTAL STRUCTURE CHANGES IN OXYGEN-DEFICIENT $YBa_2Cu_3O_{7-\delta}$ SUPERCONDUCTING THIN FILMS

J. Ye, A. Ishii and K. Nakamura
Surface and Interface Division, National Research Institute for Metals,
1-2-1, Sengen, Tsukuba-shi, Ibaraki 305, Japan

The structural properties of high-T_c $YBa_2Cu_3O_{7-\delta}$; thin films with different oxygen contents have been analyzed using X-ray diffraction. It is well known that the superconducting properties of $YBa_2Cu_3O_{7-\delta}$ depend strongly on the oxygen deficiency δ, and for bulk YBCO the c lattice parameter increases linearly from 11.68 to 11.82 Å with δ increasing from 0.1 to 0.9. In thin films, however, no such a correspondence has been found, because even under different growth conditions the c lattice parameter varies in a wide range from 11.7 to 12 Å. Moreover, since δ-values are usually subject to large uncertainties, a quantitative study of structural changes due to oxygen deficiency remains difficult.

Recently, we have succeeded in controlling oxygen deficiency in epitaxial YBCO films grown on MgO or $SrTiO_3$ substrates by equilibrating the oxygen potential of the thin films with that of bulk YBCO pellets of known oxygen deficiency. The X-ray diffraction experiments revealed that both the c lattice parameters and the 00ℓ intensities change dramatically with the oxygen deficiency. After a systematic analysis, a relationship between the value of $I(005)/I(006)$ and the oxygen deficiency has been established. Therefore, the oxygen deficiency of the films can be determined accurately, in spite of the significant variation of c lattice parameters depending on the growth conditions. Furthermore, structure analyses from the measured 00ℓ integrated intensity data show that the Cu-O and Ba-O bond lengths increase with increasing oxygen deficiency. This observation is consistent with that reported by Jorgensen et al. in a neutron powder diffraction (1990), supporting a "charge-transfer" model which accounting for the decrease of T_c with oxygen deficiency.

Jorgensen, J.D., et al. (1990). *Phys. Rev.* B**41**, 1863-1877.

16Q-07

STRUCTURAL CHARACTERIZATION OF Fe/X (X:Ag,Cu,Ta) MULTILAYER FILMS PREPARED BY DC SPUTTERING

Y.Haga, T.Sugiyama, Y.Nakamura and O.Nittono
Department of Metallurgical Engineering, Tokyo Institute of Technology,
2-12-1 Oh-okayama, Meguroku, Tokyo, 152, Japan

Microstructures influence the magnetic properties, mechanical properties, conductivities and other properties of metallic multilayer films. The investigation of microstructures of multilayer films is therefore important. Generally, X-ray diffraction (XRD) is used for structure analysis of multilayer films. In that method, we assess crystal structures in the films by comparing observed diffraction profiles with the calculated ones. Many reports about the effects of interface roughness, compositional gradient or layer thickness fluctuations on XRD profiles of superlattices have been published. However quantitative estimation of these factors for metallic multilayer films is especially difficult. Combination of XRD methods with other techniques such as transmission electron microscopy (TEM) and scanning electron microscopy (SEM) is often necessary.

In our work, we characterize structural features of Fe/X (X: Ag,Cu,Ta) multilayer films prepared by double-facing-target-type DC sputtering on Si(111) at room temperature. The deposition rate for Fe was 0.02nm/s. That needed to prepare multilayer films for other elements with various layer thickness ratios ranged from 0.02nm/s to 0.2nm/s. The perfection of film periods and crystallinity were investigated by X-ray diffraction (θ-2θ measurement). To observe detailed structure in the films and to estimate the film parameters used to calculate XRD profiles, we also studied the film structures with cross-sectional TEM (XTEM), field-emission SEM (FE SEM), and scanning tunneling microscopy (STM). Fe/Ag multilayer films were polycrystalline. Strictly speaking, those films consisted of many columns and each column contained small linked particle-like grains. Most Fe grains were bcc with a <110> preferred orientation relative to the film normal. Ag grains were fcc and had a <111> preferred orientation to the film normal, with some stacking faults. The orientations of these grains were irregular in the film plane, but it seemed that the grains had orientation relationships to each other at the inter/grain interfaces. The interface roughness gradually increased with film thickness. In particular some multilayer films containing thick Ag layers had very rough interfaces. We will report similar results for other multilayer films. In addition, we will report magnetic properties of multilayer films measured by a vibrating sample magnetometer(VSM).

16Q-08

X-RAY STANDING WAVES IN 100Å-THICK EPILAYERS UNDER GRAZING-INCIDENCE DIFFRACTION CONDITIONS

O. Sakata, I. Kawamoto and H. Hashizume, Res. Laboratory of Engineering Materials, Tokyo Institute Technology, Yokohama 227, Japan

Jach and Bedzyk (1990) demonstrated the feasibility of the grazing-incidence X-ray standing wave (GIXSW) method to determine the in-plane position of monolayer Iodine atoms adsorbed on Ge surface. The emission data were well fitted by a simple theory assuming excitation of the I atoms by GIXSW's produced from the substrate Ge crystal. This approximation is no longer valid for epilayers as thin as 100Å. The extremely shallow penetration of X-rays under the grazing-incidence condition demands dynamical diffraction in the epilayer crystal to be taken into account. Figure 1 shows Sr*K* emission data observed from 100Å-thick $CaSrF_2$ epilayers on GaAs(111) substrate diffracting 17.5 KeV synchrotron X-rays with the $(2\bar{2}0)$ planes at a glancing incidence angle slightly larger than the critical angle of total external reflection for GaAs. The observed emission profile is far from the prediction of the simple theory (dotted curve) but close to the solid curve calculated including the epilayer diffraction for Sr atoms lying on the diffracting $(2\bar{2}0)$ planes ($Z = 0$). If the fluorescing lattice Sr atoms were located midway ($Z = 0.5$), we would observe the broken profile which is quite different from the one for $Z = 0$. The present theory assumes perfect-crystal epilayers interfacing to a perfect substrate. Attempts to include lattice distortion in the theory would provide a closer fit to the data whereby structure parameters at the hetero-epitaxial interface would be more precisely characterized.

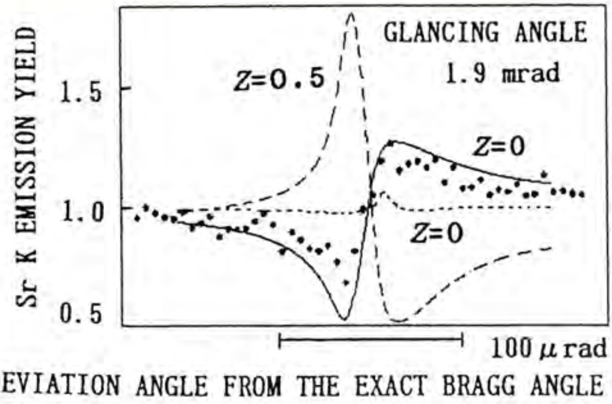

Jach, T. and Bedzyk, M.J. (1990) *Phys. Rev.* B42, 5399-5402.

16Q-09

OBSERVATION OF CTR SCATTERING FROM AlAs MOLECULAR LAYERS IN GaAS USING AN IMAGE PLATE DETECTOR

T.Shimura and J.Harada, Department of Applied Physics,
Nagoya University, Chikusa-ku, Nagoya, 46401, Japan

The interference fringe between two crystal truncation rod (CTR) scatterings from AlAs molecular layers in GaAs was observed with an Imaging Plate (IP). The rod-shaped X-ray CTR scattering emanates along the surface normal direction from each Bragg point. Analysis of that scattering provides difference information about crystal surfaces and interfaces. The IP X-ray area detector combines the advantages of dynamic range from 1 to 10^5, high sensitivity and unlimited count-rate capacity. Its use in conjunction with synchrotron radiation is very effective for studying the crystallography not only of proteins as shown by Sakabe1) but also of surfaces1),2). In this paper we demonstrate a most interesting observation with CTR scattering. Our GaAs/AlAs/GaAs sample was grown on a GaAs(001) substrate by the MBE method. The nominal numbers of molecular layers of GaAs, AlAs and GaAs were 1240, 125 and 1240 respectively. Oscillation photographs were taken at the BL-6A2 of Photon Factory, KEK. The intensity distribution of the CTR scattering around the 002 Bragg point is represented in Fig.1 Each dot is obtained by integrating the intensities across the CTR scattering with background subtracted. It is possible to interpret the Laüe-function like distribution as an interference fringe between two CTR scatterings from the interfaces. The solid line indicates model calculations in which numbers of molecular layers, lattice spacings and roughnesses of the AlAs interfaces are adjusted. Careful investigation showed that the lattice spacing and the number of molecular layers of AlAs can be obtained to within ±0.002Å and ±1 molecular layer, respectively. Estimated roughnesses of the AlAs interfaces were less than 4 molecular layers.

[1] N.Sakabe; Nucl.Instr. and Meth. **A303** (1991) 448
[2] T.Shimura and J.Harada; Acta Cryst. A**46** (1990) suppl. C-374
[3] J.Harada, T.Shimura, M.Takata, K.Yakushiji and K.Hoshi;
J.Cryst.Growth **104**(1990) 773

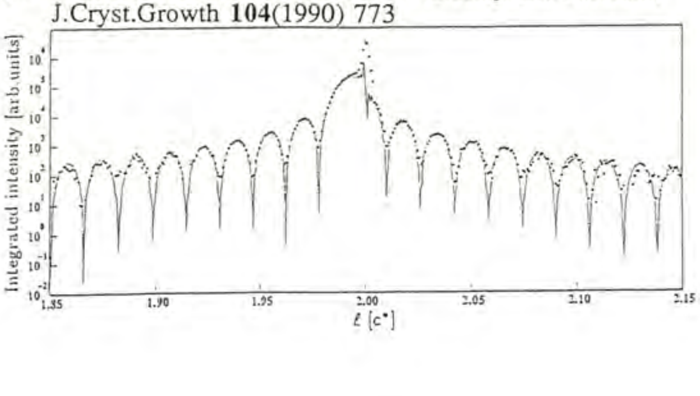

16Q-10

MISFIT ACCOMMODATION OF Pt/Au/BUFFER Ag TRILAYERS GROWN ONTO Si, MgO AND NaCl SUBSTRATES

Akira Sugawara and Osamu Nittono
Department of Metallurgy, Tokyo Institute of Technology,
2-12-1 Oh-okayama, Meguro ku, Tokyo, 152, Japan

In recent years, interface structures of metallic superlattice films grown on single crystal substrates(e.g. Si, GaAs, MgO et al.) have been extensively studied in connection with their physical properties. In general, lattice misfits between two metals are large, so misfit accommodation may be important to their growth and properties. However, most specimens were grown at low temperature and contained large stacking fault densities. This might affect the misfit accommodation. In this study, we have demonstrated differences in misfit accommodation at Pt/Au interfaces grown onto thick and annealed Ag buffer layers on Si(001), MgO(001) and NaCl(001). The lattice misfit is about 3.8% between Au and Pt and 0.2% between Au and Ag, respectively.

All the Pt(0.5~10nm)/Au(30nm)/buffer Ag(about 200nm) films were deposited onto Si(001), MgO(001) and NaCl(001) single crystal substrates at 563K by Xe^+ ion beam sputtering. First an Ag buffer layer was deposited, and then annealed above 620K for several hours. The Pt/Au bilayer was deposited later. After dissolving the Ag buffer layer in nitric acid, a Pt/Au bilayer film was mounted on a grid and investigated by transmission electron microscopy (JEM-200CX) at room temperature.

In all cases, parallel epitaxy was observed among the buffer Ag, Au and Pt layers. Since Au layers were thin, no misfit dislocations were introduced at Au/Ag interfaces. At an early stage of Pt growth on an Au layer, pseudomorphism was observed. However, following misfit accommodation, the Pt/Au interface features alter. For NaCl substrate, the stacking fault density was relatively large. Two stages of introduction of misfit dislocations were observed. First mixed dislocations were introduced by a slip mechanism. Edge-type dislocations were introduced by a climb mechanism in the next stage. By contrast, for Si and MgO substrates, stacking fault density was low and slipped dislocations were scarce. The results suggest that misfit accommodation is greatly affected by internal defects and by the surface flatness of the Ag buffer layer.

16Q-11

X-RAY DIFFRACTION ANALYSIS OF RTP PROCESSED Cu/In/Se STACKED THIN LAYERS

F. Camillo and M. Donat, Dpto de Tecnologia de Materiales, Instituto Universitario Technologico Dr F.R.P., Aptdo Postal 40347, Caracas - Venezuela, and
H. Galindo, A.B. Vincent, J.M. Martin and D. Gómez de Andérez, Facultad de Ciencias, Universidad de Los Andes, Mérida - Venezuela.

Stacked layers of Cu/In/Se have been processed by rapid thermal processing (RTP) via strong incoherent light. Films of 250 nm thickness were formed by evaporation, in a chamber at 10^{-6} torr, of copper, indium and selenium layers in stoichiometric proportions 1:1:2 on Corning 7059 glass substrates. The films obtained were subsequently treated on an apparatus which simulates the effect of a commercial rapid thermal processor (RTP) controlled with a PC microcomputer. We were able to refine the process and could obtain better films in the 260 to 290°C range. The corresponding X-ray diffraction analysis shows the presence of a phase having chalcopyrite structure in the processed films with a particular set of the RTP parameters. An investigation of the influence of these parameters showed that these must be well controlled in order to avoid unwanted secondary phase or strong segregations. Synthesis of ternary $CuInSe_2$ by this technique is also discussed.

16R-12

CRYSTAL STRUCTURES OF ADENYLYL-2'-5'-ADENOSINE TRIHYDRATE AND TETRAHYDRATE:

A study of molecular conformation under different hydrations

R Krishnan and T P Seshadri, Department of Physics, Indian Institute of Science, Bangalore 560 012, India.

Water mediated structural transformations play an important role in biological molecules. A well known example is the polymorphism of DNA double helix caused at different hydrations. However, there are not many examples of nucleic acid fragmetns studied under different hydrations by single crystal methods. Only two mononucleotides 5'd-dCMP.Na_2 and 5'-IMP.Na have been reported. Interestingly the deoxynucleotide showed conformational changes while the ribo nucleotide did not. This study was undertaken to study the effect of hydration on the molecular conformation of A2'p5'A.

The crystals of both the hydrated forms of A2'p5'A were grown using vapour diffusion techniques. Cu $K\alpha$ intensity data were collected on a CAD-4 machine. The structures were solved using direct methods and were refined to R factors of 0.108 and 0.129 for the tetrahydrate (I) and trihydrate (II) forms respectively.

Our analysis showed that **the 2'5' sugar phosphate backbone in A2'p5'A(II) is remarkably similar to that in A2'p5'A(I).** All the conformational features of A2'p5'A(I) namely, *syn/anti* geometry for the adenine bases, *C2' endo/C3' endo* mixed sugar puckering and intramolecular base — O4' stacking are also found in A2'p5'A(II). The two hydrated forms of A2'p5'A can be superposed with an R.M.S deviation of less than 0.53 Å in their coordinates. Though the two hydrated forms have totally different unit cell parameters, their volumes are very nearly the same because their cell content differs by only two solvent molecules per asymmetric unit. But the packing of the A2'p5'A molecules in their respective unit cells are significantly different. Consequently, the intermolecular interactions are very different in both the forms. However, their water nucleotide interactions are not very different as the conformations of A2'p5'A in both the hydrated forms are very similar.

Crystal data for A2'p5'A(I) & A2'p5'A(II)

Formula	$C_{20}H_{24}N_{10}O_{10}P.4H_2ONH_4$	$C_{20}H_{24}N_{10}O_{10}P.3H_2O$
a=	7.956(3)Å	9.284(3)Å
b=	12.212(3)Å	15.360(3)Å
c=	36.654(3)Å	21.610(3)Å
Space group	$P2_12_12_1$	$P2_12_12_1$
v=	3561.3Å^3	3081.6Å^3

16R-13

CRYSTAL STRUCTURE OF 2,6-DI (2-FURYL)-3,5-DIMETHYL PIPERIDIN-4-ONE

N Sukumar and M. N. Ponnuswamy, Department of Crystallography and Biophysics, University of Madras, Guindy Campus, Madras 600 025, India, and
J. C. Thenmozhiyal and R Jeyaraman, Department of Chemistry, Bharathidasan University, Tiruchirapalli 620 024, India.

Most nitrosamines are known to exhibit carcinogenic properties. It has also been observed that by blocking the α position of the ring nitrogen atom by methyl groups in cyclic nitrosamines, carcinogenic activity is reduced. Some of the N-nitroso ureas are used as antitumor agents or antibiotics. In view of the general interest in their utility and reactivity, several N-nitrosopiperidines and N-nitrosopyrrolidines have been synthesized and their conformations studied. The aim is to understand the stereodynamics of N-nitrosopiperidines and to correlate the stereochemistry with their Cancer/anticancer properties.

Crystal Data: $C_{15}H_{17}NO_3$, Triclinic, $P\bar{1}$,
a=8.915(1), b=11.4790(9), c=7.0986(4)Å,
α= 103.83(6), β= 98.317(6), γ= 93.644(8),
V= 694.27Å^3, Z=2.

The piperdin ring is in a slightly "distorted chair" conformation. One of the furyl rings assumes "half-chair" conformation whereas other furyl ring exists in "twisted" conformation. The dihedral angle between the furyl rings is 12.0(5)°. The packing of the molecules are governed by N-H...O hydrogen bonding and Van der Waals interaction.

16R-14

STRUCTURAL STUDY OF l-OCTADECANOL BY PSPC SYSTEM

H.Kobayashi and N.Nakamura, Department of Chemistry,
Ritsumeikan University, Kita-ku, Kyoto, 603, Japan.

l-Octadecanol was recrystallized several times from n-hexane. The sample was judged to be thoroughly pure by gas chromatograph equipped with a glass capillary column. It is known that l-octadecanol exhibits phase transition behaviour on cooling process from the molten state. In this study, a sample temperature control apparatus was newly designed, and constructed by a gas furnace system equipped with a proportional integrated differential (PID) controller. Moreover, a position sensitive proportional counter (PSPC) system was used as a detector in order to make quick measurements. The cooling rate from the molten state was 0.1°C/min.

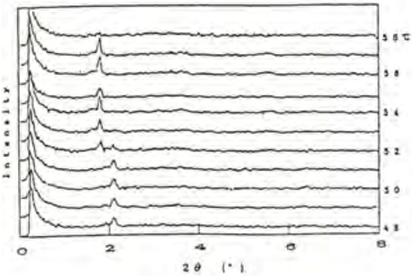

Figure 1 SAXS patterns of l-octadecanol

Small angle X-ray scattering (SAXS) patterns are shown in Figure 1. From 57 to 52°C, the peak was observed at 2θ=1.8°. The intensity of the peak increased with decreasing temperature till 55°C, but after that it decreased gradually. The peak vanished at 51°C. From 52°C, another peak appeared at 2θ=2.1°. The intensity of this peak increased with decreasing temperature till 50°C. In the temperature range 57 to 52°C, that is the high temperature phase, the long spacing is 48.7Å. Below 52°C, the long spacing is 41.7Å. These values are consistent with long spacings reported by Seto (1962). Detailed structural analysis results will be presented.

Seto, T. (1962). Mem. College Sci. Univ. Kyoto, A**30**, 89-107.

16R-15

CRYSTAL STRUCTURES OF MESO-1,1'-DICYANO-1,1'-DIPHENYL-ETHANE (1) AND MESO-1,1'-DINITRO-1,1'-DIPHENYLETHANE (2)

L. L. Koh, H. H. Huang, K. Y. Sim, Y. L. Lam and Y. Xu
Chemistry Department, National University of Singapore
Singapore 0511

Crystal structures of 1 and 2 have been determined by X-ray Diffraction.

Crystal data:

(1) C_6H_5-CH(CN)-CH(CN)-C_6H_5
monoclinic, C2/c, Z=4
a=19.044, b=5.794, c=12.494 Å, β=115.28°
R=0.046 for 710 observed reflections

(2) C_6H_5-CH(NO_2)-CH(NO_2)-C_6H_5
monoclinic, $P2_1/n$, Z=2
a=5.597, b=8.185, c=14.389, β=90.51°
R=0.051 for 604 observed reflections

Compound 1 exists in the *trans* conformation. The crystal structure is disordered. The central C atom and part of the phenyl ring bonded to the central C atom are disordered over two sets of sites each with s.o.f. of 0.50. The CN group, the outermost C atom of the phenyl ring and the H bonded to the central C atom are ordered.

Compound 2 exists in the *trans* conformation. The crystal structure is also disordered. However, in this case, only the central C atom is disordered. The disorder is best described by a four-site disordered model with s.o.f. of 0.45, 0.25, 0.20 and 0.15.

Interesting features of the structures will be discussed in the presentation.

16R-16

EFFECT OF THE TRIMETHYL SUBSTITUTENT ON C-O BOND LENGTHS AT THE BETA POSITION: SOME STRUCTURAL STUDIES

Jonathan M. White* and Glen Robertson, Research School of Chemistry,
Australian National University, G.P.O Box 4, Canberra, ACT 2601
**Present Address:* Chemistry Department, University of Melbourne
Parkville, Victoria 3052

Results of low temperature (130 K) crystal structure analyses for seven β-trimethylsilyl substituted cyclohexylnitrobenzoate esters are presented. For those molecules (three) with the Si-C and C-O bonds antiperiplanar the C-O bond lengths are increased by 0.014 Å av. [Δ/σ min = 2.9] compared with that in the silicon free analogue. For those molecules (four) with the Si-C and C-O gauche no such systematic lengthening of the C-O bonds is observed. The result is in qualitative agreement with that [$\Delta l \propto \cos^2$(Si-C-C-O)] predicted from ab initio MO calculations on a simple model complex, and is attributed to the effects of interactions between the Si-C σ and C-O σ* orbitals. It is suggested that that existence of the observed ground state effect constitutes compelling, if circumstantial, evidence that the major kinetic effects known to result from the presence of a β-silicon substituent also have their genesis in the same σ-σ* interactions.

16R-17

SEQUENTIAL BASE-PROMOTED CLEAVAGE OF C-S BONDS IN A COORDINATED CROWN THIOETHER

M.A. Bennett, L.Y. Goh* and A.C. Willis, Research School of Chemistry, Australian National University, Canberra, A.C.T., Australia. (* on leave from Department of Chemistry, University of Malaya, Kuala Lumpur.)

Treatment of the arene-ruthenium(II) salt $[Ru(\eta^6\text{-}C_6Me_6)(1,4,7\text{-trithiacyclononane})](PF_6)_2$ (**1**) with one equivalent of KOH reversibly cleaves one C-S bond to give the mono-cationic chelate tridentate vinyl thioether complex **2**. Treatment of **2** with more KOH or KO-*t*-Bu irreversibly cleaves a second C-S bond to give the neutral complex **3**, which contains vinyl mercaptan and a bidentate vinyl thioether thiolate ligand. Finally, in the presence of an excess of KO-*t*-Bu, the vinyl group of **3** couples with one of the methyl carbon atoms on the $\eta^6\text{-}C_6Me_6$ ring to give complex **4**; this process is thought to involve a Michael addition to the vinyl group of a carbanion formed by deprotonation of coordinated $\eta^6\text{-}C_6Me_6$. Complexes **2**, **3** and **4** have been characterized by X-ray crystallography, and their structures will be compared.

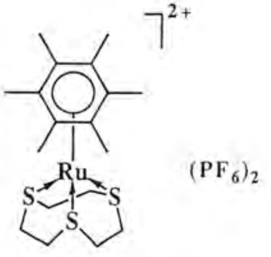

1

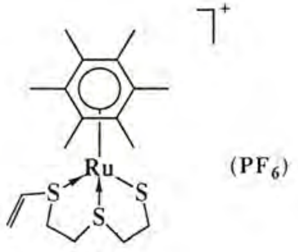

2

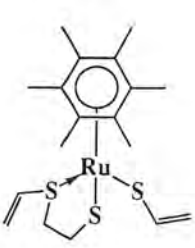

3

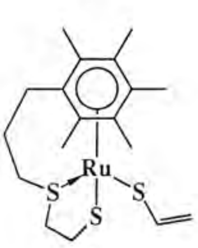

4

16R-18

STRUCTURES AND PROPERTIES OF BILAYER-FORMING AMPHIPHILES $C_nAzoC_mN^+Br^-$

Guiqing. Xu, Kenji Okuyama, and Masatsugu Shimomura
Faculty of Technology, Tokyo University of Agriculture and Technology, Koganei, Tokyo 184, Japan.

Totally synthetic bilayer-forming amphiphiles, $C_nAzoC_mN^+Br^-$, show two typical aggregation states depending on the number of carbon atoms in the spacer (m) and tail (n) parts. These are the side-by-side arrangement (H-aggregate) and the head-to-tail arrangement (J-aggregate) of azobenzene chromophores. The former arrangement was observed for compounds with the relation of m-n=2, and the latter was observed for $C_nAzoC_5N^+Br^-$ (n=6-12).

By heating, the H-aggregate changes to the J'-aggregate which is very similar to the J-aggregate. Interestingly, the odd-even effect on transition temperatures from the H- to the J'-aggregate was observed. That is, transition temperatures for compounds with odd number of m and n were higher than those for the even number compounds, by about 40^oC. According to the X-ray structural analyses, both structures of the J'-aggregates for odd and even compounds were similar to each other, but those of the H-aggregates were different. In the case of the H-aggregates, the detailed structures in the hydrophilic region were different between the odd and even number compounds (for example, chain conformation, hydrogen bond distance, and ionic interaction). These structural differences of the H-aggregates seem to be caused a big odd-even effect on the transition temperatures from the H- to the J'-aggregate.

16R-19

CRYSTAL STRUCTURE OF 1,18-DIBROMOOCTADECANE

T.Yamamoto and N.Nakamura, Department of Chemistry, Faculty of Science and Engineering , Ritsumeikan University, Kita-ku, Kyoto 603, Japan, and Y.Yoshimura, Department of Mathematics and Physics, Faculty of Science and Engineering , Ritsumeikan University, Kita-ku, Kyoto 603, Japan.

The sample used here, 1,18-Dibromooctadecane, was recrystallized from ethanol. Single crystal was grown from xylene solution. Crystal structure analysis was carried out on a crystal with size about (0.2×0.1×0.01mm); intensity data from Rigaku-Denki AFC-5 automated four-circle diffractmeter equipped with Cu-$K\alpha$ radiation from a rotating anode; unit-cell parameters from angular values of 25 reflections with $20° \leqq 2\theta \leqq 40°$, 2703 unique reflections with $2\theta < 120°$ ($-6 \leqq h \leqq 6$, $0 \leqq k \leqq 38$, $-6 \leqq l \leqq 6$) were measured by ω-scan mode with scan speed $5°\ \mathrm{min}^{-1}$, and scan ranges $(1.2+0.5\tan\theta)°$ for reflection with $0° \leqq 2\theta \leqq 120°$; below $\sin 40° / \lambda$, 606 reflections with $|F| > 3\sigma(|F_o|)$ were used in the refinement ; no significant intensity variation for three standard reflections; no absorption correction. The initial coordinate of the C atoms and Br atom set with reference to the peak on least-squares plane by direct methods with MULTAN84 (G.Germain &M.M.Woolfson,1984) ; all other atoms located after several least-squares cycles and Fourier calculations; block-diagonal least-squares refinement, $\Sigma\omega(|F_o| - |F_c|)^2$ minimized, anisotropic thermal parameters for all non-H atoms; 18H atoms refined isotropically; 158 parameters, R=0.0962, wR=0.1164.

G.Germain, P.Main and M.M.Woolfson, (1970). Acta Cryst.B26, 274

16R-20

2D-NMR STUDY ON THE CONFORMATION OF A DODECACYCLOPEPTIDE

L.H. Lai[1], L.B. Ma[1,2], Z.W. Miao[1], X.J. Xu[1], 1: Department of Chemistry, Peking University, Beijing 100871, China; 2: Beijing Institute of Microchemistry, Beijing 100091, China

Cyclopeptide is a useful template for de novo designing of four-helix-bundle proteins by acting as a supporting scaffold for the helix. As a part of our study on de novo protein design, we have synthesized a series of cyclopeptides and studied the solution conformation of one dodecacyclopeptide by 2D-NMR:

Phe—>Lys—>Pro—>Gly—>Lys—>Gly
↑ ↓
Gly<—Lys<—Gly<—Pro<—Lys<—Phe

2D-NMR spetra were recorded on a Bruker AM 500MHz spectrometer. Complete assignment was obtained by analysis of COSY and NOESY spectra. DIANA distance geometry calculations were then carried out with 62 NOE distance constraints. 10 top structures with lowest target function values among the 100 obtained were considered as final results. The backbone root-mean-squares between these ten structures was 0.29±0.06A and all heavy atoms was 1.24±0.19A. Structure analysis showed that this cyclopeptide contains two β-turns and two γ-turns. All the side chains of the four lysine residues face towards the same side of the ring, providing good anchor positions for the assembly of synthesized helix elements.

16S-31

METAL COMPLEXES OF BENZOQUINONEDIIMINE AND RELATED DIIMINES

Shie-Ming Peng, Department of Chemistry, National Taiwan University

Benzoquinonediimine has a low lying π^* orbital which can form π-bonds with metal d_π orbitals. The energy of d_π relative to that of π^* will affect the electron population on the π^* orbital, altering the bonding type and the oxidation states of the ligand, namely, opdi, s-bqdi, bqdi.

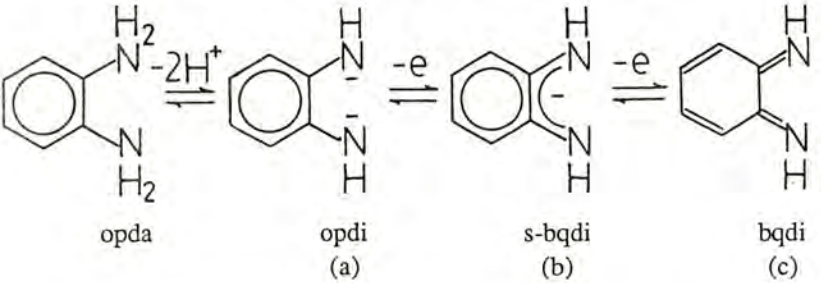

We have synthesized dozens of new complexes of (a), (b), (c) types and determined their single crystal structures. We can assign the oxidation states according to the bonding geometries of the ligands and further identify the oxidation states of the metal.

The results are summarized as follows:

1) Mono-ligand metal complexes: A series of Ru complexes, $RuCl_2(P(C_6H_5)_3)_2L$ (L= bqdi and related diimines) has been synthesized. Bonding of (a), (b), (c) types can be obtained by slightly tuning π^* energy levels from various diimine ligands.

2) Bis-ligand metal complexes: Two s-bqdi ligands are coordinated to the metal ion in a planar geometry. Two bqdi ligands are coordinated to the metal ion in a tetrahedral geometry.

3) Tris-ligand metal complexes: Three s-bqdi ligands are coordinated to metal ion in a trigonal prismatic geometry. Three bqdi ligands are coordinated to metal ion in a octahedral geometry.

Recently, we have applied ^{15}N NMR to identify the oxidation states of ligands according to chemical shifts. The results are consistent with those from X-ray diffraction.

16S-32

CRYSTAL STRUCTURES OF FOUR TRANSITION METAL COMPLEXES

Tian–Huey Lu, Tahir Tahirov, Bor–Hann Chen and Chung–Sun Chung
National Tsing Hua University, Hsinchu, Taiwan 300, R.O.C.

Crystal Structures of four transition metal complexes have been investigated. They are (1) nickel(II) complex of the deprotonated anion of 3,6,6,9–tetramethyl –4,8–diaza–3,8–undecadiene–2,10–dione dioxime, $[Ni(N_4O_2C_{13}H_{23})](C\ell O_4)$; (2) isothiocyanato[3,10–dimethyl–4,9–diaza–3,9–dodecadiene–2,11–dione dioximato(1–)]copper(II), $[Cu(NCS)(N_4O_2C_{12}H_{21})]$; (3) trans–dichloro (C–meso–3,5,7,7,10,12,14,14–octamethyl–1,4,8,11–tetraaza–cyclotetradeca –4,11–diene) cobalt(III) perchlorate. $[CoC\ell_2(N_4C_{18}H_{36})](C\ell O_4)$, and (4) carbonato (C–rac–5,7,7,12,14,14–hexamethyl–1,4,8,11–tetraazacyclotetradecane) cobalt(III) perchlorate, $[Co(CO_3)(N_4C_{16}H_{36})](C\ell O_4)$. Their crystal data are (1) monoclinic, $P2_1/c$, Z=4, a=7.161(3), b=18.945(3), c=13.949(4) Å, β=103.472(1)°, R_f=0.039, R_w=0.04; (2) orthorhombic, $Pn2_1a$, Z=4, a=7.5322(7), b=12.652(4), c=17.985(4) Å, R_f=0.034, R_w=0.036; (3) triclinic, P1, Z=1, a=6.974(4), b=8.530(1), c=11.061(2) Å, α=98.47(1), β=106.56(3), γ=93.02(3)°, R_f=0.072, R_w=0.085, and (4) orthorhombic, $P22_12_1$, Z=2, a=7.185(5), b=9.552(3), c=16.742(3) Å, R_f=0.064, R_w=0.085. (1) The Ni(II) atom is four coordinated in a distorted square plane formed by the four donor N atoms. The six–membered ring is in chair form. (2) The Cu(II) ion is five coordinated in a distorted square–pyramidal geometry with the four N atoms equatorial and a N–bound isothiocyanate axial. The Cu(II) ion deviates 0.298(2) Å from the best plane formed by the four N atoms towards the fifth coordinated N atom. (3) Aside from the perchlorate group, the molecule has a non–crystallographic inversion center at the Co(III) ion. The Co(III) ion is in the tetragonally distorted octahedral geometry with four N atoms equatorial and two chlorine atoms axial. The two five–membered rings are in gauche form. One six–membered ring is in boat form, the other in twist conformation. (4) A two–fold axis passes through the Co(III) ion and the carbon atom of the carbonate group, and thus only half a molecule needs to be located. The Co(III) ion is six coordinated. The macrocyclic ligand is in a folded structure. The two six–membered rings are in chair form and the two five–membered rings in gauche form. This work was supported by the National Science Council, ROC, under grants NSC81–0208–M007–110 and NSC81–0208–M007–86.

16S-33

COMPLEXES OF SOME FIRST TRANSITION SERIES ELEMENTS WITH 4,4'-DIPYRAZOLYLMETHANE

John A. Broomhead, Gaye Camm and Meta Sterns
Chemistry Department, Faculty of Science,
Australian National University, Canberra, ACT 2601, Australia.

The ligand 4,4'-dipyrazolylmethane (dpzm) reacts with chlorides MCl_2 (M=Mn, Fe, Co, Ni, Cu), in aqueous or ethanolic solutions, to give complexes of composition $MCl_2(dpzm)_2$, insoluble in water and ethanol, sparingly soluble in N,N-dimethylformamide (dmf) and, with the exception of the nickel complex, soluble in dimethylsulphoxide. The five complexes, which could only be prepared as microcrystalline precipitates, were found, by X-ray powder diffraction, to be isomorphous. Recrystallization of the copper complex from dmf yielded deep blue crystals of a solvate $[CuCl_2(dpzm)_2]$.2dmf, the structure of which was determined by single crystal X-ray structure analysis. Attempts to crystallize the other complexes were unsuccessful.

Crystal data: $CuCl_2C_{14}H_{16}N_8.2C_3H_7NO$; monoclinic, $P2_1/c$ (No.14)
a 8.673(1), b 17.572(2), c 8.535(1)Å, β 97.34(2)°, Z 2.

The structure comprises polymeric chains $[CuCl_2(dpzm)_2]_\infty$, with copper atoms linked by double dipyrazolylmethane bridges. Copper is in a distorted octahedral environment, with axial chlorine atoms at 2.799(2)Å and four coplanar equatorial nitrogen atoms at 2.007(5)–2.030(5)Å. The dimethylformamide molecules are accommodated in channels between the $[CuCl_2(dpzm)_2]_\infty$ chains and are easily lost on exposure of the crystals to air, with resulting breakdown of the crystal structure. The X-ray powder diffraction pattern of the decomposition product shows it to have the same structure as the unsolvated precipitates $MCl_2(dpzm)_2$.

16S-34

POLYMORPHIC STRUCTURES OF $M(HCOO)_2.2(NH_2)_2CO$: M=Mn,Cd,Co,Mg,Zn

N.Achiwa, M. Fujino, H. Takakura, M. Shiono, Department of Physics, Faculty of Science Kyushu University, Higashi-ku, Fukuoka, 812, Japan., N. Koyano, Ridwan, I. Shibuya, Research Reactor Institute, Kyoto University, Kumatori, Osaka-fu 590-04, Japan, and K. Yamagata, College of Science and Engineering, Iwaki Meisei University, Chuodai,Iwaki,Fukushima-ken 970, Japan

New family compounds M bis-formate bis-urea (abbreviated as MFoUr) belong to two kinds of space group, $P4_12_12$ (M=Mn, Cd and Co) or $C2/c$ (Mg, Zn and Co) as we have reported previously[1,2]. Among them MnFoUr and CoFoUr show a characteristic two dimensional magnetism. The structure refinements show very similar features in both types of structures;(1) a layer of two dimensional squared network of (metal-formate)$_4$ is stacked layer by layer along the *c*-axis, (2) metal ions are surrounded octahedrally by the four square-planar oxygen atoms belonging to different formate ions and by the other two oxygen atoms of urea molecules, and (3) urea molecules connected with metal ions which belong to the upper and lower layers are reversely coupled by two O··H-N hydrogen bonds, therefore the urea molecules act as supporters between these layers. The essential difference between the tetragonal and the monoclinic structures is attributed to the ordering of the two asymmetric molecular units A and B. In the monoclinic structure, the squared network plane of (metal-formate)$_4$ consists of A-B-$\overline{A}-\overline{B}$ quasi-square rings where $\overline{A}$ ($\overline{B}$) is the inversion of the A (B). While in the tetragonal structure the squared network consists of A-A'-B'-B rings where the A (B) is coupled with A' (B') along the 2_1 axis. In both compounds the layers are connected only by hydrogen bonds through urea molecules. For the tetragonal compounds, two kinds of chirality are expected, $P4_12_12$ or $P4_32_12$. Here we also report the absolute structure for CdFoUr.

1) Fujino M., Achiwa N., Koyano N., Shibuya I., Ridwan & Yamagata K., J. Magn. Magn. Mater. 104/107 (1992) 851-852.
2) Yamagata K., Achiwa N., Hashimoto M., Koyano N., Ridwan, Iwata Y., & Shibuya I., Acta Cryst. (1992). C48 793-795.

16S-35

CRYSTAL AND MOLECULAR STRUCTURE OF ZINC(II) AND COBALT(II) COMPLEXES WITH 4,5-DIAZAFLUOREN-9-ONE

N Venkata Lakshmi and K. Ravikumar, Laboratory of Crystallography,
Indian Inst. of Chemical Technology, Hyderabad 500 007, India,
G Prasuna and M V Rajasekharan, School of Chemistry, University of
Hyderabad, Hyderabad, India

4,5-diazafluoren-9-one (dafone) was prepared by known procedures (Henderson, Jr., 1984). Solutions of Zinc(II) (and Cobalt(II)) chlorides are treated with dafone solution in molar ratio in acid medium. Upon evaporation these gave good single crystals of the respective complexes (MCI_4(dafone $H)_2.2H_2O$, M=Co, Zn). The Zinc complex solution was yellow in colour throughout whereas the Cobalt complex solution was pale pink to start with and turned dark green just before crystallization.

Crystal data: λ(Mo *Kα*)=0.71069Å

$ZnCl_4(dafoneH)_2.2H_2O$, monoclinic, *C*2/*c*, a=16.783(3), b=12.087(2), c=13.912(2)Å, and β=116.51(2)°. Z=4, R=0.043 and R_w=0.047.

$CoCI_4(dafoneH)_2.2H_2O$, monoclinic, *C*2/*c*, Z=4, R=0.045 and R_w=0.048.

The crystallographic data revealed that both structures are isomorphous. The unit cell consists of protonated dafone as cation, $(CI_4)^{2-}$ anions and water molecules of hydration. The metal atom lies on a crystallographic two fold axis such that only half the molecule comprises the asymmetric unit. The water molecule connects the dafone ring and the $(MC_4)^{2-}$ via hydrogen bonding.

Henderson, Jr. L.J., Fonezek, F.R. & Cherry R (1984). *J Am Chem Soc* **106**, 5876-5879.

16S-36

STUDY ON BIS{*trans*–[BIS(DIPHENYLPHOSPHINO)ETHYLENE]}–TRICARBONYLIRON(0) AND *cis*–[BIS(DIPHENYLPHOSPHINO)–ETHYLENE]TRICARBONYLIRON(0)

Lung-Shiang Luh and Ling-Kang Liu, Institute of Chemistry, Academia Sinica, Taipei, Taiwan 11529, R. O. C.

Two routes have been employed in the synthesis of (*trans*-$Ph_2PCH=CHPPh_2)_2$-$Fe(CO)_3$, **1**, and (*cis*-$Ph_2PCH=CHPPh_2)Fe(CO)_3$, **2**. Method **A** proceeds with the Me_3NO oxidative decarbonylation of (maleic acid)$Fe(CO)_4$, followed by a precipitation of maleate salt in the presence of either *trans*-$Ph_2PCH=CHPPh_2$ or *cis*-$Ph_2PCH=CHPPh_2$. Method **B** is a low temperature quenching of (*cis*-cyclooctene)$_2Fe(CO)_3$ with either *trans*-$Ph_2PCH=CHPPh_2$ or *cis*-$Ph_2PCH=CHPPh_2$. Complexes **1** and **2** have been characterized with spectroscopic methods and X-ray diffraction. X-ray crystallographic data for the title compounds : **1**, monoclinic, space group $P2_1/c$, a = 11.532(2) Å, b = 20.454(2) Å, c = 22.652(6) Å, β = 104.49(2)°, V = 5173(2) $Å^3$, Z = 4; 2547 data with $I_o > 2.5\sigma(I_o)$ were refined to R = 0.049, Rw = 0.051. **2**, monoclinic, space group $P2_1/c$, a = 10.064(1) Å, b = 15.164(2) Å, c = 17.379(2) Å, β = 101.136(7)°, V = 2602.2(5) $Å^3$, Z = 4; 2274 data with $I_o > 2.5\sigma(I_o)$ were refined to R = 0.035, Rw = 0.037. Complex **1** has a trigonal-pyramidal Fe(0) center with two diaxially-coordinated, unidentate *trans*-$Ph_2PCH=CHPPh_2$. Compound **2** has a trigonal-pyramidal Fe(0) center with one chelating *cis*-$Ph_2PCH=CHPPh_2$ occupying one axial and one equatorial sites, conforming to the *cis*-form.

16S-37

STRUCTURE OF IODINE{[3,3'-(1,3-PROPANEDIYL-DINITRILO)BIS(2-BUTANONE OXIMATO)]-N,N'N",N'''} (2,2,2-TRIFLUOROETHYL)COBALT(III)

Silvano Geremia, Asadur Rahman*, Ennio Zangrando and Lucio Randaccio, Dipartimento di Scienze Chimiche, Universita di Trieste, 34127 Trieste, Italy.

* *Permanent address:* Department of Physics, University of Dhaka, Dhaka-1000, Bangladesh.

The compound is a coenzyme B_{12} model of the type $L[Co(DO)(DOH)_{pn}]R$. Deep brown crystals of the compound were used in collecting intensity data with an Enraf-Nonius CAD-4 diffractometer. The total number of reflexions measured was 4107 with 2948 unique reflexions ($I>3\sigma(I)$). The structure was solved by Patterson methods and subsequent Fourier syntheses.

Crystal data:
$Co(C_{11}H_{19}N_4O_2)(C_2H_2F_3)I$, FW 508.17, F(000) 250, monoclinic, space group *C2/c*, *a* 28.928(7), *b* 7.558(1), *c* 17.142(4)Å, *β* 104.92(1)° V 3621.53(2)Å^3, T 293K, d_{calc} 1.864 gms/cc, μ 26.74 cm^{-1}, λ 0.7107Å, *R* 0.027.

The Co atom forms a distorted octahedral polyhedron with axial Co-I and Co-C distances 2.6505(8) and 2.034(7)Å respectively. The average Co-N distance of 1.896Å compares well with those reported by Geremia et al, 1992, and by Randaccio et al, 1989. The fluorine atoms in $C_2H_2F_3$ are partially disordered.

Silvano Geremia, Asadur Rahman and Ennio Zangrando, (1992) *Acta Cryst* **C48**, (in press).

L Randaccio, N Bresciani Pahor, E Zangrando and L G Marzilli (1989) *Chem Soc Rev* **18**, 225-250.

16S-38

EXAFS STUDIES OF MONOMERIC/DIMERIC EQUILIBRIA OF NITRIDO-TECHNETIUM(VI) COMPLEXES IN SOLUTION

G.A. Williams, L.J. Martin and D.L. Samuels, Australian Radiation Laboratory, Yallambie, Victoria 3085, Australia; and
M. Nomura, KEK Photon Factory, Tsukuba-Shi, Japan.

The behaviour of $Cs_2[TcNCl_5]$ in various concentrations of hydrochloric acid and in non-coordinating acids such as p-toluenesulfonic acid has been studied by the EXAFS technique. The solution chemistry is complex; previously salts of $[TcNCl_4]^-$, $[TcNCl_5]^{2-}$ and $[TcNCl_4(OH_2)]^-$ have been isolated and evidence for the presence of $[TcNCl_4\text{-}O\text{-}TcNCl_4]^{4-}$, $[TcNCl_2(\mu\text{-}O)_2TcNCl_2]^{2-}$ and $[TcN(OH_2)_3(\mu\text{-}O)_2TcN(OH_2)_3]^{2+}$ has been obtained by a variety of techniques. The EXAFS spectra enable a study of the equilibria and species present in solutions of $Cs_2[TcNCl_5]$ in hydrochloric and sulphuric acids, p-toluenesulfonic acid, trifluoromethanesulfonic acid, Na(OH) and water. Of particular interest is the structural identification of the aqua cation and of the $[Tc_2N_2O_2(OH)_4]^{2-}$ anion in solution.

In order to measure EXAFS spectra from the radioactive technetium solutions, special leak-proof sample cells had to be designed, manufactured, filled with the aqueous solutions at ARL, leak-tested, and transported in appropriate packaging to the Photon Factory independently of the experimentalists. At the Photon Factory, two measurement periods each of about 24 hours were available on the EXAFS facility on beam-line BL-10. In all, 19 cells were successfully transported to Japan. In most cases the EXAFS spectra obtained were of a high quality.

The Japanese software for EXAFS analysis was provided and has been commissioned at ARL. Qualitative Fourier analyses and quantitative evaluations of the spectra are presented which show the monomeric and dimeric structures of species present in the various solutions, and the equilibria among monomeric, dimeric μ-oxo and dimeric di(μ-oxo) species have been quantified from the measured EXAFS spectra.

X-RAY STRUCTURAL STUDIES OF A NOVEL DELOCALISED TRIPHOSPHAZENE $(CF_3)_2P{=}N{=}P(CF_3)_2{=}N{=}PPh_3$ AND THE TRIOSMIUM CLUSTER COMPLEXES $Os_3(CO)_{11}[(CF_3)_2P{=}N{=}P(CF_3)_2{=}N{=}PPh_3]$

H.G. Ang, W.L. Kwik and Y.M. Cai, Department of Chemistry, National University of Singapore, Lower Kent Ridge Road, Singapore 0511.

The molecular structures of the title compounds were determined by single crystal x-ray diffraction methods. The most significant and unusual feature is that the four phosphorus-nitrogen bond lengths within free ligand and the complex are nearly equidistant. Furthermore, all these lie within the range of 1.518-1.584 Å expected for a P=N double bond. In addition, the two P-N-P segments within the P(IV)=N=P(VI)=N=P(V) moiety approach near linear structures, with the P(IV)=N=P(VI) and P(VI)=N=P(V) angles being 153.1° and 148.18° in L, and 162.4° and 154.1° in C, respectively. The central phosphorus atom is four-coordinated and hexavelent. This would suggest that the unsymmetical PNPNP segment is highly delocalised presumable due to the strong electron withdrawing CF_3 moiety.

Crystal data L: $[C_{21.5}H_{15}F_{11.5}N_2P_3]$ Monoclinic, Space Group $P2_1/n$, $\underline{a}$ = 11.94(2) Å, $\underline{b}$ = 14.368 Å, $\underline{c}$ = 15.576(3) Å, β = 92.17(3)°.

C: $[C_{33}H_{15}N_2O_{11}F_{12}P_3Os_3]$ Triclinic, Space Group $P\bar{1}$, $\underline{a}$ = 9.154(2) Å, $\underline{b}$ = 12.208(2) Å, $\underline{c}$ = 21.478(4) Å, α = 73.10(3)°, β = 78.90(3)°, γ = 68.92(4)°.

Ang H.G., Cai Y.M., Kwik W.L. and Rheingold A.L., J.C.S. Chem. Commun., (1990) 1580.

Ang H.G., Cai Y.M., Kwik W.L., E.C. Morrison and D.A. Tocher., J. Organometal. Chem., 403(1991)383.

Ang H.G., Cai Y.M., Kwik W.L., Leong W.K. and D.A. Tocher, Polyhedron 10(1991)881.

Ang H.G., Cai Y.M., Koh L.L., Kwik W.L., J.C.S. Chem. Commun., (1991)850.

NOVEL NEUTRAL MOLECULES CONTAINING THE As=N=P MOIETY. THE X-RAY STRUCTURES OF $(CF_3)_2As{=}N{=}PPh_3$, $[Os_3(CO)_{11}((CF_3)_2As{=}N{=}PPh_3)]$ AND $[Os_3(CO)_9(\mu\text{-}H)_2((CF_3)_2As{=}N{=}PPh_3)]$

H.G. Ang, W.L. Kwik and Y.W. Lee, Department of Chemistry, National University of Singapore, Lower Kent Ridge Road, Singapore 0511, and A.L. Rheingold, Department of Chemistry and Biochemistry, University of Delaware, Newark, Delaware 19716, USA.

The first perfluoro-alkyl arsinous azide $(CF_3)_2AsN_3$ undergoes Staudinger reaction with PPh_3 to give the novel perfluoro-alkyl arsino phosphinimine $(CF_3)_2As{=}N{=}PPh_3$ **1** with a short As-N bond length of 1.783(10) Å . In complexation of **1** with triosmium clusters to give $[Os_3(CO)_{11}((CF_3)_2As{=}N{=}PPh_3)]$ **2** and $[Os_3(CO)_9(\mu{-}H)_2((CF_3)_2As{=}N{=}PPh_3)]$ **3** it has been shown from X-ray crystallography that **1** assumes a highly delocalized electronic structure over the unsymmetrical As=N=P segment with a significantly short As-N bond. Enhanced delocalisation upon complexation of 1 is reflected in the increase in As-N-P angles from 126.6(6)° in **1** to 135.4(9)° and 133.0(8)° in the complexes **2** and **3**, resulting in a further shortening of the As-N bond from 1.783(10) Å in **1** to 1.716(13) Å and 1.739(16) Å in **2** and **3** respectively. These molecules represent the first examples of neutral compounds containing a highly delocalized As=N=P non-linear heterocummulene moiety with quadrivalent arsenic center.

Crystal data:

1 $CF_3)_2As{=}N{=}PPh_3$, orthorhombic, space group *Fdd2*, $a = 19.114(5)$, $b = 42.918(8)$, $c = 10.378(3)$ Å, $U = 8513(3)$ Å^3, $Z = 16$.

2 $Os_3(CO)_{11}[(CF_3)_2As{=}N{=}PPh_3]$, monoclinic, space group $P2_1/n$, $a = 10.849(6)$, $b = 24.117(9)$, $c = 14.618(8)$ Å, $\beta = 102.76(4)°$, $U = 3730.2(34)$Å^3, $Z = 4$.

3 $Os_3(CO)_9(\mu\text{-}H)_2((CF_3)_2As{=}N{=}PPh_3)$, monoclinic, space group $P2_1/n$, $a = 13.7457(16)$, $b = 15.0939(17)$, $c = 18.3746(23)$, $\beta = 109.935(9)°$, $U = 3583.8(7)$Å^3, $Z = 4$.

16S-41

X-RAY CRYSTAL STRUCTURE OF $[\{WCl_3(PMe_2Ph)_2\}_2\{(\mu\text{-}NC_6H_4N\text{-}1,4\}]$. THE FIRST STRUCTURAL CHARACTERISATION OF A BINUCLEAR COMPLEX CONTAINING A 1,4-PHENYLENE DIIMIDO BRIDGE.

W. Clegg, R. J. Errington, D. C. R. Hockless, J. M. Kirk, and C. Redshaw. Department of Chemistry, The University of Newcastle Upon Tyne, Newcastle Upon Tyne. NE1 7RU. UK.

The d^0-d^0 phenylenediimido bridge complex $[\{WCl_4\}_2\{\mu\text{-}NC_6H_4N\text{-}1,4\}]$ may be obtained by treatment of $WOCl_4$ with $C_6H_4(NCO)_2$-1,4[1] or, alternatively, from the reaction between WCl_4 and the diazide $C_6H_4(N_3)_2$-1,4.[2] This polymeric compound is presumably chlorine bridged by analogy with the structurally characterized $[\{W(NC_6H_4Me\text{-}_4)Cl_4\}_2]$,[3] and reacts with PMe_2Ph to give the binuclear d^1-d^1 tungsten (V) complex $[\{WCl_3(PMe_2Ph)_2\}_2\{\mu\text{-}NC_6H_4N\text{-}1,4\}]$. Single crystal X-ray structural analysis shows the two *mer*, *trans*-$WCl_3(PMe_2Ph)$ fragments to be linked in an eclipsed conformation by a linear, π-bonded 1,4-phenylenediimido bridge.

Crystal data: $[\{WCl_3(PMe_2Ph)_2\}_2\{\mu\text{-}NC_6H_4N\text{-}1,4\}]$ monoclinic, space group $P2_1/c$ (No 14). a=25.262(3), b=10.781(1), c=20.655(2) Å, β=96.79(13)°.

The adoption of an eclipsed conformation, rather than a less sterically demanding staggered conformation of phosphine ligands suggests that electronic factors may be playing a part, although the two unique molecules of the title complex have significantly different torsion angles. It is also interesting to note that the phenyl rings of the phosphines are all directed into the region between the metal atoms, which would seem to suggest that the chlorine *trans* to the imido group is more sterically active than the phenylenediimido bridge.

1. R. J. Errington, C. Redshaw. Unpublished results.
2. D. Antonello, R. J. Errington. Unpublished results.
3. W. Clegg, R. J. Errington. (1987) Acta Cryst. C43, 2223.

MOLECULAR STRUCTURE OF TUNGSTEN-PHENOXIDE

N. Kanehisa, Y. Kai and N. Kasai, Department of Applied Chemistry, Faculty of Engineering, Osaka University, Suita, 565, Japan, and H. Yasuda, Department of Applied Chemistry, Faculty of Engineering, Hiroshima University, Higashi-Hiroshima, 724, Japan, and Y. Nakayama, and A. Nakamura, Department of Macromolecular Science, Faculty of Science, Osaka University, Toyonaka, 560, Japan.

The use of bulky aryloxy or alkoxy metal compounds of group 4-6 as an alternative to the cyclopentadienyl compounds is of current interest in organometallic chemistry. We have reported a facile method for synthesizing a new series of pure mono- and bis-(phenoxy)metal halides. In a series of structural studies on early transition metal phenoxides we have isolated and crystallized the bis-(phenoxy)tungsten halide, $WCl_4[2,6\text{-}(i\text{-}Pr)_2C_6H_3O]_2$ (**1**), as dark red crystal. The molecular structures of tris-phenoxy tungsten halide, $WCl_3[2,6\text{-}(i\text{-}Pr)_2C_6H_3O]_3$ (**2**), and bis-phenoxy derivative, $WCl_4[2,6\text{-}(C_6H_5)_2C_6H_3)]_2$(**3**), have been reported by Quignard et. al.(1987), and also the molecular structure of tungsten bis-phenoxy derivative, $WCl4[2,6\text{-}(CH_3)_2\text{-}C_6H_3O]_2$ (**4**) have been determined by us.

In order to elucidate the structural characteristics of the series of early transition metal-phenoxides, the X-ray structure analysis of Complex **1** has been carried out. The integrated intensity data were measured on a Rigaku four-circle diffractometer with graphite monochromatized MoKα (λ=0.71069 Å). The determination and refinement of the crystal structure of **1** was carried out by using the TEXSAN software system. R and R_w are 0.086 and 0.063, respectively without the hydrogen atoms.

Crystal data: $WCl_4O_2C_{24}H_{28}$, Formula Weight 674.2, Crystal System Monoclinic, Space Group $P2_1/n$ (No.14), a=9.697(2), b=17.115(2) c=16.799(2)Å, β= 91.80(1)° Z=4, Dc=1.607 g/cm^3.

Molecular Structure of **1** has six-coordinated geometry for the central tungsten atom, and octahedral coordination sphere as well as **2**, **3** and **4**. In complex **2**, three phenoxy groups occupy the meridional sites. In complex **1**, two phenoxy groups occupy the *cis* position as same as in complex **3**, while in complex **4** *trans*.

Quignard F., Leconte M., Basset J-M., Hsu L-Y., Alexander J.J. & Shore S. G. (1987). *Inorg. Chem.* **26,** 4272

STEREOCHEMISTRY AND CRYSTAL STRUCTURE OF DIPHENYLTIN DICHLORIDE COMPLEXES WITH *meso*– OR rac–BIS(PHENYLSULFINYL)ETHANE

H G Wang, X K Yao, R J Wang, J X Bao and P X Shao, Central Lab. and Department of Chemistry, Nankai University, Tianjin, 300071, China.

The bidentate ligands, $RS(O)C_2H_4S(O)R$, exist as diastereoisomeric *rac* and *meso* forms which have different melting points X-ray crystal structure analyses proved that the higher melting isomer is of the *meso*-form when R groups are methyl (Svinning *et al., 1976)* and phenyl (Cattalini *et al., 1979;* Pelizzi *et al., 1976)*. In a previous paper (Zhu et al, 1990), X-ray diffraction results revealed that triphenyltin chloride (TPTC) reacts with either *meso-* or *rac*-bis-(phenylsulfinyl)ethane (BPSE) to give the same crystal in which the ratio of TPTC:BPSE is 2:1 and the ligand, BPSE, is the meso-isomer. In this work, 1:1 complexes of diphenyltin dichloride (DPTC) with *meso-* or *rac*-BPSE were prepared and their crystal structures were determined by X-ray diffraction methods. DPTC•*meso*-BPSE (I) is monoclinic $P2_1/a$, with $a = 18.549(5)$, $b = 12.672(4)$, $c = 22.401(3)$ Å, $\beta = 90.15(2)°$, $Z = 8$; $R = 0.049$. DPTC•*rac*-BPSE (II) is monoclinic $C2/c$ with $a = 20.584(4)$, $b = 12.726(1)$, $c = 20.230(5)$ Å, $\beta = 96.91(3)°$, $Z = 8$; $R = 0.036$. In each complex, the tin atom has a distorted octahedral coordination with two oxygen and two chlorine atoms occupying the equatorial positions, and the bidentate BPSE bridges between two Sn atoms to give a one-dimensional chain After the complexing reaction, *meso*-BPSE retains its configuration in crystal I, but one of the S atoms of *rac*-BPSE in crystal II is dipositional disordered Reasonable thermal parameters for S atoms were obtained when the occupancies of 0.5 were assigned to these positions. Although both environments of the positions can meet the demands of tetrahedral geometry for the S atoms, their chirals are inverse to each other, which means that about half the *rac*-BPSE ligands invert their configurations in the complexing reaction with DPTC.

Cattalini, L , Michelon, G , Marangoni, G & Pelizzi, G (1979) *J Chem. Soc., Dalton* Trans, 96-101

Pelizzi, G , Michelon, G ~ Bonivento, M (1976) *Cryst Struct Commun,* **5**, 617-620

Svinning, T , Mo F & Bruun, T (1976) *Acta Cryst* , B32, 759-764

Zhu, F C , Shao, P X, Yao, X K , Wang, R J & Wang, H G (1990) *Inorg Chim.* Acta, **171**, 85-88

16S-44

COORDINATION OF TETRAMETHYLETHYLENEDIAMINE WITH HALOGEN BRIDGED LEAD(II)

H. Miyamae, Y. Hatanaka, Y. Iijima, G. Hihara and M. Nagata, Department of Chemistry, Josai University, Keyakidai, Sakado-shi, Saitama 350-02, Japan.

Structure determinations of 1:1 adducts of 'Me$_4$en'*(N, N, N', N'* – tetramethylethylenediamine) with lead(II) halides (PbX$_2$, X=Cl, Br, I) are described. Colourless PbX$_2$.Me$_4$en crystals obtained by slow evaporation of appropriately stoichiometric solutions in ethanol at room temperature. were used for single crystal X-ray studies at 295 - 298 K.

Crystal data:

PbC1$_2$.Me$_4$en. Orthorhombic, space group *P*2l*nb* (No. 33),
a 8.102(19), *b* 15.096(34), c 9.258(29)Å
V 1132(5)Å^3. D_x 2.313 g.cm^{-3}. μ_{Mo} 15.44 mm^{-1}.

PbBr$_2$.Me$_4$en. Monoclinic, space group $P2_1/n$ (No. 14),
a 18.370(5), *b* 8.213(3), c 18.734(5)Å, β 117.95(2)°
V 2497(1)Å^3. D_x 2.442 g.cm^{-3}. μ_{Mo} 19.91 mm^{-1}.

PbI$_2$.Me$_4$en. Monoclinic, space group $P2_1/n$ (No. 14),
a 17.295(3), *b* 9.226(2), *c* 8.499(1)Å, β 88.93(1)°
V 1355.9(4)Å^3. D_x 2.709 g.cm^{-3}. μ_{Mo} 17.01 mm-1.

The results show the lead atoms to be in six-coordinate, highly distorted octahedral environments. In the chloride complex, the environment of four chloride and two nitrogen atoms is almost trigonal prismatic, with the suggestion that any stereochemically active lone pair at the lead atom might be accumulated at the centre of a Cl$_4$ square face, the four Pb-Cl distances ranging from 2.88 to 3.00(1) Å. In the iodide complex, the I-Pb-I bond angle *trans* to the chelating ligand is considerably enlarged, again possibly suggestive of a sterically active lone pair in a quasi-trigonal bipyramidal array. In this description, the axial Pb-I bond lengths (< > 3.223(2) Å) are shorter than the equatorial values (< > 3.323(2) Å). The bromide is still under investigation.

16T-45

CRYSTALLIZATION AND PRELIMINARY X-RAY STUDIES OF CALOTROPIN DII, A CYSTEIN PROTEASE FROM *Calotropis gigantea*

Bankim Das, Sreya Ghosh, Sampa Pain, Indrani Dey, Goutam Biswas, Bishnu P Mukhopadhyay, N K Sinha and Asok Banerjee, Biophysics Department, Bose Institute, P1/12 C.I.T. Scheme VIIM, Calcutta - 700054, India.

Rectangular needle shaped crystals of Calotropin DII, a single chain polypeptide of Mr 24163, have been obtained by a microdialysis. The enzyme crystallised in a monoclinic structure with space group $P2_1$. The unit cell dimensions are a=48.689(1)Å, b=31.972(1)Å, c=131.597(1)Å, β=97.735(3)°.

The density measurement indicated the presence of four polypeptide molecules in the unit cell. The V_M & Vs values are 2.1Å ^{3}/D and 43% respectively. The crystals are stable at room temperature (293K) and also with irradiation by X-rays, diffracting diffracts to at least 1.8Å resolution. Among the possible 22296 reflections, 11219 independent unique reflections have been collected using an area detector. A three dimensional structure solution by the molecular replacement method is in progress.

16T-46

CRYSTALLIZATION OF PROTEIN DISULFIDE ISOMERASE FROM BOVINE LIVER

G.Kurisu, C.Uematsu, T.Shiba, S.Harada, Y.Kai and N.Kasai,
Department of Applied Chemistry, Faculty of Engineering,
Osaka University, Suita, Osaka 565, Japan.

Protein disulfide isomerase (PDI) is an abundant protein which is loosely attached to the luminal side of the ER membrane. It catalyzes the formation of correct disulfide bonds of newly synthesized proteins in the ER lumen. PDI exists as a dimeric molecule which consists of chemically identical polypeptide chains of 57,000 molecular weight. In order to study its biological function based on its three-dimensional structure, PDI has been crystallized. PDI was isolated from bovine liver according to the procedure described by Lanbert & Freedmann. The purity of the enzyme was checked using SDS-PAGE analysis and reverse-phase chromatography. Crystallization was attempted using salts, polyethylene glycol and organic solvents as precipitants. The screening of crystallization conditions was performed by the batch method. Although crystals of PDI appeared in a wide variety of conditions, the best crystal was obtained from 20-30% polyethylene glycol 8000. (pH5.0-8.0) The shape of the crystals was tetragonal bipyramidal. We are searching for optimum conditions to grow the tetragonal bipyramidal crystals using the hanging drop vapor diffusion method.

16T-47

CRYSTALLIZATION AND X-RAY DIFFRACTION STUDY OF PHOSPHIOLIPIDASE A$_2$ FROM THE VENOM OF *Agkistrodon halys* PALLAS

Gui Lulu, Niu Xiutian, yang Jian, Bi Ruchang,Liu Zhengjiong, Institute
of Biophysics, Academia Sinica, Beijing 100101, China, and
Zhou Yuanchong, Lin Nianqin, Shanghai Institute of Biochemistry,
Academia Sinica, Shanghai, China.

The acidic phospholipase A_2 from *Agkistrodon halys* Pallas consisting of 124 residues belongs to a class of phospholipase A_2 which possesses a function of inhibiting platelet aggregation.The enzyme was purified by previously described techniques (*Acta Biochemica et Biophysica Sinica* **16**,664(1984)) and crystallized by a vapour diffusion method. The crystals were obtained from aliquots, containing 2,5Hexandiol, 0.lmg/L Na_2O_8-HCl and l5mg/ml protein, which were equilibrated against 65% 2,5Hexandiol solution. The crystals grow as long hexagonal prisms and diffract to a resolution better than 2.5Å. Some crystal data were determined on a CAD 4 diffractometer. The space group is $P6_1$ with cell dimensions $a=b=83.2$Å and $c=32.6$Å. There is only one molecule per asymmetric unit. Diffraction data have been collected to 2.65Å resolution using an area detector. The orientation and position of the PLA_2 molecule in the unit cell have been determined by a molecular replacement method using the known structure of C.atrox PLA_2 as search structure. Preliminary structure analysis has shown that the overall folding of this molecule is similar to that of C.atrox PLA_2. Structure refinement is in progress.

16T-48

TWO CRYSTAL FORMS OF BOVINE HEART CYTOCHROME *c* OXIDASE

E. Yamashita, Y. Morimoto, T. Tsukihara, Faculty of Engineering, The University of Tokushima,Tokushima 770, and
Y. Fukumoto, Faculty of Engineering, Tottori University, Tottori 680,
K. Shinzawa-Ito, S. Yoshikawa, Faculty of Science, Himeji Institute of Technology, Kamigouri Akou, Hyougo 678-12, Japan.

Cytochrome *c* oxidase is a key enzyme of the respiratory chain in the mitochondria. It catalyzes the oxidation of cytochromes by molecular oxygen and couples this reaction to translocation of protons across the mitochondrial inner membrane. The proton gradient produced by this reaction is utilized for ATP synthesis. Our aim is to determine the structure in order to clarify the mechanism of the enzyme reaction. Two different crystal forms were obtained: a hexagonal form crystallized from solution with a low salt concentration, and a tetragonal form crystallized by salting-out with ammonium sulfate. The space group of the hexagonal form was $P6_2$ or $P6_4$ with unit cell constants $a=b=208.7$Å, $c=282.3$Å. The tetragonal crystal space group was $I4_1$ with $a=b=253.2$Å, $c=507.1$Å.

Intensity data for both crystals were collected using a Weissenberg camera for macromolecular crystals with synchrotron radiation at the Photon Factory, Tsukuba. A total of 7,000 reflections with $F>3\sigma(F)$ at 7Å resolution were obtained by the use of six hexagonal crystals. The *R*-factor and correlation function for each pair of data sets of hexagonal crystals show that the quality of the intensity data decreased steeply over 10Å resolution.

Intensity data for the tetragonal crystal were collected by using several crystals. Part of the data has been processed. By some criteria the tetragonal crystals are of higher quality than the hexagonal form.

16T-49

STRUCTURE ANALYSIS OF *SERRATIA* PROTEASE FROM *SERRATIA* SP.E-15

K. Hamada, H. Hiramatsu and T. Fujiwara, Faculty of Science, Shimane University, Matsue 690, Japan, Y. Katsuya, Hyogo Prefecture Institute of Industrial Technology, Kobe 654 , Japan, Y. Hata, Institute for Chemical Research, Kyoto University, Uji 611, Japan, and M. Sato and Y. Katsube, Institute for Protein Research, Osaka University, Osaka 565, Japan.

Serratia protease, isolated from culture media of *Serratia* sp. E-15, is a Zn-requiring metalloprotease consisting of a single polypeptide chain of 470 amino acid residues (Mr 50,600). The function and the substitute specificity of this enzyme are similar to those of thermolysin, but the molecular weight of *serratia* protease is larger than that of thermolysin (Mr 34,600) and also the homology of the amino acid sequence between both enzymes is quite low. Crystals were obtained from 28% saturated ammonium sulfate by a microdialysis method. The crystals were space group $P2_12_12_1$ with cell dimensions $a = 109.2$, $b = 150.9$, $c = 42.6$ Å and $Z = 4$. The intensity data from the native and Sm-derivative crystals were collected on an IP-diffractometer (R-AXIS IIa). Initial protein phases at 5.0 Å resolution were obtained by single isomorphous replacement supplemented anomalous-scattering information from Sm-derivative data (SIRAS), and then the phases were gradually extended to 3.0 Å resolution using solvent-flattening procedure (Wang, 1985). A total of 6 phase-extension steps were required. After each phase-extension, phase refinement was carried out at constant resolution. An electron density map at 3.0 Å resolution shows a polypeptide folding, although there are some ambiguous positions. The molecule has an ellipsoidal shape with approximate 95x40x40 Å. The analysis of the detailed structure is in progress.

Wang, B. C. (1985). *Methods Enzymol.* **115**, 90-112.

16T-50

X-RAY STRUCTURE ANALYSIS OF NEUTRAL PROTEASE FROM *STREPTOMYCES CAESPITOSUS*

A. Nagara, T. Kinoshita, S. Harada, Y. Kai and N. Kasai, Department of Applied Chemistry, Faculty of Engineering, Osaka University, Suita, Osaka 565, Japan and
S. Tunazawa and F.Sakiyama, Institute for Protein Research, Osaka University, Suita, Osaka 565, Japan

A neutral protease, *i.e.,* a zinc-containing metalloendoprotease from *Streptomyces caespitosus,* has been crystallized. The crystals diffract to better than 1.5Å resolution with a rotating anode X-ray generator. Protein phase angles were calculated by the multiple isomorphous replacement method using two heavy-atom derivatives ($HgCl_2$ and CH_3HgCl). A 6Å resolution electron density map clearly showed molecular boundaries and the folding pattern of the polypeptide chain could be traced on a 2.5Å resolution electron density map. A large cleft, located on the molecular surface, was proved to be the active site of the enzyme by structure analyses of inhibitor-complex crystals. A catalytically essential zinc atom was also identified in the active site cleft as the highest electron density peak. Model building of the protease is in progress based on the amino acid sequence of 132 amino acid residues which has been determined recently by the authors.

Crystal data: orthorhombic, space group $P2_12_12_1$
$a = 55.21, b = 55.27, c = 37.60$Å

S.Harada, K.Kitadokoro, T.Kinoshita, Y.Kai & N.Kasai (1991). *J.Biochem.* **110**, 46-49

16T-51

THREE-DIMENSIONAL STRUCTURE OF OLIGO-1,6-GLUCOSIDASE AT 3 Å RESOLUTION

Y. Hata, Institute for Chemical Research, Kyoto University, Uji, Kyoto 611, Japan, H. Kizaki, K. Watanabe and Y. Suzuki, Department of Agricultural Chemistry, Kyoto Prefectural University, Shimogamo, Sakyo-ku, Kyoto 606, Japan, and Y. Katsube, Institute for Protein Research, Osaka University, Suita, Osaka 565, Japan.

From comparative studies on five oligo-1,6-glucosidases of various *Bacillus* species with different ranges of growth temperature, it has been proposed that the enhanced thermostability of these enzymes would be gained by increasing the frequency of proline occurrence at β-turns. In order to elucidate the mechanisms of function and thermostability of the enzymes from their structures, we have analysed the crystal structure of the enzyme from *B. cereus*. Hexagonal pillar-shaped crystals were obtained by a hanging drop vapor diffusion method (Watanabe, Kitamura, Hata, Katsube, & Suzuki, 1991). The crystals belong to the hexagonal space group $P6_2$ with cell constants a=b=106.0 Å, c=120.0 Å and with one molecule (Mr=66,000, 558 residues) in the asymmetric unit. The Hg-, U- and Sm-derivative crystals were prepared by a soaking method. Intensity data were collected using synchrotron radiation (λ=1.04Å) at $BL6A_2$ station in KEK-PF, Japan. Diffraction patterns were recorded on Fuji imaging plates and processed by the program package WEIS. The structure was determined by MIR method using 12319 reflections (81.6%) up to 3 Å resolution. The molecule of the enzyme is composed of three structural domains. The N-terminal domain has a $(\alpha/\beta)_8$-structure with an additional α-helix. The sub-domain and the C-terminal domain have β-sheet structures. The active site of the present enzyme is expected to lie in the C-terminal side of the parallel β-sheet of the N-terminal domain from comparison in the primary and tertiary structures with amylases. Oligo-1,6-glucosidase of *B. thermoglucosidasius* has 14 extra prolines which may be responsible for the increase in thermostability, compared with that of *B. cereus*. The present structure of the *B. cereus* enzyme suggests that most of the prolines are located in the second sites of β-turns.

Watanabe, K., Kitamura, K., Hata, Y., Katsube, Y. & Suzuki, Y. (1991). *FEBS Lett.* 290, 221-223.

16T-52

THREE-DIMENSIONAL STRUCTURES OF ASPARTATE AMINOTRANSFERASE FROM *ESCHERICHIA COLI* AT 1.8 Å RESOLUTION

A. Okamoto, Faculty of Science, Osaka University, Toyonaka, Osaka 560,
K. Hirotsu, and T. Higuchi, Faculty of Science, Osaka City University,
Sumiyoshi, Osaka 558, Japan.

Aspartate aminotransferase (AspAT) catalyzes the reversible transamination of α-amino group from L-aspartate to α-ketoglutarate and is essential in nitrogen and carbon metabolism in the cell. In eukaryotic cells, two genetically distinct isoenzymes of AspAT (the cytosolic enzyme and the mitochondrial one) occur, whereas only a single form of AspAT has been found in prokaryotic cells. The overall sequence homology between *E. coli* and vertebrate enzymes is about 25%, and all the important residues for catalysis are conserved. However, the activity of *E. coli* AspAT is lower than those of the enzyme from higher animals, and the *E. coli* AspAT shows a broad substrate specificity.

The enzyme is in α_2 dimeric form with a subunit molecular weight about 45000. Each subunit has one pyridoxal phosphate (PLP) forming Schiff base with a lysine residue at the active site. The *E. coli* AspAT was overproduced in the cell. Crystals of wild type AspAT and wild type AspAT 2-methylaspartate (2-MeAsp) were grown from Na_2SO_4 solution at pH 7.0 by hanging drop vapour diffusion. X–Ray data for these crystals were collected to a resolution of 1.8Å on a screenless Weissenberg type camera using synchrotron radiation at the Photon Factory ($6A_2$ station), KEK. Refinements were performed using the coordinates of the AspAT-2MeAsp (2.5 Å resolution) as starting models, by the program XPLOR. The *R*-values reduced to 0.21 and 0.22 for AspAT and AspAT-2-MeAsp, respectively.

AspAT consists of two identical subunits related by the crystallographic two-fold axes. The subunit was divided into a small domain (from N-terminus to T47 and from M326 to C-terminus) and a large domain(the remaining amino acid residues). The overall structures of AspAT and AspAT•2-MeAsp in *E. coli* were similar to those in higher animals in the 'open' form and 'closed' form, respectively. The conformational change from 'open' to 'closed' found in higher animals also occurred in *E. coli* AspAT. This movement is explained by a rotation of the small domain toward the large domain to close the active site. However, this rotation is 5° in *E. coli* AspAT, compared to 13° found in chicken mitochondrial AspAT.

In the present study, we present the high-resolution X-ray structures of E. *coli* AspAT in 'open' and 'closed' forms.

16T-53

STRUCTURE OF THE ACTIVE-SITE MUTANTS OF *ESCHERICHIA COLI* ASPARTATE AMINOTRANSFERASE

I. Miyahara, K. Hirotsu and T. Higuchi, Faculty of Science, Osaka City University, Sumiyoshi, Osaka 558, Japan and
A. Okamoto, Faculty of Science, Osaka University, Toyonaka, Osaka 560, Japan

Aspartate aminotransferase (AspAT) has a coenzyme, pyridoxal 5'-phosphate (PLP) in the active site and catalyzes the reversible transamination reaction

L-aspartate + 2-oxoglutarate = oxaloacetate + L-glutamate

via the 'ping-pong bi-bi mechanism' . The enzyme is in α_2 dimeric form with a subunit molecular weight 45000. Each subunit has one PLP forming Schiff base with a lysine residue at the active site, and is divided into a small and large domain. Our recent X-ray study confirmed that the gross conformation of *E. coli* AspAT and spatial arrangement of the active site residues are essentially identical to those of pig cytosolic and chicken mitochondrial AspATs. The substantial movement of the small domain from 'open to 'closed', depending on the binding of substrates found in higher animals' AspATs, also occurred in *E. coli* AspAT.

X-Ray structures of the active-site mutants will be very informative in assigning functional roles to the active site residues in the catalytic process. Crystals of R292V (the mutant enzyme with Val in place of Arg292), Y70W·2-methylaspartate (2MeAsp), and H143N-succinate were grown from $(NH_4)_2SO_4$ or PEG4000 solution at pH 7.0 by hanging drop vapor diffusion. X-ray data for these crystals were collected to resolution 2.1~2.2Å on a screenless Weissenberg type camera using synchrotron radiation at the Photon Factory, KEK, Japan. Refinements, performed using the coordinates of the wild type AspAT or the wild type AspAT 2MeAsp by the program XPLOR, reduced the *R*-Values to 0.21, 0.19 and 0.22 for R292V, Y70W·2-MeAsp, and H143N succinate, respectively.

The conformations of R292V and H143N succinate were quite similar to those of AspAT in 'open' form and of AspAT·2-MeAsp in 'closed' form, respectively. The conformation of Y70W·2-MeAsp is between open and closed' forms. R292V shows a striking change in substrate specificity, increasing reactivity toward aromatic amino acid substrates.The structure of Y70W shows that 2-MeAsp binds the active site of this mutant enzyme, but does not form a Schiff base with PLP, which is always found in AspATs. The activity of H143N was reduced by only 30%, probably indicating that His143 is not obligatory for catalysis. The roles of R292, Y70, and H143 will be presented on the basis of the detailed structures of the mutant enzymes.

16T-54

X-RAY STRUCTURE ANALYSIS OF ASPARTIC PROTEINASE FROM *Irpex lacteus*

H.Mizuno and N.Oogami,National Institute of Agrobiological Resources,Tsukuba,Ibaraki 305,Japan,H.Kobayashi,K.Kasamo, National Food Research Institute,Tsukuba,Ibaraki 305,Japan, and I.Kusakabe and K.Murakami,Institute of Applied Biochemistry, University of Tsukuba,Tsukuba,Ibaraki 305,Japan.

Aspartic proteinase from Irpex lacteus has milk-clotting activity. This enzyme is the first example to have no disulfide bonds in the family of aspartic proteinase. The sequence identity is 28.2% with pensillopepsin,28.5% with rhizopuspepsin,27.9% with bovine chymosin,and 27.1% with porcine pepsin.

Crystals have recently been obtained by the hanging drop method using ammonium sulfate,and belong to the space group $P2_1$,cell dimensions a=54.5,b=79.6,c=37.5A,β=96.8° (Kobayashi et al.,J.Mol.Biol(1992) in press).

Diffraction data set to 2.5A resolution was measured on a four-circle diffractometer using one crystal.
A preliminary structure analysis was examined by molecular replacement (program XPLOR) using a superposition of four known structures of aspartic proteinases as the search model. The R-factor for the translation function solution was 0.516 for all data 8.0-3.5A. The simulated annealing and model fitting are in progress.

16T-55

STRUCTURE OF CHIMERIC 3-ISOPROPYLMALATE DEHYDROGENASE AND ITS THERMOSTABLE MUTANTS

M. Sakurai, K. Onodera, H. Moriyama, N. Tanaka, K. Numata, H. Kirino, T. Oshima, Y. Katsube1), M. Sato1), Faculty of Bioscience and Biotechnology, Tokyo Institute of Technology Midori-ku, Yokohama 227, Japan. 1)Institute for Protein Research, Osaka University, Suita, Osaka 565, Japan.

Several kinds of chimeric 3-isopropylmalate dehydrogenase have been produced by hybrid genes between Thermus thermophilus HB8(thermophile, T) and Bacillus subtilis (mesophile, M). Their thermostability is intermediate between that of the parent compounds. We report here the three dimensional structures of 4M6T, 2T2M6T and its mutants, 2T2M6T-I93L and 2T2M6TS82R. Here, 4M6T is composed of the 40% mesophile region and 60% thermophile region, and 2T2M6T is constructed by replacing the first 20% of 4M6T to the corresponding thermophile.

Crystallizations were achieved by the hanging drop vapor diffusion method using 1.0 - 2.0 M ammonium sulfate. We found that the request on match salting out reagent for 2T2M6T may be a consequence of the increase of exposed polar residues and decrease of exposed hydrophobic residues.

Crystals of all enzymes were isomorphous with that of the intact thermophilic enzyme(l0T) which has space group $P3_221$, a=b=78.6Å, c=158.1Å. The structures were solved by molecular replacement and refined by PROLSQ. The R-factor was 0.20 for 4M6T within 2.2Å resolution and 0.19 for the others within 2.1Å, respectively.

Few differences were observed between all the structures l0T, chimeric enzymes and its mutants. The deviations of the Ca positions from l0T were correlated with their temperature factors, except for residues between 110 and 112, which were shifted more than expected from the temperature factors. The uncorrelated movement may bring stress on the molecule and depress its thermostability from that of l0T. In the case of 2T2M6T-S82R, an extra hydrogen bond was found between R82 and E87 via a water molecule, which may cause the mutant to recover its thermostability.

Onodera, K. et al (1991). *J. Biochem.* **109**, 1-2.
Imada, K. et al (1991). *J. Mol. Biol.* **222**, 725-738.

16T-56

CRYSTAL STRUCTURE OF RIBONUCLEASE U_2 AT 1.8 Å RESOLUTION

S. Noguchi and Y. Satow, Faculty of Pharmaceutical Sciences, University of Tokyo, Hongo, Bunkyo-ku, Tokyo 113, Japan,
C. Sasaki and T. Matsuzaki, Research Center, Mitsubishi Kasei Corp., Midori-ku, Yokohama, Kanagawa 227, Japan and
T. Uchida, Mitsubishi Kasei Institute for Life Sciences, Minamiooya, Machida, Tokyo 195, Japan.

Ribonuclease(RNase) U_2 of *Ustilago sphaerogena* is a purine specific RNase consisting of 114 amino-acid residues and preferentially hydrolyses 3'-5' phosphodiester bonds of adenine. The structure of a type II crystal ($P2_12_12_1$, a=49.32Å, b=61.27Å, c=34.95Å) was determined by a molecular replacement method using the structure of RNase T_1, which has a 32% sequence identity to RNase U_2, as a search model. The model was subjected to extensive model building and refinement cycles with programs X-PLOR and PROLSQ. The present model has been refined to an R-factor of 0.166 for 9807 reflections from 8 Å to 1.8 Å spacing, with rms deviations from ideal bond lengths and from ideal bond angles being 0.012 Å and 1.5° respectively. Fourier syntheses with Bijvoet anomalous differences phased by the model without sulfur atoms confirmed three disulfide bond positions as obvious peaks.

As compared with RNase T_1, RNase U_2 has an outward protruding beta-hairpin with a type I turn at residues 73-76, and an alpha helix at residues 16-32 inclined about 10°. The inclination can be ascribed to a two-residue shortening at the RNase U_2 loop region which follows the helix. The arrangement of Glu62, Arg85, and HislOl side chains at the catalytic site is similar to that of RNase T_1. These side chains are hydrogen-bonded to a sulfate ion which marks a phosphate binding site. Part of the presumed base-recognition site is covered with Tyr78 and Ser80 residues of a neighbouring molecule. The side chain of Glu46, which is widely conserved in microbial RNases and plays an important role in guanine recognition in the case of RNase T_1, extends away from the base-recognition site.

16T-57

STRUCTURE ANALYSIS OF PHOSPHOLIPASE A_2 FROM THE VENOM OF *TRIMERESURUS FLAVOVIRIDIS*

E. MATSUEDA, A. SUZUKI, T. YAMANE and T. ASHIDA,
School of Engineering, Nagoya University, Nagoya 464-01, Japan

Phospholipase A_2 (PLA_2) from the venom of snake, *Trimeresurus flavoviridis, is* a homo-dimeric enzyme which hydrolyzes the β-ester linkage of phosphatidylcholine. A subunit is composed of 122 residues with MW 14,000. Crystals of PLA_2 were obtained using polyethylene glycol 6,000 as a precipitant at pH 4.9, but these crystals were heavily twinned. To obtain non-twinned crystals, repeated seeding was performed using the crushed twinned-crystals as seeds (Shinoda et al., 1990). The crystals belong to space group $P2_1$ with a=44.1, b=55.7, c=48.8A, and β=92.4°. An asymmetric unit contains one dimer. The structure analysis proceeded with the molecular replacement method. All diffraction data for this method were collected on a four-circle diffractometer. Self- and cross-rotation searches were performed using the fast rotation function with 8.0-4.0Å data. The integration radius was 23Å. Self-rotation search resulted in an almost unique set of peaks (40% height of origin), from whose positions, two subunits in the asymmetric unit are related by a non-crystallographic 2-fold(or 2_1) axis. Cross-rotation searches were performed using different two subunits of venom dimeric PLA_2 from the Western Diamondback rattlesnake (68% sequence homology) as a search model. In both cases of the search model, the two highest peaks indicate the same two orientations of the target subunit. These orientations lead to the same non-crystallographic diad symmetry found in the self-rotation search. Thus the orientation of the protein is uniquely determined. A translation search is in progress using both the Crowther & Blow method and the *R*-factor minimization procedure.

Shinoda, Y., Shouji, A., Yamane, T., Suzuki, A., Ashida, T., Kihara, H. & Ohno, M. (1990). *J. Biochem.* **107**, 84-86.

CRYSTAL STRUCTURE OF CHICKEN GIZZARD G-ACTIN•DNASE I COMPLEX AT 2 Å RESOLUTION

K. Sasaki, K. Sakabe*, N. Sakabe#, H. Kondo+, and M. Shimonura†,
Coll. of Medical Technology, Nagoya University, Higashi, Nagoya 461.
* Department of Chemistry, Faculty of Science, Nagoya University, Chikusa, Nagoya 464.
\# National Lab. for High Energy Physics, Tsukuba, Ibaraki 305.
\+ Department of Biology, Faculty of Science, Nagoya Univ. Chikusa, Nagoya 464.
† Faculty of Education, Tokohagakuen University, Sena 1000, Shizuoka 220, Japan.

Although the homology between skeletal muscle actin and smooth muscle actin is high, the super-structure of skeletal muscle and differ from that of smooth muscle. For instance there is no troponin in smooth muscle. It would be interesting to understand the structural differences between both actins, at atomic level. We started an atomic level crystal structure analysis of smooth muscle actin; chicken gizzard G actin•DNase I complex in 1977. Crystals of the complex were prepared from a mixture of 2mM ATP, 2mM $MgCl_2$, 0.1mM $CaCl_2$, 1mM NaN, 8%(W/V) polyethylene glycol and 0.05M imidazole buffer at pH 6.6. The crystal system is orthorhombic with space group $P2_12_12_1$. The cell dimensions a=42.02, b=225.3 and c=77.4Å, differ from those of skeletal muscle actin (Suck et al, Proc. Natl. Acad. Sci., 1981, **78**, 4319). Intensity data were collected on the Weissenberg camera for macromolecular crystallography at BL6A2 combined with imaging plate and image reader BA100. The data were processed using Program "WEIS". Initial phases were calculated with five heavy atom derivatives (YB, PCMB, MMA, FMA, and BrATF) using the MIRA method. The figure of merit was 0.69 at 2.5Å resolution. Chain tracing was carried out on a mini-map. Each atom was then assigned by PS390 using "FRODO". Coordinates thus obtained were refined using the "XPLOR" program. The R value is 0.194 with a restrained B value, including 100 water molecules, for 10-2 Å resolution data. The chain is very similar to that of skeletal muscle G-actin (Kabsch et al, Nature 1990, **347** 37) except for 4 N-terminal and 10 C-terminal residues. The position of 373 cystein was confirmed by biochemical analysis with crystals of a C^{14}PCMB derivative prepared by soaking (H. Hayashi and H. Kondo, Private communication). Their actin used for crystallization was treated by protease and 3 terminal residues are cut from the original. One has a residue at the N-terminal end additional tothat in chicken gizzard actin. The different structure at both terminals might be caused by primary structure differences from each other. The relation of structure to function will be discussed.

16T-59

STRUCTURE OF CARBONIC ANHYDRASE II: REFINEMENT AND COMPARISON WITH OTHER KNOWN CARBONIC ANHYDRASE (CA) STRUCTURES.

Vinay Kumar and K.K. Kannan, Solid State Physics Division, Bhabha Atomic Research Centre, Bombay-400085, India.

The crystal structure of Buffalo Carbonic anhydrase (II) enzyme (BCAII) (Vinay et al., 1989) has been refined against 2.1Å resolution data collected using synchrotron radiation at Photon Factory, Japan. Refinement of the structure was carried out using PROLSQ suite of programs and manual model building against Fourier maps on IRIS-4D graphics using TOM. Except for two residues on $-NH_2$ terminus and two residues elsewhere, all the residues could be located and fitted in the Fourier maps. The stereochemistry of the final model is good with rms displacement of 0.016Å for bond distances and 22° for staggered torsion angles. The R-factor for the final model with 2040 non-hydrogen protein atoms and 230 solvent molecules is 19.1%. The rms shift for postitional parameters in the final PROLSQ cycle was 0.020Å. The refined structure of BCAII was compared with other known CA structures viz., HCAI and HCAII. The three structures were observed to be highly homologous with the maximum rms displacement of about 1Å for 1024 main chain atoms, in contrast to the sequence similarity of 60%. The maximum deviation of about 5Å in the polypeptide chains is observed in an external loop region. Alignment of sequences of six CA isoenzymes (Okuyama et al., 1992) reveals about 16% identity (40 AA residues). The comparison of the 3D structures helps in elucidating the vital role of many invariant residues. It is being proposed that the invariant Glu117 residue, which is buried and not in the active site, may be essential for the catalysis by CA enzymes. Similarily, invariant Pro30 and Arg254 may be vital for the structural integrity of CA enzymes. The details will be presented.

Vinay Kumar., Kannan, K.K & Chidambarm, R. (1989). Current Science, 58, 344-348.
Okuyama, T., Sato, S., Zhu, L.X., Waheed, A & Sly, S.W. (1992). Proc. Natl. Acad. Sci. USA, 89, 1315-139.

16T-60

METAL-PROTEIN INTERACTION: BINDING OF MERCURY TO CARBONIC ANHYDRASE I ENZYME

S. Chakravarty, V.S. Yadava and K.K. Kannan, Solid State Physics Division, Bhabha Atomic Research Centre, Bombay 400 085, India.

It is well known that metal ions play an important role in the stability and functioning of enzymes. Two structures, an organo-metallic sulfonamide, namely, 3-acetoxy Mercury, 4- amino benezene sulfonamide, complexed to the Zn^{2+} containing (holo) - Human Carbonic Anhydrase I enzyme and an inorganic salt $Hg(Cl)_2$ complexed to the apo-enzyme (Zn^{2+}-free HCAI) have been refined using PROLSQ package. The R-factors are 0.192 and 0.197 respectively. The refined structures show that the Mercury ion does not remain bonded to the benzene ring which binds in the active site of the enzyme in the former complex. Instead, it coordinates to the sulfhydryl group of CYS 212 nearly 12Å away from the active site. In the Hg^{2+} + apo - HCAI structure Hg^{2+} binds to CYS 212, and replaces Zn^{2+} at the active site as well. Although the phenomenon of sulfhydryl group coordinating to Mercury is well known and has been reported earlier by Kannan et al for Carbonic Anhydrase enzyme, the present refinement shows for the first time multiple occupancy sites of Mercury near CYS 212. Two Mercury sites with occupancies 0.59 and 0.20 have been located in this region and there is a static disorder of residue 212 where the sulfhydryl group shows two possible conformations around one of the Mercury sites. Two partial occupancy Mercury binding sites have also been identified upon refinement for the first time in the organometallic complex structure but not in the inorganic salt complex. One of these is in the vicinity of the 182-186 turn and the other is near LEU 189. The protein structure in the region of residue 189 shows a drastic change of conformation as compared to the native enzyme in both the cases. Mercurials complexed to HCAII isozyme reported in literature, however, do not induce the changes mentioned above in the structure probably because Cys 206 of HCAII is located on the surface of the protein and Cys 212 of HCAI is buried in the structure. Also mercury ion is not bound to His 64 or any of the other active site residues of the HCAI holo enzyme unlike that reported for HCAII. The details of these studies and a thorough comparison will be presented.

Kannan, K.K., Vaara, I., Notstrand, B., Lovgren, S., Borell, A., Fridborg, K. & Petef, M. (1977). Drug Action at the Molecular Level, edited by G.C.K. Roberts, pp. 73-91. London, U.K.

16U-61

STRUCTURE AND MOLECULAR MOTION IN THE ALKALI METAL SALTS OF PENICILLIN V

Alison J. Edwards, Keith Prout, Christopher M. Dobson, Jamila Fattah, Stephen J. Heyes, Jocelyn E. Taguchi, J. Mark Twyman, David J. Watkin and Michaela Wendeler. Chemical Crystallography and Inorganic Chemistry Laboratories, Oxford University, Parks Road, Oxford OX1 3PD, U. K.

NMR studies suggest that there is a substantial motion of side chains within the lipophilic interior of globular proteins. Specifically, the phenyl side chains undergo 180° flips with a rotational barrier of less than 100 kJ mol^{-1}. Although this has been interpreted as evidence of a fluid structure for proteins there is scattered evidence that similar motions occur in molecular crystals.

We have systematically examined a series of organic molecular crystals, the free acid and the Li^+, Na^+, K^+ (above and below the second order phase change at about 80°C) and Cs^+ salts of Penicillin V (phenoxypenicillin) by X-ray crystallography and solid state MAS-NMR to determine whether similar side chain rotations can occur in the crystal and to relate any side chain motion to structure.

Phenyl ring flips have been characterized in all the Pen V derivatives studied to date and a wide range of rates and activation energies for the process in the various environments has been determined. In addition a second type of molecular motion has been observed in the KPenV system. At room temperature the structure consists of four formula units per asymmetric unit, whilst above the phase change at 305 K this is reduced to two. Careful consideration of the X-Ray diffraction and solid state nmr evidence leads to the conclusion that the structure existing above the phase change is an example of dynamic disorder occuring in the crystalline state.

16U-62

CRYSTAL STRUCTURE OF THE DNA FRAGMENT d(CCGGGCCCGG)

M.A. Viswamitra and D.Champion Christdoss Selvakumar, Department of Physics,Indian Institute of science, Bangalore and Jawaharlal Nehru Centre for Advanced Scientific research, Indian Institute of Science campus, Bangalore - 560 012, India.
N.Gautham, Department of Biophysics and crystallography, Madras university, Madras - 600025, India.

Single crystal X-ray diffraction studies have thrown significant light on the fine structural details of the double helix and its several polymorphic forms. In our laboratory we have recently crystallised and solved the structure of the DNA fragment d(CCGGGCCCGG) a self complementary decamer duplex.

Crystals suitable for data collection (0.5mm × 0.3mm × 0.2mm) were grown in a period of two to three weeks from a droplet containing 0.1 mM DNA, 0.3 mM $MgCl_2$, 0.5 mM sodium cacodylate, 0.1mM spermine tetrachloride with 15%(v/v) MPD (2-methyl 2,4 pentanediol) against 80%(v/v) MPD in the reservoir. Precession photographs confirmed the space group to be $P2_12_12_1$ with the cell dimensions $a = 24.592$, $b = 43.535$ and $c = 46.689$ Å. Intensity data was collected on the Enraf Nonius CAD4 Diffractometer to 2.5 Å resolution providing 1659 unique reflections.

Structure solution attempted with MERLOT (Paula Fitzgerald, 1988) with the coordinates of an homologous B-DNA decamer sequence d(CCAGGCCTGG) (Heinemann and Ailings, 1989) did not yield any solutions. The multidimensional search procedure ULTIMA (Dov Rabinovich and Zippora shakked, 1984) provided strong peaks for the input A-DNA model generated using the fibre diffraction coordinates given by Arnott and Hukins (Arnott.S and D.W.L. Huckins,1972). Preliminary refinement shows the fragment to adopt the A-DNA conformation. Further refinement is in progress and the full structure will be reported elsewhere.

Arnott and Hukins, Biochem. Biophy. Res. Comm.,47,1504 - 1509 (1972).
Dov Rabionvich and Zippora shakked, Acta cryst,A40, 195 - 200 (1984).
Heinemann. U and Ailings. C, J. Mol. Biol.,210, 369 - 381 (1989).
Paula Fitzgerld, J. Appl. Cryst.,21, 273 - 278 (1988)

16U-63

MOLECULAR STRUCTURE OF AN RNA DUPLEX WITH FOUR SUCCESSIVE NON-WATSON-CRICK BASE PAIRS

S. Fujii, Y. Tanaka, T. Sakata and H. Hiroaki, Faculty of Pharmaceutical Sciences, Osaka University, Suita, Osaka 565,
S. Uesugi, Faculty of Engineering, Yokohama National University, Kanagawa 240 and
T. Tanaka, Protein Engineering Research Institute, Suita, Osaka 565, Japan

Thermal denaturation and NMR studies show that a tridecaribonucleotide, r(UGACWCGGCUC) forms a stable intramolecular hairpin structure in aqueous solution. Crystals of this RNA oligomer belong to space group C_2 with a=38.49Å, b=32.30Å, c=38.76Å and β=117,56° with one molecule per asymmetric unit. Diffraction data were collected to a Bragg spacing of about 1.8Å, and the molecular replacement method was applied. The stem region of the molecule is considered to adopt the A-form. To determine the precise position of the stem region, rotation, PC and translation functions were calculated. The remainder of the structure including 39 solvent water molecules was found by iterative phasing and refinement. The current R factor is 17% for 2654 reflections ($\geq 1\sigma$). In the crystal lattice, two base-paired RNA strands, related by a crystallographic 2-fold axis, constitute the A-form double helix structure. Standard Watson-Crick (W&C) pairings are formed in the terminal four base pairs on either end, whereas non-W&C base pairs are found as a four successive base pair array (U=G, U=C, C=U and G=U) in the middle of the duplex formation. 5'-End base, U is not involved in base pairing of this duplex formation, and connects the duplexes by U-U base pairing. Several of the water molecules that were observed provide more stabilization of non-W&C base pairing by hydrogen bonding with base atoms and the 2'-hydroxy group of ribose.

Sakata, T., et al. (1990). *Nucleic Acids Res.* **18**, 3831-3839.

16U-64

CRYSTAL STRUCTURE OF BOC-D-VAL-ALA-LEU-ALA-OME

Vasantha Pattabhi and C. Sadasivan, Department of Crystallography and Biophysics, University of Madras, Guindy Campus, Madras-600 025, India, and
S. Durani and V. Bobde, Department of Chemistry, ndian Institute of Technology Powai, Bombay-76, India.

Several tetrapeptides with D-residues introduced at different positions have been synthesised. The aim of this project is to systematically study the change in conformation of the short peptides in the presence of D-residues. One such peptide viz Boc-D-val-ala-leu-ala-OMe has been crystallised from aqueous butanol and its crystal structure has been determined. The compound crystallises in the orthorhombic system, space group $P2_12_12$, a=9.464(5)Å, b=35.615(5)Å, c=9.703(2)Å, V=3270(3)$Å^3$. The structure has been refined using bond length constraints for the leu, val side chains and the solvent molecule. R=0.091, R_W=0.127 for 1324 observed reflections with I>2.5.σ(I). The molecule is in the extended β conformation with deviations at the leu residue. The molecules are extended along the longest axis, viz b and packed in an anti parallel β sheet with four N-H...O hydrogen bonds of length ranging from 2.89 to 3.08Å. The solvent molecule has been located. Energy calculations on this and other related molecules indicate that the crystallographically observed conformation is not the lowest energy conformer but is one among a few other possibilities. Obviously packing forces may be the deciding factor.

16U-65

UNUSUAL CONFORMATIONAL FLEXIBILITY IN N1-SUBSTITUTED UNCOMMON PURINE NUCLEOTIDES: CRYSTAL STRUCTURE OF 1-ALLYL-ISOGUANINE and 1-ALLYL-XANTHOSINE

Yen-Chywan Liaw+, Ji-Wang Chern# and Andrew H.-J. Wang+

+Laboratory of Structural Biology, Institute of Molecular Biology, Academia Sinica, Taipei, Taiwan, ROC. #Institute of Pharmaceutical Research, National Defense Medical Center, Taipei, Taiwan, ROC.

Several new N^1-substituted uncommon purine nucleosides, including doridosine (1-methyl-isoguanosine; m-iG), 1-allyl-isoguanosine (a-iG) and 1-allyl-xanthosine (a-X), have been synthesized and tested as agonists for the adenosine receptors. Some have smooth muscle relaxant or negative chronotropic activities. The x-ray crystal structure of these compounds has been determined at atomic resolution in order to understand the structure-activity relationship. The structures were solved by direct methods and refined by full-matrix least-squares refinement procedure. The crystallographic parameters are : a-iG, space group $P2_1$, a=10.573 (1) Å, b=21.955 (2) Å, c=14.360 (1) Å, b=110.65 (1)°, no. of 3σ Fo's=4585, R=0.047; a-X, space group $P2_12_12_1$, a=16.015 (2) Å, b=16.239 (1) Å, c=5.3723 (5) Å, no. of 3σ Fo's=1169, R=0.031. In the a-iG crystal, there are *four* independent molecules (with different conformation) per asymmetric unit. While all four molecules adopt *anti* c_{CN} glycosyl torsion angle, their riboses have three distinct puckers ($C^{2'}$-exo, $C^{2'}$-endo and $C^{1'}$-exo). In contrast, the a-X structure adopts a *syn* c_{CN} glycosyl torsion angle, which is stabilized by an intramolecular hydrogen bond between the N^3 of purine base and the $O^{5'}$ of the ribose (in $C^{2'}$-endo pucker). Both purine bases (1-allyl-isoguanine and 1-allyl-xanthine) are mainly in the keto tautomer form. For the isoguanine base, the averaged N^1-C^2 bond distance (1.42 Å) is significantly longer than that (1.375 Å) of the guanine base. For the xanthine base, N^3 nitrogen has an imino proton attached which is unambiguously located in the electron density map. The surprising flexibility in the ribose ring of these N^1-substituted uncommon purine nucleosides suggests that the ribose moiety may not participate in the binding of nucleoside to the adenosine receptors.

16U-66

CONFORMATIONAL ANALYSES OF AC-RING BICYCLIC COLCHICINE ANALOGUES

R.J. Greenwood and M.F. Mackay, Department of Chemistry, La Trobe University, Bundoora, Victoria 3083, Australia.

The alkaloid colchicine (1) is a potent antimitotic agent (Brossi, M. *et al.*, *J. Med. Res. Rev.*, 1988, 8(1), 77) which exerts its effect by binding to the cyctoskeletal protein tubulin, and thus inhibits its polymerization to microtubules. The existence of two partial binding sites on tubulin has been established, one for the A-ring and one for the C-ring. In view of this, and the potent antimitotic properties of the AC-ring analogues, structure-activity studies of colchicine analogues lacking the central B-ring could provide insights into the mode of the colchicine-tubulin interaction. We have used molecular mechanics to calculate the low energy conformations of six bicyclic analogues (3)-(8) whose X-ray structures are known. There is in general good agreement between the minimized and X-ray structures, all of which mimic the structure of isocolchicine (2), the inactive isomer of colchicine. However, the magnitudes of the barriers to rotation about the central C-C bond indicate that the analogues could assume the colchicine structure in solution and so achieve the configuration necessary for binding to tubulin.

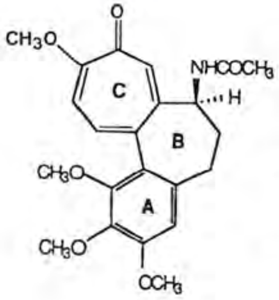

(1)

(2)

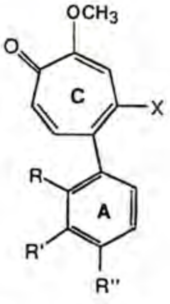

(3) $R = R' = R'' = OCH_3$, $X = H$
(4) $R = R' = R'' = OCH_3$, $X = Cl$
(5) $R = R' = OCH_3$, $R'' = X = H$
(6) $R' = R'' = OCH_3$, $R = X = H$
(7) $R = R'' = OCH_3$, $R' = X = H$
(8) $R'' = OCH_3$, $R = R' = X = H$

16U-67

ABSOLUTE CONFIGURATION AND CONFORMATION OF A NOVEL ANTIALLERGIC AGENT KW4099

N.Hirayama, Department of Biological Science and Technology,
Tokai University, 317 Nishino, Numazu, Shizuoka 410-03, Japan
T.Sugaya, S. Tomioka, Sakai Research Labs., Kyowa Hakko Kogyo Co.Ltd., 1-1-53 Takasu-cho, Sakai, Osaka 590, Japan,
E.Ohshima and N.Obase, Pharmaceutical Research Labs.,
Kyowa Hakko Kogyo Co.Ltd., Nagaizumi, Shizuoka 411, Japan.

The title compound is a novel antiallergic agent and also possesses thromboxane A_2 antagonist activity. X-ray analysis of the methyl ester of the title compound has been undertaken to determine its absolute configuration. Optical resolution has been successfully accomplished by use of (+)- or (-)-BNPPA(2,2'-(1,1'-binaphthyl)phosphoric acid). Crystallization of the (+)-BNPPA salt from a methanol solution gave well-formed colourless prisms. The results indicate that BNPPA acts as an excellent crystallization agent because many attempts at crystallization of KW4099 and its methyl ester have failed. BNPPA may be quite useful for crystallization of natural products.

Crystal data: $C_{30}N_{34}NO_3S.C_{20}H_{10}O_4P.CH_4O$ orthorhombic. $P2_12_12_1$, $Z=4$, $a=16.465(2)$, $b=30.163(3)$, $c=9.061(1)$ Å, μ (Cu $K\alpha$)=14.0 mm^{-1}

The absolute configuration of an asymmetric carbon is determined to be R by agreement with the (+)-BNPPA with the known chirality. The 6,11-dihydrodibenz[b,e]oxepin skeleton adopts a folded conformation. The conformation of the skeleton is considered to be important for biological activity. The dihedral angle between the two phenyl rings is 43.3°. The angle is 34.2° in the methyl ester of isoxepac (Matsuzawa, E.S., Hirayama, N., Ohshima, E. & Obase, H. Acta Cryst. in the press).

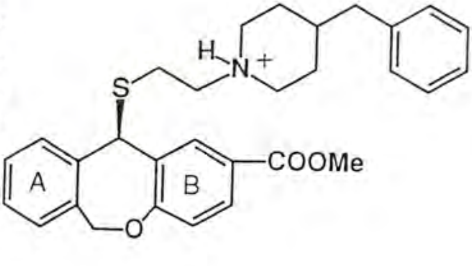

STRUCTURE DETERMINATION OF THE BLUE FLOWER PIGMENT, COMMELININ, FROM *Commelina communis*

A Nakagawa*, K.Yoshida§, T.Kondo†, T.Kawai¶ and the late T.Goto¶
*Photon Factory, KEK, 1-1 Oho, Tsukuba, Ibaraki, 305, Japan
§School of Life Studies, Sugiyama Jogakuen University, Chikusa, Nagoya, 464, Japan
†Chemical Instrument Center, Nagoya University, Chikusa, Nagoya, 464-01, Japan
¶Laboratory of Organic Chemistry, Faculty of Agriculture, Nagoya University, Chikusa, Nagoya, 464-01, Japan

Commelinin is a blue pigment from blue-flower, *Commelina communis* (Japanese name:Tsuyukusa). It is a metalloanthocyanin consisting of six malonylawobanins, six flavocommelinins and two magnesium ions. Its molecular weight is about 9000. We have solved the crystal structure of Cd-commelinin, in which the complexation metal Mg^{2+} is replaced with Cd^{2+}, elucidating the mechanism of flower coloration.

Cd-commelinin crystals, obtained from aqueous-ethanol solution. have space group *P*321 with cell dimensions a=b=31.329Å and c=33.590Å. As there are two commelinin molecules in a crystallographic unit cell, there is one-third of a molecule in the asymmetric unit (containing a total of 210 non-hydrogen atoms and about 60 solvent atoms). Diffraction data for Cd-commelinin was collected using the Weissenberg camera for macromolecular crystallography (Sakabe, 1991) with imaging plates (Miyahara *et al.*, 1986) on BL-6A_2 at the Photon Factory, KEK, using an X-ray wavelength 1.04Å to a resolution of 0.75Å. For a total of 19588 independent reflections the merging *R*-factor based on F^2 was 6.66%.

One direct method solution using SHELXS-86 (Sheldrick, 1990) showed two very strong peaks at positions corresponding to Cd ion positions determined from Patterson maps. Interpretation of electron density peaks calculated from this solution using SHELXS-86 was carried out on a computer graphics system using FRODO (Jones, 1978). At the initial stage of model building, a total of 63 peaks were assumed as parts of molecule; the *R*-factor calculated for these positions was 39.8% at 1.0Å resolution. Cycles of model building into different Fourier maps, and refinement of the atomic parameters using the XTAL program system(Hall and Stewart, 1990) finally revealed the entire atomic structure of Cd-commelinin. The present atomic parameters, refined to an R-factor of 13.2% at 1.0Å resolution (10164 reflections), include 30 water molecules. Anisotropic thermal parameters are applied to 207 atoms where the isotropic thermal factors, U, are smaller than 0.2.

Cd-commelinin is a novel type supramolecule which has several kinds of association that include self-association, co-pigmentation and an intramolecular sandwich type association. Once a molecule is formed, not only coordination of metal ions, but also strong hydrophobic stacking and hydrophilic interaction make a quite stable molecule.

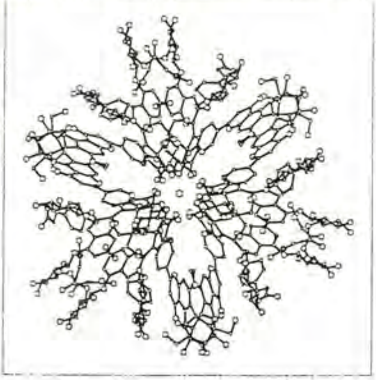

Hall, S.R. & Stewart, J.M. (1990) Eds. *Xtal3.0 Reference Manual*. Univ. Western Australia and Maryland
Jones, T.A. J. *Appl. Cryst.*, **11**, 268 (1978)
Miyahara, J. *et al.* (1986) *Nucl. Inst. Methods*,**A246**, 572
Sakabe, N. (1991) *Nucl. Inst. Method,* **A303**, 448
Sheldrick, G.M. (1990) *Acta Cryst.* **A46**, 467

STRUCTURAL STUDIES ON β-(l$\rightarrow$3) LINKED OLIGOSACCHARIDES

K. Noguchi and K. Okuyama, Faculty of Technology, Tokyo University of Agriculture and Technology, Koganei, Tokyo 184, Japan and
S. Kitamura and K. Takeo, Department of Agricultural Chemistry, Kyoto Prefectural University, Shimogamo, Kyoto 606, JAPAN.

Recently, much attention is being denoted to β-(l$\rightarrow$3) glucan for their physical properties and physiological functions, such as gel formation properties, antitumor effects, and various immunological activities. These functions are known to be closely related to their molecular conformations. For better understanding of the conformation of β-(l$\rightarrow$3) linked polysaccharides, crystal structures of two oligosaccharides were determined by X-ray diffraction methods.

Crystal data: methyl 3-*o*-β-D-glucopyranosyl-β-D-glucopyranoside(1), $C_{13}H_{24}O_{11}$, orthorhombic, $P2_12_12$, a=14.548(2), b=24.252(7), c=4.938(1)Å, Z=4;*o*-(2,3,4,6-tetra-*o*-acetyl-β-D-glucopyranosyl)-(l$\rightarrow$3)-*o*-[2,3,4,6-tetra-*o*-acetyl-β-D-glucopyranosyl-(l$\rightarrow$6)]-*o*-(2,4-di-*o*-acetyl-β-D-glucopyranosyl)-(l$\rightarrow$3)-1,2,4,6-tetra-*o*-acetyl-β-D-glucopyranose(2), $C_{52}H_{70}O_{35}$, monoclinic, $P2_1$, a=12.709(4), b=27.767(9), c=9.567(4)Å, β=105.07(2)°, and Z=2.

The β-(1$\rightarrow$3) linkage conformation of 1 is similar to that of β-D-laminarabiose (Takeda, Yasuoka, & Kasai, 1977). The intramolecular hydrogen bond between O_5 and O_4' [2.77(1)Å] almost equals that in β-D-laminarabiose. The conformations of two β-(1$\rightarrow$3) linkages observed in 2 resemble to each other, but differ from that in 1. These two linkages' conformation are also similar to those in other acetylated β-(1$\rightarrow$3) linked disaccharides (Takeda, Kaiya, Yasuoka, & Kasai, 1978; Perez, Vergelati, & Tran, 1985). The existence of (1$\rightarrow$6) branched glucose residue from the central residue in 2 does not affect β-(1$\rightarrow$3) linkage conformation. The dihedral angles around C_1-O_1 bonds depend on the exo-anomeric effect. As a result, linkage conformations are influenced by intramolecular hydrogen bonding, the size of substituents, and the exo-anomeric effect. The dihedral angle around the C_1-O_6 bond is also influenced by the exo-anomeric effect. The orientation of O_6 at the β-(1$\rightarrow$6) linkage has a *gauche-trans* conformation. The conformation around the C_6-O_6 bond is *trans*.

Perez, S., Vergelati, C. & Tran, V. H. (1985). *Acta Cryst.* B**41**, 262-267.
Takeda, H., Kaiya, T., Yasuoka, N. & Kasai, N. (1977). *Carbohydr. Res.* **62**, 27-37.
Takeda, H., Yasuoka,N. & Kasai,N. (1977). *Carbohydr. Res.* **53**,137-152.

16U-70

CRYSTAL STRUCTURES OF MODIFIED NUCLEOSIDES 5'-O-TOSYL ADENOSINE AND 2'-O-TOSYL ADENOSINE.

D.Prahadeeswaran and T.P. Seshadri, Department of Physics, Indian Institute of Science, Bangalore 560 012, INDIA.

Crystal structure analyses of the title compounds were undertaken as a part of our program to understand the conformational flexibility of the 2'-5' and 3'-5' nucleic acid fragments. In the modified nucleoside 5'-O-tosyladenosine, instead of a phosphate group, a sulphonyl group with a bulky phenyl ring is attached in its 5'-position. In 2'-tosyladenosine the same group is attached in its 2'-position. Crystals of 2'-O-tosyladenosine (compound I) were grown by slow diffusion of water into DMSO solution. Weissenberg photograph confirmed the space group to be $P2_1$ with the cell dimension $a = 7.359(3)$, $b = 7.873(3)$, $c = 16.098(5)$ Å and $\beta = 96.0(2)°$. The structure was solved by direct methods using SHELX-86. The R-factor converged to 0.059 for 1936 unique reflections. An intra molecular stacking between the adenine base and the phenyl ring was observed in this structure. The glycosidic torsion angle about the C(l')-N(9) bond is 62.3(4)° which falls in the range associated with *syn* conformation and the sugar puckering is C2'-endo. The *syn* conformation of the adenine base is stabilised by a N3···O5' intramolecular hydrogen bond as in A2'p5'C and A2'p5'A.

The 5'-O-tosyladenosine (compound II) crystals were grown by slow evaporation of acetone solution. The Weissenberg photograph confirmed the space group to be $P2_12_12_1$ with cell dimension $a = 8.045(1)$, $b = 8.937(1)$, $c = 26.773(2)$ Å. The Cu $K\alpha$ intensity data consisting of 1472 reflections with $F(obs) \geq 3\sigma(Fobs)$ were collected on a CAD-4 diffractometer. The structure was solved by MULTAN 82 and refined by full matrix least square and difference fourier methods to an R-factor of 0.044. The glycosidic torsion angle about the bond C(l')-N(9) is -166.2(4)° which falls in the *anti* conformation and the sugar puckering is C3'-endo. The torsion angle about C5'-O5' is -142.8(4)°.

Unlike compound I the phenyl ring of compound II assumes a folded shape with respect to the adenine base.

16U-71

METAL ION-PURINE BASE INTERACTIONS: ZINC(II) AND CADMIUM(II) COMPLEXES OF 8-METHYLTHIOTHEOPHYLLINE. X-RAY CRYSTAL STRUCTURE AND SOLUTION STRUCTURE OF BIS(8-METHYLTHIOTHEOPHYLLINATO)DIAQUAZINC(II)

M. H. Skipworth and M. R. Taylor, School of Physical Sciences, The Flinders University of South Australia, G.P.O. Box 2100, Adelaide, SA 5001, Australia, and J. C. Avila-Roson, M. A. Hidalgo, J. Suarez-Varela and E. Colacio, Facultad de Ciencias, Universidad de Granada, 18071 Granada, Spain.

The complexes $[M(H_2O)_2L_2]$, (where $M=Zn^{2+}$ or Cd^{2+} and L is the 8-methylthiotheophyllinato anion) have been prepared and characterised by means of I.R. ^1H and ^{13}C-NMR spectral studies. Structure determination of $[Zn(H_2O)_2L_2]$ at 293 K by single crystal X-ray diffraction methods revealed that the zinc(II) ion is co-ordinated at the N7 of the two monodentate L anions and the two water molecules. This gives rise to a ZnN_2O_2 environment with local C_{2v} symmetry. Co-ordination of the zinc ion is approximately tetrahedral with small deviations from the ideal angles due to large steric factors and crystal packing.

The molecules of the complex are held together by intermolecular hydrogen bonds and base-base stacking interactions where the interbase stacking distance is 3.40 Å. These interactions link the molecules in extended chains which run through the structure. Bond lengths and angles in this compound do not significantly differ from those reported for free theophylline and its N7 complexes [1,2].

Crystal Data: $[Zn(H_2O)_2L_2]$ monoclinic, spacegroup $C2/c$ (No.15), Z 4
a 14.6615(6), b 8.6664(3), c 17.253(1) Å, β 94.22(1)°.

1. Colacio, E., Romerosa, A., Ruiz, J., Roman, P., Gutierrez-Zorrilla, J. M. & Martinez-Ripoll, M. (1989). *J. Chem. Soc. Dalton Trans.* 2323 and references therein.

2. Cozak, D., Marhy, A., Olivier, M. J. & Beauchamp, A.L. (1986). *Inorg. Chem.* **25**, 2600 and references therein.

16V-72

MOLECULAR LIBRATION AND A POSSIBLE STRUCTURAL PHASE TRANSITION IN CRYSTALLINE 4,4"-DIFLUORO-p-TERPHENYL

H. Saitoh, K. Saito, Y. Yamamura, H. Matsuyama, K. Kikuchi, M. Iyoda and I. Ikemoto, Department of Chemistry, Faculty of Science, Tokyo Metropolitan University, Hachioji, Tokyo 192-03, Japan.

Crystals of a molecule having (a) soft internal degree(s) of freedom often show an interesting phase transition associated with a change in the molecular conformation. The first three members of so-called *p*-polyphenyls shows a "twist" phase transition at a low temperature and studies have been made in detail for a long time. Study on the analogous compounds has a crucial importance for getting a unified understanding of the mechanism of the "twist" transitions. We have chosen 4,4"-difluoro-p-terphenyl (DFTPH) as a sample compound taking into account of the results of the study on 4,4'-difluorobiphenyl. The molecule of DFTPH was synthesized by the coupling reaction of p-fluorophenylzinc chloride and p-diiodobenzene using $Ni[P(C_6H_5)_3]_4$ as a catalyst. The crystal structure of DFTPH was determined at room temperature by single-crystal X-ray diffraction.

Crystal data : $F-(C_6H_4)_3-F$ monoclinic, space group $P2_1/a$
a 7.868(2), b 5.741(1), c 14.129(3)Å, β 93.27(2)°,
V 637.2(2)Å^3

The structure is iso-structural with that of *p*-terphenyl and a molecule lies on an inversion center. The molecular geometry assuming an ordered single central ring is planar within 0.03 Å, and the apparent squared amplitude amounts to 250(10) deg^2 of libration of the central ring around the long molecular axis. The large amplitude implies the disordered nature of the structure. When the carbon atoms on the central ring are split, two central rings, which have opposing conformation with respect to the outer rings, remain planar within 0.04 Å. The dihedral angle between two conformations is 22.1(1)°, and the amplitudes of libration of each central ring shrinks to 90(10) deg^2. The potential barrier height $V(O)$ at the planar conformation is estimated as about 1 kJ·mol^{-1} in the crystal using the method by Baudour (1991). The height is much smaller than 4.57 kJ·mol^{-1} for *p*-terphenyl and, consequently, the possible "twist" transition of DFTPH will occur at a lower temperature.

Baudour, J. L. (1991). *Acta Cryst.* B**47**, 935-949.

16V-73

X-RAY DIFFRACTION STUDY OF PHASE TRANSITIONS AND STRUCTURES OF $(KBr)_{1-x}(KCN)_x$ MIXED CRYSTALS

Y.Yoshimura, T.Okazaki and K.Shimaoka, Sci. Eng. Ritsumeikan U.,
56-1 Tojiin-Kitamachi, Kita-ku, Kyoto 603, Japan.

Crystal structures and phase transitions of $(KCN)_{1-x}(KBr)_x(x=0.9, 0.8)$ mixed crystals were studied by X-ray diffraction (precession) method. The crystal structure of the mixed crystals at room temperature has a NaCl type cubic structure, with linear CN^- ions achieving the required symmetry by rapid reorientation in the site of octahedral symmetry. The mixed crystals undergo phase transitions associated mainly with the change in the orientation of the CN^- ions, which is the same mechanism in the case of the phase transitions of alkali cyanides; NaCN, KCN and RbCN. A crystal structure of the mixed crystals in a low temperature phase [L.T.P.] is considered to be isostructural with the metastable phase of KCN crystal in the temperature range from 165 to 158 K, if the crystal has been once subjected to the phase transition at 168K before cooling.

Precession photos of the mixed crystals were taken at the temperature range between room temperature and 83 K. A structural change was observed from cubic to a L.T.P. at about 138 K for $x=0.9$ and 106 K for $x=0.8$. A variety of diffraction photographs indicating a coexistence of various forms were obtained below the phase transition temperature. Paying attention to the presence of splitting and superlattice reflections, a triclinic and a monoclinic forms were found in the L.T.P. of $(KCN)_{0.9}(KBr)_{0.1}$ crystal. Triclinic form: The space group $P\bar{1}$ and the lattice constants are $a_T=9.45(1)$, $b_T=4.41(1)$, $c_T=4.59(1)$Å, $\alpha_T=121.0(5)^\circ$, $\beta_T=119.0(5)^\circ$ and $\gamma_T=90.0(1)^\circ$ at 85 K. Monoclinic form: The space group $A2/m$ and the lattice constants: $a_M=4.61(1)$, $b_M=4.59(1)$, $c_M=7.55(1)$Å and $\beta_M=122.5(5)^\circ$ at 85 K. In the L.T.P. of the $(KCN)_{0.8}(KBr)_{0.2}$ crystal a new triclinic form was found. The lattice constants of the triclinic lattice are $a_T=6.46(1)$, $b_T=6.45(1)$, $c_T=6.45(1)$Å, $\alpha_T=90.1(5)^\circ$, $\beta_T=87.10(10)^\circ$ and $\gamma_T=92.8(5)^\circ$ at 85 K. Crystallographic relationships between these forms and the cubic lattice will be presented.

16V-74

PACKING EFFECT IN SOLID-STATE POLYMERIZATION OF DIETHYNYLBENZENE DERIVATIVES BY γ-IRRADIATION

R. Kitagawa, N. Kanehisa, Y. Kai and N. Kasai, Department of Applied Chemistry, Faculty of Engineering, Osaka University, Suita 565, Japan, Y. Yamamoto, and S. Takahashi, Institute of Scientific and Industrial Research, Osaka University, Ibaraki 567, Japan

Investigation of solid-state polymerization of crystalline monomers has attracted increasing attention during last three decades. From the viewpoint of crystal engineering, structural studies on the correlation between crystal structures and their reactivities are interesting. This paper is concerned with the inherent reactivities of a series of crystalline diethynylbenzene derivatives (I-IV) in solid-state polymerization, which is initiated by radicals generated upon irradiation with γ rays. Effects of the molecular packing in the crystals on the reactivities are discussed.

I(o)

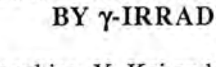

I(p)

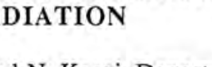

II(o)

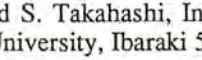

II(m)

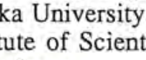

III

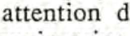

IV

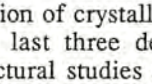

In a series of studies on the correlation between crystal structures and solid state polymerization of diethynylbenzene derivatives, many variation of molecular packings were revealed by X-ray crystal structure analyses. One of the important structural factors for determining molecular packings is the position of two ethynyl substituents in the benzene ring, *ortho, meta,* and *para*. The second substituent in the benzene ring is also important in deciding the molecular packing. Only the replacement of methyl group by methoxy causes definite differences in their crystal structures. The interatomic distances between the acetylene carbons of neighbouring molecules correlates well with the solid state polymerization activities of the monomer crystals. The monomer IV shows a unique dimerization reaction in a chain mode. The mechanism of the initial stage of dimerization reaction was simulated by energy optimization based on its crystal structure.

16V-75

ASYMMETRIC PHOTOSYNTHESIS IN A CHIRAL CRYSTAL ENVIRONMENT

Hidenori Kogo, Akiko Sekine, Yuji Ohashi, Rikiya Matsukawa*, Kyuichi Miyamoto* and Fumio Toda*.
*Department of Chemistry, Tokyo Institute of Technology, O-okayama, Meguro-ku, Tokyo 152, Japan and *Department of Industrial Chemistry, Ehime University, Matsuyama 790, Japan.*

It has been found that the α-oxo amide (1) is transformed to β-lactam (2) on exposure to visible light in the solid state as shown in Fig.1.

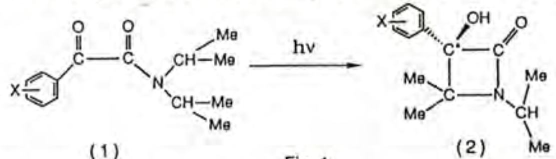

Fig. 1

When the substituents (X) bonded to the phenyl ring are m - Cl (1b), o - Me (1d) and m - Me (1e) groups, the corresponding chiral products (2b,d,e) were obtained with about 100 % enantiomeric excess. On the other hand, the α-oxo amides with X= o - Cl (1a), p - Cl (1c) and p - Me (1f) did not reveal such an asymmetric synthesis. In order to clarify the factors which influence on the above difference, the crystal structures of (1a) - (1f) were determined. Moreover, the absolute structures of (1b) and the β-lactam (X= m -Cl, 2b) were determined using anomalous dispersion technique, in order to elucidate the mechanism of cyclization. The crystals revealing the asymmetric induction, (1b), (1d) and (1e) have a chiral space group, $P2_12_12_1$, whereas (1a), (1c) and (1f), which gave racemic β-lactam, have the centrosymmetric space group, $P2_1/n$, Pbca and Pbca, respectively. The asymmetric synthesis clearly depends on whether the molecular packing in the reactant crystals is chiral or not. The molecular structures of the six crystals have very similar conformation to each other. The absolute structures of the reactant and product crystals clearly suggest that the process of the cyclization is controlled topochemically, that is, a new bond is formed between the two carbon atoms with very short contacts (C ... C = 2.85 Å) and then a four - membered ring is made.

Author Index

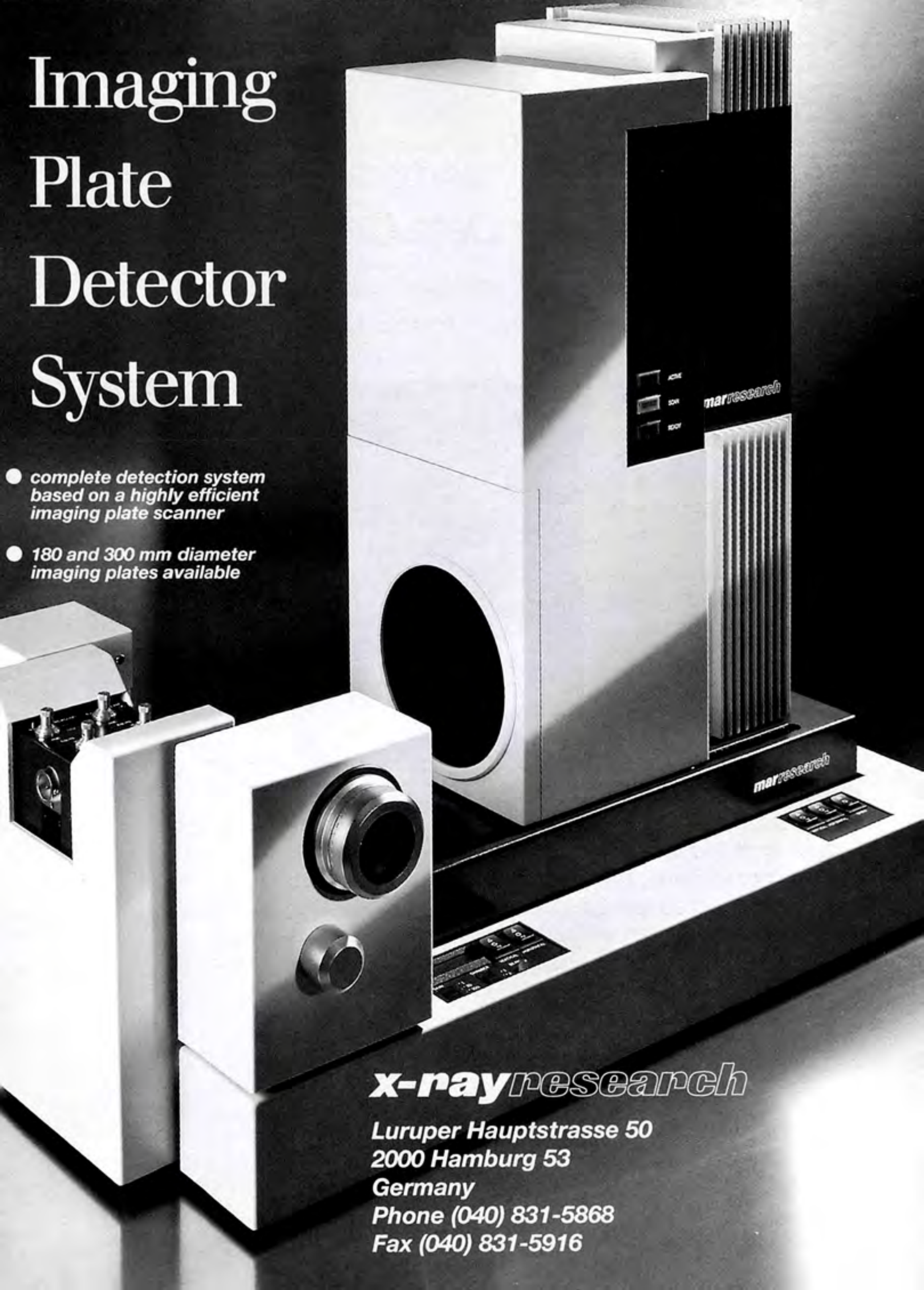
ACTIVE
SCAN
READY
marresearch
marresearch

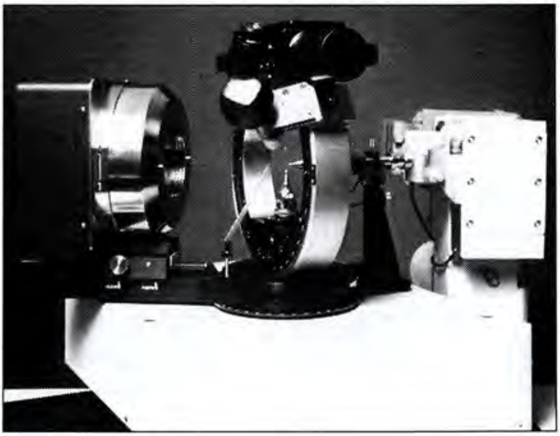

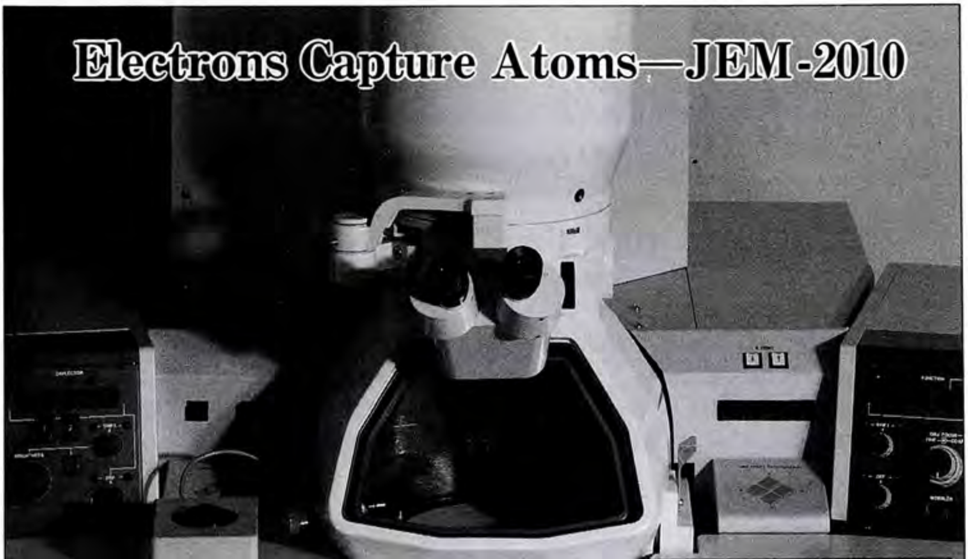

Configuration	Resolution	Spherical aberration coefficient	Chromatic aberration coefficient
UD-UHR	0.194nm	0.5mm	1.0mm
UD-HT	0.23nm	1.0mm	1.4mm

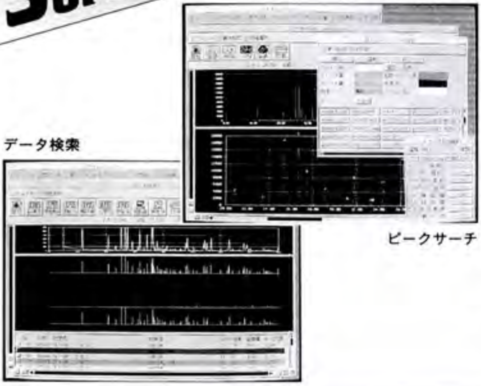


M18XHF
SRA


SRA